Review on the Degradation Mechanisms of Metal-N-C Catalysts for the Oxygen Reduction Reaction in Acid Electrolyte: Current Understanding and Mitigation Approaches

Kavita Kumar, Laetitia Dubau, Frédéric Jaouen, Frédéric Maillard

A Review on the Degradation Mechanisms of Metal-N-C Catalysts for the Oxygen Reduction Reaction in Acid Electrolyte: Current Understanding and Mitigation Approaches

Kavita Kumar, [1] Laetitia Dubau, [1] Frédéric Jaouen, [2,] * Frédéric Maillard [1,] *

1. Univ. Grenoble Alpes, Univ. Savoie Mont Blanc, CNRS, Grenoble INP, LEPMI, 38000 Grenoble (France). E-mail : frederic.maillard@grenoble-inp.fr

2. ICGM, Univ. Montpellier, CNRS, ENSCM, F-34293 Montpellier (France). E-mail : frederic.jaouen@umontpellier.fr

Contents

ABSTRACT

One bottleneck hampering the widespread use of fuel cell vehicles, in particular of proton exchange membrane fuel cells (PEMFCs), is the high cost of the cathode where the oxygen reduction reaction (ORR) occurs, due to the current need of precious metals to catalyse this reaction. Electrochemists tackle this issue in the short/medium term by developing catalysts with improved utilization or efficiency of platinum, and in the longer term, by developing catalysts based on Earth-abundant elements. Considerable progress has been achieved in the initial performance of Metal-Nitrogen-Carbon (Metal-N-C) catalysts for the ORR, especially with Fe-N-C materials. However, until now, this high performance cannot be maintained for sufficiently long time in operating PEMFC. The identification and mitigation of the degradation mechanisms of Metal-N-C electrocatalysts in the acidic environment of PEMFCs has therefore become an important research topic. Here, we review recent advances in the understanding of the degradation mechanisms of Metal-N-C electrocatalysts, including the recently identified importance of combined oxygen and electrochemical potential. Results obtained in liquid-electrolyte and PEMFC device are discussed, as well as insights gained from *in situ* and *operando* techniques. We also review the mitigation approaches that the scientific community has hitherto investigated to overcome the durability issues of Metal-N-C electrocatalysts.

KEYWORDS: Oxygen Reduction Reaction; Non-Precious Metal Catalysts; Degradation Mechanisms; Durability; Stability.

1. Introduction

Introducing the "British Petroleum (BP) Statistical Review of World Energy 2019: an unsustainable path", [1] Spencer Dale, BP chief economist, said: "There is a growing mismatch between societal demands for action on climate change and the actual pace of progress, with energy demand and carbon emissions growing at their fastest rate for years. The world is on an unsustainable path." These sentences perfectly illustrate the societal concerns associated with the continuously growing carbon dioxide (CO_2) emissions and the resulting global warming. The development of hybrid vehicles and full electric vehicles is part of the solution to these issues. While for low driving range, a Li-ion battery pack is lighter than a proton exchange membrane fuel cell (PEMFC) system (stack and pressurized H_2 tank dimensioned for this range), above a certain threshold of driving range, the PEMFC system becomes the lighter solution. [2] The fundamental reason for this is that batteries are power devices with limited specific energy while hydrogen-fuelled PEMFCs are intrinsically better suited for obtaining a high specific energy (and therefore a large mileage). Indeed, H_2 has a high specific energy of 33.3 kWh kg^{-1}, three times higher than that of any other fuel and more than hundred fifty times higher than that of a Li-ion battery's active material (250 Wh kg^{-1}). The interested reader is referred to Refs [3, 4] for values of specific energy, energy density and specific power ranges for PEMFC and for a broad selection of Li-ion and advanced "post-Li-ion" cells). PEMFC systems with compressed H_2 tanks are therefore currently best positioned to replace thermal engines in automobiles for the market segment of long distances, maintaining both a high autonomy and a short refuelling time. [5] In these devices, the hydrogen oxidation reaction (HOR) and the oxygen reduction reaction (ORR) take place at the anode and cathode, respectively. [6] Both reactions need to be catalysed, and the most efficient and robust catalysts in PEMFC environment are Pt or Pt-alloy nanoparticles (NPs) supported on high surface area carbon. However, the scarcity and the high cost of Pt, and of platinum group metals (PGM) in general, hinders the global commercialization of PEMFCs. [7] Comprehensive review articles on the degradation mechanisms of Pt-based/C nanoparticles have been also published in the recent years, and the interested reader is referred to Refs. [8-11]. Three main approaches are considered to reduce the catalyst's cost in a PEMFC: i) reducing the PGM content in the electrodes while maintaining or improving the power performance; ii) recycling PGMs contained in aged membrane electrode assemblies (MEAs), [12] iii) replacing PGM by more abundant and cheaper metals. [13] The third solution is particularly attractive from cost and sustainability viewpoints. Indeed, by replacing PGM-based catalysts by electrocatalysts based on more abundant transition metals such as Fe, Mn or Co, the price of a PEMFC stack could become at least 50 % cheaper, even for relatively low production volumes (in the context of the automotive industry) of 500,000 units per year. [14] Moreover, electrocatalysts based on non-precious-metals are tolerant to most species that strongly contaminate PGM surfaces, originating either from the H_2 fuel (CO in trace amount of 10-20 ppm, sulphur species), air (chlorides on coastal area, air impurities from combustion engines in urban areas, such as CO_2, NO_x, SO_x) [15, 16] and from PEMFC stack components (*e.g*. alcohols, inorganic and organic anions).

The most mature class of non-precious metal electrocatalysts for the ORR in acid medium consists in 3d transition metal (Fe, Co, Mn) embedded in a carbon matrix (C) doped with nitrogen (N), referred to as Metal-N-C catalysts in what follows. Their beginning-of-life (BoL) ORR activity strongly depends on their physical and chemical structure, namely the nature and coordination of the metal centres, [17-20] the metal content, [17-21] the redox potential of the metal, [19, 20, 22] the basicity of N-containing groups [18-20, 23-25] and the pore size distribution in the

carbon phase. [19, 20, 22] Similar to PGM electrocatalysts, the mass-normalized activity for the ORR of Metal-N-C electrocatalysts, i_m, can be expressed as (**Equation 1**): [26]

$$i_m = TOF \times ASD \times F/N_a \quad (1)$$

$$ASD = \upsilon \times SD \quad (2)$$

Where i_m is the mass-normalized activity (A g^{-1}_{powder}) at a given electrode potential (E), ASD is the gravimetric density of electrochemically accessible sites for the ORR (site g^{-1}_{powder}), TOF the turnover frequency of the active sites (electrons $site^{-1}$ s^{-1}, for the same E value), F Faraday's constant (C mol^{-1}), N_a Avogadro's number (mol^{-1}). In turn, ASD, is related to the total number of sites (labelled SD, in mol g^{-1}_{powder}), via the ratio of active sites located on the surface to all active sites, υ (**Equation 2**). From these equations, it is explicit that enhanced mass-normalized activity can be obtained by either increasing the value of SD, TOF or υ. [27] Increasing υ is achievable for example by preferentially localizing active sites on the carbon surface. [28]

The use of SD and ASD descriptors also raises the question of the nature of the active sites for the ORR. Two main forms of metal species exist in Metal-N-C catalysts: i) single metal atom coordinated to several nitrogen atoms in the carbon matrix (Metal-N_x sites) and ii) inorganic metal NPs (carbides, nitrides, sulphides, depending on precursors used and pyrolysis conditions).[19, 20] Following extensive research efforts, a consensus has now been reached that the major contributors of ORR activity in PGM-free Metal-N-C catalysts comprising multidunous metal species are the Metal-N_x sites, these sites comprising most likely four nitrogen atoms. [18, 29-31] The structure and texture of the carbon matrix also play a crucial role for the ORR activity and long-term stability of Metal-N-C catalysts.[21] Micropores are essential to host Metal-N_x moieties, [22, 32] while mesopores and macropores ensure efficient transport of oxygen (O_2) molecules and reaction products to and from the active sites, respectively.[25, 33, 34] Moreover, the chemical environment around Metal-N_x moieties can also significantly modify their TOF. An illustration of this can be found in recent works showing that mild and reversible surface oxidation of carbon (for example due to hydrogen peroxide (H_2O_2), see **section 2.4**) leads to decreased TOF values via weakened O_2-binding. [33, 35, 36]

The identification, quantification and implementation of the most active sites [26, 27, 29, 30, 33, 35-40] and ORR activity/structure relationships [41-48] remain the most popular subjects of study in the field of Metal-N-C catalysts. Objectives of performance and activity have been set for PGM-free cathodes in PEMFC device. The United States Department of Energy (US DoE) has defined the objective of ORR activity at 0.9 V in H_2/O_2 PEMFC at 44 mA·cm^{-2}, [49] comparable to Pt/C cathode's activity, while the European Fuel Cells and Hydrogen Joint Undertaking (FCH-JU) set an even higher target of 75 mA·cm^{-2} at 0.9 V in H_2/O_2 PEMFC and a performance of 0.6 A·cm^{-2} at 0.7 V in H_2/air PEMFC (0.42 W·cm^{-2}). [50] Recent years have witnessed considerable progress in the initial performance of Metal-N-C cathodes. Several studies have reported ORR activities above 20 mA·cm^{-2} [28, 31, 49, 51-54] and up to 0.041 A cm^{-2} at 0.9 V in H_2/O_2 PEMFC, [55] while H_2/air PEMFC current densities of 0.3-0.4 A·cm^{-2} have been achieved at 0.7 V at 80°C. [51, 55, 56] While further progress on activity and power performance of Metal-N-C cathodes is still needed to envision the replacement of Pt in high power density PEMFCs, the achievements

and rate of progress witnessed on these topics during the last decade holds promise, at least for low- to medium-duty PEMFC applications. The interested reader is referred to Refs [51, 57, 58] for reviews on the recent progress on initial activity and power performances of Metal-N-C layers for PEMFC. Beyond gains in ORR activity, the development of novel electrode architectures that are specific for Metal-N-C catalysts is acutely needed to increase the power performances with air feed. [59]

While steady progress has been achieved in the past decade regarding the BoL activity and power performance of Metal-N-C catalysts, little progress has been achieved regarding their stability and durability. Moreover, a negative correlation has been identified between the initial ORR activity of Metal-N-C catalysts and their durability in PEMFC operation. [11, 60] Exacerbated performance loss with time is observed for Fe-N-C catalysts with high microporous area, corresponding also to the initially most active ones. [11] This holds especially true for doubly-pyrolyzed Metal-N-C catalysts, the ORR activity of which is not stable over the long term. [60, 61] Only a few Metal-N-C materials but with low initial activity have shown promising durability in PEMFC. [62] Their activity and PEMFC performance is however significantly below the state-of-the-art reached with ultralow Pt cathodes. [63] While restricted performance loss during operation in PEMFC for several hundreds of hours has been reported for some Fe-N-C cathodes with interesting ORR mass activity, the durability tests were typically performed under a galvanostatic or potentiostatic hold of the cell, corresponding to a low cathode potential and therefore also to a mixed control by ORR kinetics and mass-transport of the cathode performance. [64] Complete cell polarization curves before and after a durability test identified that the apparent stable performance during the potentiostatic hold at 0.4 V or 0.5 V was an interplay of decreasing ORR activity with time and increasing mass-transport properties with time. [65] Durability of non-PGM cathodes is especially challenging at cathode potentials ≥ 0.6 V, [64-66] which by virtue of the positive linear relation between energy efficiency and operating PEMFC voltage, corresponds to the desired range of operating cathode potential for high efficiency. Beside the restricted durability of Metal-N-C cathodes under galvanostatic or potentiostatic operation, further accelerated performance loss associated with voltage cycling needs to be considered, and in particular start-up/shutdown (SU/SD) of a fuel cell vehicle, potentially leading to transient high cathode potentials (typically > 1.0 V) and fast rate of carbon corrosion. [21, 66-68] The accelerated stress test (AST) proposed by the US DoE for MEA testing in PEMFC is composed of 30,000 square-wave load cycles between 0.60 and 0.95 V at 80°C with H_2 and N_2 fed at the anode and cathode, respectively. [69] The loss in initial mass activity should not exceed 40 % after 30k load cycles for a given cathode electrocatalyst to pass. However, this AST was designed for carbon-supported Pt-based nanoparticles, whose degradation is essentially driven by Ostwald ripening and is not affected by O_2. As such, it is ill-suited to study the durability of Metal-N-C catalysts, since a significant fraction of these materials' performance decay arises from H_2O_2 produced during the ORR, and associated radicals, as will be discussed in the present review. [70-73] Indeed, Fe but also Co cations (free cations but also possibly as Metal-N_x sites) are recognized catalysts to form, by reaction with H_2O_2, reactive oxygen species (ROS) such as superoxide ($^{\bullet}O_2^-$), hydroxyl ($^{\bullet}OH$) and hydroperoxyl ($^{\bullet}OOH$) radicals, which can degrade the catalyst, ionomer and proton-exchange membrane (PEM). [74, 75] Overall, the current status of non-PGM Metal-N-C cathode catalysts is that of an unsatisfactory compromise between high initial activity (or power) performance and durability, not fulfilling simultaneously the three main criteria for industrial application, namely low cost, high performance and high durability. While Metal-N-C catalysts have a lower cost than Pt-based catalysts, the low performance (in $W_{electric}$ per cm^2

of geometric MEA area) of the currently most durable Fe-N-C cathodes would result in PEMFC stacks with much increased volume and mass to reach a given electric power output, should Pt-cathodes be replaced by Fe-N-C ones. This is not economically viable for transportation application, not only simply due to the increased size and mass of the stack, but also due to the non-negligible cost of other components of a PEMFC stack (PEM, ionomer, gas diffusion layer, bipolar plates, etc). Ideally, the durability of PGM-free cathode layers should ultimately be comparable to that of Pt-based cathodes, or the performance loss during the lifetime of a product be low enough so that it is acceptable by the customers. PEMFCs have broad application markets, ranging from heavy-duty vehicles to portable electronics and backup power systems, with diverse operating conditions and device specifications. Precise goals of Metal-N-C layer durability are therefore premature at this stage, but certainly the durability of Metal-N-C materials in acid medium must be significantly improved compared to the current status, for replacing Pt-based materials in any of the envisioned PEMFC applications.

In the last years, research in the field of PGM-free catalysts for PEMFCs has increasingly integrated studies of their stability and durability in various operating conditions, as well as the fundamental understanding of their degradation mechanisms. Herein, we review the current understanding of the degradation mechanisms of Metal-N-C catalysts and cathode active layer (AL) in acidic environment. The main identified degradation mechanisms for Metal-N-C catalysts are discussed first, concluding with complex phenomena arising from a combination of "stressing factors" and also discussing modifications of the mass-transport properties through the cathode AL during PEMFC operation. The recently investigated strategies to mitigate these different degradation mechanisms are then presented and discussed, including switching to non-iron metals for mitigating Fenton reactions and modified syntheses for improved selectivity towards 4-electron ORR and/or for imparting radical scavenging properties. Several review papers published in the past 5 years have focused on the stability and durability of PGM-free catalysts for PEMFCs. [51, 76-86] The present review has the distinct features of presenting the most recent understanding and status of i) degradation mechanisms (including the recently identified importance of combined O_2 and electrochemical potential in the degradation), ii) methodological studies performed in PEMFC environment and combined with advanced end-of-test (EoT) MEA characterisation, and iii) by-design approaches to improve the durability of PGM-free catalysts and ALs. In citing and discussing the literature in the field, we focused on the studies where not only stability or durability was measured *per se*, but where those measurements were combined with sufficient characterisation before, during and/or after the electrochemical measurements, in order to shed light on the degradation mechanisms.

2. Degradation mechanisms of Metal-N-C oxygen reduction electrocatalysts in acid medium

We review in this section the main degradation mechanisms of Metal-N-C electrocatalysts identified in the literature, starting in each subsection with the understanding gained in rotating disk electrode (RDE) or flow cell environments (liquid acidic electrolyte) and continue, when available, to the understanding gained in PEMFC environment, either with *in situ*/ *operando* techniques or from EoT characterization of MEAs or cathode AL. The main differences in experimental conditions between experiments in liquid acidic electrolyte and in

PEMFC are i) the temperature (often room temperature (RT) is employed in RDE studies but typically 80°C in PEMFC) and ii) less water available in PEMFC environment.

For clarity, we first define for PGM-free Metal-N-C catalysts and use in a self-consistent way the words stability, durability, *in situ* and *operando* (**Table 1**). In addition, we generally refer to as i) load conditions, for experiments involving a change of the cathode potential comprised between 0.0 and 1.0 V *vs*. the reversible hydrogen electrode (RHE) as the lower and upper limits; and ii) SU/SD conditions, for experiments where the lower limit is ≥ 1.0 V *vs*. RHE. The primary reason for distinguishing between stability (no ORR) and durability (ORR occurring) in acidic medium is due to the occurrence of specific degradation mechanisms during ORR on PGM-free catalysts, which do not occur or have limited effects on PGM-based catalysts. The low importance for the durability of PGM-based materials of H_2O_2 and ROS formed *operando*, but high importance for Metal-N-C catalysts, is a key example of the need to specifically differentiate between degradation mechanisms that are related to ORR from those that are not, for Metal-N-C catalysts. According to **Table 1**, three important conditions are therefore defined, namely i) Stability under load conditions, ii) stability under SU/SD conditions, and iii) durability. Stability in conditions i) is a necessary but non-sufficient condition for reaching durability. Stability under SU/SD conditions ii) is closely related to carbon corrosion, and this effect can be studied either in the presence or absence of O_2, since the herein definition of SU/SD (lower potential limit ≥ 1.0 *vs*. RHE) excludes in practice the ORR. In accordance with the definition of stability and durability, we employ in the present review the words *in situ* and *operando* for techniques that allow probing Metal-N-C materials in the absence of ORR (*in situ*) or in the presence of ORR (*operando*).

Table 1. Definition of stability and durability in the present review.

	Definition	**Operation modes**
Stability	No changes in the local coordination, in the number of metal-based active sites in Metal-N-C and in their TOF, in the absence of ORR in acidic medium	Load
		SU/SD
Durability	No changes in the local coordination, in the number of metal-based active sites in Metal-N-C and in their TOF, during ORR in acidic medium	Load
In situ	Measurements probing Metal-N-C while it is subjected to an electrochemical potential in acidic medium, in the absence of ORR	Load
		SU/SD
Operando	Measurements probing Metal-N-C during ORR in acidic medium	Load

As will progressively emerge from this review, the degradation mechanisms of PGM-free catalysts are not only set by the particular material studied, but also by the experimental conditions applied. Examples of the latter are the upper and lower potential limits applied (UPL and LPL, respectively), the absence or presence of O_2 in the environment and the

temperature. These experimental parameters play a key role not only on the overall degradation rate but also on which is the predominant degradation mechanism. Therefore, to provide the reader with the key experimental information from the literature in a single format, all AST involving potential cycles are labelled as [low potential – high potential - duration of each cycle (for stepped potential) or scan rate (for scanned potential) – number of cycles – nature of the atmosphere – temperature] and [potential – duration – atmosphere – temperature] for liquid and solid electrolyte, respectively. For liquid acidic electrolyte, the nature of the atmosphere corresponds to the gas used to saturate the electrolyte, while in PEMFC it corresponds to the cathode feed. Also, as Metal-N-C catalysts can feature aggregates with size 1 µm *i.e.*, exceed the thickness required to correctly measure the mass activity of an ORR catalyst and the fraction of H_2O_2 generated, [87-89] the reproducibility of the data is a key parameter.

2.1 Modelling degradation mechanisms at single-atom sites and its kinetics

Holby *et al.* [90] recently investigated with density functional theory (DFT) the stability towards demetalation of a divacancy Fe-N_4 site in graphene (**Figure 1a**). The general dissolution reaction is (**Equation 3**):

$$H_aO_bFeN_4C_z + n\ H^+ \rightarrow Fe_{aq}^{x+} + H_{n+a}N_4C_z + (x - n)\ e^- + b/2\ O_2 \quad (3)$$

H_aO_b represents oxygenated species adsorbed axially atop Fe coordinated by four nitrogen atoms. During dissolution, the metal atom becomes an aqueous cation with electric charge *x*, leaving behind a cavity (referred to as □-N_x in what follows). The latter can in turn bind protons, to reach the most stable configuration. The simplest case of **Equation 3** is when a = b = 0 (no axial ligand), and n = 2:

$$FeN_4C_z + 2\ H^+ \rightarrow Fe_{aq}^{2+} + H_2N_4C_z \quad (4)$$

The authors assumed that the dissolved species is Fe^{2+}, in line with the classical Pourbaix diagram for Fe. Metastable pseudo Pourbaix diagrams were constructed with DFT. The stability of the metal-free N_4 cavity was first studied as a function of the number of protons. $H_2N_4C_{138}$ was found to be the most stable structure, followed by $H_3N_4C_{138}$. Then, the regions of stability were investigated for FeN_4C_{138}, O_2-FeN_4C_{138} and OH-FeN_4C_{138}, for a fixed Fe^{2+} concentration. The calculations showed that FeN_4C_{138}, without axial ligand, is not stable at pH below *ca* 6.5, at 10^{-9} M Fe^{2+} (**Figure 1b**). The acid stability of O_2-FeN_4C_{138} and OH-$FeN_4N_4C_{138}$ bilayer structures were found to be much improved, as shown in **Figure 1c** for O_2-FeN_4C_{138} with a stability domain now extend to acidic pH and to a broader range of potential. Therefore, the calculations show that the Fe-N_4 site is strongly stabilized by OH and O_2 axial ligands. When the ligands are ORR intermediates, the results suggest that the sites are prone to dissolution only between each ORR turnover cycle, when the site is under-coordinated for a short time. In contrast, a Fe-N_4 site with permanently bound OH species (as is probably the case in O_2-free

electrolyte, with no turnover of adsorbed species) should be highly stable, even in acidic conditions.

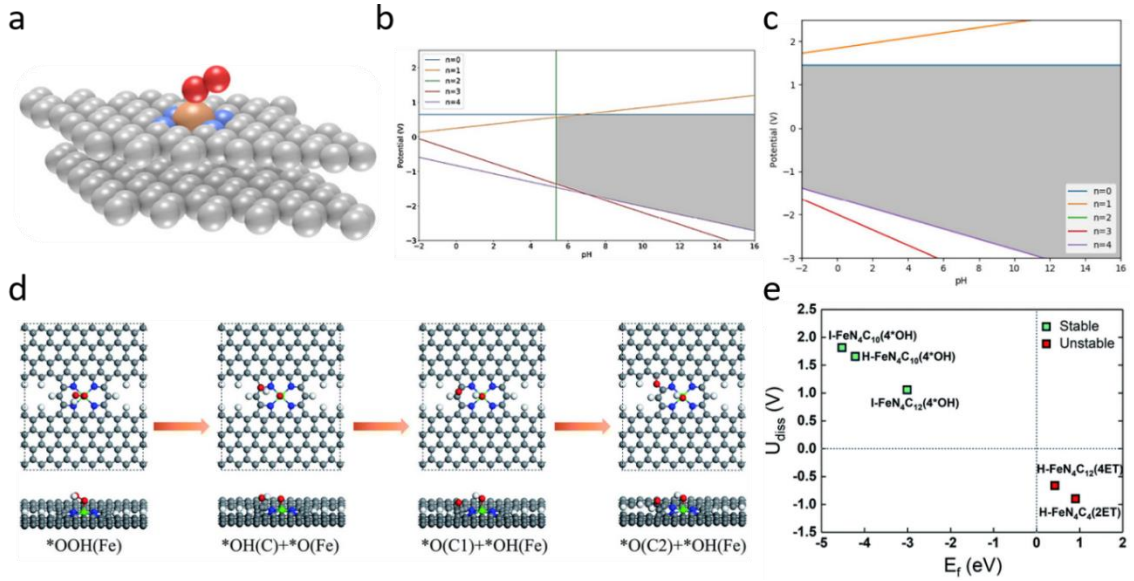

Figure 1. Modelling the effect of specific carbon corrosion triggered by ORR on Fe-N_4 sites. a) Edge view of O_2-FeN_4C_{138} relaxed bilayer structure; b) FeN_4C_{138} stability as function of pH and potential with $[Fe^{2+}] = 10^{-9}$ M with *n* the number of protons exchanged during the dissolution reaction (**Equation 3**); c) O_2-FeN_4C_{138} stability domain with $[Fe^{2+}] = 10^{-9}$ M. The shaded area indicates the stability domain *vs*. dissolution for all considered dissolution reactions, with *n* the number of protons exchanged during the dissolution reaction (**Equation 3**). DFT results on carbon reversible or irreversible oxidation triggered by ORR near Fe-N_4 sites. d) Upper and side views of H-FeN_4C_{12} structure during ORR turnover cycle leading to irreversible carbon oxidation; e) calculated energy of formation (E_F) and dissolution potential (U_{diss}) of different surfaces with one Fe-N_4 site embedded and four OH or ether functional groups (labelled ET). Figures a, b and c, reproduced with permission from Ref. [90]. Copyright [2020] American Chemical Society. Figures d and e, reproduced with permission from Ref. [91]. Copyright [2021] The Royal Society of Chemistry.

Modelling the effect of specific carbon corrosion triggered by ORR on Fe-N_4 sites was recently reported by Tan *et al*. [91] The irreversible degradation of Fe-N_4 sites caused by local carbon oxidation near the active site was investigated with DFT calculations for different sites, including FeN_4C_{12}, FeN_4C_{10}, FeN_4C_8 and FeN_4C_4. Two sites are in-plane sites with no C-H bonds in the vicinity of Fe-N_4 (labelled I-FeN_4C_{10} and I-FeN_4C_{12}) and the remainder are sites hosted in micropores and that feature C-H bonds located near Fe. These are labelled with the prefix H- (*e.g.* H-FeN_4C_4). The authors investigated with DFT the resistance to metal dissolution by calculating the energy of formation, E_F, and the dissolution potential, U_{diss}. With the definitions of E_F and U_{diss} adopted by the authors, the sites with negative E_F value are considered thermodynamically stable, and those with $U_{diss} > 0$ V *vs*. the standard hydrogen electrode (SHE) are regarded as electrochemically stable. For the un-oxidized surfaces, all sites were thermodynamically and electrochemically stable, except H-FeN_4C_8. The durability of the five other sites (during ORR cycle) was examined in the case of oxidized carbon surface. Carbon oxidation triggered by ORR on Fe-N_4 was simulated by assuming a dissociation pathway, involving adsorption of O_2 on Fe, forming $^*OOH$, then dissociating into $^*O$ and $^*OH$ on Fe and a secondary site (adjacent C-atom), respectively, and finally protonation to form two water molecules. In the course of this ORR turnover cycle, the carbon oxidation pathways were explored, including the possible formation of epoxy, ether and OH functional groups. In the next step, the H from OH on the carbon site is abstracted by Fe, forming an epoxy group (3rd step in **Figure 1d**). The latter may then displace a C atom and enter the carbon lattice,

irreversibly altering the geometry of the active site (4th step in **Figure 1d**). Depending on the chemistry of carbon atoms adjacent to the ligating nitrogen atoms, it was found that the adsorption of oxygenated species atop the carbon can be reversible or irreversible. The most stable oxidized form was with ether functional groups (H-FeN_4C_4, H-FeN_4C_{12}) or with OH groups (I-FeN_4C_{10}, H-FeN_4C_{10} and I-FeN_4C_{12}). The calculated E_F and U_{diss} values in the case of 4 oxygen functional groups present nearby Fe-N_4 is shown in **Figure 1e**. The figure reveals that H-FeN_4C_{12} is destabilized with 4 ether groups, and H-FeN_4C_4 destabilized with only 2 ether groups. The other three sites remained thermodynamically stable even in the presence of 4 OH-groups. These results are in general agreement with the intuition that in-plane Fe-N_4 sites should be more robust than edge sites.

In parallel to pure *ab initio* approaches undertaken to assess the stability of various Fe-N_4 sites embedded in defective graphene sheets, simpler kinetic models have been applied to interpret experimentally observed deactivation rates of Fe-N-C catalysts in PEMFC. Yin and Zelenay [92] applied and compared the efficiency of different kinetic models in fitting the experimental decay of ORR activity in PEMFC. The latter was measured at high cell voltage where the current density is controlled by the ORR kinetics. The two models are a) autocatalytic degradation, and b) first-order degradation. Model a) assumes two steps, the first being the formation of a deactivating intermediate catalysed by the active site (noted 'D' in **Equation 5**), and the second being the degradation of the active site by this intermediate (noted 'S' in **Equation 6**). The kinetic current density at fixed potential was assumed proportional to the site density (noted as 'ASD' in the present review but '[S]' in the equations from the authors).

$$S + R \rightarrow S + D \quad (5)$$

$$S + D \rightarrow S' + E \quad (6)$$

Where *S* and *S*' are the active and inactivated sites, *R* is the reagent involved in the formation of the deactivating species *D*, and *E* is the product(s) of the reaction between *D* and *S*. Assuming first-order and irreversible kinetics, these two reactions lead to a system of first-order ordinary differential equations to numerically solve [S] (the site density on the surface of the catalyst) and [D] as a function of time ([R] was assumed to be constant). Alternatively, additional assumptions could be made (high formation and removal rates of D compared to its consumption rate via **Equation 7**, and quasi steady-state for [D]) to obtain the following analytical solution for [S]:

$$[S] = (k \cdot t + 1/[S]_0)^{-1} \quad (7)$$

Where *t* is time, *k* is a constant (related to the kinetic constants of **Equations 5-6**) and $[S]_0$ the value of [S] at $t = 0$. Reorganizing **Equation 7**, the ratio $[S]/[S]_0$ can be expressed as:

$$[S]/[S]_0 = ([S]_0 \cdot k \cdot t + 1)^{-1} \quad (8)$$

Assuming the ORR turnover frequency of site *S* is unmodified over time, the ratio $[S]/[S]_0$ is also equal to the ratio $j_k/j_{k,0}$ where j_k is the ORR kinetic current density at a fixed cathode potential (high), leading to pure kinetic control. **Equation 8** was referred to as the logistic decay model by Yin and Zelenay. [92] Fitting this equation with experimental curves of $j_k/j_{k,0}$ involves only one fitting parameter, namely the mathematical product $[S]_0 \cdot k$ (noted as $1/t_0$, in Ref. [92]). In deriving this analytical solution, it was also implied that the experimental conditions during which the degradation of active sites occur were kept constant (*e.g*. temperature, pressure, cathode potential)

The second model investigated by Yin and Zelenay is a simple first-order degradation kinetics of active sites as a function of time (**Equation 9**).

$$S \rightarrow S' \quad (9)$$

This leads to an exponential decay of [S] with time (**Equation 10)**:

$$[S]/[S]_0 = \exp(-kt) \quad (10)$$

As discussed above, the ratio $[S]/[S]_0$ is also equal to the ratio $j_k/j_{k,0}$ (assuming unmodified TOF for *S* over time).

A third model was studied, considering two types of active sites A and B with different ORR kinetics, but each assumed to obey a simple first-order degradation kinetics, according to **Equation 11**. This leads to two independent exponential decays over time for each active site's density. The total current density is then described by the sum of two exponential decays.

$$j_k/j_{k,0} = C \cdot \exp(-k_1 \cdot t) + (1-C) \cdot \exp(-k_2 \cdot t) \quad (11)$$

This model was included following the double exponential decay model proposed just earlier by Dodelet's group, [93] and that involves three parameters, C, k_1 and k_2 (C and (1-C) describe the relative contributions of sites A and B to the initial activity).

The authors then investigated the ability of each model to fit experimental data of normalized current density $j/j_{t=0}$ versus time, measured in PEMFC with Fe-N-C cathodes. **Figure 2a** shows the best fit for each model, for a potentiostatic hold at 0.84 V. The data shows a fast-initial decay of current, followed by a slower decay later on. The logistic decay model (with one fitting parameter) resulted in a good fit, almost as good as that obtained with the numerical solution (exact form of the autocatalytic decay model). In contrast, the single exponential decay model could not properly fit the data over the entire time scale. The double exponential

decay model (with three fitting parameters) could also properly fit the data. The models were then applied with the cell being at open-circuit potential (OCV) for most of the time, with short potential holds at 0.84 V to record *j*(0.84 V) from time to time. **Figure 2b** shows that in such conditions (no ORR taking place during the degradation), similar observations can be made, with the logistic decay, autocatalytic decay and double exponential decay models resulting in good fits, while the single exponential decay does not. Moving to degradation conditions of high current density, namely potentiostatic hold at 0.40 V, **Figure 2c** shows that none of the models perfectly fitted the data in this case. This is not unexpected, since at high current density, gradients of O_2 concentration and therefore intermediate species concentration, and degradation rates, build up through the cathode AL. Such gradients and ensuing mathematical complexity are not considered in these simple models. The models were also applied to experimental data obtained on another and more durable Fe-N-C catalyst from Dodelet's group. **Figure 2d** shows that a similar observation was made as in **Figure 2a** and **Figure 2b** regarding which kinetic degradation models could reproduce the data and which could not.

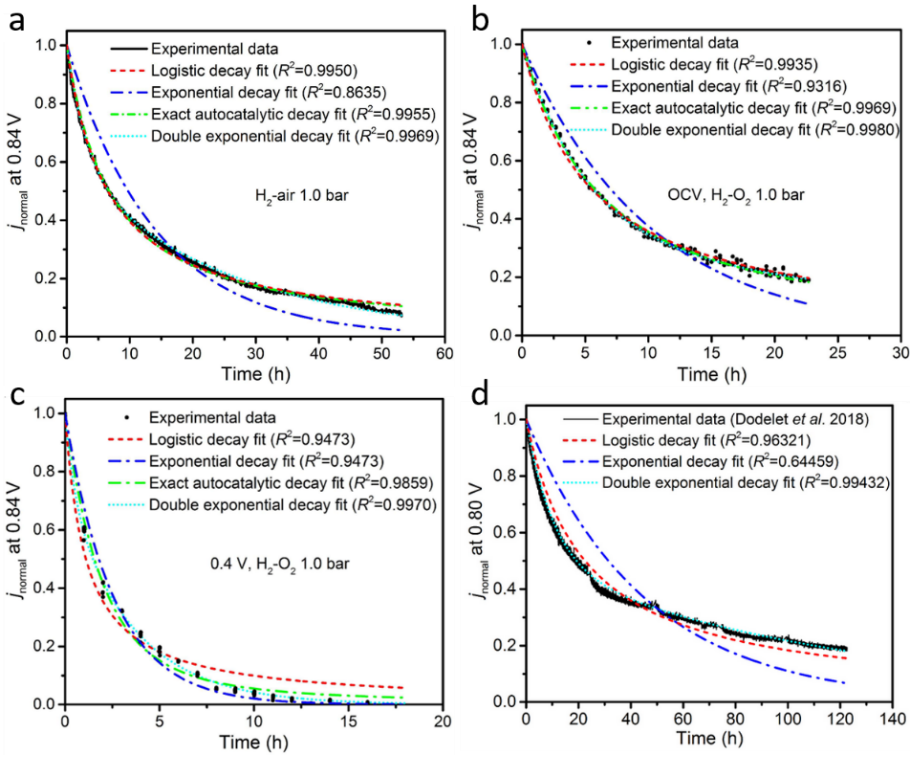

Figure 2. Normalized current density at 80°C in PEMFC recorded (at 0.84 or 0.80 V) *vs*. time and its fitting with various kinetic degradation models. a) Normalized current density of a cyanamide-polyaniline derived Fe-N-C cathode in a H_2/air PEMFC continuously held at 0.84 V; b) Normalized current density of same Fe-N-C cathode in a H_2/O_2 PEMFC continuously held at OCV, except for short acquisition of current at 0.84 V; c) Normalized current density of same Fe-N-C cathode in a H_2/O_2 PEMFC continuously held at 0.40 V, except for short acquisition of current at 0.84 V; d) Normalized current density of a Fe-N-C cathode prepared from ZIF-8 and Ar+NH_3 pyrolysis (from Dodelet's group) in a H_2/air PEMFC continuously held at 0.80 V, except for acquisition of polarization curve every 25 h. Figures a, b, c and d, reproduced with permission from Ref. [92]. Copyright [2018] The Electrochemical Society.

All these analytical models can however be the result of many different fundamental degradation mechanisms, even if the autocatalytic model suggests deactivation by an intermediate species, possibly a ROS. In contrast, the double exponential decay model suggests two decoupled degradation events, possibly related to two different active sites, or to two different mechanisms occurring at different time scales. Interestingly, durability data

acquired in PEMFC at a lower temperature of 25°C by Dodelet's group showed mainly one early decay between 0-15 h, but the quasi absence of decay afterwards, in contrast to the durability data recorded at 80°C. [93] In the latter case, the logistic decay model could not properly fit the data, but the double exponential decay model could (see Figure 5 in Ref. [94]). This suggests that the degradation mechanism leading to the decay rate observed at longer times in PEMFC at 80°C is very significantly mitigated at 25°C.

To summarize **section 2.1**, DFT works predict that axial ligands atop Fe strongly stabilize Fe-N_4 sites embedded in graphene sheets against Fe demetallation, and that a strong coordination of C atoms present in the second coordination sphere of Fe is important to avoid the irreversible displacement of C by O atoms during ORR on Fe-N_4. Different semi-empirical kinetic models of deactivation can reproduce the observed ORR activity decay of Fe-N-C materials in PEMFC operated at low current density, while for PEMFC durability test at high current density, none of the proposed models could properly reproduce the data. This is likely associated with complex gradients of local current density throughout the thick Fe-N-C cathode at high current density, and ensuing complexity that is not taken into account in the proposed kinetic models of deactivation.

In the remainder of this review, we focus on the fundamental degradation and deactivation mechanisms that lead to these phenomenological observations of poor durability.

2.2 Demetalation in the absence of carbon corrosion and oxygen reduction reaction

Demetalation from Metal-N-C in conditions where the carbon matrix is not corroded or surface-oxidized can first be generally discussed with the stability expectations predicted by the Pourbaix diagrams. This degradation mechanism corresponds to Stability/Load mode, according to **Table 1**. Fe-, Co- Cr- and Mn-N-C materials are the main reported ORR-active Metal-N-C catalysts in acid medium. [35, 95-97] Unfortunately, all crystalline structures of these metals are unstable at sufficiently low pH and at typical electrochemical potential of operating PEMFC cathode (0.5-0.9 V *vs*. RHE). **Figure 3** summarizes the huge underlying stability challenge of implementing PGM-free catalysts in acidic medium, beside the activity challenge. Only Fe shows a domain of stability in acidic medium, with Fe_2O_3 being the stable form in acidic conditions but only at high potential, typically > 0.6 V *vs.* RHE for pH ≥ 2 (**Figure 3c**). Moreover, while Fe_2O_3 has some ORR activity in alkaline medium, [98-101] it has negligible activity in acidic medium. [80, 102, 103] It will be shown later in this review that Fe_2O_3 is a main degradation species observed with EoT characterization of Fe-N-C catalysts following a durability test in acid medium. Recently, a Sn-N-C catalyst comprising Sn-N_x sites was reported to be highly active in acid medium. [104] This expands the family of ORR-active Metal-N-C materials beyond 3d transition metals, with potential advantages with respect to the mitigation of Fenton reactions. The fundamental reasons for the possible stability of Metal-N-C materials under load conditions in acid medium are:

i) Strong stabilization of 3d metal cations by nitrogen ligands in Metal-N_x pockets (single-metal-atom sites),

ii) Protection of metallic or metal-carbide particles by a thin overlayer of (nitrogen-doped) carbon.

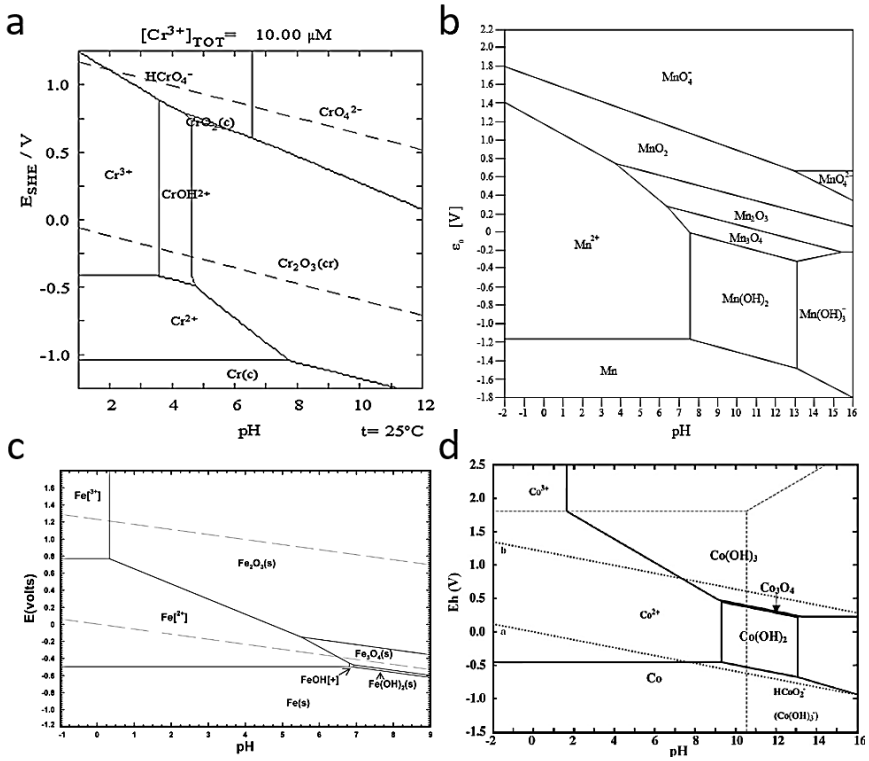

Figure 3. Pourbaix diagrams for a) Cr, b) Mn, c) Fe and d) Co. Figure c) reproduced from Ref. [105].

Based on Pourbaix diagrams for Cr, Mn, Fe and Co, the stability of Metal@carbon core@shell structures requires a defect-free carbon layer around metallic particles in the pristine materials, and the resistance of the carbon layer towards carbon corrosion in operating conditions. For the Metal-N_x sites, stability in acidic conditions in the absence of other stressing conditions (*e.g.* absence of O_2, and temperature and electrochemical potential sufficiently mild to avoid or minimize carbon corrosion) is related to the competition between metal cations and protons for occupying the □-N_x cavities (see **section 2.1**). Unpyrolyzed Metal-N_4 macrocycles supported on carbon can be a useful proxy for understanding the behaviour of Metal-N_x sites from Metal-N-C materials in acidic medium. [106, 107] In general, for a particular metal and oxidation state, metal-phthalocyanines (Metal-Pc) are more difficult to demetalate than metal-porphyrins, related to the fact that the central cavity is somewhat smaller in phthalocyanines. [108] Among Metal-Pc compounds, Fe is recognized to lead to the highest ORR activity, [97] and Fe-Pc have therefore been studied by many groups for ORR in different pH conditions. [97, 107, 109, 110] The simplest Fe(II)Pc macrocycle has been shown to be relatively stable in acidic medium when cycled between 0.1 and 0.9 V *vs.* RHE in O_2-free acidic medium. [106, 111, 112] However, when cycled in the presence of O_2, the same Fe(II)Pc macrocycles become highly unstable, [106] as will be discussed in detail in **section 2.6**. The demonstrated stability of well-defined Metal-N_4 macrocycles in acid medium (in the absence of O_2, in this subsection) in the potential region where ORR is targeted was the rational background for the development of Metal-N-C catalysts with Metal-N_x sites. These observations lead to the idea of integrating similar active sites in a conductive carbon matrix, by applying heat treatments. [97, 113, 114] This approach however introduces strong heterogeneities of active sites and metal speciation, which has for a long time slowed down the progress and fundamental understanding of pyrolyzed Metal-N-C materials. In recent years, optimized selection of precursors and pyrolysis conditions have however led to the preparation of Metal-N-C catalysts that are free or quasi-free of metal aggregates and only or mostly comprise Metal-

N_x sites. [18, 28-30, 54, 95, 103, 104] On the other hand, high metal contents can be used to prepare a second type of pyrolyzed Metal-N-C catalysts that contain only metallic species, surrounded or not by a protective carbon layer (Metal@C or Metal@N-C sites). [21, 115, 116] We discuss below the demetalation in Stability/Load mode (absence of O_2) of Metal-N-C materials containing only or mostly Metal-N_x sites, and then of those containing mostly or only Metal@(N)C sites, differentiating studies in liquid acidic electrolyte from studies in PEMFC.

2.2.1 Studies in liquid acidic electrolyte

Choi *et al.* [117] reported in 2015 the first online study of Fe demetalation from a Fe-N-C catalyst comprising 91 % of Fe as Fe-N_x sites and the remainder as metallic Fe (labelled FeNC-dry-1). No loss of ORR activity was observed after potential cycling degradation test [0.1 – 0.4 V *vs.* RHE – 500 mV s^{-1} – 5 k – Ar – 20°C] in 0.1 M $HClO_4$, but online inductively coupled plasma mass spectrometry (ICP-MS) results showed signal for Fe leaching in the electrolyte at potentials < 0.77 V *vs.* RHE. The results were interpreted as the leaching of ORR-inactive (or poorly active) Fe species in such conditions, assigned to the minor fraction of Fe present as metallic Fe particles. It was inferred that the Fe particles are not perfectly protected by a carbon layer in that particular sample, leading to a passivating Fe-oxide layer at open circuit potential (OCP). As seen in the Pourbaix diagram (**Figure 3c**), such a passivating layer is stable down to *ca*. 0.75 V *vs*. RHE at pH 1. When further decreasing the potential however, the oxide layer is reduced, leading to Fe^{2+} leaching in the electrolyte, detected online by ICP-MS. These conclusions were supported by a follow-up paper, investigating FeNC-dry-1 and two other Fe-N-C catalysts comprising either only Fe-N_x sites (FeNC-dry-0.5) or mostly metallic Fe particles (FeNC-wet-1), as shown by ^{57}Fe Mössbauer spectroscopy (**Figure 4a-c**). [118] It was shown that the demetalation rate linearly scales with the absolute amount of Fe present as Fe particles (**Figure 4d-e**). Such demetalation did however not lead to significant ORR activity loss, since these materials contain a significant fraction of Fe as Fe-N_x sites, with much higher activity per Fe atom than Fe@N-C particles.

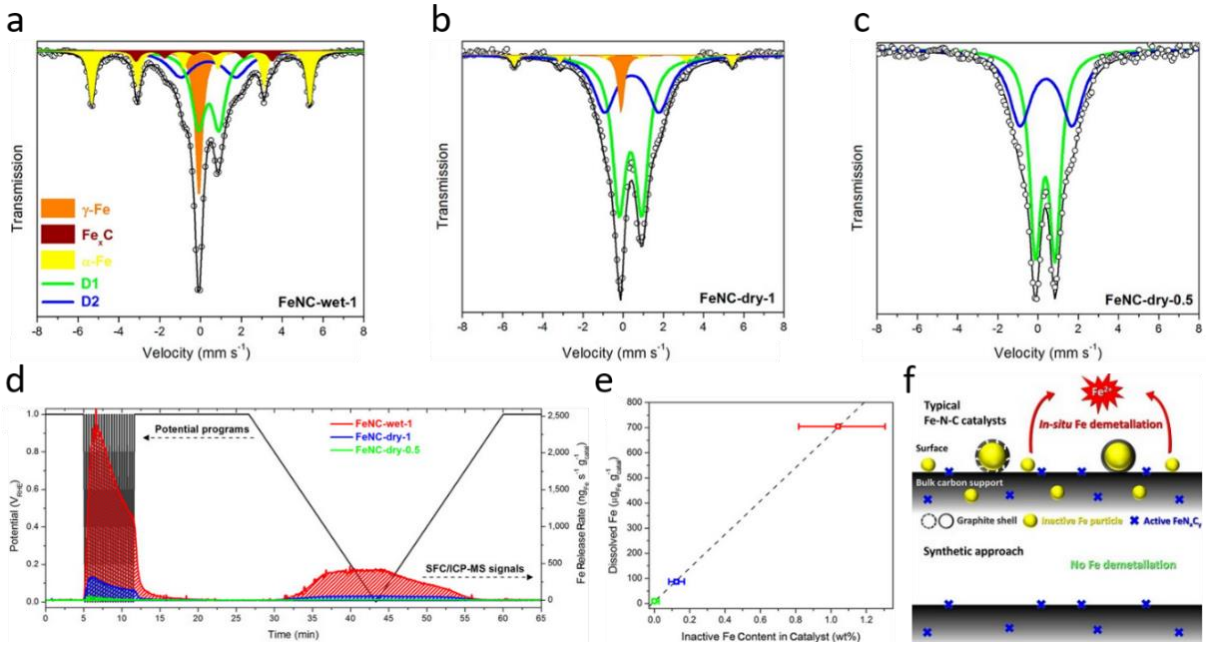

Figure 4. ^{57}Fe Mössbauer spectra at room temperature of a) FeNC-wet-1, b) FeNC-dry-1, c) FeNC-dry-0.5, d) online Fe dissolution rate during 20 fast cycles and 1 subsequent slow cycle in Ar-saturated 0.1 M $HClO_4$ electrolyte, e) Positive correlation between the cumulative amounts of Fe dissolved during the 20 fast cycles and the total content of crystalline Fe structures in the catalysts, f) scheme of leaching trends for Fe from different

Fe sites in load-cycling conditions in de-aerated acid electrolyte. Figures a, b, c, d, e and f reproduced with permission from Ref. [118]. Copyright [2016] American Chemical Society.

Overall, the results demonstrated good acid stability of Fe-N_x sites, in the potential range 0.0 – 1.0 V *vs.* RHE, in de-aerated acid electrolyte, while Metal@(N)C particles unexpectedly leached Fe cations, due to imperfect carbon shells (**Figure 4f**). Together with the DFT results from **section 2.1**, the acid stability of most Fe-N_x sites suggests that OH or H_2O axial ligand is still present at low potential, stabilizing the sites.

The investigation of the stability of Metal-N-C catalysts in such conditions was then extended to a series of three Fe-N-C and three Co-N-C catalysts, at higher electrolyte temperature (80°C) and prolonged cycling by Kumar *et al.* [21] Two Fe-N-C catalysts and two Co-N-C catalysts were prepared that comprise only Metal-N_x sites (prepared by flash (FP) or ramp pyrolysis (RP), $Fe_{0.5}$FP, $Fe_{0.5}$RP, $Co_{0.5}$FP, $Co_{0.5}$RP), one Fe-N-C catalyst comprising only Fe_3C particles ($Fe_{5.0}$RP) and one Co-N-C catalyst ($Co_{5.0}$RP) comprising only metallic Co particles. While the most active materials are those based on Metal-N_x sites (with Fe > Co), the initial ORR activity of $Fe_{5.0}$RP and $Co_{5.0}$RP is however interesting in acid medium (**Figure 5a**), and can be assigned to Fe@N-C and Co@N-C particles. Such sites seem to have a lower TOF than Metal-N_x sites. However, a higher metal loading on N-C is achievable and, in optimized materials, this effect might compensate for their lower TOF. For these six materials, a linear relation was found between the absolute loss of metal content during the AST, locally monitored by energy-dispersive X-ray spectroscopy (EDXS), and the ORR activity loss after AST [0.6 – 1.0 V *vs.* RHE – 3s/3s – 10k – Ar – 80°C] in 0.1 M H_2SO_4 (**Figure 5b**). [21] This result suggests that the ORR decay in load-cycling conditions and inert atmosphere is related to the demetalation of the active sites (Metal-N_x sites or metallic particles), but that the nature of the active sites remained the same after the AST. Fe-N_x and Co-N_x sites featured excellent stability during load-cycling in de-aerated 0.1 M H_2SO_4, retaining between 60 and 100 % of their initial ORR activity after 10,000 cycles between 0.6 and 1.0 V (**Figure 5b**, four labels "$Metal_{0.5}$"). In contrast, 80-90 % of the initial ORR activity was lost after the same AST on $Fe_{5.0}$RP and $Co_{5.0}$RP (**Figure 5b,** two labels $Metal_{5.0}$). Unfortunately, while one could have expected similar or even higher stability in such AST conditions for Metal@N-C particles *vs.* Metal-N_x sites, the opposite was observed for this particular series of catalysts. This is assigned to imperfect (porous) graphene shells around the metallic particles, offering access for the acidic electrolyte. Other syntheses approaches resulting in a uniform encapsulation by carbon may result in Metal@N-C sites with improved stability during load-cycling. [119]

Among the four Metal-N-C materials with Metal-N_x sites, $Fe_{0.5}$RP was more stable than $Fe_{0.5}$FP while $Co_{0.5}$FP was slightly more stable than $Co_{0.5}$RP after 10k potential cycles. $Fe_{0.5}$RP was then subjected to extended cycling, [0.6 – 1.0 V *vs.* RHE – 3s/3s – 30k – Ar – 80°C] in 0.1 M H_2SO_4. The decrease in ORR activity at 0.8 V *vs*. RHE after that AST was only 25%, reaching the US DoE target of less than 40 % loss of activity after such an AST for PGM-free catalysts. [21] As we shall see later, this protocol performed in the absence of O_2 does not correctly predict the activity loss observed on PGM-free catalysts in O_2-saturated acidic electrolyte when catalysing the ORR. The load-cycling AST in O_2-free environment had initially been defined for Pt-based catalysts, for which the main degradation mechanisms are carbon corrosion, Pt dissolution and agglomeration, independent of the nature of the atmosphere. [8, 120]

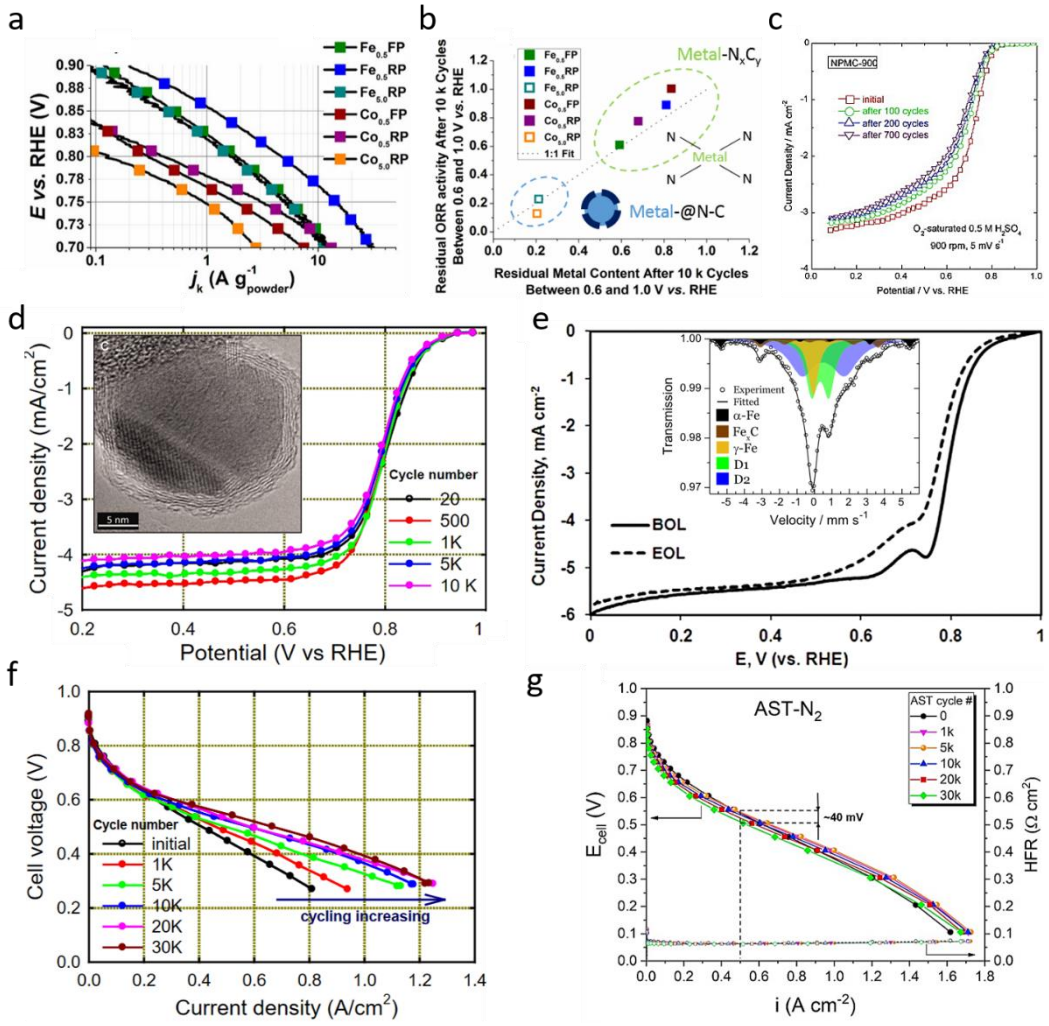

Figure 5. ORR activity before and after load cycling in de-aerated acidic solution of Fe-N-C and Co-N-C catalysts comprising either Metal-N_x sites or Metal@N-C particles. a) initial ORR Tafel plots at 25°C, b) Linear correlation between the normalized ORR activity at 0.8 V *vs*. RHE ($j_{final}/j_{initial}$) and the normalized metal content (final metal content/initial metal content) of Metal-N-C catalysts after AST [0.6 – 1.0 V *vs*. RHE – 3s/3s – 10k – Ar – 80°C] in 0.1 M H_2SO_4. [21] RDE polarisation curves for c) a Fe-Co-N-C catalyst before and after AST at RT in N_2 saturated 0.5 M H_2SO_4 between 0.8 and 1.2 V *vs*. RHE. [121] d) PANI-FeCo-C(1) before and after [0.6 – 1.0 V *vs*. RHE – 50 mV s^{-1} – 10k – N_2 – RT] in 0.5 M H_2SO_4 (inset: representative HR-TEM image). [64] e) Fe-N-C catalyst before and after [0.6 – 1.0 V *vs*. RHE – 3s/3s – 10k – N_2 – 60°C] in 0.5 M H_2SO_4. [122] f) H_2/O_2 PEMFC polarisation curves with PANI-FeCo-C(1) cathode before and after [0.6 – 1.0 V *vs*. RHE – 50 mV s^{-1} – 10k – H_2 anode/N_2 cathode – 80°C]. [64] g) 0.6 – 0.95 V stepped potential AST with cathode under N_2 atmosphere (denoted AST-N_2). A single H_2/air polarisation curve is acquired after 1 k, 2 k, 5 k, 10k, 20k and 30k cycles in N_2. [71] Figures a and b, reproduced with permission from Ref. [21]. Copyright [2018] American Chemical Society. Figure c, reproduced with permission from Ref. [121]. Copyright [2010] Elsevier. Figures d and f, reproduced with permission from Ref. [64]. Copyright [2011] Science. Figure e, reproduced with permission from Ref. [122]. Copyright [2015] Elsevier. Figure g, reproduced with permission from Ref. [71]. Copyright [2020] Elsevier.

These recent results shed light on the different active site's reactivity in acid and their stability in de-aerated load-cycling conditions. While a number of studies previously reported RDE AST of Metal-N-C materials, the metal speciation and quantification were not sufficient to interpret the observed (in)stability and to relate it to the type of active sites in presence. Popov's group reported the stability for a Fe-Co-N-C material that had been acid leached after pyrolysis, but no structural characterisation was provided. The activity at 0.7 V *vs*. RHE was divided by at least a factor of two after AST [0.8 – 1.2 V *vs.* RHE – 10 mV s^{-1} – 0.7 k – N_2 – RT]

in 0.5 M H_2SO_4 (**Figure 5c**). [121] The chosen upper limit of 1.2 V however might have triggered carbon corrosion, even at room temperature. Zelenay's group reported high stability after AST [0.6 – 1.0 V *vs.* RHE – 50 mV s^{-1} – 10k – N_2 – RT] in 0.5 M H_2SO_4 for the PANI-FeCo-C(1) catalyst (**Figure 5d**). [64] High-resolution transmission electron microscopy (HR-TEM) showed the presence of metallic particles covered by a thin graphite shell (**Figure 5d inset**), but the simultaneous presence of Metal-N_x sites and their contribution to ORR activity cannot be excluded due to the localized information provided by HR-TEM. Assuming the ORR activity of polyaniline (PANI)-FeCo-C(1) mainly originated from Metal@N-C particles, the uniform and defect-free coverage by carbon might have been the rationale for its high stability. Serov *et al.* [122] reported on a Fe-N-C catalyst prepared by hard templating with silica and comprising 90 % of Fe as Fe-N_x sites and 10 % as metallic Fe and Fe_3C (**Figure 5e**). The authors reported only *ca* 25 mV loss at -1 mA cm^{-2} after a stepped AST [0.6 – 1.0 V *vs.* RHE – 3s/3s – 10k – N_2 – 60°C] in 0.5 M H_2SO_4. Based on the previously discussed studies, this can be rationalized as the stability of Fe-N_x sites, mainly accounting for the ORR activity of this material.

Before shifting to PEMFC environment in the next subsection, we discuss the demetalation and deactivation of ammonia-treated Fe-N-C materials following an acid wash (no ORR). While an ammonia-treatment of Fe-N-C catalysts increases strongly their initial ORR activity, especially in PEMFC conditions, [123] this goes hand-in-hand with a faster deactivation compared to Fe-N-C materials that are initially less active. [124] Herranz *et al.* [124] showed that an NH_3-treated Fe-N-C has a highly basic character, assigned to highly basic N-groups formed during the pyrolysis in ammonia (NH_3). It was also shown that after acid-wash (AW), the catalyst showed a high drop in ORR-activity (*ca* 80-90 %, **Figure 6a**), but that this drop was partially reversible by removing (*via* a mild annealing treatment) bisulphate anions that adsorbed during the AW (**Figure 6a**). The reversible activity decay and recovery upon repeated AW was assigned to the adsorption/desorption of the electrolyte's anions on protonated nitrogen groups, while the irreversible decay (*ca* 50 % loss of ORR activity, **Figure 6a-b**) was correlated with a loss of *ca* 50-75 % of the Fe bulk content in the acid-washed catalysts (**Figure 6c**). The irreversible decay was therefore assigned to the demetalation of a fraction of Fe-N_x sites that are unstable in acid medium, possibly due to the involvement of highly basic N-groups in such Fe-N_x sites. Further experimental proof to the ORR activation but destabilization in acid medium of Fe-N_x sites by NH_3 pyrolysis will be discussed in **section 2.6**.

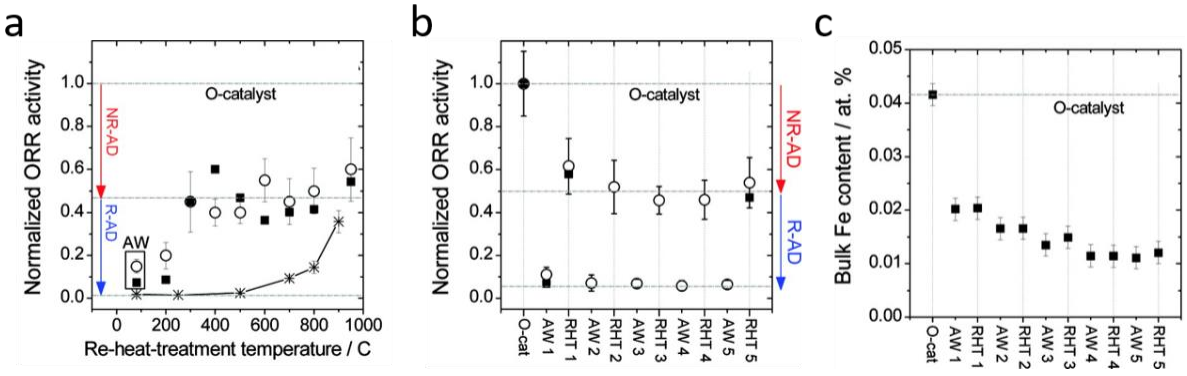

Figure 6. Reversible and irreversible ORR activity decay for an NH_3-pyrolyzed Fe-N-C catalyst following acid-wash (AW) and re-heat-treatment (RHT). a) Activity normalized to that of the original catalyst (O-catalyst) for the acid-washed catalyst (AW catalyst) and AW followed by RHT in argon at different temperatures. The activity was measured in RDE (open circles) and PEMFC (filled squares). The stars show the activity of a N-C powder to which Fe salt was added before the RHT, to assess the annealing temperature at which novel Fe-N_x sites may be formed during the annealing. b) Normalized ORR activity for five successive acid-washing/reheat-treatment cycles. Each

acid-washing lasted 24 h in a pH 1 H_2SO_4 solution. Each AW catalyst was re-heat treated for 1 h at 950°C in argon. c) Bulk Fe content at each step of the five-acid washing/re-heat-treatment cycles. (N)R-AD stands for (non)-recoverable activity decay. Figures a, b and c, reproduced with permission from Ref. [124] Copyright [2011] American Chemical Society.

2.2.2 Studies in PEMFC

While potentiostatic hold or load-cycling AST with N_2-fed cathode are not typically used in PEMFC environment to study stability, one such experiment was reported by Wu *et al.* [64] for the PANI-FeCo-C(1) catalyst whose RDE results are shown in **Figure 5d**. **Figure 5f** shows the H_2/O_2 PEMFC polarization curves before and after cycling the cell between 0.6 and 1.0 V with N_2 feed at the cathode during cycling. No loss in ORR activity at *e.g.* 0.8 V can be seen after such an AST while, at high current density, an improvement in the performance was observed. This was rationalized by improved mass-transport properties of the cathode, likely due to the dissolution of non-reactive phase of the catalyst, and improved accessibility of the remaining active sites.

Recently, Osmieri *et al.* [71] reported on the performance loss in PEMFC of a Fe-N-C cathode comprising Fe-N_x sites, after an AST involving potential steps between 0.60 and 0.95 V, comparing the results obtained when feeding the cathode either with N_2 or air during the AST. In this subsection, we shall discuss only the results observed with N_2, while the comparison between N_2 and air feed will be discussed in **section 2.6**. The initial H_2/air polarisation curve and the ones recorded after 1 k and up to 30k cycles in N_2, *i.e*. AST [0.60 – 0.95 V – 30k – 3s/3s – N_2 – 80°C], are shown in **Figure 5g**. Little performance or kinetic loss is observed even after 30k load cycles in N_2, with only 40 mV decrease in cell voltage at 0.5 A·cm^{-2}. The high-frequency resistance (HFR) did not change during the AST (**Figure 5g**, right hand-side axis), indicating that the proton conductivity through the membrane and/or through the cathode AL did not decrease significantly. No statistically meaningful change was observed in the high-angle annular dark field scanning transmission electron microscopy (HAADF-STEM) image of the Fe-N-C cathode before and after the load cycle AST in N_2. Overall, the results are in line with the reported high stability of Fe-N-C with Fe-N_x sites when subjected to load cycles in deaerated acidic solution. [21, 64, 122]

As a final note of this subsection, it is highlighted that while the demetalation from active sites may be measured either online or at EoT for RDE and flow cell setups based on liquid acid electrolyte, the demetalation from metal-based active sites in a PEMFC cathode may not be easily detected by either online or EoT electrode characterisation, due to the possibility of metal cations to i) exchange with protons in the Nafion ionomer and membrane, [125-126] or ii) to reprecipitate as metal oxides. [103] Both events would impede detecting a demetalation, resulting in unchanged metal content in the cathode or MEA. In this case, the average change of metal speciation in the cathode should be investigated with spectroscopic or imaging methods, in order to detect if novel metal phases appeared after the AST and if others decreased in content, intensity or frequency of occurrence.

As a summary of **section 2.2**, Fe-N_x and Co-N_x sites were found relatively stable to load cycling conditions in O_2-free conditions and in a broad range of potentials (0-1 V *vs*. RHE), both in RDE and PEMFC setups. For Metal-N-C materials comprising a minor or major amount of core@shell Metal@N-C particles, the observed demetallation often stems from metallic cores, not from single metal atom sites. Metal-N-C catalysts whose initial activity is steered by Metal@N-C particles were found poorly stable to load cycling conditions, with significant activity decay, even in the absence of ORR. The goal of less than 40 % loss in activity after 30k

cycles of load cycling at 80°C in O_2-free acid medium has been achieved for several Metal-N-C catalysts comprising Metal-N_x active sites. While this is a necessary criterion for achieving durability during PEMFC operation, it however does not mean that it is sufficient, as discussed in the next sub-sections.

2.3 Bulk carbon oxidation reaction

Carbon is the major element in Metal-N-C catalysts, representing typically 90-95 at. % of the material's composition. The carbon matrix covalently hosts the Metal-N_x sites and supports and surrounds the Metal@(N)C particles, serving as the long-range electronic conductor for both types of active sites. [127] Hence, surface or bulk carbon oxidation reaction (COR) during operation of Metal-N-C catalysts can affect the active sites' TOF, selectivity, stability/durability, but also the electronic conductivity of the entire AL as well as its mechanical integrity, in the case of extended bulk COR. For reasons that will become more obvious in **section 2.6**, we make a clear distinction between surface-restricted COR (**Equation 12**, **Equation 13** and **Equation 14** restricted to a mono-layer, with oxygen functional groups formed on the top surface) and bulk COR, leading to the irreversible formation of gaseous CO_2 and CO (**Equation 15 and Equation 16**). [67]

$$C_{(s)} + H_2O_{(l)} \rightarrow C - OH_{(s)} + H^+ + e^- \quad (12)$$

$$C - OH_{(s)} \rightarrow C = O_{(s)} + H^+ + e^- \quad (13)$$

$$C = O_{(s)} \rightarrow C - OOH_{(s)} + H^+ + e^- \quad (14)$$

$$C_{(s)} + 2H_2O_{(l)} \rightarrow CO_{2(g)} + 4H^+ + 4e^- \qquad E° = 0.207 \text{ V } vs. \text{ SHE} \quad (15)$$

$$C_{(s)} + H_2O_{(l)} \rightarrow CO_{(g)} + 2H^+ + 2e^- \qquad E° = 0.512 \text{ V } vs. \text{ SHE} \quad (16)$$

This subsection focuses on the occurrence and effects of bulk COR in Metal-N-C cathodes, while surface oxidation is discussed later in the frame of the effect of H_2O_2 on Metal-N-C (**section 2.4**). From thermodynamics, the onset of COR to CO_2 and CO is 0.207 and 0.512 V *vs.* the SHE, respectively. However, the COR rate is kinetically limited, being in practice negligible at room temperature below 1.0 – 1.1 V *vs*. RHE, [128, 129] but increasing with temperature [117, 130, 131] and relative humidity. [132-134] High COR rate at the cathode has been identified as a main degradation mechanism during uncontrolled SU/SD of PEMFC with Pt/C cathodes. [135, 136] During these events, a transient H_2/air front is created in the anode (air fed to the H_2-filled anode channels for stop, and *vice versa* for a start), leading to local reduction current at the anode and triggering the need for a local oxidation current at the cathode, which can only be either water oxidation reaction or COR. Local increase of the cathode potential up to 1.6 V *vs*. RHE has been reported. [135] Note that such mechanism is operative only if the anodic catalysts is able to reduce O_2 (which is the hallmark of Pt-based catalysts). This implies that this problem could be eliminated using a fully HOR-selective catalyst at the anode.

This subsection is therefore mainly related to the stability SU/SD degradation mode in **Table 1**, and discusses the effect of COR on the structure, activity and PEMFC performance of Metal-N-C catalysts with respect to i) the metal speciation, ii) structural and physicochemical properties of the AL.

2.3.1 Studies in liquid acidic electrolyte

The effect of high potentials on a Fe-N-C catalyst comprising mainly Fe-N_x sites was studied by multiple techniques by Choi *et al*. [117] The AST consisted in cycling the potential between 1.2 and 1.5 V *vs*. RHE in Ar-saturated 0.1 M $HClO_4$. The electrolyte temperature during the AST was 20, 50 or 70°C. It was first shown that the temperature during the AST plays a critical role on the extent of deactivation. When conducted at 20°C, the AST resulted in restricted ORR activity loss even after 5k cycles (**Figure 7a**). After the same AST at 50 and 70°C, the Fe-N-C material showed a dramatic loss of ORR activity after 5k cycles (**Figure 7b-c**). The increasing extent of deactivation with temperature was assigned to strongly increased COR rate with temperature, as supported by the increasing oxidation current with temperature, seen at high potential in the cyclic voltammograms (CVs, **Figure 7d**). The onset potential (E_{onset}) for the oxidation current is *ca*. 1.0 V *vs*. RHE, in line with previous studies on carbon black supports for Pt/C. [120, 129, 137] Direct proof for COR was given by a flow cell coupled online to differential electrochemical mass spectroscopy (DEMS). **Figure 7e** shows the detection of CO_2 and then of CO when the potential becomes higher than *ca*. 0.9 and 1.2 V *v*s. RHE, respectively, at 50°C. The effect of COR on a same catalyst's particle was investigated with identical location – STEM (IL-STEM) and identical-location energy-dispersive X-ray spectroscopy (IL-EDXS). Thin carbon protrusions located at edges of the pristine catalyst's particle disappeared after the potential cycling (elliptic circles in **Figure 7f**) while the particle dimensions were reduced by 5–15 %. Such a reduction could significantly reduce the electric connection between particles in a Fe-N-C layer, leading to decreased through-plane electric conductivity of the AL and, eventually, collapse of the electrode structure. By comparing results obtained with online DEMS (CO_2 detection) and online ICP-MS (for online detection of Fe leached), a proportional correlation between the Fe leaching rate and the CO_2 production rate was obtained. This correlation supported the hypothesis that COR indirectly triggers the destruction of Fe-N_x sites, by removing the carbon atoms surrounding the Fe-N_x sites.

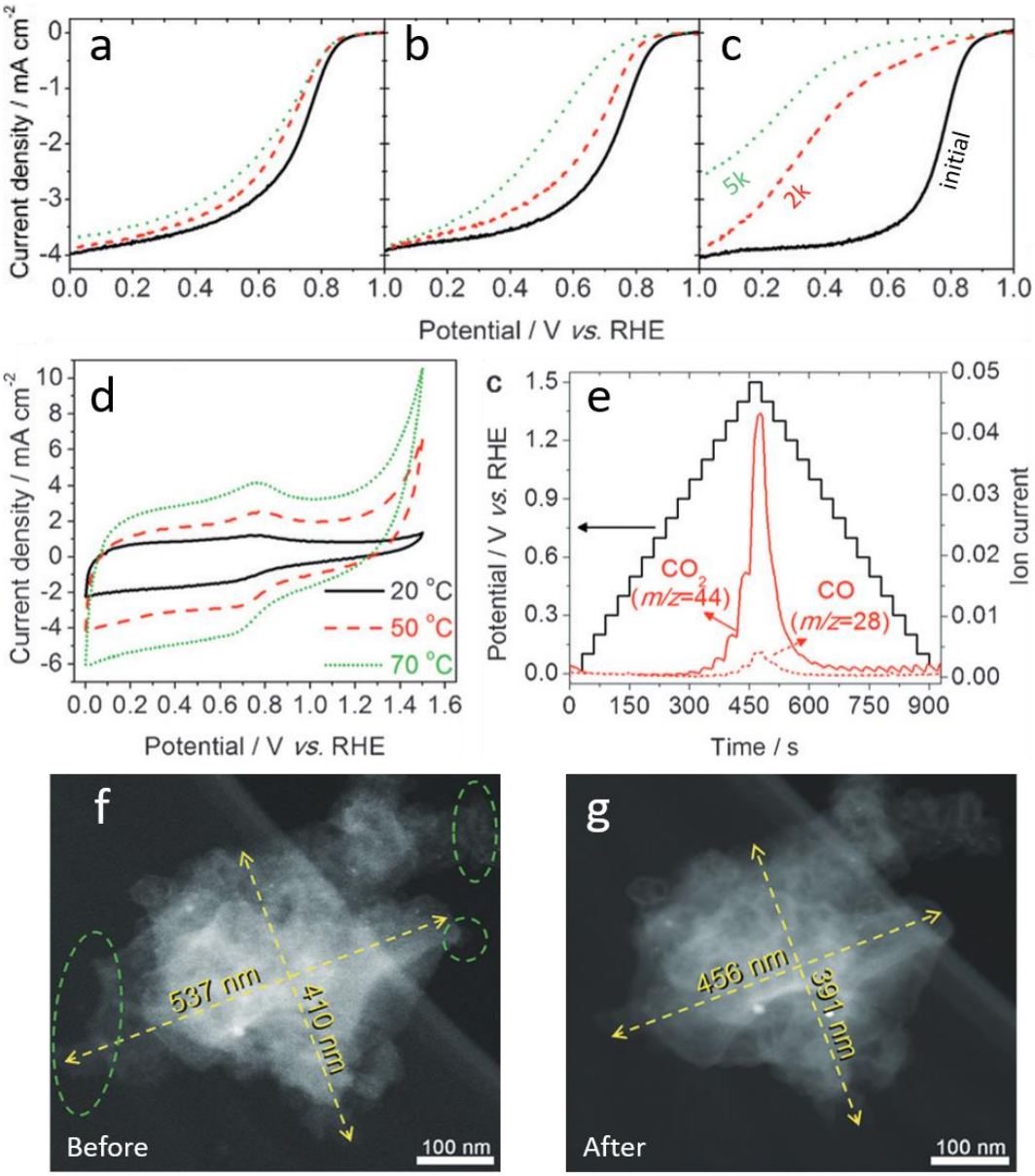

Figure 7. Combined effects of high potential and temperature on the ORR activity and COR rate. a) ORR curves before (solid black curve) and after 2 k (dashed red curve) or 5 k (dotted green curve) cycles [1.2 – 1.5 V *vs.* RHE – 500 mV s^{-1} – 5k – Ar – 20°C] in 0.1 M $HClO_4$. The ORR activity was measured in O_2-saturated 0.1 M $HClO_4$. b) Same but the AST was performed at 50°C; c) same but the AST was performed at 70°C. [117] d) Cyclic voltammograms in N_2-saturated 0.1 M $HClO_4$ of the fresh Fe-N-C electrode, as a function of electrolyte temperature. e) Online flow cell/DEMS results acquired at 50°C in de-aerated 0.1 M $HClO_4$. f) – g) morphology of a same Fe-N-C particle acquired with identical-location TEM before and after the AST [1.2 – 1.5 V *vs.* RHE – 500 mV s^{-1} – 5k – Ar – 50 °C]. Figures a, b, c, d, e, f and g, reproduced with permission from Ref. [117]. Copyright [2015] Wiley.

A study from Kramm's group investigated the effect of the nature of the transition metal in Metal-N-C materials on their resistance to stability tests in SU/SD mode. [138] In the current approaches of pyrolytic synthesis of Metal-N-C, the carbonaceous phase is often formed simultaneously with the metal-based active sites. Hence, the nature of the metal may influence the final morphology and graphitic character of the carbonaceous matrix, especially when Metal-N_x sites along with metal clusters form during pyrolysis. Metallic Fe, Co and Ni particles are known to catalyse graphitization and/or growth of carbon nanotubes (CNTs) at high temperature. Eight monometallic (including 7 non-PGM and also Ru) and 4 bimetallic

Metal-N-C catalysts were prepared from metal acetate, ZIF-8 and phenanthroline. The SU/SD protocol was [1.0 – 1.5 V *vs*. RHE – 500 mV s^{-1} – 5k – O_2 – RT] in 0.1 M H_2SO_4. Despite the presence of O_2, no ORR can occur during this AST due to the high potential. All Metal-N-C suffered from significant ORR activity loss after this SU/SD protocol, with examples shown in **Figure 8a-b**. Interestingly, these results agree with those of Linse *et al.* [139] who performed SU/SD tests with MEAs based on various Pt/C loadings and various Pt wt. % on carbon, and reported that COR in SU/SD was the main degradation mechanism. In the search for a structural descriptor for describing the activity loss during the SU/SD protocol, *ex situ* characterization of the pristine catalysts by X-ray photoelectron spectroscopy (XPS), X-ray diffraction (XRD) and Raman spectroscopy revealed a positive correlation between the content of [pyridinic nitrogen + N from Metal-N_4 sites] and the ratio D_3-band/*G*-band from Raman spectroscopy (**Figure 8c**). This was rationalized in that the D_3-band signal (located at *ca*. 1500 cm^{-1} and assigned to defective carbon, molecular fragments or functional groups) in Raman spectra may intimately be related to in-plane defects in graphene, created by in-plane Metal-N_4 sites in particular. The variation of the D_3-band/*G*-band between Raman spectra acquired before and after the SU/SD-AST was then compared with the variation in the kinetic ORR current density before and after the SU/SD-AST. A general positive correlation was found, if the materials were separated in two groups, namely the monometallic and bimetallic ones (**Figure 8d**).

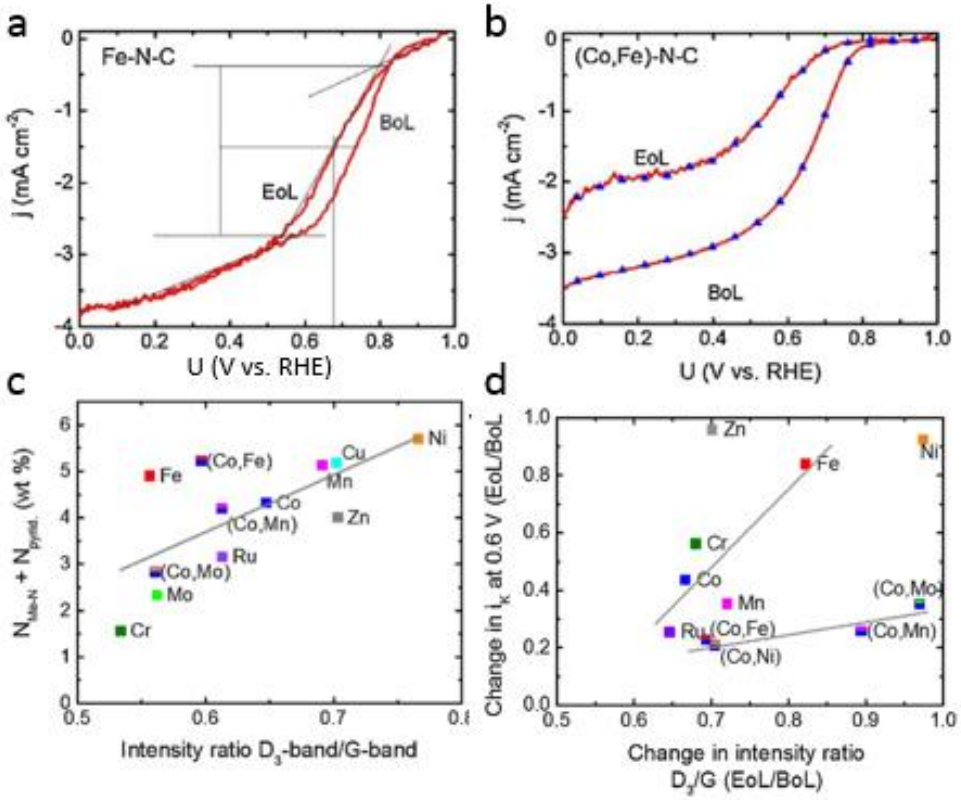

Figure 8. Effect of the nature of the metal in Metal-N-C and Co-M_2-N-C materials on their degradation during a stability SU-SD protocol. ORR polarisation curves before and after SU/SD cycles from a) Fe-N-C and b) Co, Fe-N-C. c) Positive correlation between the sum of $N_{pyridinic}$ and $N_{Metal\text{-}N4}$ from X-ray photoelectron spectroscopy and the ratio of D_3/G bands from Raman spectroscopy. d) Positive correlations between the ratio i_k (after SU/SD)/i_k (before SU/SD) and the ratio (D_3/G (after SU/SD)) / (D_3/G (before SU/SD)). Note: in d), the *y*-axis definition implies a positive correlation between y-axis value and material stability. Figures a, b, c and d, reproduced with permission from Ref. [138]. Copyright [2015] Elsevier.

Overall, the results identified Fe-N-C as the least unstable to the SU/SD protocol (smallest loss in ORR activity, **Figure 8d**), while the four bimetallic Co-M_2-N-C materials behaved as the Co-N-C and were clearly more unstable when subjected to the same protocol (**Figure 8d**). The authors concluded that COR leads to oxidation on the edges of graphitic crystallites and also to the direct or indirect disintegration of Metal-N_4 sites (correlated with a decrease in the D_3 band intensity).

The stability in SU/SD cycling conditions was also investigated for the family of six Metal-N-C materials whose stability in load-cycling de-aerated conditions is reported in **section 2.2.1** (**Figure 5a-b**). Despite higher average graphitization for the Metal-N-C materials with higher metal content, as reflected by their d_{002} interlayer spacing being closer to that of graphite (**Figure 9a**), those materials suffered from similar or even stronger ORR activity loss after 10k cycles of SU/SD cycles compared to the four other Metal-N-C with more amorphous carbon matrix (**Figure 9c**). These findings are similar to the work of Castanheira *et al.* [120] who reported no or mild effect of the degree of graphitization of the carbon support in Pt/C on the extent of deactivation in SU/SD conditions. Raman spectra before and after the SU/SD protocol revealed a relative decrease of the D_3 band intensity (at 1495 cm^{-1}) compared to the *G* and *D* bands for all six materials, in line with the report from Kramm's group. [138] This supports that the disordered carbon domains of the catalysts were preferentially corroded during the SU/SD-AST. However, the decrease in the D_3 band was more marked for the $Fe_{5.0}$RP and $Co_{5.0}$RP catalysts compared to the $Fe_{0.5}$RP and $Co_{0.5}$RP ones, as shown for the two cobalt catalysts in **Figure 9b** and **Figure 9d** (black and red curves). In contrast to the case after a load-cycling protocol in de-aerated acidic solution for the same set of materials (**Figure 5b**), there was no correlation between the remaining activity after the SU/SD-AST and the remaining amount of metal in the catalysts (**Figure 9c**). The somewhat counterintuitive result of higher ORR activity loss after SU/SD-AST for graphitic Metal-N-C materials *vs.* amorphous ones may be assigned to the different nature of the ORR active sites, Metal@N-C particles in the graphitic materials and Metal-N_x sites in the amorphous materials. For the former, the COR probably removes or induces enhanced porosity in the N-C graphitic shell surrounding the metallic particles, and massive metal leaching then ensues due to the thermodynamic instability of such phases in acidic medium. For Metal-N_x sites in contrast, the sites that survived the SU/SD-AST can still be stable in acidic medium. Moreover, Metal-N_x sites that were buried in the N-C matrix in the pristine materials may be accessible to O_2 after the SU/SD-AST, thereby mitigating the ORR activity loss resulting from the destruction of a fraction of the Metal-N_x sites that were electrochemically accessible in the pristine materials. Importantly, the $Co_{0.5}$RP material was distinctly more resistant to the SU/SD protocol, retaining *ca* half of its activity after AST [1.0 – 1.5 V *vs*. RHE – 3s/3s – 10k – Ar – 80°C] in 0.1 M H_2SO_4 (**Figure 9c**).

This improved resistance to the SU/SD protocol with a Co-N-C catalyst *vs*. other Fe-N-C catalysts in that study contrasts with the results from Martinaiou *et al.* [138] where the Co-N-C was less resistant to the SU/SD protocol than the Fe-N-C material (both materials made with an otherwise identical synthesis). These results show that it is difficult to deconvolute the effect of the nature of the metal as part of the active sites from the effects it has on the carbon structure and morphology during the pyrolysis. Pyrolysis conditions (such as flash *vs*. ramp mode) also play an important role on the carbon morphology and local structure around Metal-N_x sites, although this is not always easy to evidence (*e.g.* no clear difference in carbon structure between $Co_{0.5}$FP and $Co_{O.5}$RP).

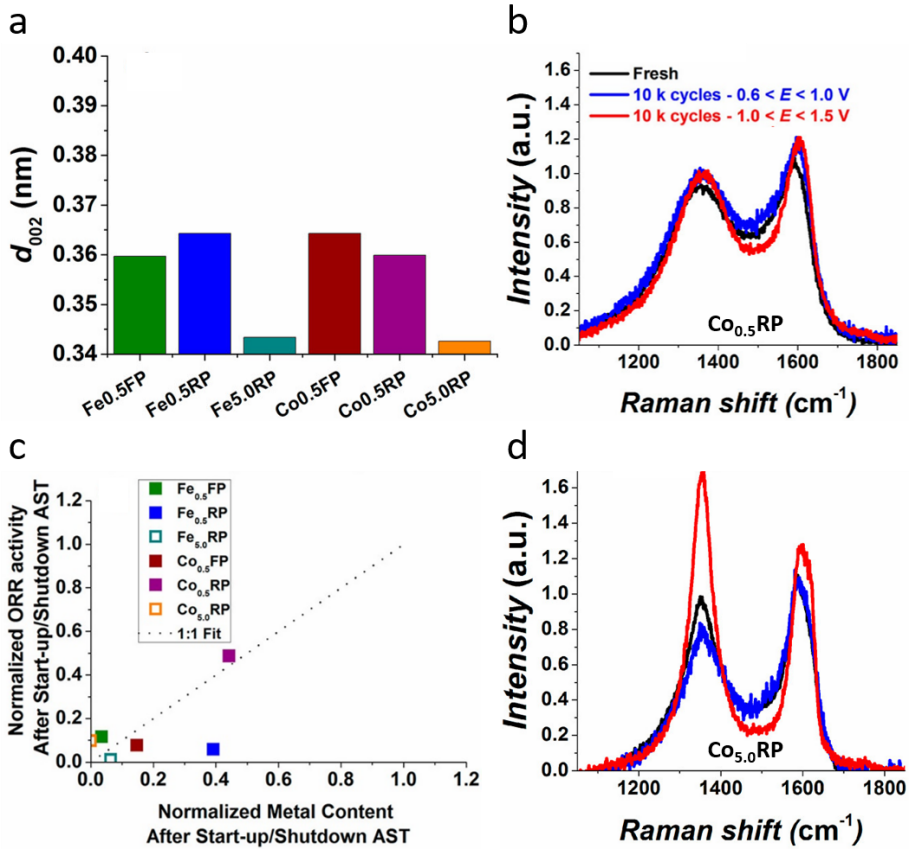

Figure 9. Effect of SU/SD-AST on Fe-N-C and Co-N-C materials with different graphitization level and type of metal-based active sites. a) Average interlayer spacing between graphitic layers (d_{002}); Raman spectra before and after 10k cycles at 80°C for b) $Co_{0.5}RP$ and d) $Co_{5.0}RP$; d) lack of linear correlation between the normalized ORR activity at 0.8 V *vs*. RHE ($j_{final}/j_{initial}$) and the normalized metal content (final metal content/initial metal content) of Metal-N-C catalysts after the SU/SD-AST [1.0 – 1.5 V *vs*. RHE – 3s/3s – 10k – Ar – 80°C] in 0.1 M H_2SO_4. Figures a, b, c and d, reproduced with permission from Ref. [21]. Copyright [2018] American Chemical Society.

2.3.2 Studies in PEMFC

Besides the important differences in experimental conditions in RDE and PEMFC environments (temperature, relative humidity), differences in carbon corrosion rate are also expected due to the increasing importance of some parameters at high current density in PEMFC *vs*. RDE studies, in particular the electronic conductivity through the cathode AL after a SU/SD-AST.

Serov *et al.* [140] reported the dramatic effect of SU/SD AST, applied to a scaled-up Fe-N-C material (from Pajarito Powder – material with mostly Fe-N_x sites but also Fe@N-C sites) with otherwise promising durability in PEMFC operating at U = 0.65 V. The carbon corrosion AST was [1.0 – 1.5 V – 2 V s^{-1} – 5k – N_2 – 80°C] and resulted in severe performance loss (brown curves in **Figure 10a**) with current density at U = 0.4 V dropping from *ca*. 0.7 A cm^{-2} to less than 0.1 A cm^{-2}. Using a focused ion beam coupled to a scanning electron microscope (FIB-SEM), the authors also provided evidence of decreased macroporosity in the AL after the SU/SD-AST, [140] suggesting that the AL collapsed due to COR and loss of connectivity between the Fe-N-C agglomerates. Goellner *et al.* [141] observed a comparable PEMFC performance decay with another Fe-N-C catalyst after [0.9 – 1.4 V – 3s/3s – 0.3k – N_2 – 80°C] (**Figure 10b**), but the cycle included a stepped potential with a 3 s hold at 1.4 V, different from the triangular SU/SD at 2 V s^{-1} applied in Serov *et al*. [140] The duration spent for each cycle at $E \geq 1.4$ V was in fact only 1/20th second in Serov *et al.*, but 3 seconds in Goellner *et al*. The same trends are however observed, the SU/SD protocol leading not only to strongly decreased ORR kinetic

activity but also to drastically higher absolute value of the slope of the polarization curve, typically associated with higher Ohmic loss or mass-transport issues after the SU/SD protocol. Further insights were obtained with electrochemical impedance spectroscopy (EIS), showing the formation of a straight line in the Nyquist EIS plots at high frequency after only 50 SU/SD cycles, and this feature extending with increasing cycling (**Figure 10c**). Based on porous cathode EIS modelling, [142, 143] such a straight line is specific for combined limitation of the cathode performance by both kinetics and charge (proton or electron) conduction through the cathode AL. The intercept of the EIS spectrum with the real axis at high frequency (zoom of **Figure 10c**) shows an increasing value with increasing number of SU/SD cycles. While this might *a priori* be assigned to increased PEM resistance (possible if Fe cations pollute extensively the membrane), this hypothesis was excluded with the following experiment: only the anode and PEM were hot pressed together, and the cathode only positioned against the PEM-anode. At the end of the SU/SD, the cycled PEM-anode was replaced by a fresh PEM-anode. The PEMFC performance remained very low, indicating that the entire performance loss and increase in HFR during the SU/SD cycling can be assigned to the cathode. [141] The surge of a HFR component from the cathode AL is possible from EIS cathode modelling if both the conduction of protons and electrons through the cathode AL are limiting its performance. [141] Following estimation of the decrease in electronic conductivity through the cathode before/after SU/SD and feeding into a model of porous electrode, it was concluded that the decreased electronic conductivity through the cathode could not fully account for the huge drop in performance. Strongly decreased density of active sites after SU/SD protocol might have implied local O_2 transport issues (the remaining few active sites need to "work" more than initially to reach a same cathode current density) and long-range O_2 transport issues due to flooding of meso- and macropores (increased hydrophilicity after COR).

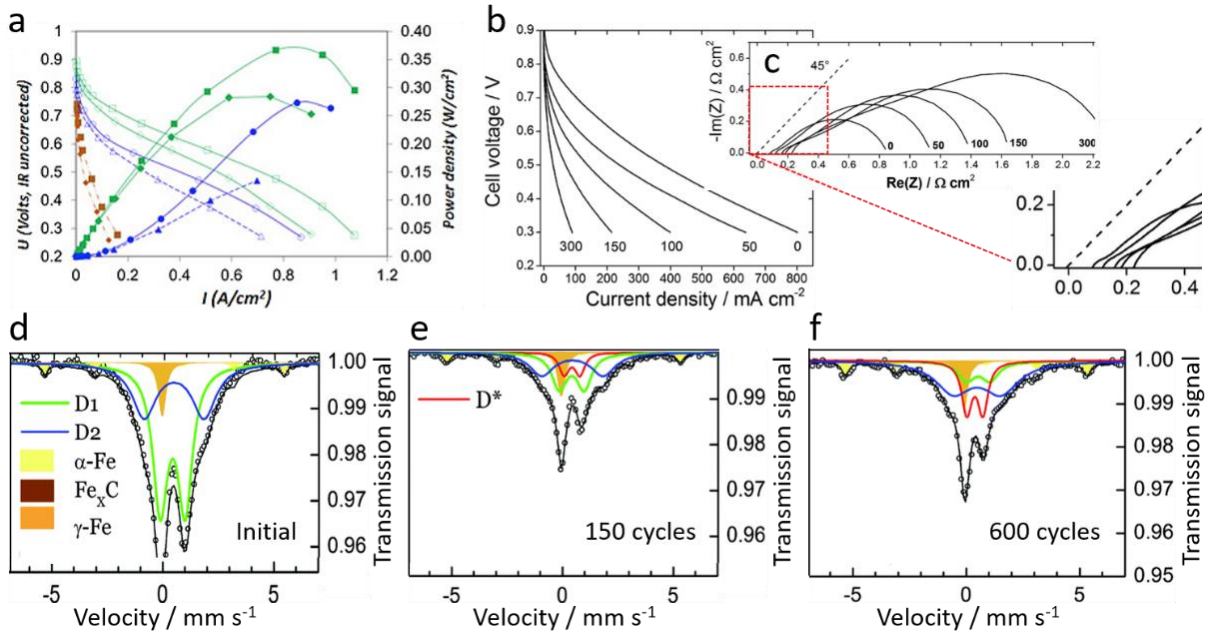

Figure 10. Effect of SU/SD-AST stability protocol in PEMFC on Fe-N-C cathodes. a) H_2/air polarisation curves for a Fe-N-C obtained by silica templating, before and after a 100 h hold at 0.65 V (blue curves), and after [1.0 – 1.5 V *vs*. RHE – 2 V s^{-1} – 5k – N_2 – 80°C] (brown curves). Figure a, reproduced with permission from Ref. [140]. Copyright [2016] Elsevier, b) H_2/O_2 polarisation curves for a Fe/N/C cathode derived from ZIF-8 after 50 and up to 300 SU/SD cycles with stepped potential [0.9 – 1.4 V – 3s/3s – N_2 – 80°C]; c) corresponding Nyquist plots of the impedance spectra acquired at 0.1 A cm^{-2} (the inset shows the HFR region); ^{57}Fe Mössbauer spectra of another Fe-N-C cathode (labelled Fe/N/C-dry and containing mainly Fe-N_x sites) in d) pristine state, e) after 150 SU/SD

cycles and f) after 600 SU/SD cycles in PEMFC at 80°C. Figures b, c, d, e and f, reproduced with permission from Ref. [141]. Copyright [2014] The Royal Society of Chemistry.

Changes in the Fe speciation before and after SU/SD cycles in PEMFC were also investigated by ^{57}Fe Mössbauer spectroscopy, for two Fe-N-C catalysts derived from ZIF-8 and labelled Fe/N/C and Fe/N/C-dry. The former contained a high amount of metallic Fe particles along with Fe-N_x sites, while the latter contained mainly Fe as Fe-N_x sites. For both catalysts, a trend of decreasing signal of the Fe-N_x sites with SU/SD cycling was observed, while the signal for metallic Fe and Fe_3C particles decreased only by a small amount (Figure 7 in Ref. [141]). **Figure 10d-e-f** shows the ^{57}Fe Mössbauer spectra for the pristine Fe/N/C-dry cathode as well as for after 150 and 600 SU/SD cycles. The spectra were acquired in transmission mode through the whole cathode separated from the rest of the MEA, so that the absolute quantity for a specific Fe species (one spectral component) is proportional to the component's signal intensity. The signal intensity of the doublet components D1 and D2 (assigned to Fe-N_x sites) decreased after 150 cycles by factors of 5.2 and 2.8, respectively. The strong correlation between the ORR activity decrease (divided by 6 after 150 cycles) and the decrease in D1 intensity suggests that the site associated with D1 is more ORR active than the ones associated with D2. Recently, a combined experimental and theoretical investigation supports the assignment of D1 to a FeN_4C_{12} site coordination with oxygen adsorbate axially bound to the central Fe cation (implying D1 is a surface-active site) and of D2 to FeN_4C_{10} or FeN_4C_{12} active sites in different spin states but without axially-bound oxygen adsorbate (suggesting it might a site buried in the carbon matrix). [144] These recent assignments and surface *vs*. bulk locations of D1 and D2 are in line with the observations in **Figure 10d-e-f**, reporting exacerbated loss of D1 intensity relative to D2. After electrochemical SU/SD cycling in PEMFC, a new doublet component with lower quadrupole splitting than D1 appeared, labelled D* and that was assigned to ferric hydroxide nanometric particles (**Figure 10e-f**). Such particles are magnetically disordered at room temperature due to their small size, leading to a doublet component with spectral parameters matching those of D*. While the leaching and reprecipitation of Fe either from Fe-N_x sites or from metallic particles could lead to *D**, the comparison of Mössbauer spectra of cycled Fe/N/C and Fe/N/C-dry cathodes strongly suggested that *D** in this case formed mainly from the transformation of metallic iron (Fe) and iron carbide (Fe_3C) particles into ferric (hydr)oxide (FeO_x), once exposed to the acidic electrolyte after the removal of their carbon protective layer by COR. As discussed in **section 2.6**, EoT ^{57}Fe Mössbauer measurements of Fe-N-C cathodes at low temperature of -268 °C allow a better separation between the signals for ferric (hydr)oxide and the doublet D1 assigned to one type of Fe-N_x sites.

To summarize **section 2.3**, all SU/SD protocols significantly degrade all Metal-N-C materials, as expected since the metal-based active sites are intimately connected to the carbon matrix in such materials. Perhaps counterintuitively, the Metal@N-C sites seem to deactivate and leach out the metal even faster than Metal-N_x sites in SU/SD protocols. When comparing Fe-N_x sites and Co-N_x sites, there seems to be diverging results on the stability trend to SU/SD protocol. Not only the nature of the metal but also the synthesis procedure of Metal-N-C materials and detailed carbon morphology and structure therefore seem to control the degradation rate during SU/SD protocol. Beyond ORR activity loss, SU/SD protocols lead to a loss of carbon and drastic decrease of performance in PEMFC due to loss in electronic conductivity through the cathode layer and collapse of the electrode structure.

2.4 Effect of hydrogen peroxide in the absence of oxygen reduction reaction

Hydrogen peroxide (H_2O_2) is the only stable intermediate or by-product of the ORR in acid medium and can be a particularly important stressing factor for PGM-free cathode catalysts and MEAs during ORR. Fenton reactions are expected to occur in acidic medium between transition metal cations (either solvated, bound in the Nafion ionomer, in metal-oxide particles or even as Metal-N_x sites in the N-C matrix) and H_2O_2, leading to the continuous formation of ROS. While Fe and copper (Cu) cations are the most researched Fenton catalysts due to their importance in biology, other transition metal cations may also lead to Fenton reactions. For example, Strlic *et al.* [145] studied the homogeneous catalysis of a Fenton-like reaction by various transition metal cations in aqueous solution. It was found that, at pH 7, the Fenton-like reactivity was in the order Cu(II) > Cr(III) ~ Co(II) >> Fe(III) ~ Mn(II) >> Ni(II) > Zn(II) > Cd(II). While the metal cation coordination, pH and environment in that study differ from those under ORR electrocatalysis by Metal-N-C materials in acidic conditions, the results generally show that one cannot simply assume that switching to Fe-free Metal-N-C catalysts will avoid or even decrease Fenton reactions.

The amount of H_2O_2 produced during ORR on Metal-N-C materials is usually measured with a RRDE setup. Due to the low ORR activity of Metal-N-C materials in acid, relatively high loadings are typically deposited on the working electrode for RRDE measurements. In such conditions, the apparent H_2O_2 content detected at the ring electrode may underestimate the peroxide production locally near the active sites, due to possible peroxide electro-reduction or decomposition before it diffuses out of the AL. Bonakdarpour *et al.* [146] clearly showed this effect for a particular Fe-N-C catalyst which resulted at 0.35 V *vs*. RHE in an apparent % peroxide < 7 % at 800 $\mu g \cdot cm^{-2}$ but of 70-95 % at 20 $\mu g \cdot cm^{-2}$. Recently, Ünsal *et al*. [147] also showed that the quality of the thin-film electrode, namely the size of the aggregates composing the Metal-N-C catalyst, does not influence the mass activity of the catalyst but determines the H_2O_2 yield measured at the ring electrode. While subsequent studies showed that other Fe-N-C and Metal-N-C catalysts can show much lower % peroxide than 70 % at low loading, the general trend of increasing % peroxide with decreasing catalyst loading has been confirmed by several laboratories. [70, 148, 149] This supports that the "true" peroxide production is significant for most if not all PGM-free catalysts.

An early study from Wiesener [150] looked into the effect of peroxide on the load/durability of Co-N-C by regularly adding a controlled amount of H_2O_2 in O_2-saturated acidic solutions and analysing the ORR activity as a function of time, with or without addition of H_2O_2. However, disentangling the effects of applied electrochemical potential, presence of high concentration of peroxide in the bulk of the solution and the ORR electrocatalysis itself is difficult and may hide the fundamental degradation mechanism triggered by the presence of peroxide, or may lead to interrelated effects leading to more severe degradation than the sole presence of peroxide is able to impinge (see **section 2.6**). Three studies were then reported in 2003 and 2009 on the effect of *ex situ* treatment of Fe-N-C catalysts by H_2O_2. [151-153] Lefèvre *et al*. [151] prepared different Fe-N-C catalysts (Fe acetate or Fe-porphyrin precursors, 0.2 or 2.0 wt. % Fe before pyrolysis) and measured first their ORR activity in an RDE setup, but without rotating the electrode. The position of the O_2 reduction peak observed in such conditions was reported as V_{pr} (filled symbols in **Figure 11a**). As was shown later the same year, the V_{pr} value is proportionally correlated with the logarithm of the kinetic current density times the Tafel slope value, so that a change of 70-90 mV in the V_{pr} value typically corresponds to a 10-fold variation in ORR kinetic activity. [154] The catalysts were then immersed for 5 h in a solution of

pH 1 containing also 5 vol. % of H_2O_2 (simulating the local environment near Fe active sites with 5 % H_2O_2 production during ORR). The ORR activity measured after this peroxide treatment was dramatically decreased (empty symbols in **Figure 11a**). Control experiments by treating selected catalysts with acid only (no peroxide) showed some activity loss, but less than with peroxide (stars symbols in **Figure 11a**). The Fe content was measured before and after peroxide treatment, and positively correlated with the change in V_{pr} (**Figure 11b**, filled symbols), from which the authors concluded that the loss in ORR activity is explained by the Fe loss during the acidic peroxide treatment, in turn related to a loss of active sites. However, this attractive qualitative conclusion is not in line with the quantitative analysis that a change of one Tafel slope in the V_{pr} value (*i.e.* a change in ΔV_{pr} of 70-90 mV) should correspond to a one order of magnitude decrease in the number of active sites.

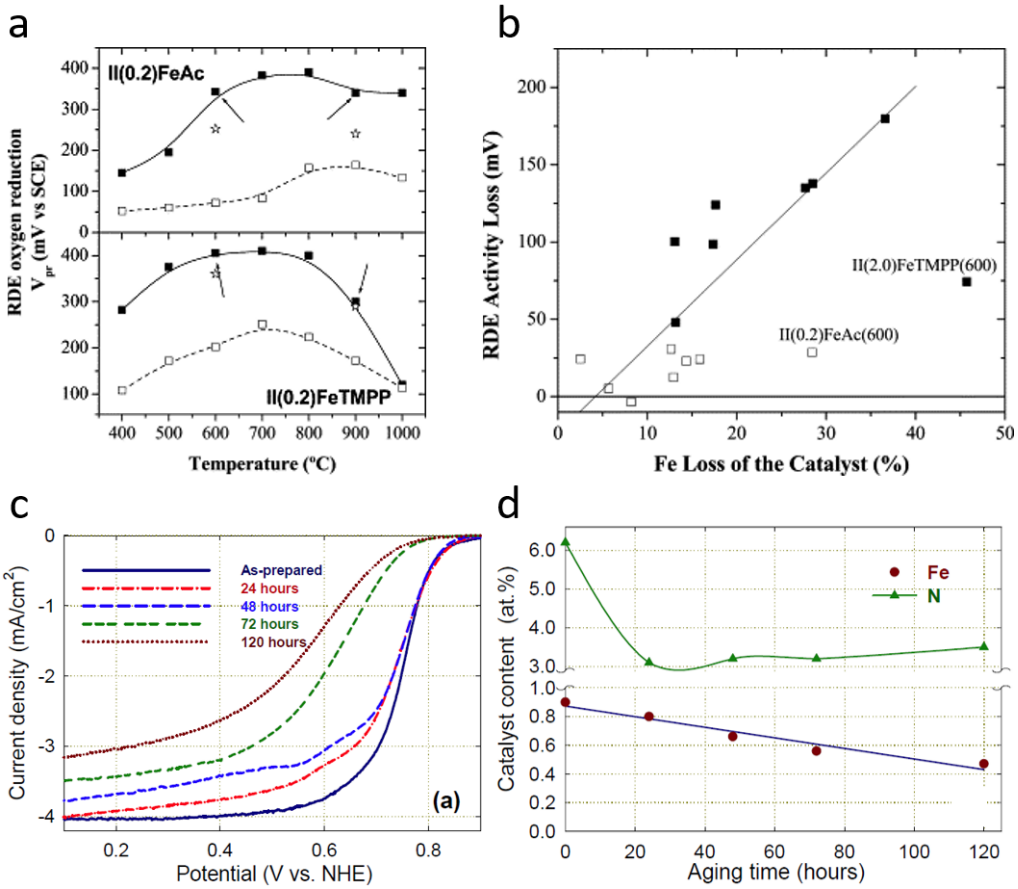

Figure 11. Early studies on the effect of *ex situ* peroxide treatment. a) ORR activity at pH 1 reported as V_{pr} before (filled symbols) and after (empty symbols) acidic peroxide treatment for two different Fe-N-C series prepared at various pyrolysis temperatures. The star symbols in a) report the activity after acidic treatment but without peroxide. b) Correlation between the change in ORR activity (ΔV_{pr}) and the loss of Fe content during H_2O_2 acidic treatment. Filled symbols correspond to H_2SO_4 + 5 vol. % H_2O_2 treatment, and empty symbols to H_2SO_4 treatment only. c) ORR polarisation curves for the as-prepared Fe-N-C and after treatment for different duration in water + 10 wt. % H_2O_2 at 80°C. d) X-ray photoelectron spectroscopy-determined Fe and N contents corresponding to the data in c). Figures a and b, reproduced with permission from Ref. [151]. Copyright [2003] Elsevier. Figures c and d, reproduced with permission from Ref. [153]. Copyright [2009] The Electrochemical Society.

Therefore, **Figure 11b** actually shows that the ORR activity decreased by a factor between 10x and 1000x for a relative decrease of the Fe content of only 15-40 %. The ORR activity loss induced by acidic peroxide treatment seems therefore not proportionally related to the loss of Fe content, if related at all. Schulenburg *et al.* [152] studied a pyrolyzed Fe-N-C catalyst prepared from an Fe porphyrin and carbon black. The material was investigated for ORR

activity in acid medium, Fe content and Fe speciation as-synthesized, after an acid wash, and after an acid wash followed by H_2O_2 treatment, adding a 30 vol. % H_2O_2 solution drop-by-drop to the acid-washed Fe-N-C. It was observed that the ORR activity of the as-synthesized and acid-washed samples were comparable (slightly higher after acid wash), while the Fe content was much lower after acid wash (0.47 % Fe *vs*. 2.05 % Fe for as synthesized Fe-N-C). ^{57}Fe Mössbauer spectroscopy identified that the Fe_3C and metallic Fe phases were removed by the acid wash, but that other doublet components (related to Fe-N_x sites and or superparamagnetic Fe oxide NPs) remained. In contrast, the ORR activity after acid wash + peroxide treatment resulted in a dramatic decrease of the ORR activity, while the Fe content and ^{57}Fe Mössbauer spectrum were similar to those observed after the acid wash. In the third early study, Wu *et al.* [153] applied a different *ex situ* H_2O_2 treatment, keeping the H_2O_2 concentration fixed (10 wt. % in water at 80°C) but varying the duration of immersion of the PANI-derived Fe-N-C catalyst. It was found that the ORR activity does not decrease much up to 48 h of treatment, but then dramatically dropped after 72 h of treatment (**Figure 11c**). The N content determined by XPS showed a sharp decrease in the first 24 h of treatment but remained stable afterwards, while the Fe content slowly but steadily decreased with increasing duration of peroxide treatment (**Figure 11d**). There was no quantitative correlation however between Fe content and ORR activity: i) no significant loss of ORR kinetics was observed after 24-48 h of peroxide treatment while during that time the Fe atomic content decreased by only 0.2 at. %; then ii) from 48 to 72 h of treatment the polarization curve negatively shifted by *ca*. 100 mV in the kinetic region while the Fe atomic content decreased again only by *ca*. 0.2 at. % (**Figure 11c-d**).

In summary, these early studies revealed a dramatic effect of *ex situ* peroxide treatment (in acidic or neutral conditions) on the ORR activity of different Fe-N-C catalysts in acid, but the mechanism behind this effect was unclear. In 2015, Goellner *et al.* [35] reinvestigated the effect of peroxide on a Fe-N-C and Co-N-C catalyst. The metal speciation was investigated before and after H_2O_2 treatment with extended X-ray absorption fine structure (EXAFS) and X-ray absorption near-edge structure (XANES) spectroscopy, as well as ^{57}Fe Mössbauer spectroscopy for the Fe-N-C. The *ex situ* peroxide treatment was conducted by immersing a given amount of each catalyst in deionized water + 30 wt. % H_2O_2 at 80° C, with different volumes of peroxide added so as to cover a targeted range of ratio of (moles H_2O_2) / (catalyst mass). The metal K-edge XANES and EXAFS spectra of the pristine Fe-N-C and Co-N-C catalysts had strong similarities with those of corresponding Metal (II) phthalocyanines, indicating the presence of metal mainly as Metal-N_4 sites. RDE of the pristine and H_2O_2-treated catalysts showed continuously decreasing ORR activity with increasing amount of H_2O_2 per mass of catalyst used during the *ex situ* H_2O_2 treatment, as shown in **Figure 12a** for Fe-N-C. However, Co-N-C showed less ORR activity decay, the activity after treatment with 10^{-2} mol H_2O_2 mg^{-1} being divided by ca 7 for Fe-N-C, but only by ca 3 for Co-N-C. For both catalysts, no significant changes in the metal coordination were identified by Co and Fe *K*-edge EXAFS, XANES and ^{57}Fe Mössbauer spectroscopies (see **Figure 12b-d** for XANES and Mössbauer spectroscopic results on Fe-N-C). This information combined with the restricted loss of bulk metal content (**Figure 12e**) suggested that the major fraction of Metal-N_4 sites survived the peroxide treatment, but that their site-specific ORR activity (or TOF) had been decreased. The only noticeable change was revealed by XPS, identifying an increase in the oxygen content from 4-5 at. % for pristine Fe-N-C and Co-N-C to 9-12 at. % for Fe-N-C and Co-N-C treated with 10^{-2} mol H_2O_2 mg^{-1}. O_{1s} narrow scan spectra identified a specific increase in the hydroxyl and epoxy groups, known to result in strong distortion of the graphene layers. Surface oxidation of carbon (different from

bulk COR) thus seemed to be the main degradation route during reaction with H_2O_2, impacting the TOF of otherwise unmodified Metal-N_x sites.

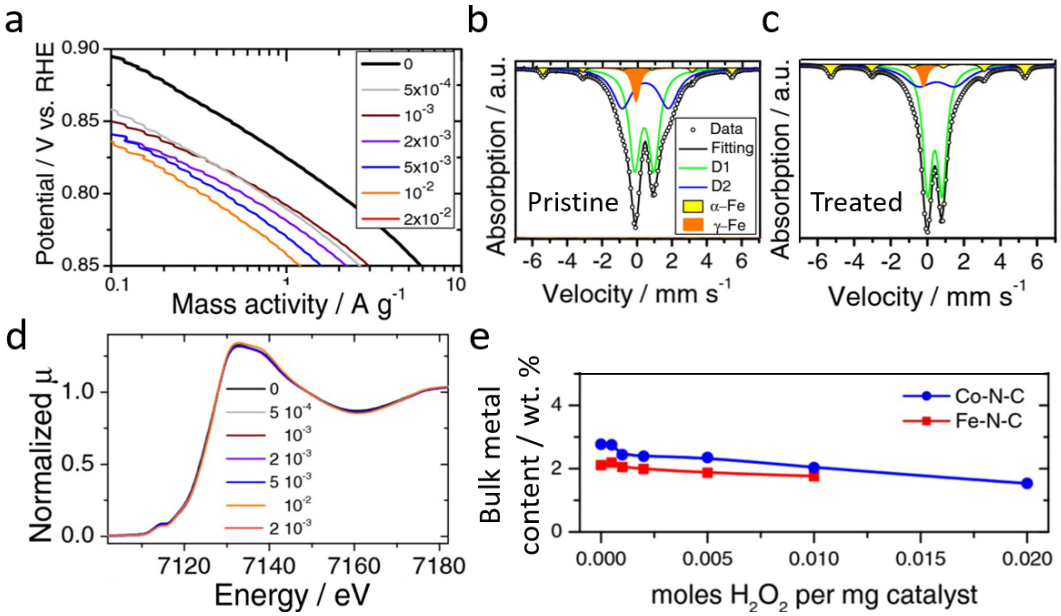

Figure 12. ORR activity loss induced by peroxide treatment without apparent structural change. a) ORR Tafel plots from RDE of pristine Fe-N-C and after *ex situ* treatment at various ratios of moles H_2O_2/mg Fe-N-C (indicated in the legend). b) ^{57}Fe Mössbauer spectra of the pristine Fe-N-C. c) ^{57}Fe Mössbauer spectra of the Fe-N-C after treatment with 10^{-2} moles H_2O_2/mg Fe-N-C. d) Fe K-edge XANES spectra of Fe-N-C and peroxide-treated Fe-N-C. e) Bulk metal content of Fe-N-C and Co-N-C *vs*. the ratio of moles H_2O_2/mg Metal-N-C used during the peroxide treatment. Figures a, b, c, d, and e, reproduced with permission from Ref. [35]. Copyright [2015] The Electrochemical Society.

Further insights on the elusive deactivation mechanism of Fe-N-C by H_2O_2 were revealed by Choi *et al.* [36] in a subsequent study on the same Fe-N-C catalyst as investigated in Ref. [35], and labelled FeNC-1. *Ex situ* peroxide treatment was performed at 20, 50 or 70°C in a pH 1 solution with 5 wt. % H_2O_2 (samples labelled as FeNC-1-T, where *T* is temperature) and it was observed that the ORR activity and selectivity for the four-electron O_2 reduction decreased with increasing treatment temperature (**Figure 13a-b**). The Tafel slope increased after treatment at 70°C, indicating a change in the rate determining step. As in Ref. [35], the material did not show any sign of structural or chemical modification after peroxide treatment (Fe K-edge EXAFS, XPS, inductively coupled plasma atomic emission spectroscopy (ICP-AES), ^{57}Fe Mössbauer, N_2 sorption isotherms, Raman spectroscopy), except for the increased oxygen content measured by XPS. The results suggested again that the peroxide treatment only modified the top-surface of FeNC-1, oxidizing the carbon surface indirectly via the formation of ROS via Fenton reactions with Fe, but without resulting in bulk COR. Besides the oxygen content, three other surface-specific descriptors were found that correlate with the ORR activity change, namely the work function (WF), the potential of zero charge (E_{pzc}) (**Figure 13c-d**) and the surface basicity.

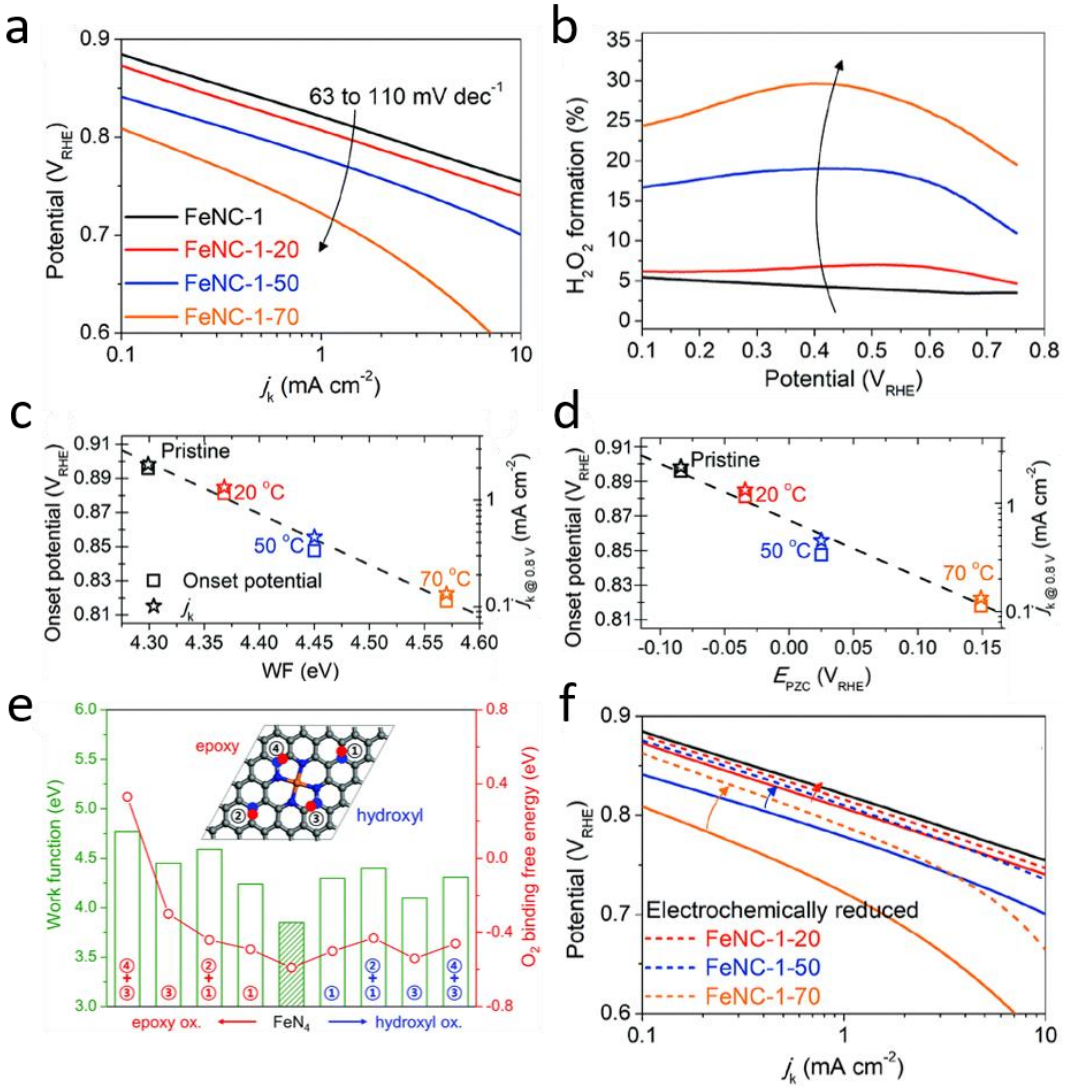

Figure 13. Mechanism of surface deactivation by peroxide treatment. a) ORR Tafel plots from RRDE of pristine and peroxide-treated Fe-N-C-1; b) corresponding ORR selectivity; c) ORR activity *vs*. WF; d) ORR activity *vs*. E_{pzc}; e) DFT results reporting the calculated WF of the surface and O_2 binding energy on a Fe-N_4 site, with or without surface oxygen groups in the graphene sheet; f) recovery of ORR activity *via* electrochemical reduction of the surface after peroxide treatment. Figures a, b, c, d, e and f, reproduced with permission from Ref. [36]. Copyright [2018] Royal Society of Chemistry.

These three correlations are explained on the basis of modulation of the TOF of Fe-N_x moieties by the electronic properties of the surrounding carbon surface. The WF, E_{pzc} and basicity of the carbon surface are inter-related and modified by the carbon surface oxidation. Furthermore, DFT calculations correctly reproduced the increase in WF triggered by the addition of surface oxygen groups and identified that the latter decreased the O_2 binding energy at the Fe centre, a key descriptor for ORR catalysis (**Figure 13e)**. These findings were confirmed in a recent theoretical and experimental study by Jung *et al.* [155] showing that hydrogen or oxygen-containing carbon surface groups control the ORR selectivity of a Co-N-C catalyst. Interestingly, such changes are reversible: Choi *et al.* [36] showed that Fe-N-C catalysts treated by peroxide recover to a large extent their initial ORR activity (**Figure 13f**) and selectivity after applying an electrochemical reduction protocol similar to that employed for reducing graphene oxide. This clearly shows that the TOF of Fe-N_x sites is modulated by the long-range chemical state of the carbon surface, and that such properties cannot be tracked

by techniques used to probe Fe. In a follow-up study, Choi's group investigated the effect of the pH-value at which the peroxide treatment is performed, and found increasing deactivation of Fe-N-C with decreasing pH down to pH 1. [156] Peroxide treatment at pH 6 already resulted in significant deactivation, while treatment at pH ≥ 12 resulted in no deactivation. Nitrone spin-trap coupled to electron paramagnetic resonance (EPR) experiments also evidenced the formation of ROS by exposing Fe-N-C to H_2O_2 in acidic solutions, but absence of ROS in alkaline conditions. [156]

In summary, due to the poor activity of Metal-N-C catalysts towards the electroreduction and the chemical disproportionation of H_2O_2 in acidic conditions, even minute amount of peroxide produced during the ORR can accumulate over time. This in turn triggers Fenton reactions between transition metal cations and peroxide, leading to ROS. It has recently been shown that the *ex situ* peroxide treatment of Fe-N-C and Co-N-C materials with Metal-N_x sites in neutral to acidic conditions leads to surface oxidation, decreasing the TOF of the Metal-N_x sites. Co-N-C catalysts seem to be less affected by *ex situ* exposure to a given amount of H_2O_2 compared to Fe-N-C catalysts. Moreover, the *ex situ* exposure of Fe-N-C to H_2O_2 was shown to increase the H_2O_2 yield during ORR, constituting an evil circle for the *operando* deactivation of Metal-N-C cathode ALs in PEMFC. Further studies are needed, especially on Metal-N-C catalysts with Metal@N-C sites and on Metal-N-C catalysts with Metal-N_x sites integrated in more graphitic carbon structures, in order to obtain a broader view on the effect of exposure to H_2O_2. In addition, oxidation of the carbon surface might negatively impact the transport properties of the AL, due to increased hydrophilicity in particular. Finally, it is noteworthy that the exposure of Fe-N-C to H_2O_2 in alkaline conditions did not modify its ORR activity and selectivity, opening interesting perspectives for application in anion-exchange membrane fuel cell cathodes, with advantages over PGM-catalysts with respect to their general insensitivity to fuels such as methanol [157-159] and $NaBH_4$. [101]

2.5 A spinoff of Metal-N-C surface-oxidation: improved catalysts for H_2O_2 electro-synthesis

Today, H_2O_2 is industrially produced via the anthraquinone oxidation process (>5 million tons per year), for utilization as an oxidizing agent for wastewater treatment, pulp and paper bleaching, chemical synthesis. The scaled-up electrosynthesis of H_2O_2 would offer several advantages over the existing process, as it does not involve organic solvents, it can achieve high concentrations of H_2O_2 directly, and could be produced on-site, eliminating the risks and costs associated with the transport of H_2O_2 from few large chemical plants as is done today. [160]

While Metal-free N-C materials are generally highly selective for the two-electron ORR [161-164] they display also a high overpotential, which has a negative impact on the energy efficiency of an electrochemical device whose purpose is the H_2O_2 electrosynthesis. The overpotential for Metal-free N-C materials is especially high in mildly to strong acid electrolytes, and those pH values are preferable for the chemical stability of hydrogen peroxide. H_2O_2 electrosynthesis in PEM-based electrolyser is thus particularly appealing, as it results in concentrated H_2O_2 in pure water. [165]

The new understanding that H_2O_2 (intentionally added to the electrolyte as a stressor, or produced during the ORR) leads to the surface-oxidation of the carbon matrix of Metal-N-C materials, and to higher % H_2O_2 produced by Fe-N_4 sites during ORR, [36] resulted in an interesting spinoff. Taking advantage of this effect, one can intentionally modify the surface

of Metal-N-C catalysts with the goal of electrochemically producing H_2O_2. [166, 167] Surface oxidation resulted in a strongest selectivity effect for Co-N-C, among Fe-, Mn- and Co-N-C catalysts, increasing the peroxide yield from ca 25 to 85 % at 0.6 V *vs.* RHE in acid medium. [166] The oxidation effect was visible also in a reduced activity toward the H_2O_2 to H_2O electroreduction reaction, explaining the higher peroxide yield after the oxidative treatment. In another example, a Co-N-C material with combined high contents of Co-N_4 sites and oxygen functional groups was prepared from graphene oxide. [155] Alternatively, oxygen functional groups can be formed *in situ* by scanning the potential to a high electrochemical potential, before conducting H_2O_2 electrosynthesis. [155] While it may appear counterintuitive that single metal atom site of the Metal-N_4 type can be selective for four-electron reduction, low peroxide yields are usually observed, especially with Fe-N-C materials hosting Fe-N_4 sites. DFT works showed that the O-O bond cleavage in Fe-N-C is facilitated through a cooperative effect, one end of the O_2 molecule being bound to the Fe-N_4 metal cation and the other end to a carbon atom in the second coordination sphere. [168] Forming oxygen functional groups on such carbon atoms can therefore drastically reduce the ability of Fe-N_4 sites, and Metal-N_4 sites in general, to carry out the four-electron ORR.

Degradation effects and mechanisms of Metal-N-C materials applied for the H_2O_2 electrosynthesis have not yet been studied in detail. For non-pre-oxidized Fe-N-C materials, their *in situ* surface oxidation during break-in could lead to increased rate of H_2O_2 production, as a result of an increase in selectivity of the oxygen reduction towards H_2O_2. Prolonged operation would however likely result in carbon corrosion and the loss of Metal-N_4 sites and decreased electric conductivity through the AL. While Fe-N-C materials with an oxidized surface are promising catalysts for H_2O_2 electro-synthesis, the current optimum balance between high selectivity toward two-electron ORR and low overpotential seems to favour Co-N-C over Fe-N-C materials, [169] due to intrinsic optimum HO binding on the Co-N_4 centre. While the degradation mechanisms discussed in the present review regarding Fe-N-C catalysts for ORR in acidic medium for electric power generation in PEMFC will likely be transposable to Co-N-C catalysts for H_2O_2 electro-synthesis, in-depth studies will be needed on the latter topic to go beyond the phenomenological observation of decreased efficacy of the device. [170] The rate and predominance of the different degradation types discussed in the present review indeed strongly depend on the electrolyte pH, AL thickness, temperature, operating regime of the device (cell voltage and/or current density), peroxide concentration, etc; factors that will vary significantly from PEMFC for electric power generation to an electrolysis cell for H_2O_2 synthesis.

2.6 Combined effects of electrochemical potential and oxygen reduction reaction

As reported in **section 2.2** and **section 2.4**, while some Metal-N-C materials have shown high stability to load cycles in de-aerated acidic medium, such materials suffer from a reduced TOF of their Metal-N_x sites when exposed to H_2O_2 in acidic conditions, while the number of Metal-N_x sites was quasi-unmodified [152]. From these two *a priori* independent stressing factors (electrochemical potential and H_2O_2), one would expect the main degradation mechanism of Metal-N-C materials during load cycles in O_2-containing environment or steady-state ORR electrocatalysis to be comparable to that reported for *ex situ* peroxide treatment (no COR, no loss of Metal-N_x sites but reduced TOF of Metal-N_x sites due to top-surface oxidation). While the rate of peroxide production during ORR for a given cathode AL is of course related to the applied potential, the mechanism by which H_2O_2 deactivates/degrades the AL is *a priori* not expected to depend on the potential, and this is what is meant with “two *a priori* independent

stressing factors". Recent studies however revealed that the degradation phenomena observed during ORR on Metal-N-C ALs are different from those observed when simply contacting them with H_2O_2. These studies are discussed below.

2.6.1 Studies in liquid acidic electrolyte

As introduced in **section 2.2**, Metal-phthalocyanines and Fe-phthalocyanines in particular can be good molecular proxies for studying the single metal atom sites of pyrolyzed Metal-N-C materials. In this subsection, we thus discuss first the phenomena observed with different iron phthalocyanines supported on carbon, before switching to pyrolyzed Fe-N-C materials. Iron(II) phthalocyanine supported on Vulcan carbon black was investigated by Baranton *et al*. [106] The authors showed that the ORR activity decreased rapidly when applying a constant potential of 0.5 V *vs.* RHE (**Figure 14a**) or while potential cycling (inset of **Figure 14a**). *In situ* infrared (IR) reflectance spectroscopy revealed that the spectral signature changed from Fe(II)Pc to H_2Pc over 3 h of potentiostatic hold at 0.5 V *vs*. RHE in O_2-saturated 0.5 M H_2SO_4 solution (**Figure 14b-c**), in line with the decreased ORR current density. One should note however that the current density at 0.5 V *vs.* RHE (shown in **Figure 14a**) is strongly diffusion-limited and therefore largely underestimates the true decrease in ORR kinetics. From the inset of **Figure 14a**, one can infer *ca*. 100 mV negative shift in the kinetic region, implying that the ORR activity dropped by at least 90 %. Importantly, the authors wrote that "in 0.5 M H_2SO_4 argon (Ar)-saturated electrolyte, no degradation of the FePc/C electrode was observed from electrochemical and IR reflectance spectroscopy measurements". It was therefore concluded that a combined effect of O_2 adsorption on Fe(II) and protonation is likely causing the demetalation, and such an effect may occur during one of the ORR steps on Fe(II)Pc. While Fe(II)Pc undergoes a strong conformational change from in-plane to out-of-plane location of the Fe(II) cation upon adsorption of oxygenated adsorbates, [171] the change is similar for H_2O, OH or O_2 adsorbates. This suggests that one of the ORR steps in acid medium triggers the demetalation, not only the adsorption event. The authors proposed that an electron transfer from the out-of-plane Fe(II) to the adsorbed O_2 or oxygenate intermediate might result in a transient Fe(III) state, destabilized in acid medium in the out-of-plane configuration due to its lower ionic radius than Fe(II). Such a mechanism was also proposed earlier by Meier *et al.* [112] for polymeric Fe(II)Pc, where enhanced demetalation was also observed in O_2- *vs*. N_2-saturated 6 N H_2SO_4. It is also possible that demetalation occurs when Fe(II)N_4 is under-coordinated (no axial ligand) during each turnover cycle, as discussed in **section 2.1**. More recently, Chen *et al.* [111] studied with electrochemical tip-enhanced Raman spectroscopy (TER) the durability of an Fe (II) phthalocyanine monolayer on Au(111) in air-saturated 0.1 M $HClO_4$. The ORR activity decreased rapidly when it was subjected to a potential hold at 0.4 V *vs*. RHE in air-saturated solution, but was much more stable in N_2-saturated solution (**Figure 14d-e**). A 15 min hold at 0.4 V *vs.* RHE in O_2-saturated 0.1 M $HClO_4$ led to irreversible changes in the TER spectra, in particular the disappearance of the 593 and 751 cm^{-1} peaks and appearance of peaks at 724 and 795 cm^{-1} (**Figure 14f**). Analysis of the "altered" spectrum demonstrated that it corresponds to H_2Pc. Since no alteration of the spectrum was observed in inert-gas saturated 0.1 M $HClO_4$ at the same potential, the authors concluded that the ORR catalysis by Fe(II)Pc is responsible for the demetalation, not the electrochemical potential *per se*. In line with Baranton *et al*, [106] they mentioned the strong out-of-plane distortion of FePc upon O_2 adsorption and possible transient presence of Fe(III) in out-of-plane configuration during the ORR, as a result of electron transfer from the Fe cation to the oxygen adsorbate. Since the degraded product of FePc and all the spectral lines after degradation could be assigned to

H_2Pc in which the macrocyclic structure is retained (**Figure 14g**), the authors concluded that FePc demetalation during ORR proceeded without breaking bonds (no carbon corrosion). [111]

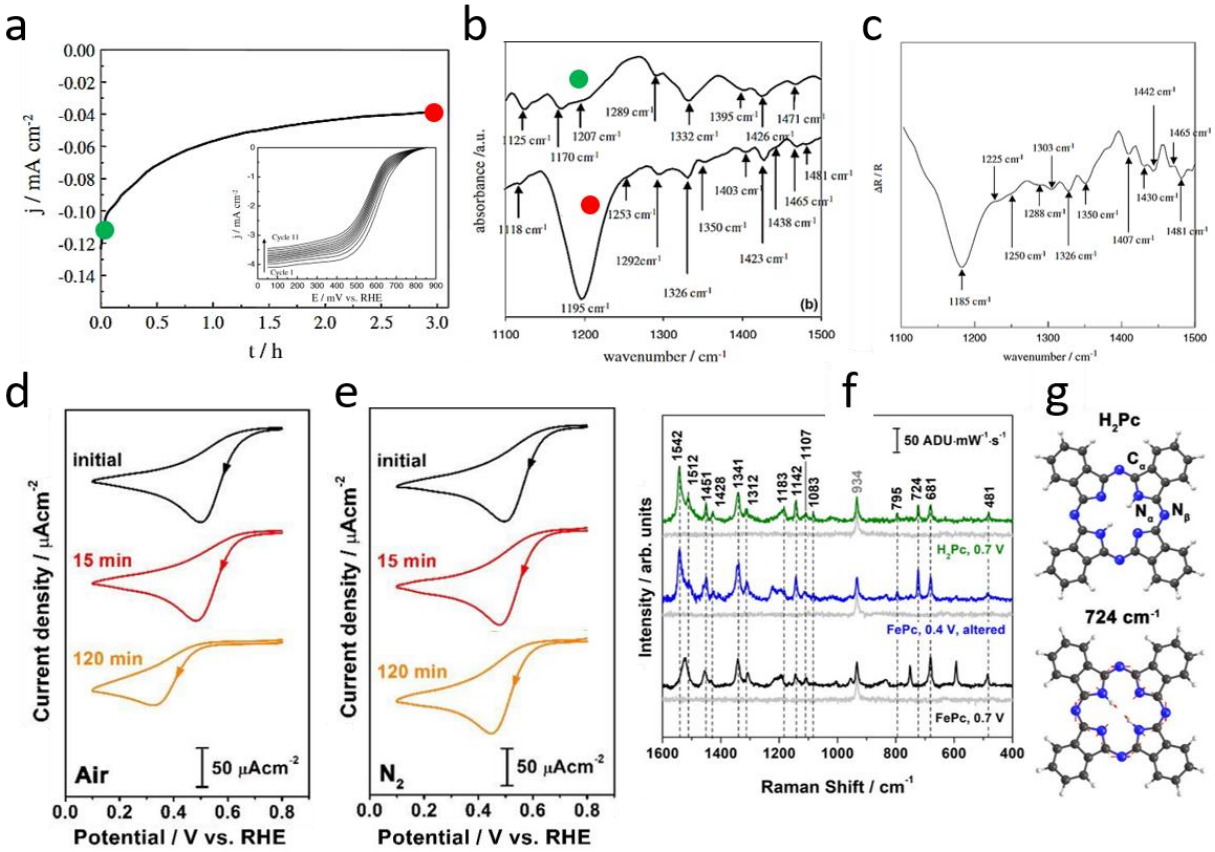

Figure 14. Degradation of Fe(II)Pc when catalysing ORR in acid medium. a) Current density *vs*. time at 0.5 V *vs*. RHE for FePc/carbon in O_2-saturated 0.5 M H_2SO_4 at 20°C. The inset shows the change in the first 11 cycles. b) First and last IR spectra recorded during the 3 h potential hold shown in a). Arrows indicate characteristic wavenumbers. c) Infrared spectrum of H_2Pc in ethanol. d) Cyclic voltammograms of FePc/Au(111) measured in air-saturated 0.1 M $HClO_4$ before and after a potential hold at 0.4 V *vs*. RHE for different durations in d) air-saturated 0.1 M $HClO_4$ and e) N_2-saturated 0.1 M $HClO_4$. f) EC-TER spectra of FePc/Au(111) at 0.7 V and 0.4 V *vs.* RHE (black and blue) and H_2Pc at 0.7 V *vs*. RHE (green) in aerated 0.1 M $HClO_4$. The blue spectrum was acquired after 15 min of potential hold at 0.4 V *vs*. RHE in aerated solution. Note that after personal communication with the corresponding author of Ref. [111], it was found that electrode potentials were incorrectly reported versus Ag in the original reference. They are here correctly reported *vs*. RHE. g) Calculated geometry and displacement vectors (red arrows) for the H_2Pc vibration at 724 cm^{-1}. Figures a, b and c, reproduced with permission from Ref. [106]. Copyright [2005] Elsevier. Figures d, e, f and g, reproduced with permission from Ref. [111]. Copyright [2019] American Chemical Society.

Interestingly, the durability in O_2-rich acidic medium of the simplest Fe phthalocyanine was however improved significantly for a FePc with diphenylphentioether peripheral groups. [172] These bulky and out-of-plane electron-donating groups modify not only the electric charge distribution in the macrocycle but also provide a high degree of steric hindrance. [173] This might possibly prevent the protons from easily accessing the N_4 cavity during ORR, slowing down the demetalation rate. While the underlying reason for the improved durability is yet unclear, it may provide bottom-up explorative approaches for improved durability of Fe-N_x sites.

While many studies checked and/or focused on the load/stability of pyrolyzed Metal-N-C materials in acidic solutions saturated in inert gas, [21, 121, 140, 153] very few investigated load/durability in acidic solutions saturated in O_2. The historical reason is that AST in (R)RDE had been defined for PGM-based/C catalysts, for which the main degradation mechanisms are

not related to the presence of O_2 and the occurrence of ORR, but mainly related to dissolution/reprecipitation of the metal NPs and particle agglomeration. [174]

Regarding pyrolyzed Metal-N-C materials, perhaps the most striking evidence that their degradation mechanism in acidic medium differs between inert-gas and O_2 saturation may be found in our recent work. [70] We showed that the same load cycling protocol ([0.6 V – 1.0 V *vs.* RHE – 3s/3s – 10k – 80°C]) in Ar-saturated (Ar-LC) or O_2-saturated (O_2-LC) applied to a Fe-N-C catalyst derived from ZIF-8 material and comprising only Fe-N_x sites (labelled $Fe_{0.5}$RP, and previously discussed in **section 2.2.1** and **section 2.3.1**) resulted in a 4-fold higher ORR activity loss with O_2- (O_2-LC) *vs.* Ar (Ar-LC) saturation of a pH 1 electrolyte (**Figure 15a**). By combining information obtained from cyclic voltammetry, nitrite stripping, transmission electron microscopy (TEM), Raman and EDXS spectroscopies, the main reasons for this difference were identified. Nitrite stripping showed an unexpected increase in the ASD after O_2-LC (**Figure 15b**), in contrast with the strong ORR activity decrease. Characterization of the Fe-N-C AL after O_2-LC by TEM (**Figure 15d**), XRD and Raman spectroscopy showed the presence of nanometric Fe-oxide particles that formed from the reprecipitation of Fe cations leached from Fe-N_x sites. Nitrite stripping on a control Fe_2O_3/N-C material revealed that this technique not only senses surface Fe-N_x sites but also Fe-oxides. The increased ASD by nitrite stripping observed after O_2-LC therefore only indicated that a higher number of Fe atoms were exposed on the surface after O_2-LC, but not only in the form of Fe-N_x sites. This implies that the SD number obtained from nitrite stripping overestimated in this case the number of Fe-N_x sites, and also that the average TOF derived from that SD-value underestimated the TOF of Fe-N_x sites remaining after O_2-LC (**Figure 15c**). A comparison of Raman spectroscopy and CVs before and after O_2-LC (**Figure 15e-f**) supported the occurrence of COR. In particular, the Raman spectrum after O_2-LC was very similar to that observed after 500 cycles of 1.0/1.5 V *vs.* RHE, conditions known to lead to COR (**Figure 15f**). This unexpected carbon corrosion during O_2-LC in turn explained how a higher SD value could be detected after O_2-LC by nitrite stripping: COR resulted not only in the destruction of initially surface-exposed Fe-N_x sites (re-precipitating as Fe-oxides) but also in the formation of a new carbon surface and the exposure (and attack) of Fe-N_x sites that were initially not surface-exposed.

The sensitivity of the COR occurring during O_2-LC to the temperature, the UPL and LPL limits applied during the AST was investigated. Similar ORR activity loss was observed after O_2-LC at 25°C and 80°C, and also for square cycles of 0.3-0.7 V and 0.6-1.0 V. This is in strong contrast with expected effects of temperature and potential for classical electrochemical COR. In particular, an increase in temperature from 25 to 80°C is known to increase the rate of classical COR by a factor x20 to x40. [141, 175] H_2O_2 formed *via* ORR during O_2-LC seemed to play a key role in this special carbon corrosion mechanism, since lower loadings (thinner layers) of $Fe_{0.5}$RP resulted in a mitigated loss of ORR activity, which was assigned to the lower residence time of H_2O_2 in thinner layers in an RDE setup. We hypothesized that H_2O_2 and/or ROS formed from H_2O_2 and Fe (Fe-N_x sites or Fe oxides) are responsible for carbon corrosion at such low potential, which we named as ROS-induced carbon corrosion. [70] We note that while being low, these potentials are still above the thermodynamic potential for COR (forming CO or CO_2 products). It will be important in the future to identify if this ROS-induced carbon corrosion also occurs in PEMFC and if it takes place only in dynamic mode (stepped or scanned potential) or also in steady-state mode (fixed potential or current density). Dynamic modes might perturb the passivating layer of surface oxides existing on carbon surfaces, favouring its attack by peroxide and/or ROS. Last, the study showed that the Fe cations leached from Fe-N_x sites

either re-precipitated as Fe-oxides (observed after O_2-LC at 80°C) or diffuse away in solution (observed after O_2-LC at 25°C). Low temperature usually applied in RDE setups may explain why Fe-oxide particles had typically not been observed as a degradation product of Fe-N_x sites previously. The temperature changes the Pourbaix diagram of Fe, with higher temperature broadening the stability domain of ferric oxides in acidic medium. [176]

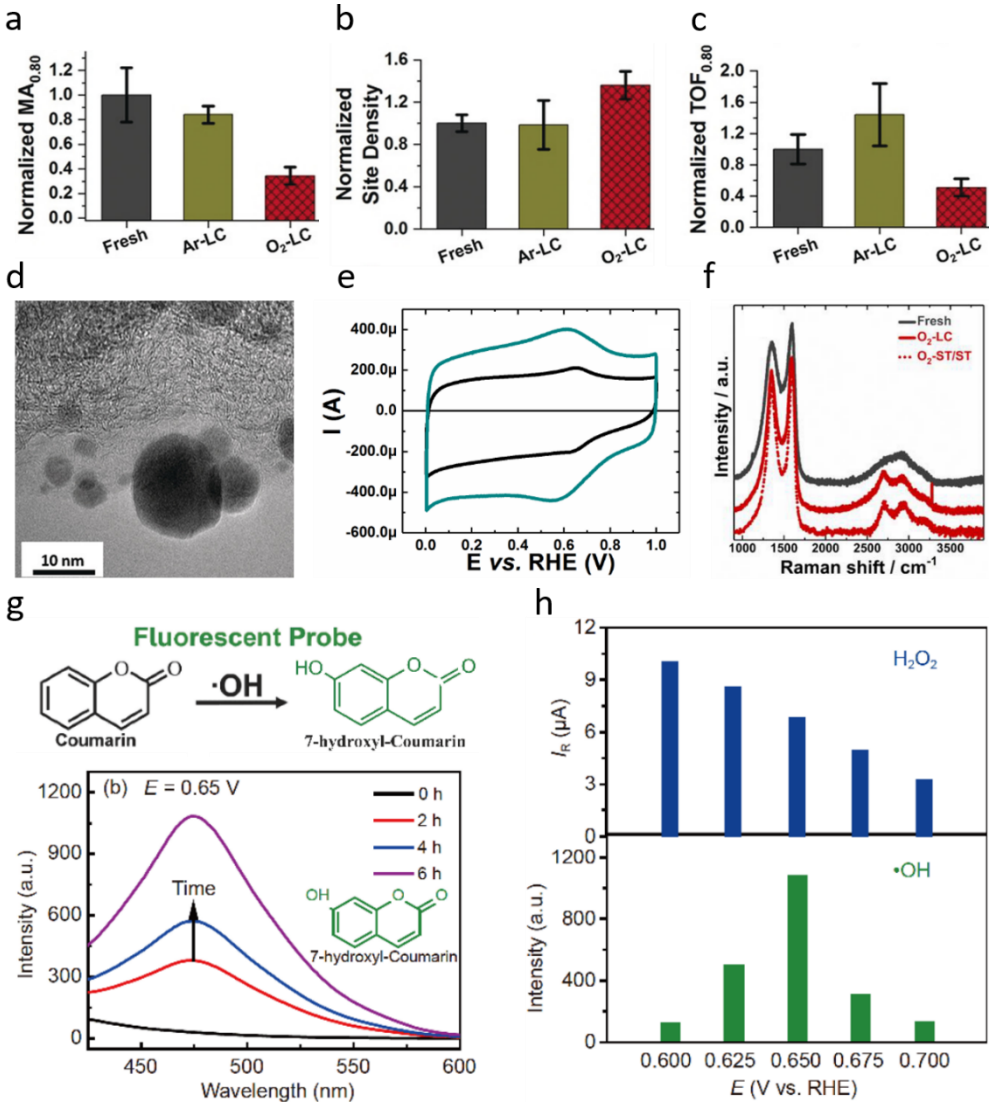

Figure 15. Effect of O_2 on the degradation of Fe-N-C catalysts. a-f) Effect of O_2 in degrading $Fe_{0.5}$RP during load cycling in pH 1 acidic solution. a) Mass activity at 0.8 V *vs.* RHE (normalized to the fresh Fe-N-C layer) for the fresh catalyst, after [0.6 V – 1.0 V *vs.* RHE – 3s/3s – 10k – 80°C] in Ar-saturated (Ar-LC) or O_2-saturated (O_2-LC) in 0.1 M H_2SO_4. b) Site density (normalized to the fresh Fe-N-C layer) measured by nitrite stripping. c) TOF (normalized to the fresh layer) obtained from the combination of ORR activity change at pH 5.2 before and after nitrite stripping and from SD values. d) TEM image after O_2-LC. e) Cyclic voltammograms obtained at 10 mV s^{-1} before (black) and after (cyan) O_2-LC at 80°C. f) Raman spectra for the fresh layer (grey), after O_2-LC (solid red) and after start-stop [1.0 – 1.5 V *vs.* RHE – 3s/3s – 0.5 k – O_2 – 80°C] in 0.1 M H_2SO_4 (dotted red). g-h) Effect of potential on the rate of •OH radical production during ORR catalysed by another Fe-N-C. g) Scheme for the conversion of non-fluorescent coumarin to fluorescent 7-hydroxyl-coumarin by •OH radical and fluorescence emission spectra of the solution with coumarin added immediately after ORR at 0.65 V *vs.* RHE, for different duration of ORR (see legend). The emission at 472 nm is characteristic for 7-hydroxyl-coumarin. h) Ring current measured in RRDE during ORR on the Fe-N-C working electrode for discrete values of potential (upper frame) and intensity of the 472 nm fluorescence signal from the solution after 6 h at each potential followed by addition of coumarin (lower frame). Figures a, b, c, d, e and f, reproduced with permission from Ref. [70]. Copyright [2020] Wiley. Figures g and h, reproduced with permission from Ref. [177]. Copyright [2020] Springer.

Different types of ROS formed *ex situ* by contacting Metal-N-C catalysts with H_2O_2 and produced *in operando* may be at the root of the different degradation mechanisms observed (*ex situ*: surface-restricted COR, no destruction of Metal-N_x sites; load cycling in oxygenated acidic electrolyte: carbon corrosion and destruction of a significant fraction of Fe-N_X sites). The hydroxyl radical is in particular regarded as a more powerful oxidant than other ROS. [75] Probably the first example of detection of ROS immediately after ORR on a Fe-N-C material was recently reported by Chen *et al*. [177]. Potentiostatic holds in RDE were performed for 6 h in O_2 saturated 0.1 M H_2SO_4, followed by quick addition of coumarin as a fluorescence probe for $^{\bullet}$OH radicals and the acquisition of fluorescence emission spectra (**Figure 15g**). Increased intensity of the signal for 7-hydroxyl-coumarin with increasing duration of the potential hold at 0.65 V supported the continuous formation of $^{\bullet}$OH during ORR (**Figure 15g**). Control experiments in O_2-saturated 0.1 M H_2SO_4 but without ORR (at open circuit potential) and Ar-saturated 0.1 M H_2SO_4 at 0.65 V confirmed the tight connection between the detection of 7-hydroxyl-coumarin and the ORR on Fe-N-C. Then, the effect of the potential value on the intensity of the signal for 7-hydroxyl-coumarin was recorded, identifying that 0.65 V resulted in the most intense signal for 7-hydroxyl-coumarin for potentials in the range 0.6-0.7 V (**Figure 15h**, lower frame).

2.6.2 Studies in PEMFC

Ferrandon *et al.* [65] studied the durability in PEMFC of a Fe-N-C derived from PANI, for which the synthesis had been previously optimized [178] and the durability in PEMFC of one of the most promising among Fe-N-C materials thus far. [64] Losses in the ORR kinetics were more pronounced after [0.6 V – 100 h – 100 % O_2 – 80°C] than after [0.4 V – 100 h – 100 % O_2 – 80°C] (**Figure 16a-b**), but in contrast the mass-transport properties improved after the 0.6 V hold, leading to even higher current density after the durability test than before at cell voltages < 0.45 V. The authors assigned this effect to the leaching of Fe spectator species (in particular Fe sulphide), improving the accessibility of the Fe-based active sites remaining after the test. The material had been previously shown by *ex situ* XANES to comprise a multitude of Fe species, and this was verified with the fresh MEA (**Figure 16c**, white columns). The linear combination fitting (LCF) of XANES spectra with a library of Fe compounds and combined with the total Fe content by ICP-MS resulted in the absolute wt. % for each type of Fe. The Fe compounds corresponding to the porphyrazin, pyridinic and pyrrolic labels are shown in **Figure 16d**, while the other labels are self-explanatory. The metallic Fe, Fe_3C and sulphide as well as organometallic Fe components disappeared after both PEMFC durability tests, but are considered merely as ORR inactive species in this Fe-N-C, due to the presence of Fe-N_x sites represented by the porphyrazin, pyridinic and pyrrolic components. Focusing on these, a dramatic drop is observed between the fresh and the operated MEAs for the pyrrolic component, and a relative drop for the pyridinic component. This suggests that these two components are related to the ORR activity. However, both the pyridinic and pyrrolic components are present in slightly smaller quantities after the 0.4 V hold compared to after the 0.6 V hold, in contradiction with the trend of ORR activity loss. The LCF analysis of XANES spectra for such a complex material is however not free of imperfections, in particular due to the strong analogy of XANES spectra between Fe nano oxides and Fe-N_4 sites, as shown later in **section 5.2**.

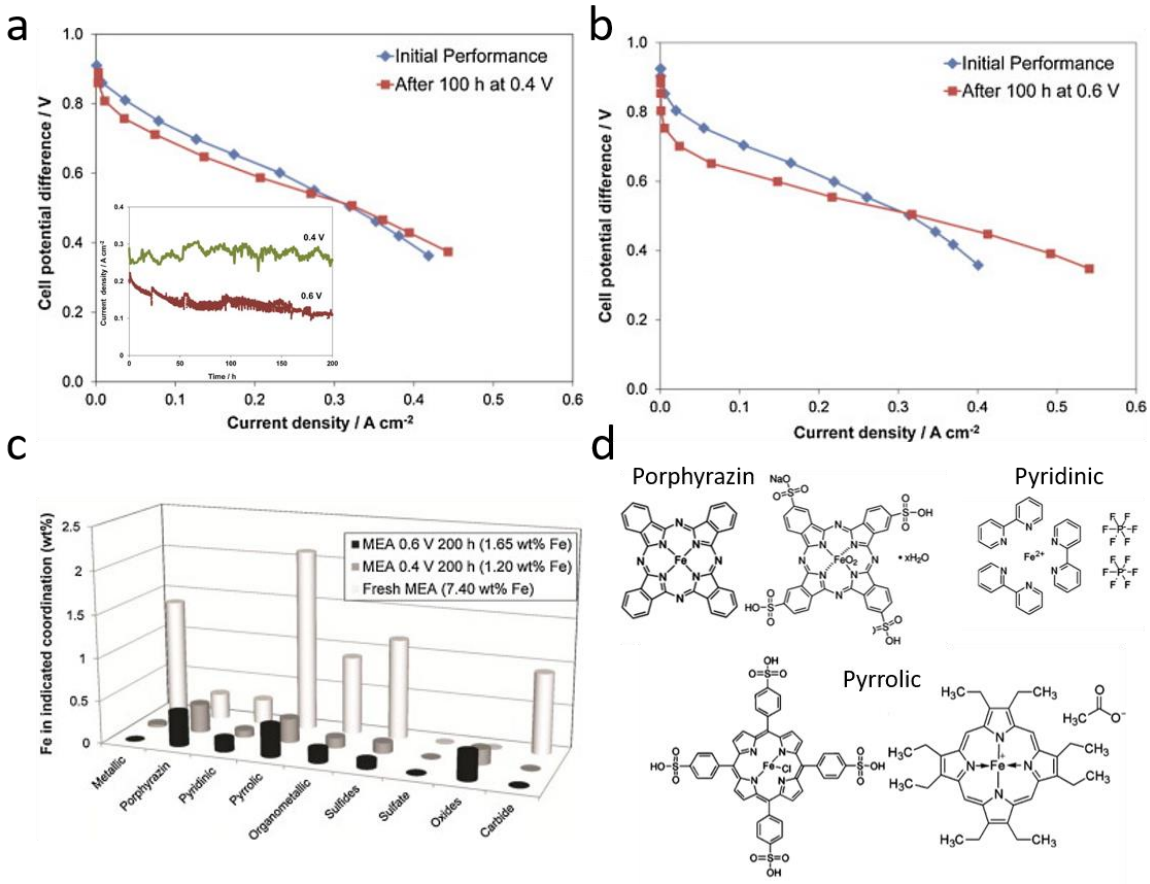

Figure 16. Durability and Fe speciation changes by XANES after PEMFC operation for a PANI-derived Fe-N-C cathode with multidunous Fe structures. H_2/air polarisation curves before and after a) [0.4 V – 100 h – 100 % O_2 – 80°C] and b) [0.6 V – 100 h – 100 % O_2 – 80°C]. The inset in a) shows the current density *vs.* time curves during 200 h holds at 0.4 and 0.6 V. c) absolute weight % of Fe for each type of Fe coordination for the fresh MEA and for MEAs after [0.4 V – 200 h – 100 % O_2 – 80°C] or [0.6 V – 200 h – 100 % O_2 – 80°C] d) the Fe compounds corresponding to the porphyrazin, pyridinic and pyrrolic labels. Figures a and b, reproduced with permission from Ref. [65]. Copyright [2013] Elsevier. Figures c and d, reproduced with permission from Ref. [178]. Copyright [2012] American Chemical Society.

Clear evidence for the destruction of Fe-N_x sites during the first 50 h of PEMFC operation of Fe-N-C cathodes was reported by Chenitz *et al.* [93] from EoT ^{57}Fe Mössbauer spectroscopy. The authors investigated the durability in operating PEMFC of a Fe-N-C catalyst prepared *via* NH_3 pyrolysis, previously known to be initially highly active but with fast degradation rate during the first 50 h of operation. [25] To investigate the durability as a function of the operating voltage, a voltage hold for 25 h was followed by a polarisation curve (lasting < 1 h), and this was repeated five times applying the same voltage for each of the 25 h segments, as exemplified in **Figure 17a** for 800 mV hold. This protocol allows extracting the value of current density at any point of the polarisation curves and plotting it *vs.* the duration of operation at 800 mV. To look into the ORR kinetics, reporting the current density at 0.8 V in the polarisation curves (*j* at 0.8 V) is usually chosen for PGM-free catalysts, and the plot of this scalar *vs.* time of operation at 800 mV is shown in **Figure 17b** (orange curve). Repeating the same protocol for other voltage holds (between 800 and 200 mV), the set of curves shown in **Figure 17b** was obtained. The figure shows that the rate of ORR activity loss of the Fe-N-C cathode during the first 125 h is quite independent of the voltage applied, even if the 400 and 500 mV holds seem to have degraded the performance a bit more compared to lower and higher voltages. From this, the authors concluded that COR (either COR, directly related to the voltage applied, or

restricted surface oxidation *via* Fenton reactions, more tightly related to the current density produced during operation) could be excluded as a main degradation mechanism of this Fe-N-C cathode during the first 125 h. Lack of extensive COR was supported by similar CVs in H_2/N_2 before and after PEMFC operation.

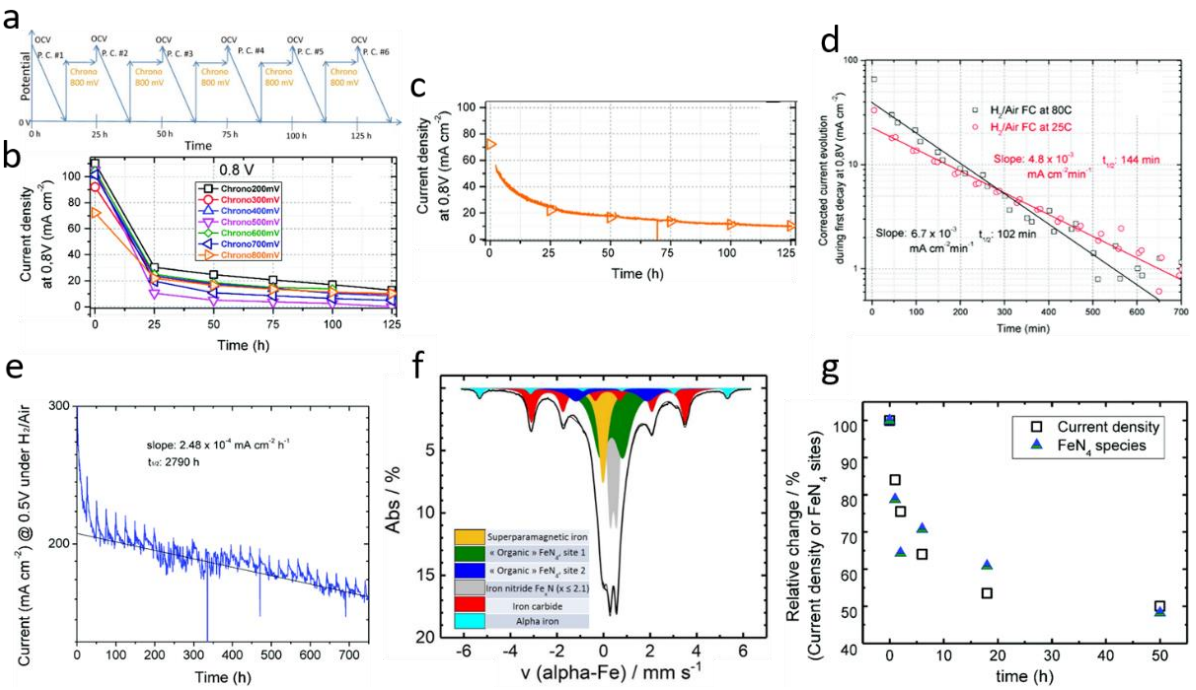

Figure 17. Durability and Fe speciation changes by Mössbauer spectroscopy after PEMFC operation for a ZIF-8 derived Fe-N-C cathode with multidunous Fe structures. a) Test protocol alternating fast polarisation curves and 5 potential holds at a fixed voltage (800 mV shown here). The duration of the polarisation curve is exaggerated in the scheme. b) Current density at 0.8 V (read on each of the 6 polarisation curves acquired for each MEA) *vs*. time of operation at a fixed cell voltage (value indicated in the legend). c) Current density *vs*. time during a continuous chronoamperometry at 0.8 V (solid curve) and the match with the reads at 0.8 V on each of the polarisation curves acquired between each of the 5 voltage holds at 800 mV. d) Semi-logarithmic Y-plot of corrected current density (at 0.8 V) *vs*. time in Zone 1 (0-700 min) for a PEMFC operating in air at 25 (red) or 80°C (black). e) Semi-logarithmic Y-plot of density (at 0.5 V) *vs*. time with the exponential decay fitting in Zone 2 (50-700 h) for a PEMFC operating in air at 25°C. f) ^{57}Fe Mössbauer spectrum of as-prepared MEA. g) Relative changes of current density at 0.6 V and of the sum of the Mössbauer components D1 and D2 (green and blue doublets in f)) as a function of the duration in PEMFC at 0.6 V. Figures a, b, c, d, e, f and g, reproduced with permission from Ref. [93]. Copyright [2018] Royal Society of Chemistry.

From continuous current *vs.* time curves acquired during voltage holds, the authors identified a first (0-25 h) and second zone (> 25 h) (**Figure 17c**), each corresponding to an exponential decay of the ORR activity with time, but with different rates of decay (see also **section 2.1** on the double-exponential decay kinetics). In Zone 1, the rate of decay corresponds to a half-life time of *ca*. 140 min at 25°C while it is > 2000 h at 25°C in Zone 2 (**Figure 17d-e**). The loss of ORR activity in Zone 1 was shown to be related to the loss of Fe-N_x active sites by EoT ^{57}Fe Mössbauer spectroscopy. The spectrum of a fresh MEA is shown in **Figure 17f**, identifying two doublet components assigned to ORR-active Fe-N_4 sites (green and blue doublets) as well as four other components assigned to Fe nitride, carbide and metallic Fe species. The relative change in the amount of Fe-N_4 sites over 50 h operation in PEMFC strongly correlated with the relative change in current density at 0.6 V, supporting the claim that the main reason for the loss of performance during this timeframe was due to direct Fe-N_4 site demetalation, not triggered by carbon corrosion (similar to the one reported for Fe(II) phthalocyanine in

oxygenated acidic medium, see **section 2.2.1**). While the authors claimed that this demetalation is specific for Fe-N_4 sites hosted in micropores, a recent study comparing two Fe-N-C materials with different microporous surface area revealed Fe demetalation in both cases, although the extent of demetalation was stronger for the NH_3-pyrolyzed Fe-N-C (with higher basicity), highlighting the importance of surface basicity in addition to the microstructure. [179] No Mössbauer spectroscopy characterisation was performed after the slower degradation at longer time (Zone 2, > 50 h), so that it is unknown if a slower demetalation of remaining Fe-N_4 sites after 50 h occurred or if the degradation mechanism was entirely different.

The relative contributions of COR and of Fe demetallation to the overall PEMFC performance loss depend on its operative conditions, namely the nature of the cathode gas feed (air or N_2), the cathode potential value, and the duration of operation (the electrical charge passed). Ünsal *et al*. [180] recently presented an approach to differentiate and quantify the impact of different degradation mechanisms on the ORR activity loss. They combined four AST protocols entailing different cathode gas feeds, potential hold values and durations on a home-made prepared Fe-N-C catalyst comprising FeN_x sites and Fe@N-C particles. They obtained quantitative insights into deactivation losses related to ORR (H_2O_2-related effect) by comparing the results of [0.5 V – 1h – air – 80°C] and [0.5 V – 1h – N_2 – 80°C] AST protocols. Similarly, a [0.8 V – 1h – air – 80°C] ASTs allowed studying the PEMFC performance decay in a potential region where lesser extent of Fe-demetallation is expected (see Refs. [117, 118]). The authors showed that the relative contribution of COR and of Fe demetallation depend on the value of the potential hold, COR contributing more to the ORR activity loss than Fe-demetallation at a high (0.8 V) potential. The opposite trend was found after holding the potential at a low (0.5 V) value. It is also interesting to note that the ALs' mass transport properties worsened after ASTs using air at the cathode, and that the increase of the mass transport overpotential correlated with the extent of ORR activity loss in the kinetic region of the polarisation curve. These important results suggest that a lower density of triple-phase boundary active sites (the sites that are ionically, electronically and diffusion connected) leads to slower O_2 diffusion, in agreement with what was previously found for Pt-based/C catalysts. [181-183] Significant differences of ionomer in thin-film and bulk properties and/or increased interfacial resistance at the FeN_x/ionomer interface may account for the observed trend. [182] Last, the authors reported that H_2O_2-related instability does not depend on the operative voltage, but rather on the ORR charge, further underlining the pivotal role of H_2O_2 in the degradation of Fe-N-C catalysts.

Li *et al.* [103] investigated the durability of two Fe-N-C catalysts derived from ZIF-8 (one obtained *via* Ar pyrolysis and the other *via* NH_3 pyrolysis, labelled as $Fe_{0.5}$ and $Fe_{0.5}$-950, respectively), and that initially comprised Fe mainly as Fe-N_x sites. Fundamental insights were first obtained via *in situ* Mössbauer spectroscopy on $Fe_{0.5}$ (in H_2/N_2 PEMFC, *i.e.* no ORR) on the nature of the two different Fe-N_x sites leading to the doublet components commonly labelled as D1 and D2 in the Fe-N-C literature (see *e.g.* **Figure 17f**). Mössbauer spectra acquired *in situ* at different potentials revealed the potential-dependence of D1 (sub-labelled as D1H and D1L, for high and low potential) and the potential-independence of D2 (**Figure 18a-d**).

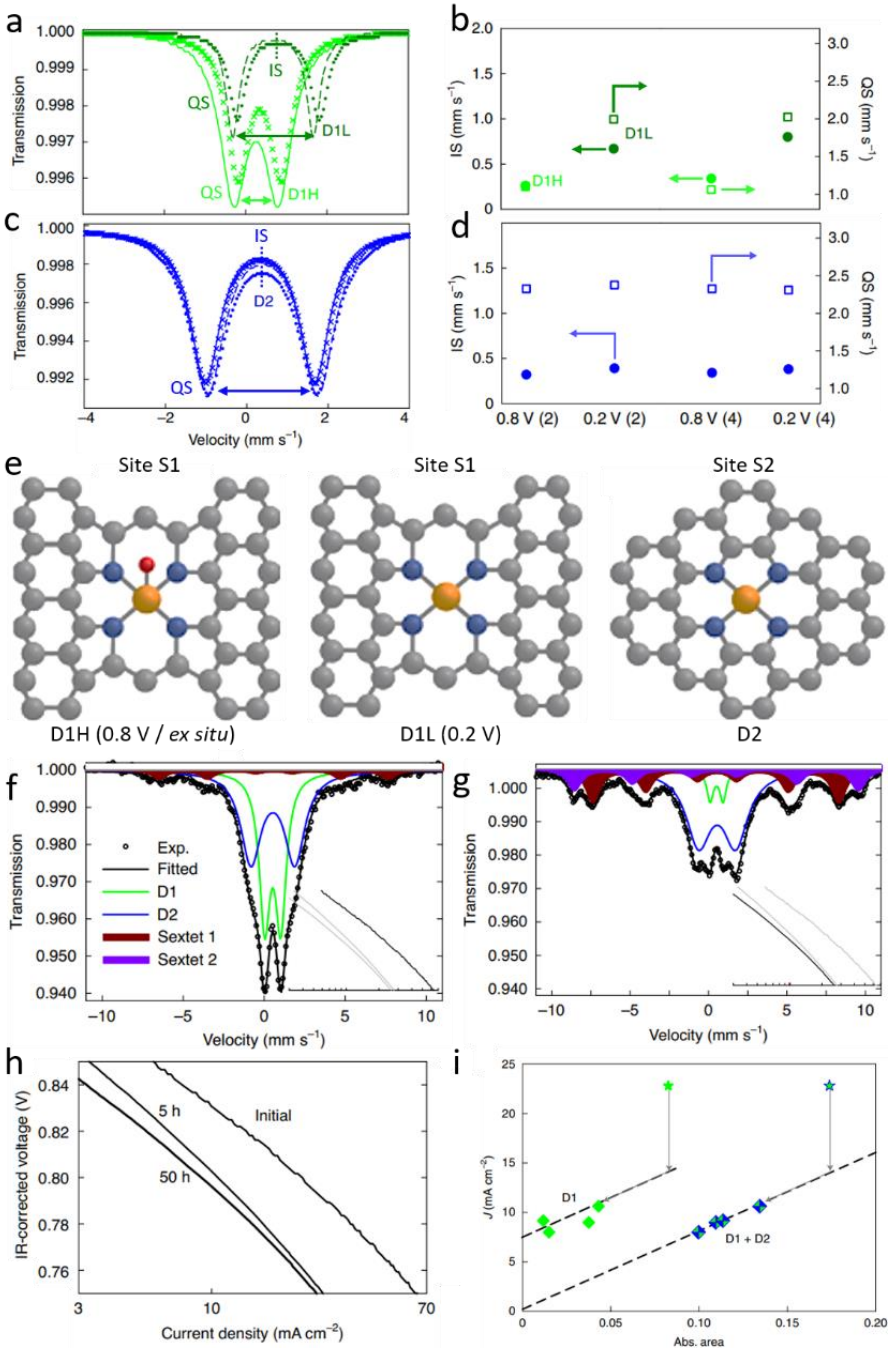

Figure 18. Different signature and durability of Fe-N_x sites S1 and S2 by *in situ* and EoT ^{57}Fe Mössbauer spectroscopy for a ZIF-8 derived $Fe_{0.5}$ cathode. a) Effect of electrochemical potential on fitted components from *in situ* ^{57}Fe Mössbauer spectroscopy in PEMFC for a) D1 and c) D2 at 0.8 V (2), 0.2 V (2), 0.8 V (4) and 0.2 V (4). The number in parentheses represents the cycle number; b) and d) show the corresponding IS and QS values of D1 (D1H and D1L) and D2. e) Scheme of sites S1 (with/without oxygenate adsorbate depending on potential) and S2. f) Mössbauer spectrum of pristine $Fe_{0.5}$ cathode. Mössbauer spectra after H_2/O_2 PEMFC operation at 80°C and 0.5 V for g) 50 h. The sextets are assigned to ferric oxides. h) Tafel plots of initial PEMFC polarisation curve and after 5 h and 50 h of operation at 0.5 V. The *ex situ* and all EoT Mössbauer spectra were acquired at -268 °C. i) The current density of $Fe_{0.5}$-cathodes at 0.8 V as a function of the absolute absorption area for D1 and D1+D2. The activity on the y-axis were obtained during the first polarisation curve (star) and after 5, 10, 25 or 50 h of operation at 0.5 V in H_2/O_2 PEMFC at 80°C (diamonds). The absolute absorption area of a given Mössbauer component on the *x*-axis is proportional to the number of corresponding sites in the cathode. Figures a, b, c, d, e, f, g, h and i, reproduced with permission from Ref. [103]. Copyright [2021] Springer Nature.

With the help of DFT applied to calculate the quadrupole splitting (QS) of different Fe-N_4 sites, D1 and D1H could be assigned to O-Fe(III)N_4C_{12} high-spin site, D1L to a Fe(II)N_4C_{12} high-spin site and D2 to a Fe(II)N_4C_{10} low or medium spin site. [103, 144] The reversible change with potential in N_2 environment between the Mössbauer spectroscopic signatures assigned to O-Fe(III)N_4C_{12} and Fe(II)N_4C_{12} (*i.e.* between D1H and D1L, **Figure 18a-b**) is triggered by the change of the Fe oxidation state at *ca.* 0.75 V *vs*. RHE. In summary, two Fe-N_x sites S1 and S2 were identified, with S1 being on the top surface (bound or not with an O-adsorbate as function of potential) and a site S2 that is either located in the bulk of the N-C matrix, or has less affinity to oxygen than S1. While *operando* Mössbauer spectroscopy in PEMFC (H_2/O_2) was then attempted, the long acquisition time (36 h) needed to record a single spectrum at a given voltage prevented its application, due to large changes in the amount and nature of Fe species during this period of operation, as shown earlier in **Figure 17g** for another Fe-N-C. EoT ^{57}Fe Mössbauer spectroscopy was therefore applied to study the fate of the two different sites S1 and S2 during PEMFC operation. The fittings indicate unmodified spectral parameters and absolute intensity for D2 with operation time, continuously decreasing signal intensity for D1 and continuously increasing signal intensity for the two sextets assigned to superparamagnetic ferric oxide (**Figure 18f-g**). The trend of decreased D1 intensity with PEMFC operation time was in line with decreased ORR activity with time (**Figure 18i**).

Quantitatively, the results reveal a linear correlation between the activity and the absolute amount of either D1 or (D1+D2) (**Figure 18i**). The data for the initial activity (star symbol) was an outlier, possibly due to a higher TOF of S1 sites during the first polarization curve, in line with recent work demonstrating decreased TOF of Fe-based sites by mild surface oxidation. [36] After 5 h of operation, a linear correlation between the overall ORR activity and either D1 or D1+D2 was observed. However, the extrapolation at x = 0 leads to a positive y-intercept, indicating significant ORR activity even in the absence of D1. The authors concluded from this that D2 also contributes to the ORR activity of $Fe_{0.5}$ cathode, and that D2 is the main contributor to ORR activity after 50 h operation in PEMFC. No changes in the carbon morphology of Fe-N-C were observed by Raman spectroscopy after potential hold at 0.5 V in H_2/O_2 PEMFC, in line with Raman results obtained for other Fe-N-C materials after potentiostatic holds at 0.6 V in H_2/air PEMFC by Chenitz *et al.* [93], potentiostatic hold at 0.2 V for a direct methanol fuel cell by Martinaiou *et al.* [184], and unchanged CV after potentiostatic hold at 0.4 V in H_2/O_2 by Chen *et al*. [185], but in stark contrast with COR observed after square-wave cycles of 0.6 V/1.0 V in O_2-saturated acid medium in RDE (see **section 2.6.1**). Potential cycling might accelerate carbon corrosion compared to voltage holds via the continuous removal of a passivating layer of oxygen functional groups and reformation of a new oxidized surface.

The same trends were observed by Li *et al*. [103] for the NH_3-pyrolyzed Fe-N-C ($Fe_{0.5}$-950) as for $Fe_{0.5}$, with strong decrease of D1 signal and unmodified D2 signal after 50 h H_2/O_2 PEMFC operation (**Figure 19a-b**). Minor differences were the presence of a higher amount of Fe oxides in the pristine $Fe_{0.5}$-950 cathode compared to the pristine $Fe_{0.5}$ cathode (compare **Figure 19a** and **Figure 18f**) and the much higher initial ORR activity of the $Fe_{0.5}$-950 cathode (compare **Figure 19c** and **Figure 18h**). The Fe oxide particles formed *operando* were nanometric (**Figure 19d**), with some match between Fe and F mapping in the aged cathode suggesting that Fe demetalation from Fe-N_4 sites and clustering into nano Fe oxide is linked to the presence of Nafion ionomer. [103]

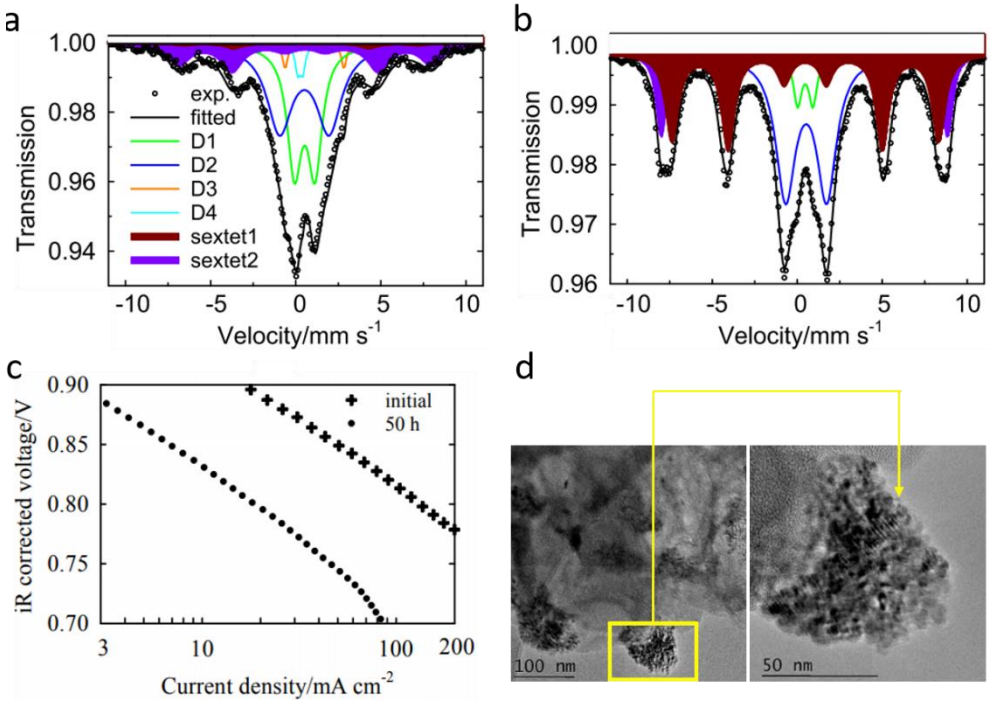

Figure 19. Different durability of Fe-N_x sites S1 and S2 by end-of-test ^{57}Fe Mössbauer spectroscopy for $Fe_{0.5}$-950 cathode derived from $Fe_{0.5}$ via NH_3 pyrolysis. a) Mössbauer spectrum of pristine $Fe_{0.5}$-950 cathode. b) Mössbauer spectrum after H_2/O_2 PEMFC operation at 80°C and 0.5 V for 50 h. The sextets are assigned to ferric oxides. c) Tafel plots of initial PEMFC polarisation curve and after 50 h of operation at 0.5 V. The Mössbauer spectra were acquired at -268 °C. d) TEM images of $Fe_{0.5}$-950 cathode after H_2/O_2 PEMFC operation at 80°C and 0.5 V for 50 h. Figures a, b, c, d, reproduced with permission from Ref. [103]. Copyright [2021] Springer Nature.

The results are in line with those of Chenitz *et al*. [93] for another NH_3-pyrolyzed Fe-N-C and indicate that demetalation from Fe-N_4 sites is a main degradation mechanism in *operando* PEMFC between 0 and 50 h operation. It however gives two important additional insights: i) the demetalation of Fe-N_4 sites is not specific to NH_3-pyrolyzed Fe-N-C catalysts and ii) the demetalation is seen only for S1 sites (located on top surface) but not at all for S2 sites (either located on top surface but with lower binding energy for O_2 than S1 sites, or not directly accessible by O_2). The data also shows that the exacerbated decrease of ORR activity in the first 50 h of operation for NH_3-pyrolyzed Fe-N-C *vs.* inert-gas pyrolyzed Fe-N-C is not due to a stronger fraction of S1 *vs*. S2 sites in the former, but to the higher TOF of S1 sites in NH_3-pyrolyzed Fe-N-C, at least during the initial polarisation curve. This higher TOF is likely due to the presence of highly basic nitrogen groups after NH_3-pyrolysis, expectedly with very short lifetime before their protonation and subsequent anion adsorption. The latter phenomenon had been shown to decrease the high ORR activity of NH_3-pyrolyzed Fe-N-C to the level of an inert-gas pyrolyzed Fe-N-C. [124] Proietti *et al.* [25] had shown that the current density at 0.5 V of an initially more active NH_3-pyrolyzed Fe-N-C decreased faster than its parent Ar-pyrolyzed Fe-N-C material, the two current *vs*. time curves meeting after *ca.* 15 h of operation at 0.5 V. This suggests that the activity decrease of NH_3-pyrolyzed Fe-N-C between 0 and 15 h of operation is the combined outcome of a parallel decrease in the TOF (which might be completed even during the first 1-2 h) and of the number of sites S1, while the activity decrease of inert-gas pyrolyzed Fe-N-C during that time period is less impacted by a decrease in the TOF, and more impacted by a decrease in the number of sites S1. After 15 h of operation and up to 50 h at least, the decrease in ORR activity is then mainly due to the decrease of the number of S1 sites *via* demetalation, both for inert-gas and NH_3-pyrolyzed Fe-N-C. We would also like to warn the reader that the above conclusions and the terminology of NH_3 or inert-gas-pyrolyzed Fe-N-C are related to the studies [80, 93] (both leaning on ZIF-8 and phenanthroline as common sacrificial precursors for the N-C matrix) and should not be regarded *stricto sensu*. For example, other syntheses of Fe-N-C not resorting to NH_3 gas during pyrolysis might result in a behaviour similar to that of NH_3-

pyrolyzed ZIF-8. Surface descriptors such as the basicity, the work function or the potential of zero charge of Fe-N-C should more precisely categorize a broad range of Fe-N-C materials than the phenomenological description of their synthesis. [18, 36, 124] Investigating the fate of nitrogen atoms, Garcia *et al.* [186] evidenced with N K-edge X-ray absorption spectroscopy (XAS) that pyridinic nitrogen coordinated to Fe was stable after load cycling in O_2-saturated 0.1 M $HClO_4$ RDE in acid medium, while the signal assigned to pyrrolic nitrogen coordinated to Fe was unstable. This result is in line with the D1 and D2 Mössbauer doublets assignments to unstable porphyrinic and stable pyridinic structures, in aerated acidic media, respectively. Interestingly, in alkaline media, both the pyrrolic and pyridinic N groups (coordinated to Fe) seemed stable.

Analogous to the study in RDE by Kumar *et al.* [70] where the effect of load cycling in N_2- or O_2-saturated medium was compared back-to-back for a given Fe-N-C. Osmieri *et al.* [71] investigated this effect for another Fe-N-C, but in PEMFC environment. While very small activity and performance loss was observed after [0.60 – 0.95 V – 3s/3s – 30k – N_2 – 80°C] (as previously discussed in **section 2.2.2**), the same load cycling but with an air-fed cathode resulted in a dramatic loss of activity and overall performance (compare **Figure 20a** and **Figure 20b**). This is further supported in **Figure 20c**, showing that a H_2/air polarisation curve recorded just before the next set of AST in N_2 is superimposed with the first H_2/air polarisation curve recorded after that set of AST in N_2 (*e.g.* see the superimposed 10k + polarization curve and 20k curves in **Figure 20c**). This implies that no measurable loss of ORR activity occurred during each additional 10k cycles in N_2. The polarisation curve was negatively shifted at 0.5 $A \cdot cm^{-2}$ by 200 mV after 30k load cycles in air. Breakdown of possible sources of performance decrease (kinetic, Ohmic, mass-transport) by EIS and analytical mathematical model of EIS and steady-state polarization curves showed that the vast majority of the performance loss during load cycling in air could be assigned to kinetic loss. Cyclic voltammetry showed a significant increase in capacitance from 250 to 350 mF cm^{-2} after 30k load cycles in air but restricted increase from 200 to 230 mF cm^{-2} after 30k load cycles in N_2. On the basis of unmodified proton and electronic resistance identified by EIS in N_2, the authors assigned the increased capacitance to increased density of oxygen functional groups on the surface of carbon (pseudo-capacitance, supported by the appearance of broad peaks in the CV) and not to COR. Raman spectroscopy or other characterization of the carbon phase after the ageing was however not reported, and it cannot be definitely excluded that some COR occurred. The introduction of oxygen functional groups should also have decreased the TOF of the Fe-N_x sites that survived the air/load cycle protocol, according to the study by Choi *et al*. [36]. The total Fe content in the cathode AL was measured before and after the various AST load cycles, identifying a decrease from 0.09 to 0.04 at. % Fe after 30k load cycles in N_2, and a higher decrease from 0.09 to 0.01 at. % Fe after 30k load cycles in air. Overall, the decrease in ORR kinetics (increased overpotential, $\Delta\eta_c$) correlated with the increased (pseudo)capacitance (ΔC) and increased loss in Fe content (**Figure 20d**). HAADF-STEM images of the cathode before and after load cycling revealed only single metal atoms (*i.e.* probably Fe-N_x sites), but in lower number after 30k load cycles in air than in N_2. This is in contrast with the report from [80] where the decrease of Fe-N_x sites during operation in PEMFC resulted in the appearance of nano Fe-oxides. The different observation by Osmieri *et al.* [71] may be due to different experimental conditions, resulting in different local electrochemical environment. Indeed, despite same duration (50 h), the local pH was probably higher in the AST of Li *et al.* [103] ([0.5 V – 50 h – O_2 – 80°C]) compared to that performed by Osmieri ([0.60 – 0.95 V – 3s/3s – 30k – air – 80°C]), thereby facilitating the precipitation of the Fe ions released in solution. The different pore structure and/or morphology of Fe-N-C catalysts or AL may also account for the observed differences. In

particular, the Nafion/catalyst ratio in the cathode AL may be a key parameter for the fate of leached Fe cations in PEMFC, and one can note that much higher ionomer content was used by Li *et al.* [103] (Nafion/catalyst mass ratio 1.5, *i.e*. 60 wt. % ionomer) than by Osmieri *et al.* [71] (35 wt. % ionomer).

In summary for **section 2.6**, the occurrence of ORR in acid medium leads to structural changes of Fe-N-C materials and loss of ORR activity, that are little or not observed when applying the same electrochemical protocol but without O_2. A significant fraction of Fe-N_x sites is destroyed, and bulk carbon corrosion can be observed in some cases, even after operation at electrochemical potentials where bulk COR would not be expected. The fate of Fe cations that left the Fe-N_x sites depends on the temperature and ionomer/catalyst interfacing, iron either being leached out in the electrolyte (RDE) or in the exhaust water (PEMFC), or reprecipitating as iron oxide in the cathode layer. From *post mortem* Mössbauer spectroscopy characterisation, the Fe-N_4 site S2 is found to be more durable than the Fe-N_4 site S1. Interconnected with this, pyridinic nitrogen atoms seem to be more stable than pyrrolic nitrogen atoms during O_2-LC protocols. In addition to decreased site density after O_2-LC, it is likely that the TOF of remaining Fe-N_x sites also decreased.

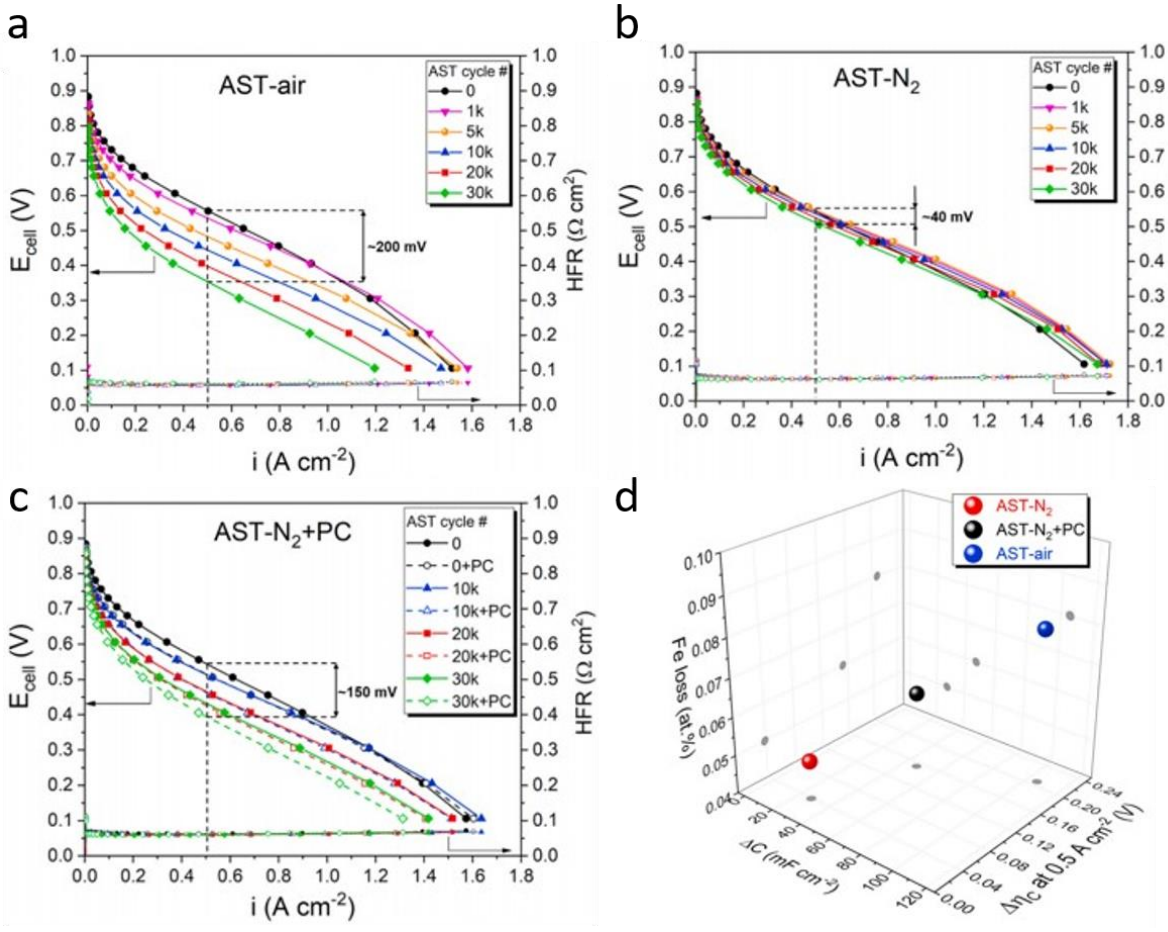

Figure 20. H_2/air polarisation curves for a Fe-N-C cathode comprising Fe-N_x sites, before and after various load-cycling AST conditions in PEMFC. a) 0.60 – 0.95 V potential steps AST with cathode under air atmosphere. Note that the AST was interrupted periodically to monitor the polarisation curves (during which ORR occurs at the cathode) after 10k, 20k and 30k cycles in N_2. b) Same as a) except that N_2 is fed constantly at the cathode, both during polarisation curve acquisition and during the potential steps AST. c) 0.60-0.95 V stepped potential AST with cathode under N_2 atmosphere, interspersed with 15 polarisation curves in different conditions (during which ORR occurs at the cathode) after 10k, 20k and 30k cycles in N_2. d) Correlations between increased kinetic

overpotential ($\Delta\eta_c$), increased (pseudo)capacitance (ΔC) and decreased Fe content after 30k load cycles in three different modes. Figures a, b, c and d, reproduced with permission from Ref. [71]. Copyright [2020] Elsevier

2.7 Charge- and mass-transport losses

While the previous sections discussed i) mechanisms related to the atomistic degradation or modification of the ORR active centres, or focused on ii) the implications on the active centres of degradation mechanisms, the present section shortly discusses other negative effects occurring during the operation of PGM-free cathodes, beside the decreased ORR kinetics. We focus here on charge- and mass-transport losses observed after load/durability testing in PEMFC. The negative effects of SU/SD-AST on the transport losses in PEMFC environment are however not discussed, since such AST lead to very fast performance loss and will have to be avoided by system and/or material approaches for any practical implementation of PGM-free layers. Perhaps the most striking example that not only ORR kinetics but also transport properties of a PGM-free cathode steer the initial PEMFC power performance and its evolution with operating time was reported by Ferrandon *et al*. [65] In this special case, the ORR activity was shown to decrease with operating time, but the transport properties of the AL improved in parallel (**Figure 16a-b**). This led to a crossing point between the beginning-of-test (BoT) and EoT polarisation curves at *ca.* 0.4 V, also resulting in unmodified current density with time when the cell was operated for hundreds of hours at 0.4 V (**Figure 16a**).

2.7.1 Water management and related O_2 transport

The flooding of different types of pores in the cathode of PGM-free layers has historically been regarded as a likely phenomenon for their poor performance in the high current density region of the polarization curve, and also for the decrease in performance over time. Metal-N-C layers are particularly prone to flooding due to i) thick ALs of 70-100 µm compared to Pt/C layers, ii) the presence of a significant amount of micropores (and in some cases only or predominantly micropores) in highly-active Metal-N-C materials and the generally accepted presence of some of the Metal-N_x sites in such micropores. A positive correlation between initial ORR activity and power performance in PEMFC and the micropore surface area of Metal-N-C has been established for a broad set of materials, but unfortunately another positive correlation links the rate of performance loss *vs*. time with the microporous surface area. [11] Enhanced flooding with operation time may be assigned to changes in the wettability of the carbon surface, which may be an outcome of surface oxidation, *e.g.* by ROS species. Increased hydrophilicity of the carbon surface is generally expected with increasing number of oxygen functional groups. [187]

A special type of flooding was recently the centre of a debate in the field of Fe-N-C catalysts, namely micropore flooding. Zhang *et al.* [67] initially proposed that micropore flooding is the main reason for the decrease of ORR activity and of power performance with time for a highly microporous Fe-N-C (derived from ZIF-8 *via* NH_3 pyrolysis), and not due to the loss of Fe-based active sites. This conclusion was derived from the similar relative trends of ORR activity and power performance loss (after normalization to their initial power or activity performance) observed for samples with very different Fe contents. The authors proposed that the high initial activity is due to initially hydrophobic micropores, allowing for fast access of O_2 *via* gas phase to the Fe-N_x active sites located in such pores. During operation, the carbon surface in the micropores might be populated with oxygen functional groups, triggering the flooding of the micropores and reduced accessibility to O_2. The measurement of carbon electrooxidation in H_2/N_2 configuration of the MEA showed an onset of electrochemical COR at *ca.* 0.5 V, giving

some support to the proposed mechanism. However, no EoT characterization had been reported to demonstrate that no Fe-based sites were lost. The mechanism of micropore flooding initially proposed by Dodelet's group was further investigated by Choi *et al.* and then by a second study from Dodelet's group. [67, 188] Choi *et al.* [188] first discussed what the initial state of humidification of micropores might be in a Fe-N-C layer, and came to the conclusion that the fully dry hypothesis of micropores proposed by Zhang et *al.* [67] is not in line with experimental observations. For fully dry micropores (case 1 in **Figure 21a**), Fe-N_x sites located in dry micropores cannot participate in the ORR because there is then no accessibility for protons, needed for the ORR. The lack of path for protons also prevents the COR, and thus the micropore would remain hydrophobic and free of water during operation, also preventing the Fe-N_x sites located herein to participate in the ORR. The authors concluded that the only two possibilities for the initial state of micropores is either "surface wetted" (case 2 in **Figure 21a**) or flooded. Case 2 holds the benefit of allowing fast O_2 access via gas-phase diffusion and some access for protons to the Fe-N_x sites located in micropores. It is then conceivable that a switch from surface-wetted micropores to flooded micropores, as a negative outcome of PEMFC operation, might drastically decrease the mass transport performance of highly microporous Fe-N-C layers. BoT PEMFC polarisation curves at 100 and 60 % RH in O_2 and air did however not result in improved mass-transport performance at lower RH, which would likely be expected for case 2. The electrochemical capacitance value measured with H_2/N_2 configuration of the MEA supported that the microporous surface area contributed to the capacitive current, in turn supporting that the state of the micropores at BoT corresponds either to the case 2 or to flooded situation. Distinguishing between these two hypotheses cannot be achieved with cyclic voltammetry since in both cases, the electrochemical surface area is the same. Instead, analysis of mass transport losses before and after PEMFC operation was undertaken. The PEMFC was operated for 4 h at 0.4 V with H_2/Air and the polarisation curves before and after the short durability test compared, with air cathode feed (**Figure 21b**). [188] The results show that a major kinetic loss occurred, which cannot be explained by a switch from surface-wetted to flooded micropores. Moreover, the mass-transport properties do not appear worse after the durability test, and even seem to be slightly improved in the air-fed EoT polarisation curve (**Figure 21b**). These results clearly demonstrate that micropore flooding is not the reason for decreased power performance during PEMFC operation of microporous Fe-N-C. This was also supported by the lack of improvement after drying the MEA by feeding dry gases while keeping the cell at 80°C for 5 h (**Figure 21b**). Choi *et al.* [188] concluded that the micropores are likely flooded already at BoT. These two papers were then followed by a second study from Dodelet's group on their NH_3-pyrolyzed Fe-N-C, agreeing with the above conclusion from Choi *et al.* [188] that the performance loss cannot be due to micropore flooding, and showing that the rate of performance loss was largely independent of the applied voltage during the PEMFC durability test. From EoT Mössbauer spectroscopy, the loss of Fe-N_x sites via demetalation was demonstrated, as discussed in **section 2.6.2**.

While micropore flooding is no longer considered an issue for the durability of Metal-N-C layers, the water management in the cathode AL as a whole still is. Tracking differences in water management and meso- or macropore flooding in the AL is however very challenging, with very few studies having attempted achieving this. Water retention curves combined with micro- and nano-X-ray computed tomography *ex situ* analysis for a fresh Fe-N-C AL were reported for example by Normile *et al*. [189]. *Operando* micro X-ray computed tomography has also been applied with a specifically designed PEMFC to investigate the location and content of liquid water in *operando* at BoT for different Fe-N-C materials. [189-191] Such methodology has

not yet been applied to Metal-N-C cathodes aged in PEMFC in order to identify whether or not changes in wettability occurred during operation. Very recently, neutron imaging has allowed assessing the water content in *operando* PEMFC through the MEA including a Fe-N-C cathode, easily differentiating the membrane and GDLs, and even the cathode AL (**Figure 21c-d**). [192] The results showed higher water content in a PANI-derived Fe-N-C cathode than in a Pt/C cathode under otherwise identical operating conditions. While this shows that BoT polarization curves with Metal-N-C ALs can be limited by water flooding in some specific pores or locations in the cathode (essentially causing O_2 mass-transport limitations), there is as yet no convincing experimental evidence that the poor durability of Metal-N-C cathodes in operating PEMFC has anything to do with changes in cathode wettability with operating time, concurring with the conclusion in Ref. [191] Several attempts to recover the performance of Fe-N-C ALs after operation by drying-out methods before restarting the cell did not lead to any performance recovery. [185, 188]

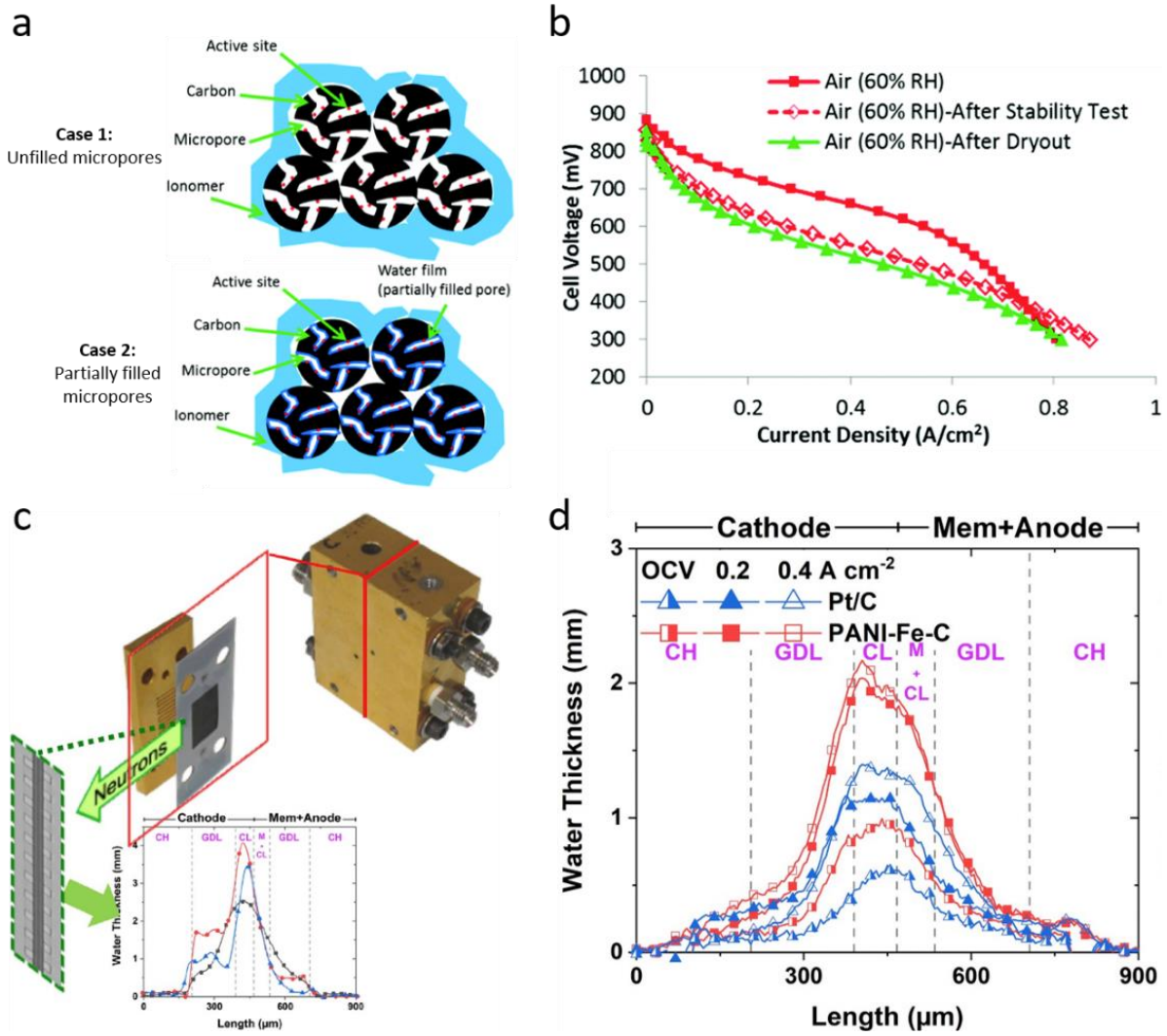

Figure 21. Nano and macroscale water flooding concerns in Fe-N-C ALs. a) Scheme for two possible cases of micropores (pore width ≤ 2 nm) in Fe-N-C catalyst at beginning-of-test, besides the case 3 of complete water flooding. [188] b) H_2/air PEMFC polarisation curves with a Fe-N-C cathode before and after a 4 h hold at 0.4 V, and also after drying-out process following the durability test. [188] c) Neutron imaging hardware and setup. [192] d) Water thickness profiles through the MEA measured by neutron imaging for MEAs with Pt/C and PANI-Fe-C cathodes, at OCV, 0.2 and 0.4 A·cm^{-2} at 50 % RH. [192] Figures a and b, reproduced with permission from Ref. [188]. Copyright [2017] Royal Society of Chemistry. Figures c and d, reproduced with permission from Ref. [192]. Copyright [2020] Elsevier.

2.7.2 Proton conductivity in the cathode active layer

Due to the thick cathode layers currently needed to maximize ORR activity and also power performance in PEMFC with Metal-N-C cathodes, the conduction of protons and perhaps, in specific cases or after severe aging, of electrons, may be an issue. Proton conduction may be limiting already the BoT performance, but could be further limiting after durability testing due to localized ionomer degradation in the cathode if ROS are produced in large quantities by PGM-free active sites, or via cationic exchange of protons by transition metal cations as a result of their leaching from Metal-N-C. These two mechanisms may also expand to some extent in the PEM, not only being restricted to the cathode AL.

Chen *et al.* [185] investigated the durability in PEMFC of a Fe-N-C prepared from nano-ZIF-8. In addition to the commonly observed drop in kinetic activity during operation, the authors observed a continuous increase of the HFR with operation time, from 70 $m\Omega \cdot cm^2$ initially to 108 $m\Omega \cdot cm^2$ after 20 h operation at 0.4 V in H_2/O_2 PEMFC (**Figure 22a**). Fe contamination in the middle of the PEM was observed *ex situ* after the test (**Figure 22b**), while EIS in N_2/H_2 configuration was performed to evaluate the proton conductivity inside the cathode layer (**Figure 22c**). The data confirmed the increase in HFR after testing (assigned to Fe contamination of the PEM) but also revealed an extended 45° line at high frequency and increased real part of the impedance at low frequency after testing, revealing that the proton conductivity in the cathode layer decreased. This was also probably due to Fe contamination and also, perhaps, due to ionomer degradation by ROS. According to theory for a perfect capacitive behaviour of porous electrodes and taking into account proton conduction through the electrode, the difference between the real part of the impedance of the vertical line that should be seen at low frequency and the HFR value should be equal to $L/(3\sigma_{eff})$, where L is the AL thickness and σ_{eff} the effective proton conductivity (assumed uniform through the layer). [142] While no clear vertical line is observed, possibly due to uneven ionomer distribution through the layer and pore size distribution, [193] the data reported by Chen *et al.* [185] clearly suggests that the proton conductivity in the cathode layer decreased after the durability test. The origin of performance loss over the entire scale of current density was then analysed with a simple analytical mathematical model including a Tafel law for ORR, membrane resistance and proton resistance in the cathode layer. The outcome is shown in **Figure 22d**, revealing the prominent role of ORR activity loss but also of losses due to decreased proton conductivity in the cathode layer and in the PEM, playing a role at high current density. [185] While this effect will not necessarily take place for all Metal-N-C layers in PEMFC (not observed for example in the work of Osmieri *et al*. [71]), it is an effect worth taking into account. One must keep in mind also that for ZIF-8 derived catalysts, the residual amount of Zn after pyrolysis can be significant, Zn being present as atomically dispersed Zn-N_x sites. These may leach during PEMFC operation, contributing to a partial cationic exchange of protons by metal cations in the cathode AL and/or elsewhere in the MEA.

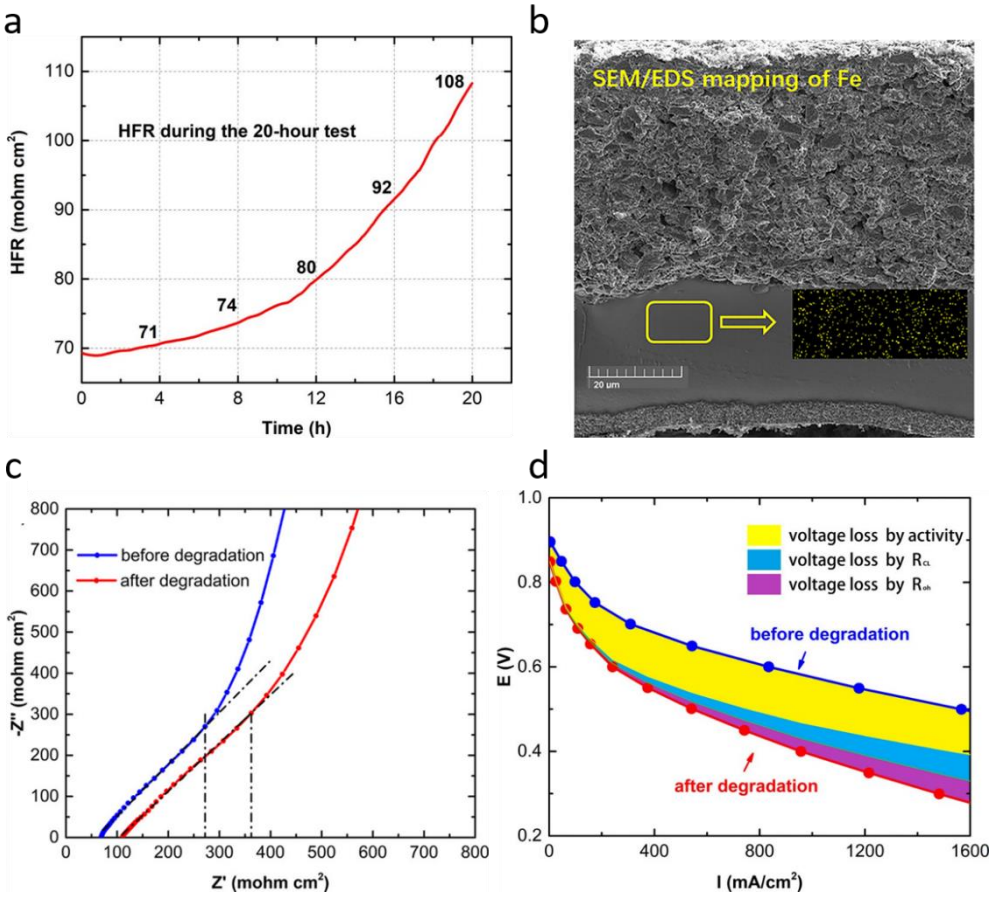

Figure 22. Effect of Fe contamination in the cathode layer and PEM during PEMFC operation. a) HFR value during the durability test at 0.4 V in H_2/O_2 PEMFC. b) Cross section SEM image of the MEA after durability test and EDXS mapping for Fe. c) Nyquist plot of the EIS in H_2/N_2 MEA before and after degradation at 0.4 V in operating PEMFC. d) BoT and EoT polarisation curve and deconvolution of the voltage loss into kinetic loss (yellow), Ohmic loss in the cathode layer (blue) and in the PEM (purple). Figures a, b, c, and d, reproduced with permission from Ref. [185]. Copyright [2019] American Chemical Society.

2.7.3 O_2-transport resistance

Besides adversely affecting proton conductivity, [194-196] water uptake [197-199] and mechanical toughness [200] of the ionomer/the membrane, the partial exchange of protons by metal cations in the ionomer of the cathode (as discussed in **section 2.6.2** for Metal-N-C catalysts) may also increase the O_2-transport resistance and thus lead to a drop of the cathode performance at high current density. [126, 195, 201-203] This effect was first studied using conventional Pt-based catalysts. Indeed, Co^{2+} and Fe^{3+} cations may be introduced in the PEMFC environment simply by corrosion of the gas feed lines, stack and tubing components, auxiliaries, or stainless-steel bipolar plates. For Pt-alloy catalysts, preferential dissolution of the non-PGM transition metal from Pt_xM alloy NPs (*e.g.* PtCo/C used at the cathode of Toyota Mirai and Mirai 2) can further increase this effect. [203] Once present in the PEMFC, these cations tend to accumulate on the cathode side due to the potential gradient formed in the polymer electrolyte during PEMFC operation, and thus an increase in current density will reinforce this trend. [204] The adverse effects of metal-cation contamination was first studied by Okada *et al.* [125] using Pt electrodes covered with a Nafion film that was previously contaminated with Li^+, Na^+, K^+, Ca^{2+}, Fe^{3+}, Ni^{2+}, or Cu^{2+} ions. The authors reported a *ca*. 40-60 % decrease of the ORR kinetic current for contamination levels comprised between 0.1 and 1 % of all cationic sites comprised in the

Nafion ionomer, which they related to a decrease of the O_2 permeability (diffusion coefficient of O_2 times O_2 concentration) in the metal-cation contaminated ionomer. Similar observations were made by Durst *et al.* [203] using Pt/C NPs, and Co^{2+}-contaminated Nafion ionomer|membrane. The authors used three different set-ups: (i) a Pt/C RDE|liquid electrolyte interface, (ii) a Pt/C RDE|polymer|liquid electrolyte interface and (iii) a Pt/C ultramicroelectrode|Nafion|gas phase. Whatever the configuration, the O_2-diffusion limited current density dropped with increasing contamination level. Chronoamperometric measurements revealed that such decrease resulted from a combination of a decreased ORR selectivity (increased % H_2O_2) and a decreased O_2 permeability in the contaminated ionomer. Choi *et al.* [117]observed lower diffusion-limited current density and a less sharp transition from the kinetic domain to the diffusion-limited domain in RDE studies, after LC or SU/SD AST of a Fe-N-C. These phenomena were assigned to Fe contamination of the Nafion ionomer in the AL, reducing the O_2 permeability. Two approaches have been used to assess the effect of cation contamination on the PEMFC performance: (i) either metallic cations are introduced (in liquid electrolyte) at the anode/the cathode, or (ii) the MEA is deliberately spiked with cations before being tested in a PEMFC. Using 10 wt. % Pt/Vulcan cathodes and 20 wt. % Pt/graphitized carbon (0.05 mg_{Pt} cm^{-2} at each electrode) and a perfluorosulfonated Nafion membrane in which 98 % of the sulfonate groups were occupied by Co^{2+} cations, Braaten *et al.* [205] recently found that the resistance to oxygen transport increased by a factor of 2 and 1.5 at 100 and 50 % RH, respectively, in agreement with the modelling performed by Delacourt *et al.* [206] The authors proposed that cation contamination compresses the hydrophilic domains of the ionomer/membrane as a result from reduced water uptake, increasing the tortuosity of the O_2 diffusion path. These results are in line with former findings. [207] Such effects are certainly important for the durability of PGM-free cathodes and deserve more experimental studies.

In summary for **section 2.7**, the flooding of micropores in Metal-N-C AL does not seem to contribute to losses in performance over time when operating a PEMFC, implying it either occurs very fast or does not occur at all. Decreased proton conductivity throughout the cathode AL after PEMFC testing is sometimes observed (but not systematically), which can be due to partial exchange of protons by metal cations, and/or chemical attack of the ionomer and related decrease in ion exchange capacity. Contamination by metal cations can also affect O_2 transport through the ionomer, but more experimental works are needed to conclude whether this applies when operating Metal-N-C AL in PEMFC.

3. Degradation mechanisms of Metal-N-C oxygen reduction electrocatalysts in alkaline medium

Besides acidic medium, of great relevance from both fundamental and industrial perspectives, Metal-N-C catalysts have also proven to be highly-efficient for the ORR electrocatalysis in alkaline medium, with electrocatalytic activity exceeding that of benchmark Pt/C NPs and being durable. [100, 101, 179, 208-216] High ORR activity mostly arises from the fact that both inner and outer-sphere electron transfer mechanisms operate in alkaline medium, not in acid. [217] Consequently, the structure-sensitivity of the ORR is less marked in alkaline than in acid electrolyte. For example, in alkaline electrolyte Metal@N-C catalysts perform slightly better than Metal-N_x sites (Metal = Fe, Co) formed upon inert-gas pyrolysis, [100] while the opposite trend was found in an acidic electrolyte when comparing the same set of materials. [21] Note however that Metal-N_x sites formed upon NH_3 pyrolysis still outperform Metal@N-C catalysts and are stable in alkaline environment. [179] In addition, Metal-N-C materials are tolerant to

anodic fuels [101, 214, 215, 218] and to common impurities present in reformed H_2 or in air [15] bringing promises for the development of high-performance anion-exchange membrane fuel cells. [219-222] In this section, slightly moving away from the scope of this Review, we therefore present the similarities but also the differences of degradation mechanisms of Metal N-C materials in acid and alkaline media. Let us first underline that the same overarching degradation mechanisms occur regardless of pH, however the details of the mechanisms, the extents of degradation, and the effects on the ORR activity of Metal-N-C catalysts can differ in acidic and alkaline media.

3.1 Demetalation in the absence of carbon corrosion and oxygen reduction reaction

Compared to acidic medium, demetalation in such conditions (only applying an electrochemical potential) is expected to be a minor issue in alkaline electrolyte due to the absence of protons. Moreover, metal cations that leave the Metal-N_x moieties will have a high probability for reprecipitating as metal (hydr)oxides at high pH, and the loss of Metal-N_x sites will not necessarily lead to a loss of total Metal content, but rather a partial or complete transformation of the metal coordination from Metal-N_x to Metal-O_x. For example, using *in situ* ICP-MS, Santori *et al*. [179] measured similar low amount of Fe leached in the electrolyte during [0.6 – 1.0 V *vs.* RHE – 100 mV s^{-1} – 5k – N_2 – RT] in 0.1 M KOH for two atomically dispersed Fe-N-C materials pyrolyzed at 1050°C either under Ar or under NH_3. This was in contrast to the case in acid medium, where the NH_3-pyrolyzed Fe-N-C material released much more Fe than the Ar-pyrolyzed one. Because of its higher initial ORR activity, the Fe-N-C material pyrolyzed under NH_3 therefore seems to be advantageous for operation in alkaline, combining high activity and stability. Another study on demetalation in the absence of carbon corrosion and ORR occurring in alkaline electrolyte was recently carried out by Ku *et al*. [223] Using a gas diffusion electrode half-cell coupled with ICP-MS setup (GDE/ICP-MS), they reported that a commercial Fe-N-C catalyst produced by Pajarito powder or a state-of-art Fe-N-C catalyst featuring exclusively FeN_x sites release only a low amount of Fe when AST is performed in Ar-saturated 0.1 M NaOH. The Fe amount released for a same AST in O_2-saturated 0.1 M NaOH was however found to be 10 times faster (discussed in subsection 3.3). Similar to what has been shown in acidic electrolyte, the leached Fe cations reprecipitate as Fe-oxides in alkaline electrolyte, and local TEM images combined with point EDXS analyses revealed that the main oxide species after AST was $Fe(OH)_3$. [216]

3.2 Bulk carbon oxidation reaction

Bulk COR is generally perceived as being much slower in alkaline than acidic medium. [224] As shown by Yi *et al*., [225] the COR proceeds differently in acid and alkaline electrolyte. Oxidation of a glassy carbon electrode in acidic media mostly leads to increased concentration in oxygen-containing surface groups, leading to ring opening and thus propagation of COR to the bulk of the carbon material. In contrast, in alkaline media, OH-species preferentially attack the edges of the carbon crystallites until they become hydrophilic and delaminate. [225] The implication is that apparent unmodified carbon structure of Metal-N-C electrodes after AST in alkaline medium is not necessarily synonym with no structural degradation, because the oxidized graphene sheets (containing Metal-N_x sites) can be nicely 'peeled off', creating a new clean carbon surface and exposing to the electrolyte fresh Metal-N_x sites in graphene sheet that is free of oxygen functional groups.

Improved graphitization of Metal-N-C can however be advantageous for improved durability in alkaline medium. Domínguez *et al*. [226] reported better durability for Fe-N_x sites and Fe-based NPs dispersed into graphene-like carbon compared to multiwalled carbon nanotubes and active carbon after [0.6 – 1.0 V *vs.* RHE – 50 mV s^{-1} – 3k – O_2 – unspecified *T*] in 0.1 M KOH. *In situ* infrared reflection spectra detected CO_2 evolution at more positive potentials ($E \geq 1.4$ V *vs*. RHE) for Fe-N-C catalyst based on graphene compared to carbon nanotubes ($E \geq 1.3$ V *vs*. RHE) and activated carbon ($E \geq 1.2$ V *vs*. RHE). In line with these findings, Sharma *et al*. [227] synthesized Co NPs supported onto carbon black using $Co(acac)_2$, a ligand that can release carbon into metal lattice. The as prepared Co/C NPs were thermally annealed in an Ar atmosphere at different temperatures *viz*. 500, 600, and 700 °C, leading to formation of a graphene shell. Increasing the annealing temperature significantly attenuated the decrease of the half-wave potential ($E_{1/2}$) after [0.6 – 1.0 V *vs.* RHE – 100 mV s^{-1} – 5k – O_2 – 25°C] in 0.1 M KOH. However, enhanced durability came at the expense of the initial ORR mass activity, as shown by the lower ORR mass activity of materials annealed at 700°C.

3.3 Combined effects of electrochemical potential and oxygen reduction reaction

The more aggressive conditions of O_2 saturated electrolyte *vs*. inert-gas saturated electrolyte observed in acidic medium seem also to apply in alkaline electrolyte. A study on the comparative degradation of two Fe-NC catalysts in inert gas or O_2 saturated alkaline electrolyte was recently carried out by Ku *et al*. [223] Using a gas diffusion electrode half-cell coupled with ICP-MS setup (GDE/ICP-MS), they reported that a commercial Fe-N-C catalyst produced by Pajarito powder or a state-of-art Fe-N-C catalyst featuring exclusively Fe-N_x sites preferentially demetalate in the presence of oxygen in alkaline medium, in line with the observations previously made in acidic electrolyte. [70, 103] The AST consisted in steps of increasing current between 0 and -125 mA cm^{-2}_{geo} in O_2-saturated 0.1 M NaOH at RT. The same AST was also reproduced in Ar-saturated 0.1 M NaOH using the values of potential experienced by the Fe-N-C catalysts during the AST in O_2-saturated 0.1 M NaOH (*ca.* 0.57 – 0.87 V *vs*. RHE). The amount of Fe being dissolved (ng_{Fe} $mg^{-1}_{Fe\text{-}N\text{-}C}$) was found to be 10 times higher in O_2-saturated electrolyte *vs*. Ar-saturated electrolyte. However, a normalization of the amount of dissolved Fe by the electrical charge that passed through each AST (ng_{Fe} $mg^{-1}_{Fe\text{-}N\text{-}C}$ C^{-1}) showed comparable dissolution rates. Discussing the possible degradation mechanisms, the authors discarded the possibility that the Fe sites could be destabilized by HO_2^- (the dominant form of hydrogen peroxide in alkaline medium) or ROS. [228] They tentatively ascribed the correlation between Faradaic charge and amount of Fe being released to the instability of the oxygen-coordinated Fe atoms during the Fe^{2+}/Fe^{3+} redox transition, and to the associated changes in coordination of the Fe cations.

While the four-electron selectivity is desired also in alkaline medium, to avoid hydrogen peroxide and ROS formation, the attack by hydrogen peroxide and ROS is less severe in alkaline medium because hydrogen peroxide is less stable in alkaline than in acid, and because the nature of the ROS is different, with less of the most aggressive OH radicals and predominantly more of the less aggressive $^{\bullet}OOH$ and $^{\bullet}H$ radicals during ORR in alkaline. Wierzbicki *et al*. [229] showed using *operando* electron-paramagnetic resonance spectrometry, that although $^{\bullet}OOH$ and $^{\bullet}H$ radical species are produced at the cathode of AEMFC, independently of the nature of the catalyst, these species are much less aggressive in alkaline *vs*. acidic environment. The effect of the treatment of a Fe-N-C by hydrogen peroxide was studied across the entire pH scale by Bae *et al*. [156] and almost negligible deactivation was

found after a treatment in a sufficiently strong alkaline electrolyte. This correlated to the absence of the •DMPO-OH adduct by electron-paramagnetic resonance (where DMPO stands for 5,5-dimethyl-1-pyrroline N-oxide).

Also similar to what has been shown in acid electrolyte, Metal-N_x sites seem to maintain their ORR activity better than zero-valent metallic NPs embedded in carbon layers. However, this does not imply that Fe-N_x sites remain intact in alkaline medium but, on the contrary, there is evidence that they partially transform over time. Mufundirwa *et al*. [213] first showed that a fraction of single Fe atoms dispersed into a N-C matrix (NPC-2000 catalyst from Pajarito powder) is transformed into Fe-based NPs after [0.6 – 1.0 V *vs.* RHE – 3s/3s – 60k – unspecified atmosphere – RT], and that this transformation is accompanied by a negligible decrease of the $E_{1/2}$. In contrast, a 60 mV decrease of $E_{1/2}$ was observed for a home-made catalyst containing initially Fe-oxide and Fe-carbide NPs after the same AST. These findings were confirmed by Sgarbi *et al*. [216] using two Fe-N-C catalysts comprising exclusively Fe-N_x sites or Fe_3C@N-C NPs (referred to as $Fe_{0.5}$RP and $Fe_{5.0}$RP, respectively in Ref. [21]). By combining Synchrotron XAS and X-ray emission spectroscopy (XES), STEM, EDXS, and ICP-MS analyses, they showed that a small fraction of the Fe was transformed into Fe oxide after [0.6 – 1.0 V – 3s/3s – 10k – 60°C] AST performed in O_2-saturated 0.1 M NaOH. Nearly 50 % of Fe-N_x sites formed $Fe(OH)_3$ while some of the Fe_3C@N-C NPs showed $Fe(OH)_3$ shell covering the Fe_3C core ($Fe(OH)_3$@Fe_3C@N-C NPs). The amount of Fe being redeposited as well as the size/density of the Fe-oxide NPs highly depends on the temperature, larger and more numerous $Fe(OH)_3$ NPs forming at 25°C *vs*. 60°C.

In contrast to the acidic medium, where Fe-oxide NP formed during AST have negligible ORR activity, such decomposition products of Fe-N_x sites or metallic particles initially wrapped in carbon layer, can contribute to some extent to the ORR activity in alkaline measured after AST due to the non-negligible ORR activity of Fe oxide in alkaline. [230, 231] The *operando* formed Fe-oxide particles can also possibly act in synergy with the untransformed Fe-N_x moieties, translating into a mild change of the apparent activity of the electrode after the AST, despite significant transformation of Fe speciation. [208] In contrast, Fe oxide shells on Fe@N-C core were less active than the native Fe@N-C particles, and catalysts based on Fe@N-C sites deactivated faster than those based on Fe-N_x sites upon potential cycling in Ar-or O_2-saturated alkaline electrolyte. [216]

Analogous to the observation in acid medium, the higher stability/durability of the S2 site *vs.* the S1 site seem also to apply in alkaline medium. The D2 site was found to be durable after 100 h operation in H_2/air AEMFC at 0.6 A cm^{-2}, while the content of the D1 site decreased by *ca*. 30 %. [232] The loss in D1 content and the loss in cell performance was however much less compared to the case of the loss observed in PEMFC for the same NH_3-pyrolyzed Fe-N-C catalyst, highlighting the advantage of high pH vs low pH for such PGM free materials. [232]

4. Mitigation strategies

4.1 Mitigation of demetalation

4.1.1 Post-synthesis removal of unstable metal species

To avoid *operando* demetalation and associated negative effects on the proton conductivity but also oxygen permeability in proton-conducting ionomers and PEMs, [125, 126] the acid-unstable metal species in Metal-N-C catalysts can be selectively removed before their

implementation in PEMFC. Acid wash is commonly used to selectively remove unstable and/or inactive metal species in Metal-N-C material, before implementing them in the acidic and oxidizing environment of a PEMFC cathode. [117, 233] Indeed, it is widely admitted that acid wash removes inactive ORR species from Metal-N-C catalysts [64] but does not remove the most ORR active sites, although such statement is contradicted by other groups. [118, 234] Using online ICP-MS, Choi *et al.* [118] showed that the application of [0.0 – 1.0 V *vs*. RHE – 100 mV s^{-1} – 0.1 k – Ar – RT] in 0.1 M $HClO_4$ removed a significant amount of Fe from an Fe-N-C catalyst initially containing both Fe-N_x sites and metallic Fe particles, without affecting the ORR activity. The leached Fe was mostly assigned to metallic Fe and Fe_3C particles, while most Fe-N_x sites survived the 100 cycles. Importantly, the Fe leaching rate was very low if no CV was applied and if the electrode was let at OCP, highlighting that a simple acid wash is not as efficient as a CV between 0.0 and 1.0 *vs*. RHE in removing acid-unstable Fe. The reason for this is that the OCP of Fe-N-C catalysts is typically > 0.7 V *vs*. RHE. At such potential, ferric (hydr)oxides can be stable in acidic pH, in equilibrium with free ferric cations in solution, (see **Figure 3c**), implying that leached Fe cations can partly reprecipitate on the catalyst in the form of ferric (hydr)oxides. Such oxides can later pollute the Nafion ionomer and membrane during PEMFC operation, when the cathode potential becomes lower than 0.7 V *vs*. RHE. An alternative acid wash method including a reducing agent ($SnCl_2$) was studied and found to be as efficient as the 0.0 – 1.0 V *vs*. RHE CVs in removing the Fe. The addition of 10 mM $SnCl_2$ to 0.1 M HCl lowered the OCP of the Fe-N-C catalyst from *ca*. 0.85 V *vs*. RHE to < 0.5 V *vs*. RHE, thereby stabilizing free ferrous cations and allowing their removal during the filtration step. Other reducing agents than $SnCl_2$ could be used to that end. Both the electrochemical acid-wash and chemical acid-wash methods can therefore be efficient for removing inactive Fe before implementation of Fe-N-C cathode and catalysts in PEMFC, but it is important to make sure the environment is in sufficiently reducing conditions to avoid reprecipitation of ferrous cations as ferric (hydr)oxides on the catalyst/cathode. For Mn, Co or Cr-N-C catalyst, such precaution should not be needed, since their Pourbaix diagrams indicate that the divalent cation is the only stable form in acidic pH between 0 and 1.0 *vs*. RHE (**Figure 3**). The removal of zinc (Zn) in a final synthetic step might also be important for Metal-N-C catalysts derived from ZIF-8 and other Zn-based MOFs. The presence of a significant amount of Zn as Zn-N_x sites in Metal-N-C catalysts derived from Zn-rich MOFs could be harmful in PEMFC operation, Zn being much prone to demetalation in acid medium. Zn can be removed by appropriate heat-treatments, due to the low boiling points of Zn (907°C) and of $ZnCl_2$ (732°C). For example, Jiao *et al.* [28] observed that the Zn content in Fe-N-C prepared via CVD of $FeCl_3$ decreased drastically between 650 and 750°C, assigned to the removal of Zn from Zn-N_x sites as $ZnCl_2$ vapour. In any case, similar poor durability was observed in PEMFC for the as-pyrolyzed and acid-washed Fe-N-C samples, indicating an intrinsic poor durability of the Fe-N_x active sites, and that poor durability is not an indirect consequence of the leaching of less active or inactive Fe species. The removal of acid-unstable transition metals from Metal-N-C catalysts before implementation in PEMFC is therefore a necessary step for durable MEAs, but not a sufficient one.

4.1.2 Chemical modification of Metal-N_x environment

The stability of Metal-N_x sites strongly depends on their local environment. This is well illustrated by Seo *et al.* [173] who reported that a Fe-Pc modified with thioester groups (Fe-SPc) features a slightly lower ORR activity than Fe-Pc but much improved durability in 0.1 M $HClO_4$, with only 20 mV decrease in the $E_{1/2}$ of Fe-SPc compared to *ca* 400 mV for FePc after a load

cycle AST in RDE [0.0 – 1.0 V *vs*. RHE – 0.1k – O_2 – 25 °C] (**Figure 23a-b**). based on DFT calculations, the authors argued that electron-donation from thioester groups to Fe cations in Fe-SPc depreciates their TOF but enhances their stability in acid media (**Figure 23c**). It was suggested that an electron charge accumulation on the Fe cation in Fe-N_4 active site can reduce the demetalation process occurring during the ORR. Alternatively, a steric effect introduced with the thioester groups might have prevented the fast protonation of the Fe-N_4 sites.

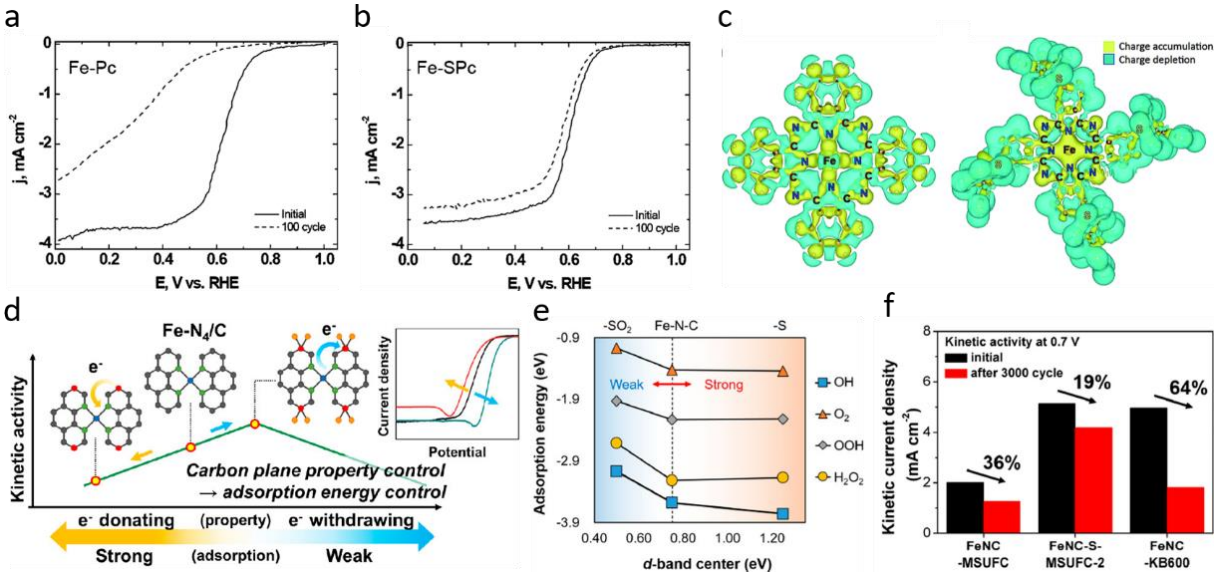

Figure 23. Correlation between the electronic and chemical composition of the carbonaceous environment, the electron density at the Fe-N_4 centre, the ORR activity and durability. ORR polarization curves of Fe-Pc/C a) and Fe-SPc/C b) before and after AST [0.0 – 1.0 V *vs*. RHE – 0.1k – O_2 – 25 °C]. The potential scan rate was not specified by the authors. [173] c) electron density on Fe-Pc and Fe-SPc. [173] d) Effect of electron-withdrawing and electron-donating groups on the kinetic activity of Fe-N-C catalysts. [235] e) Relationship between the adsorption energy of ORR intermediates and the *d*-band centre of the Fe cation in Fe-N_4. [235] f) Kinetic current density at 0.7 V *vs.* RHE before and after [0.9 – 1.1 V *vs*. RHE – 3 k – unspecified atmosphere – 25 °C]. [235] Figures a, b and c, reproduced with permission from Ref. [173]. Copyright [2014] Royal Society of Chemistry. Figures d, e and f, reproduced with permission from Ref. [235]. Copyright [2019] American Chemical Society.

By incorporating and controlling the ratio of electron-withdrawing and electron-donating functions on the carbon plane of a Fe-N-C material, Mun *et al*. [235] proposed a new strategy to increase both its ORR activity and stability (**Figure 23d**). Several sulphur-doped Fe-based catalysts were prepared using different concentrations of dibenzyl disulphide precursor. XPS analysis revealed that two main chemical sulphur structures coexist in the sample, namely thiophene-like S (C-S-C) and oxidized S (C-SO_x). While, thiophene-like sulphur-groups promote the electron enrichment of the carbon plane, increasing the energy of the *d*-orbital of the Fe cation in Fe-N_4 sites and thus increasing the adsorption of ORR intermediates, the oxidized sulphur groups lead to an opposite effect (**Figure 23e**). Therefore, the authors claimed that oxidized sulphur groups with electron-withdrawing property promoted the ORR activity whereas the thiophene-like sulphur functions reduced it, due to their electron-donating property. To reach the highest ORR activity, the sulphur doping level and ratio of oxidized-S / thiophene-like S was optimized and found to be at 0.24 at. % S with the highest oxidized-S / thiophene-like S ratio for the Fe-N-C-S-MSUFC-2 material. Moreover, this catalyst exhibited improved stability to other catalysts in the study, losing only 19 % of its initial activity after 3k cycles between 0.9 – 1.1 V *vs.* RHE (**Figure 23f**). These results on model phthalocyanines and also pyrolyzed Fe-N-S-C catalysts show that it is possible to tune the TOF of Fe-N_4 sites and

also their durability by chemically modifying the carbonaceous environment. This modifies not only the electron density at the Fe centres, but also possibly the COR on the carbon matrix. More theoretical and experimental work is needed on Metal-N-C materials doped with other elements such as S, P for tuning the TOF and durability of Metal-N_4 active sites.

4.2 Mitigation of surface and bulk carbon corrosion

As already discussed in **section 2.3**, mild corrosion of the carbon matrix yields formation of oxygen-containing surface groups, depletion of the delocalized π electrons and drop of the TOF of the Metal-N_x moieties. [36] More severe carbon corrosion leads to a decrease of the pore volume and of the pore diameters, [236] to increasing hydrophilic character [237-239] and to the destruction of the Metal-N_xC_y active sites. The COR is thermodynamically possible from 0.2 V *vs*. SHE but kinetically slow, [129] hence COR is a severe problem during start/stop periods during which the local cathode potential can reach as high as 1.5 V *vs*. RHE. [120] Former studies on Pt/C catalysts have shown that graphitic carbon supports are the most robust towards carbon corrosion due to lower content of structural defects, onto which corrosion initiates. [120] Increasing the degree of graphitization of Metal-N-C materials is therefore a promising solution to improve their durability. [240] As more graphitic materials are also more hydrophobic, this approach also reduces the probability of flooding the cathode AL. [42, 61] Nevertheless, increased degree of graphitization requires temperatures comprised between 1700 and 3000°C, [241] which are detrimental to the surface concentration of pyridinic- and pyrrolic-N [62, 242] (eventually leading to a drop of the TOF), and to the atomic dispersion (aggregation of the transition metal atoms leading to a drop in ASD value). The right trade-off between durability (more graphitic structure *i.e*. low specific surface area) and mass activity for the ORR (high ASD + high TOF) must therefore be found.

Wu *et al*. [153] prepared different PANI-based Fe-N-C catalysts, with different carbon supports such as Vulcan XC-72, BP-2000, KJ-300J and multiwall CNTs, and reported that the CNTs-based MEAs were the most stable after [0.4 V – 500 h – O_2 – 80 °C] (**Figure 24**). This was confirmed by Xia *et al.* [243] who directly grew CNTs doped with Fe-N_x sites and tested their stability with [0.9 – 1.4 V *vs.* RHE – 50 mV s^{-1} – 500 cycles – N_2 – unspecified *T*] AST protocol.

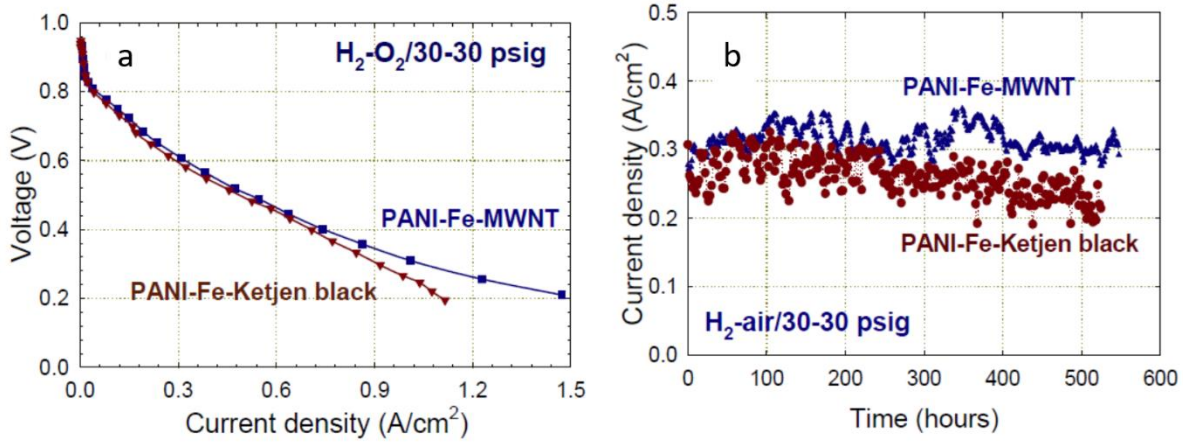

Figure 24. Fuel cell performance of PANI-Fe catalyst obtained using MWNTs and Ketjenblack as supports: (a) initial polarization plots, (b) life tests. Cell temperature 80°C; anode – 0.25 mg cm^{-2} Pt on a woven-web GDL (E-TEK), 30 pounds per square inch gauge (psig) H_2; cathode – catalyst loading 4.0 mg cm^{-2}; Nafion® 1135 membrane. Figures a and b, reproduced with permission from Ref. [153]. Copyright [2009] The Electrochemical Society.

Similarly, using a series of Fe-N-C materials prepared by wet-impregnation process of a non-microporous carbon support with various amounts (7-90 wt. %) of an Fe porphyrin (Cl-FeTMPP) followed by thermal treatment at *T* = 950 °C in Ar atmosphere during 30 min, Charreteur *et al.* [242] showed that the durability of Fe-N-C catalysts increased with the amount of Fe precursor and this was correlated to the increasing graphitic character of the carbon matrix. The material prepared from 66 wt.% Cl-FeTMPP showed no loss of performance over 15 h of PEMFC operation and higher ORR activity than materials prepared with higher amounts of Fe precursors. Counterintuitively, the more durable electrocatalyst released a large quantity of peroxide species (25-35 %) during the ORR, as measured by RRDE. These observations can be explained from different hypotheses: i) highly graphitic carbon is less sensitive to ROS and COR; ii) the peroxide species were quickly transported away from the AL; iii) the Fe-based active sites were core-shells of Fe_3C@C with no surface Fe present (and thus no ROS produced via direct contact between Fe cations and H_2O_2).

4.3 Mitigation of peroxide and reactive oxygen species effects

While all 3d transition metal cations produce some amount of ROS (mostly $^{\bullet}OH$ and $^{\bullet}OOH$ radicals) when contacted by H_2O_2 in acidic medium, [145, 244, 245] the amount and oxidative power of ROS on Metal-N-C catalysts might be mitigated by resorting to a metal different from Fe for the Metal-N_4 sites. For achieving combined high durability and high activity, the alternative Fe-free Metal-N_4 site should however simultaneously achieve i) comparable ORR activity to Fe-N_4 sites, ii) high selectivity for 4-electron ORR and iii) decreased production of ROS (or production of less oxidizing ROS) when contacted with a given amount of H_2O_2. For example, achieving iii) without achieving ii) would likely result in little to no improvement in durability, since more H_2O_2 would be produced per unit of time (PEMFC operating at a constant current density) on the Metal-N_4 site *vs.* Fe-N_4. While Co-N-C and Mn-N-C catalysts are typically less active towards the ORR than Fe-N-C catalysts and also produce more H_2O_2 during ORR [127, 246, 247] their degradation rate during PEMFC operation is significantly lower than that of Fe-N-C catalysts (see *e.g*. Figure 4 in Ref. [95]). This can be assigned to the lower reactivity of Co^{2+} and Mn^{2+} cations with H_2O_2, which is explained by the much higher redox potentials for Mn^{3+}/Mn^{2+} and Co^{3+}/Co^{2+} relative to $H_2O_2/^{\bullet}OH$, while the redox potential of Fe^{3+}/Fe^{2+} is slightly below that of $H_2O_2/^{\bullet}OH$ (**Equations 17-20**):

$$H_2O_2 + H^+ + e^- \leftrightarrow {}^{\bullet}OH + H_2O \qquad E° = 0.88\ V\ vs.\ SHE \qquad (17)$$

$$Fe^{3+} + e^- \leftrightarrow Fe^{2+} \qquad E° = 0.77\ V\ vs.\ SHE \qquad (18)$$

$$Mn^{3+} + e^- \leftrightarrow Mn^{2+} \qquad E° = 1.54\ V\ vs.\ SHE \qquad (19)$$

$$Co^{3+} + e^- \leftrightarrow Co^{2+} \qquad E° = 1.92\ V\ vs.\ SHE \qquad (20)$$

While the redox potentials of metal cations in Metal-N_4 sites may differ somewhat from those of free cations, the trends should be unchanged. Below, we review the results and understanding gained on Co-N-C and Mn-N-C catalysts and compare to Fe-N-C catalysts.

Secondly, we discuss different strategies to mitigate the negative effect of ROS, namely dual metal atom catalysts (DMACs), and ROS scavengers. Finally, we deal with recent efforts targeting selective formation of durable Fe-N_x sites.

4.3.1 Single-metal atom catalysts

4.3.1.1 Co-N-C catalysts

Co-N-C catalysts were identified some years ago as the second most active sub-class of Metal-N-C materials, typically *ca* one-order-of-magnitude less active than Fe-N-C, but also typically with a lower Tafel slope than Fe-N-C materials, leading to comparable initial performance in PEMFC at U = 0.4-0.5 V. [248] The peroxide production during ORR is usually higher on Co-N-C compared to Fe-N-C catalysts (*e.g*. 1.0-1.5 % H_2O_2 depending on the potential on Co-N-C and *ca*. 0.5 % H_2O_2 on Fe-N-C in Ref. [249], as measured at a catalyst loading of 0.6 mg_{powder} cm^{-2}). The low selectivity of Co-N_4 sites is intrinsic to its low OOH binding energy, favouring protonation of OOH and desorption of H_2O_2 rather than O-O bond splitting. This trend is the same as observed with metal-phthalocyanines, where Co-phthalocyanines usually reduce O_2 by only two-electron. Note also that H_2O_2 production strongly depends on the catalyst loading: indeed, a Co-N-C catalyst comprising only Co-N_x sites was recently shown to be highly selective for 2-electron ORR at a loading of 0.1 mg_{powder} cm^{-2}, with potential application for H_2O_2 electrochemical synthesis. [155, 169, 249] Hence, high selectivity for 4-electron ORR reported in some instances in acid medium for Co-N-C catalysts [248] might be due to high catalyst loadings and cascade reactions leading to peroxide decomposition and/or further electro-reduction rather than direct 4-electron ORR. [146]

Nevertheless, although Co-N-C catalysts with Co-N_x sites do not match the criterion ii) stated in the introduction of **section 3.3** (high 4-electron selectivity), they result in lower rates of ROS formation during ORR relative to Fe-N_x sites, due to their lower activity towards Fenton's reaction. Indeed, when contacted by given amounts of H_2O_2 in *ex situ* conditions (no electrochemical potential applied), a model Co-N-C catalyst comprising only Co-N_x sites suffered from distinctly less deactivation than the model Fe-N-C catalyst prepared identically, except for the nature of the metal (**Figure 25a-b**). [35] For example, **Figure 25a** shows that after treatment with 2 x 10^{-2} moles H_2O_2 per mg of catalyst, *ca* 60% of the Co-N-C catalyst mass could be recollected after the filtration, while no Fe-N-C could be recollected. This can be assigned to carbon loss and/or to the breaking of carbon agglomerates into small carbon particles, becoming small enough to pass through the filter. The fluoride content released by a piece of Nafion membrane immersed in the peroxide + Metal-N-C solution was used as another indicator for the amount of ROS produced during the treatment, highlighting *ca* 2x lower fluoride concentration after peroxide treatment of the Co-N-C *vs*. the Fe-N-C (**Figure 25a**). This in turn suggests less ROS were produced on Co-N-C thereby fulfilling the criterion iii) stated at the inception of **section 3.3**.

Assuming that ROS-induced carbon corrosion [70] controls the long-term durability of Metal-N-C catalysts, the differences in selectivity and ROS production therefore seem to favour Co-N-C *vs*. Fe-N-C, and a benefit can be derived from this. This has been proven by Cheng *et al*. [250] who developed two materials based on single Co or Fe atoms embedded into N-doped carbon nanofibers (CoP−N/CNFs and Fe-N/CNFs, respectively). CoP-N/CNFs evidenced much better durability than Fe-N/CNFs after [0.6 – 1.0 V *vs.* RHE – 10k – O_2 – 25 °C] in 0.1 M $HClO_4$.

Specifically, a 34 mV negative shift of $E_{1/2}$ was reported for Co-N/CNFs to be compared with 59 mV for Fe-N/CNFS. Similarly, Xie *et al*. [249] reported that the drop in current density of a PEMFC polarized at 0.7 V for 100 h with 1.0 bar H_2 on the anode and 1.0 bar air on the cathode was significantly lower for a Co-N-C cathode than for a Fe-N-C cathode (20.5 and 46.8 % drop, respectively). CO_2-emission rate measurements at the outlet of a PEMC cathode, showed more pronounced increase for Fe-N-C *vs*. Co-N-C after the gas fed to the cathode was switched from N_2 to O_2 at a cell voltage of 0.3 V, and decrease of the CO_2 emission rate after switching back to N_2. Moreover, increased demetalation was observed for Fe- *vs*. Co-based cathode in the same study.

To compensate for the lower mass activity of Co-N-C vs. Fe-N-C materials, synthesis strategies should be developed in particular those promoting an increase in ASD. An illustration of this can be found in the recent work of He *et al.* [251] who pyrolyzed Co-doped ZIF nanocrystals precursors coated with a surfactant layer at 900°C under nitrogen flow. According to the authors, the decomposition of the surfactant leads to a graphitized shell with high N content covering the ZIF-pyrolyzed nanocrystals. Pluronic 127 (M = 12600 g mol^{-1}) proved to be optimal to maximize the ORR activity ($E_{1/2}$ values of 0.95 and 0.85 V *vs*. RHE for Co-N-C@Pluronic and state-of-the-art Fe-N-C, respectively). Moreover, better 4-electron selectivity, and enhanced durability were observed during [0.6 – 1.0 V *vs*. RHE – 50 mV s^{-1} – 30k – O_2 – 25 °C] and [0.7 or 0.85 V *vs*. RHE – 100 h – O_2 – 25°C] in 0.5 M H_2SO_4. In a follow-up paper, [249] the same group used a ligand-exchange strategy in which $Co(acac)_3$@ZIF-8 was converted into $Co(mIm)_4$@ZIF-8, and then pyrolyzed. Co-N-C catalysts synthesized with acac or mIm ligands both contained 1 at. % Co but the material synthesised by the ligand exchange procedure had a comparable ORR activity than a reference Fe-N-C. Interestingly, the ORR activity dropped only by 11 % at 0.85 V for Co(mIm)–NC(1.0) after [0.6 – 1.0 V *vs*. RHE – 50 mV s^{-1} – 10k – O_2 – 25°C], much less than that for Fe(mIm)–NC(1.0), which degraded by 47 %. The choice of the ligand also has a very important role on the ORR selectivity of Co-N-C catalysts since, at identical Co atomic content, the H_2O_2 yield was as low as 2 % at all potentials with the mIm ligand. This value was 3 to 4 times lower than that observed on the Co(acac)-NC material (4-8 % H_2O_2, depending on the electrode potential). These results suggest that it is synthetically possible to modulate the selectivity of Co-N_x sites, by playing with the ligand used during the synthesis of the doped MOF. Alleviated Fenton reactions on Co-N-C or bimetallic (Fe, Co)-N-C materials [252] is thus a promising approach to synthesize efficient and more durable Metal-N-C catalysts.

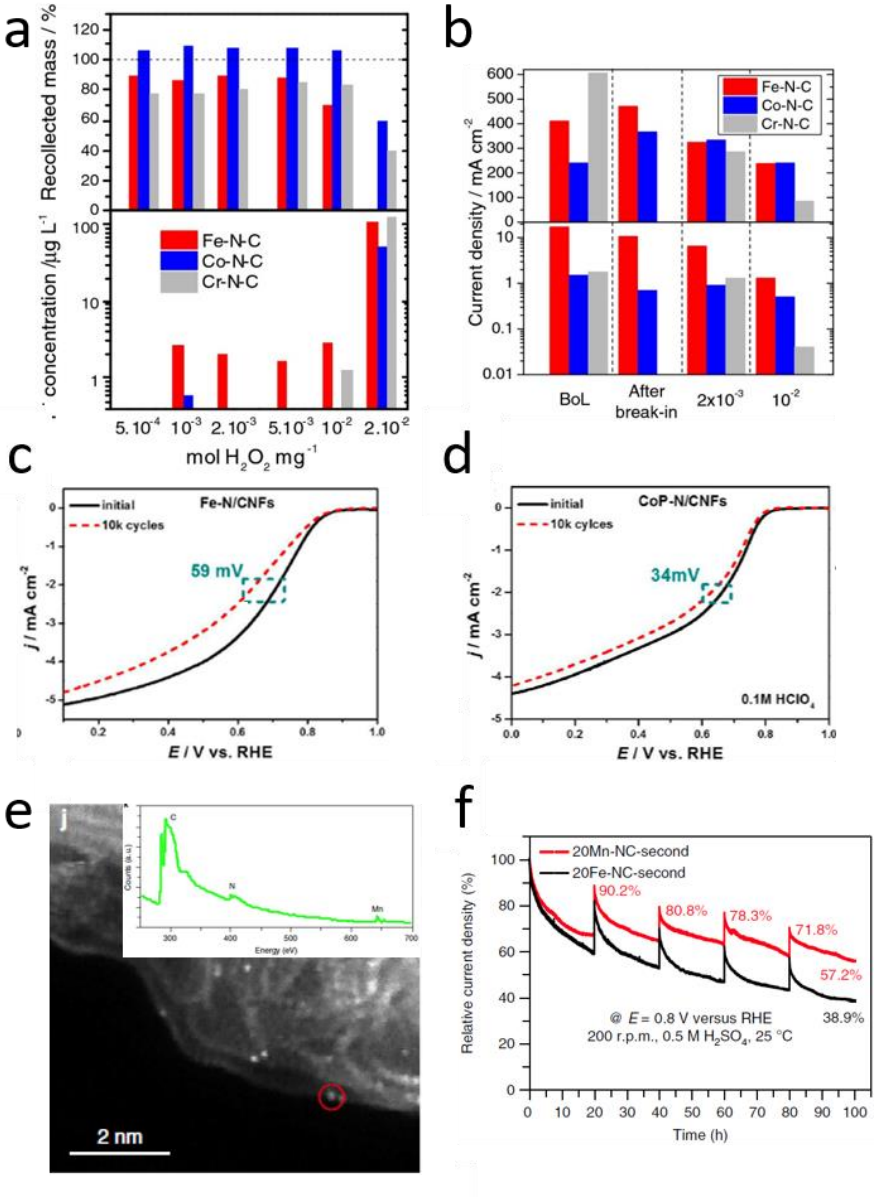

Figure 25. Comparative durability of Co-N-C, Mn-N-C and Fe-N-C catalysts. a-b) Effect of *ex situ* peroxide treatment in acid. a) Top: Relative mass of catalyst recollected after each H_2O_2 treatment (in amount ranging from $5x10^{-4}$ to $2x10^{-2}$ moles H_2O_2 per mg of catalyst) + filtration + drying; bottom: concentration in the filtrate of fluoride ions released by the Nafion membrane immersed in solution during the H_2O_2 treatment [35] ; b) current density measured in PEMFC at 0.5 V (top) or 0.8 V (bottom) for the pristine catalysts at beginning of life or after break-in, and for the catalysts treated with $2{\cdot}10^{-3}$ or 10^{-2} mol H_2O_2 mg^{-1}. [35] ORR polarisation curves for c) single Fe or d) Co atoms embedded into N-doped carbon nanofibers (Fe-N/CNFs and CoP-N/CNFs, respectively) before and after [0.6 – 1.0 V *vs.* RHE – 10k – O_2 – 25 °C] in 0.1 M $HClO_4$. [250] Structure and compared durability in PEMFC of Mn-N-C and Fe-N-C catalysts. e) Aberration-corrected high-angle annular dark field scanning transmission electron microscopy image and associated electron energy loss spectrum of 20Mn-N-C catalyst. The red circle shows the atomic site where the spectrum was recorded. f) Current density normalized to the t =0 current density for 20Mn- and 20Fe-N-C catalysts during a 100 h hold at 0.8 V *vs.* RHE, in O_2-saturated and acidic media at 25 °C [95]. A short potential cycling between 0.0 – 1.0 V was applied every 20 h during the 0.8 V hold, partially restoring the activity. Figures a and b, reproduced with permission from Ref. [35]. Copyright [2015] The Electrochemical Society. Figures c and d, reproduced with permission from Ref. [250]. Copyright [2017] American Chemical Society. Figures e and f, reproduced with permission from Ref. [95]. Copyright [2018] Nature.

4.3.1.2 Mn-N-C catalysts

Similar to Co cations, Mn cations are potentially less prone to react with H_2O_2 to form ROS. [253] Recently, Wu's group reported on a ZIF-8 derived Mn-N-C catalyst with 3.0 wt. % of Mn featuring mostly atomically dispersed Mn-N_4 moieties [95] (**Figure 25f**). The ORR activity measured by RDE in acid medium for the optimized 20Mn-N-C material (20 is atomic percent of Mn against total metal during the synthesis of Mn-doped ZIF-8 precursors) showed a $E_{1/2}$ of *ca*. 0.8 V *vs.* RHE, only slightly lower than that of a reference 20Fe-N-C material and higher than that of a reference 20Co-N-C material. Its selectivity towards 4-electron ORR (*ca* 2 % H_2O_2 only) approached that of the 20Fe-N-C reference and was higher than that of the 20Co-N-C reference. The 20Mn-N-C catalyst was also slightly more durable than 20Fe-N-C after AST [0.6 – 1.0 V *vs.* RHE – 50 mV s^{-1} – 30k – O_2 – 25°C] in 0.5 M H_2SO_4, or upon polarization at [0.8 V *vs.* RHE – 100 h – O_2 – 25 °C] in 0.5 M H_2SO_4 (**Figure 25f**). The initial performance of the 20Mn-N-C-catalyst was also investigated in PEMFC and showed peak power density of *ca*. 0.45 W cm^{-2} in O_2, only slightly lower than that of 20Fe-N-C (*ca*. 0.51 W cm^{-2}). The current density at 0.6 V and above was however significantly lower for 20Mn-N-C *vs*. 20Fe-N-C, assigned to a lower ORR kinetics.

In their second study on Mn-N-C materials, Wu's group successfully increased the ORR activity and initial performance of Mn-N-C by modifying the synthesis, resorting to aqueous acidic conditions for preparing the Mn-doped ZIF-8 catalyst precursor, then adopting a two-step doping (of both Mn and N precursors) and pyrolysis strategy (first pyrolysis at 800°C followed by a second pyrolysis step at 1100°C). Acidic conditions prevented the formation of Mn oxides. The best performing material, labelled Mn-N-C-HCl-800/1100, showed a $E_{1/2}$ of 0.815 V *vs.* RHE in RDE. High durability similar to their first report was observed, with only 14 mV loss in $E_{1/2}$ after AST [0.6 – 1.0 V *vs.* RHE – 50 mV s^{-1} – 30k – O_2 – 25°C] in 0.5 M H_2SO_4. It was also related to the increased resistance to carbon corrosion, evidenced by minimized change in electrochemical capacitance before and after AST. [254] Much improved performance in H_2/O_2 PEMFC was reached with Mn-N-C-HCl-800/1100 of that study compared to 20Mn-N-C of their previous steady, with *ca*. 0.6 A cm^{-2} at 0.6 V and peak power density of 0.6 W cm^{-2}. Also, in H_2/air PEMFC initial test, the high peak power density of 0.39 W cm^{-2} could be achieved, which is at par with the state-of-art of any PGM-free cathodes in PEMFCs. A 160 h durability test in PEMFC was performed at 0.65 V. The current density at 0.65 V after 160 h was only ca 37% of the initial one (Figure S26 in Ref. [254]). In comparing the retained current density over the first 16 h of test, the cathode based on Mn-N-C-HCl-800/1100 lost only 20 % of its initial current density, while a similarly prepared Fe-N-C lost 44 % of its current density (Figure 6f in Ref. [254]). These losses in performance at 0.65 V may however be the result of changes in ORR kinetics and mass-transport. The change in ORR kinetics could not be assessed, as the initial and final polarisation curves before and after test were not reported in that study, impeding a detailed analysis of the reason for the decayed performance at 0.65 V. In summary, despite progress in the activity and durability of Mn-N-C *vs*. Fe-N-C, the durability is still a major issue, with significant performance decay over only 160 h of test, well below the industrial targets for PEMFC application. Further fundamental works on Mn demetalation rate, and the occurrence or not of ROS during ORR on Mn-N-C materials would be of interest for further understanding and comparison to Co-N-C and Fe-N-C materials.

4.3.2 Dual-metal atom catalysts

The interest for DMACs arises from cytochrome c oxidase, an enzyme that contains an a3-CuB site facing a Fe-heme and which is the catalyst designed by nature to reduce O_2 into H_2O. [255] By definition, DMACs contain catalytic sites that involve two metal atoms in proximity, acting synergistically to optimize the binding energies of reaction intermediates [256] or to facilitate the O-O bond scission. [257] The ORR activity of DMACs closely depends on the chemical nature of the metal elements, their arrangement and orientation with respect to each other, the total number of valence electrons in the dimer, their electronegativity, and the radius of the embedded transition metal. [258] Besides the promises of enhanced ORR activity, DMACs also theoretically offer the possibility to switch the adsorption mode of O_2 from superoxo-like to peroxo-like configuration (bonding to two adjacent metal atoms so that more electrons are donated into the empty orbital of O_2). [259, 260] This could reduce the production of H_2O_2 during ORR and thus decrease the contribution of the ROS-induced carbon corrosion mechanism (see **section 2.6**). The two metal atoms can either be co-located in the same graphene sheet and form a metal-metal bond (adjacent in-plane) or be linked through an oxygen or nitrogen heteroatom (in-plane bridged), or be located in two different graphene sheets but at atomic proximity (co-facial). The interested reader is referred to recent Review articles on DMACs. [261, 262]

Characterizing pristine DMACs is challenging, and gaining insight into their degradation mechanism is even more challenging since atomic resolution before and after AST must be reached. Little work has yet been reported specifically on DMACs stability/durability in PEMFC or RDE conditions. Ye *et al*. [263] succeeded in preparing and characterizing a series of Fe_x-N-C materials featuring exclusively mono- (Fe_1), bi- (Fe_2) or tri-nuclear-Fe atom sites (Fe_3) according to STEM-HAADF and XAS characterization. The highest initial ORR activity was observed for the Fe_2-N-C catalyst. However, the Fe_1-N-C catalyst was found to be the most durable catalyst after [0.6 – 1.0 V *vs*. RHE – 50 mV s^{-1} – 20k – O_2 – RT] in 0.5 M H_2SO_4, and the lower durability of the other two materials was assigned to a decrease of the number of Fe-Fe bonds. This degradation mechanism is unique to DMACs, and therefore distinct from those discussed previously in this Review. Wang *et al*. [264] prepared a bimetallic FeCu-N-C material, inspired from the co-facial Fe-Cu structure of cytochrome c oxidase. No XRD peaks for Fe and Cu crystallographic phases were observed, and the parent Cu-N-C material had much inferior ORR activity to the FeCu-N-C and parent Fe-N-C materials. However, FeCu-N-C and Cu-N-C had improved H_2O_2 reduction activity over Fe-N-C. This is in line with an earlier work reporting similar H_2O_2 reduction activity for Fe-N-C and Cu-N-C in acid for another DMAC (poorly structurally characterized at that time, and probably comprising not only Metal-N_x sites), while Cu-N-C had negligible ORR activity *vs*. Fe-N-C. [96] In Wang's study, a lower decrease of $E_{1/2}$ after 10k cycles in O_2-saturated 0.1 M $HClO_4$ electrolyte (unspecified potential range, scan rate, and temperature) was observed for FeCu-N-C compared to the parent Fe-N-C and a benchmark Pt/C. A FeCu-N-C material prepared differently was also reported by Du *et al.* [265]. The FeCu-N-C catalyst showed a mitigated ORR activity decrease when subjected to [0.4 V *vs*. RHE – 10 h – O_2 – 25°C] in 0.5 M H_2SO_4 and in 0.1 M KOH than a commercial 20 wt. % Pt/C. Maybe the most promising DMAC was a FeCo-N-C catalyst synthesized by Wang *et a*l. [266] using a guest-node strategy and starting from a Zn/Co MOF. In RRDE, the ORR activity of the FeCo-N-C catalyst was higher than that of a commercial 20 wt. % Pt/C while its 4-electron selectivity was comparable (comparison made at fixed metal loading, Fe+Co for FeCo-N-C and Pt for the benchmark Pt/C, hence implying a thinner film for Pt/C due to the higher metal wt. % on

carbon for the latter). The peroxide amount was also lower than that measured on the parent Fe-N-C and Co-N-C catalysts. No change in ORR activity was noticed after [0.6 – 1.0 V *vs*. RHE – 50 mV s^{-1} – 50k – O_2 – RT] in 0.1 M $HClO_4$ for the FeCo-N-C catalyst. A negligible change in PEMFC voltage was observed after 100 h test at constant current density (0.6 or 1.0 A cm^{-2}) under H_2/air on FeCo-N-C, and no change was noticed in its EXAFS and XANES spectra after the AST. The high ORR activity and selectivity to the 4-electron path were attributed to a stronger O_2 binding and a more facile O-O bond cleavage on FeCo-N-C than the parent catalysts. A FeCo-N_X-C catalyst with a $FeCoN_5$ active site structure was recently synthesized by Xiao *et al*. [267] using $Fe(acac)_3$ and a Zn/Co bimetallic MOF. Higher ORR activity and lower H_2O_2 yield were observed on FeCo-N_x-C compared to the parent Co-N_x-C and Fe-N_x-C catalysts. The ORR current decreased by only 6 % after [0.85 V *vs*. RHE – 0.55 h – O_2 – RT] in 0.1 M $HClO_4$ (the AST was not performed on the parent catalysts). Similarly, a FeNi-N-C catalyst synthesized by Zhou *et al*. [268] outperformed the parent Fe-N-C in terms of ORR activity and H_2O_2 yield. The FeNi-N-C catalyst was also more stable, with only 12 mV negative shift of $E_{1/2}$ after [0.66 – 1.06 V *vs*. RHE – unspecified scan rate – 5k – N_2 – RT] in 0.1 M $HClO_4$, compared to 25 mV for the parent Fe-N-C. Finally, CoZn-N-C catalysts were synthesized by Zang *et al*. [269] and Lu *et al*. [257] The CoZn-N-C material of Zang *et al*. exhibited a 35 mV positive shift of $E_{1/2}$ compared to a commercial Pt/C. Moreover, there was only 12 mV decay in $E_{1/2}$ after [0.6 – 1.1 V *vs*. RHE – 50 mV s^{-1} – 10k – O_2 – unspecified *T*] in 0.1 M $HClO_4$, and only 15-20 mV degradation of the PEMFC voltage was noticed after [0.4 A cm^{-2} – H_2/O_2 – unspecified *T*]. Similarly, no change of the PEMFC voltage was noticed for Lu's CoZn-N-C material after [0.5 A cm^{-2} – 8 h – O_2 – unspecified *T*].

4.3.3 Reactive oxygen species scavengers

Due to the low selectivity of some PGM-free active sites (Metal-N_x sites, M@C sites or nitrogen functional groups on the remainder of the N-C surface), the amount of H_2O_2 produced locally in the AL may be much higher than in Pt-based layers, and the propensity for H_2O_2 to form ROS with 3d transition metals is also higher than with Pt. This is why solutions are needed to i) promote the reduction or decomposition of *operando* formed H_2O_2 and ii) mitigate the adverse effects of ROS.

In the acidic medium of PEMFC, there are however no known PGM-free catalysts that are stable and that can efficiently electro-reduce H_2O_2 to water. The addition of relatively low amount of Pt to Fe-N-C was studied by Mechler *et al.* in 2018, [270] in an attempt to provide improved H_2O_2 to water activity to an Fe-N-C catalyst. Amounts of Pt salt were impregnated on the Fe-N-C to result in 0.5, 1 or 2 wt. % Pt, and treated at 560°C in 5 % H_2 in N_2 for forming Pt NPs. The resulting Pt/Fe-N-C hybrid catalysts showed, surprisingly, no improved activity for peroxide reduction (**Figure 26a**), and no improved ORR activity. This was explained by the lack of CO stripping signal both before and after the PEMFC durability test, indicating the absence of gas-phase accessible Pt surface. Despite the failure to prepare a Pt/Fe-N-C hybrid with improved H_2O_2 reduction activity *vs*. Fe-N-C, the PEMFC durability of Pt/Fe-N-C with 1-2 wt. % Pt was greatly improved *vs*. Fe-N-C, (**Figure 26b**) with no significant loss even after 180 h of operation for the 2wt. %Pt/Fe-N-C hybrid. The reason for the electrochemical inaccessibility of the Pt particles and for the stabilization effect in these Pt/Fe-N-C hybrids remained however speculative.

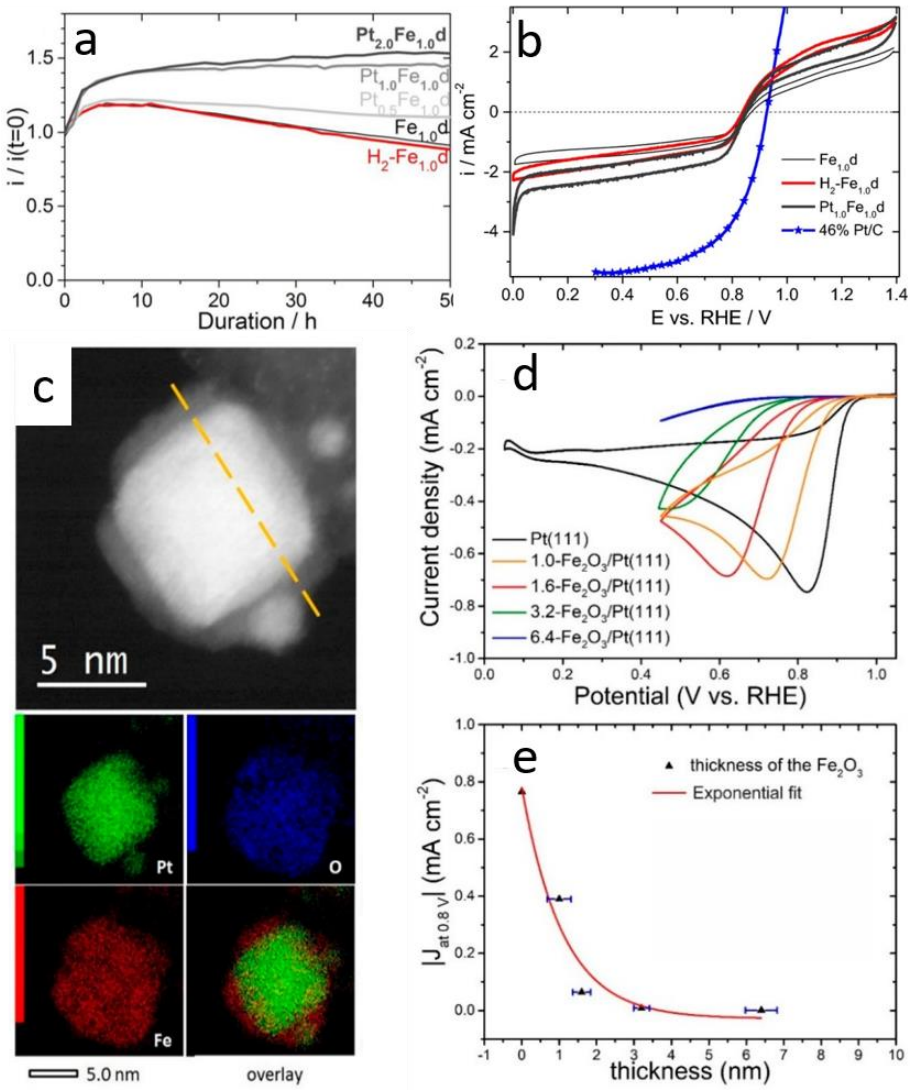

Figure 26. a) Hydrogen peroxide reduction and oxidation in N_2-saturated 0.1 M $HClO_4$ with 3 mM H_2O_2 at 1600 rpm. b) Current density in PEMFC at 0.5 V (normalized by the current density at t = 0) as a function of time. c) STEM-EDXS characterization of a single core-shell Pt@FeO_x particle in the Pt/Fe-N-C hybrid catalyst with 2 wt. % Pt; d) CVs in O_2-saturated 0.1 M $HClO_4$ for different thickness of Fe_2O_3 deposited on Pt(111); e) ORR activity at 0.8 V *vs*. RHE as a function of the thickness of the Fe_2O_3 thin-film on Pt(111). The scalar before Fe_2O_3 in the legend in d) indicates the film thickness, in nanometre. Figures a and b, reproduced with permission from Ref. [270]. Copyright [2020] American Chemical Society. Figures c, d and e, reproduced with permission from Ref. [271]. Copyright [2018] The Electrochemical Society.

Recently, HR-STEM images of the same Pt/Fe-N-C material and 2D model surface studies revealed the nature of the Pt particles and shed some light on the complex interaction between Pt and Fe in this synthesis approach. [271] First, it was revealed with high resolution STEM-EDXS that the Pt particles are covered by a thin shell of Fe-oxide, explaining the H_2O_2 and ORR inactivity of the Pt in such Pt/Fe-N-C hybrid (**Figure 26c**). While Fe_2O_3 is *a priori* known to be unstable in the ORR potential range (at least at E < 0.6 V *vs*. RHE) in acid medium, the absence of CO stripping signal after a PEMFC test at 0.5 V supported the stability of Pt core/Fe_2O_3 shell, at least from OCP down to 0.5 V. [270] To gain fundamental understanding on the stability and activity of Pt core/Fe_2O_3 shell particles, the deposition of Fe_2O_3 thin-films, with controlled thickness from 1.0 nm to 6.4 nm, was performed on Pt(111). The thin-films were shown to be stable in acid medium in the potential range 0.45 to 1.05 V *vs*. RHE. This unexpected stability (based on the Pourbaix diagram of Fe) was assigned to the stabilization

of the Fe_2O_3 thin-film by the sub-surface Pt, possibly via hybridization of the Pt 5d orbitals with Fe 3d and O 2p states at the interface. CVs on the model surface layers in the restricted potential range >0.45 V *vs*. RHE showed a strong increase of the ORR activity with decreasing Fe_2O_3 film thickness (**Figure 26d**). Note that it was verified for all films that the Pt surface was fully covered by Fe_2O_3. Further analysis showed that the ORR activity increases exponentially with decreasing film thickness of Fe_2O_3 (**Figure 26e**), supporting an electron tunneling effect from the Pt through the Fe_2O_3 overlayer.

It remains nevertheless unclear if such core-shell particles contributed to stabilize Fe-N_4 sites during operation of the Pt/Fe-N-C hybrids in PEMFC, or if the apparent stable activity over time in PEMFC was a complex outcome of decreasing ORR contribution from Fe-N_4 sites compensated by a thinning of the Fe_2O_3 shell around Pt particles, increasing the ORR activity of such core-shells. Also, while the Pt amount may appear low (1-2 wt. %), its absolute amount is not negligible due to thick Fe-N-C layers (4 mg cm^{-2}) and combined with the low performance reached hitherto with such Pt/Fe-N-C hybrids. To be of practical interest, such an approach would either require significantly improving the power performance of Pt/Fe-N-C hybrid layers, or exchanging Pt with a PGM-free metal.

In contrast to the absence of PGM-free catalysts that catalyse H_2O_2 reduction in acid medium, a number of PGM-free cations or oxides are recognized ROS scavengers in liquid acid medium and/or PEMFC environment. Cerium oxide (CeO_2), Mn oxide, Ce^{3+} and Mn^{2+} cations in particular were investigated in the context of PEMFC for protecting PEM membranes against chemical attack by ROS. [127, 272-275] Trogadas *et al*. [276] proved that CeO_2 mitigates the oxidative degradation of a PEMFC membrane, and that the ROS-scavenging property of ceria is regenerated at the end of the scavenging cycle in acidic media (**Figure 27a**). [274, 276] The challenge with Metal-N-C catalysts is that the ROS scavenger must be in close proximity of the Metal-N_4 active sites (**Figure 27b**), due to the high reactivity of ROS species and their ability to diffuse in the AL. Based on that approach, the Pacific Northwest National Laboratory (PNNL) investigated the addition of nitrogen-doped CeO_x (N-CeO_x) to Fe-N-C, in order to promote the decomposition of H_2O_2 and/or ROS. [277] The authors showed that N-doping increases the Ce^{3+}/Ce^{4+} ratio, positively impacting the ROS scavenging properties relative to undoped ceria. [278] Slightly lower % H_2O_2 during ORR was detected with RRDE by adding N-CeO_x to a reference Fe-N-C *vs*. one without N-CeO_x. Increased durability was also observed during 5,000 load-cycles in O_2-saturated acidic medium by adding 10 wt. % N-CeO_x to a Co-N-C catalyst (**Figure 27c-d**). Improved durability was also observed in PEMFC environment. While the addition of 5 wt. % N-CeO_x to an Fe-N-C cathode AL reduced the initial performance (especially at high current density, much less in the kinetic domain), it mitigated strongly the decrease in performance during a potential hold at 0.4 V compared to the reference cathode layer without N-CeO_x (**Figure 27e**). The BoL and EoL ORR activities at 0.8 V are shown in **Figure 27f**, revealing that, with N-CeO_x, the EoL ORR activity of the Fe-N-C layer is still 32% of the BoL activity, while without N-CeO_x the EoL activity dramatically decreased to 2 % the BoL value. As discussed before, ROS and/or H_2O_2 can induce carbon corrosion, especially during potential cycling. Insights on the stabilization mechanism by N-CeO_x was gained by recording CO_2 emission online. As shown in **Figure 27g-h**, the N-CeO_x/Fe-N-C composite layer maintained lower CO_2 emission at low voltage and also during the switches from high-to-low, and low-to-high potentials, as compared to the Fe-N-C layer. SEM-EDXS analyses after PEMFC operation revealed that Ce atoms were atomically dispersed through the AL. [279] Similarly, Wei *et al.* [280] embedded a phenylenediamine-based Fe/N/C catalyst with CeO_2 nanoclusters using a

hydrothermal method. AST in RDE configuration [0.6 – 1.0 V *vs*. RHE – 100 mV s^{-1} – 10k – O_2 – RT] in 0.1 M $HClO_4$ and OCV tests in PEMFC cathodes (5 h at OCV followed by polarization curve) revealed much better durability. In particular, the current density loss at U = 0.5 V was only 18% after three OCV tests for the CeO_2-modified Fe/N/C catalyst compared to 44% for the Fe/N/C reference material.

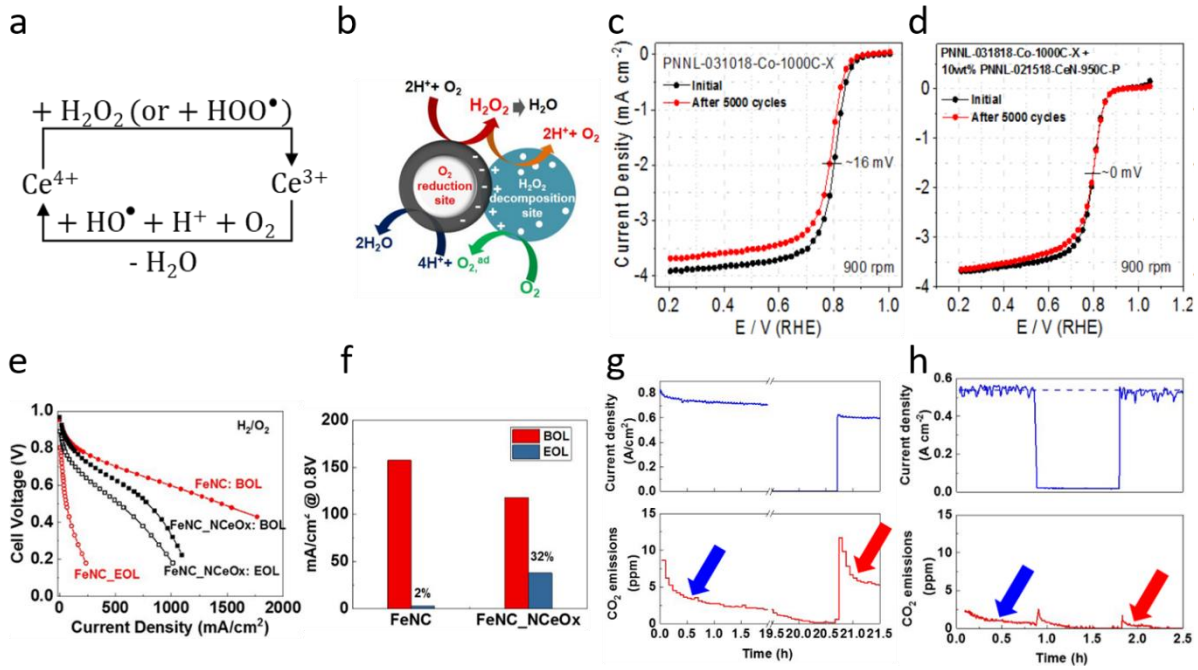

Figure 27. ROS and/or H_2O_2 scavengers for stabilizing Metal-N-C. a) Regenerative ROS scavenging mechanism of CeO_x; b) Scheme of bifunctionality with Metal-N-C and ROS scavengers in a cathode layer to decrease peroxide and ROS production during ORR [278] ; initial and EoT polarisation curve for a Co-N-C catalyst without c) and with d) 10 wt. % of N-CeO_x particles. The AST comprised potential steps between 0.6 V (3 s) and 0.95 V (3 s) with rise time of ~1 s in O_2 saturated 0.5 M H_2SO_4. [278] Improved durability in PEMFC for a composite layer N-CeO_x/Fe-N-C. e) BoL and EoL polarisation curves for a Fe-N-C catalyst from LANL with or without 5 wt. % N-CeO_x physically mixed during cathode AL preparation (the durability test consisted in cycles of the sequence 0.4V-55min/0.85V-5min) [277]; f) ORR activity at 0.8 V in PEMFC at BoL and EoL corresponding to e); CO_2 emission rate during potentiostatic control g) without or h) with N-CeO_x in the cathode layer. The cell voltage was 0.3 V, then OCP hold for 1 h and then back to 0.3 V. The corresponding current density during these potential holds is shown in the middle frame while the CO_2 emission rate is shown in the lower frame. [281] The Figures a, b, c, d, e, f, g, h are reprinted from Refs. [277, 278]. Public Domain.

Further improved durability and avoiding the decrease in performance seen by physically mixing Metal-N-C with *e.g.* N-CeO_x may be reached with bottom-up synthesis approaches, resulting in Ce^{3+} sites covalently integrated, either during or after the synthesis of Metal-N-C. The expected advantages are a shorter average distance between the Metal-N_4 sites and the ROS scavenger Ce site, a more efficient use of Ce atoms and reduced dissolution and migration of Ce atoms or CeO_x NPs in the MEA during operation. The latter is a well-known issue when using Ce^{3+} to stabilize PEM membranes. [282] For example, Li *et al.* [283] reported such a synthesis, involving the adsorption of Fe^{3+} and Ce^{3+} in 1:1 molar ratio on polypyrrole, followed by pyrolysis at 900°C in Ar and then NH_3. The addition of Ce resulted in enhanced atomic dispersion of Fe, leading to a high content of 4.6 wt. % Fe with no or low amount of Fe-Fe signal in the EXAFS Fe K-edge spectrum, and improved ORR activity relative to the parent Fe-N-C prepared identically but without Ce. XRD revealed the peaks of CeO_2 after Ar pyrolysis, but a different pattern after NH_3 pyrolysis, possibly due to N-doping of CeO_x in such conditions.

While that study did not report the stability of the material in acid medium since the focus was on alkaline medium, it is an interesting example for bottom-up synthesis to result in ORR and ROS scavenging bifunctionality in a PGM-free catalyst.

Shao *et al.* [284, 285] functionalized Fe-N-C catalysts with N-doped CeO_x or Ta-doped TiO_x NPs. The authors reported that N-doping promotes non-stoichiometric (Ce^{3+}) and oxygen vacancies, increases the peroxide scavenging ability and enhances the stability of Fe-N-C catalysts, with only 10 mV loss after ORR staircase potential steps of 0.025 V at intervals of 25 s from 1.0 to 0.0 V *vs*. RHE in O_2-saturated 0.5 M H_2SO_4 at 25°C for Fe-N-C-$NCeO_x$ compared to 31 mV for Fe-N-C (**Figure 28a**). The H_2O_2 yield was below 2 % for optimized modified Fe-N-C catalysts (**Figure 28b**), and correlated with decreased CO_2 level in PEMFC cathode. The MEA performance and activity (> 30mA cm^{-2} at 0.9 V) in H_2/O_2 of dual-active site catalyst Fe-N-C-$NCeO_x$ was better than the baseline Fe-N-C (**Figure 28c**), and so was their durability after the DOE ElectroCat protocol (**Figure 28d**). Recently, Xie *et al.* [285] demonstrated that Ta-doped TiO_x NP additives suppressed the H_2O_2 yield by 51 % at 0.7 V after [0.6 – 1.0 V *vs*. RHE – 20 mV s^{-1} – 10k – O_2 – RT] in RDE configuration. Moreover, the current density decay at U = 0.9 V in PEMFC was only 3 % compared to 33 % without scavengers after [0.4 – 0.85 V – 55 min/5 min – 20 cycles – H_2/air – 80 °C].

Beside regenerative ROS scavengers, sacrificial ROS scavengers might be used to stabilize Metal-N-C cathode layers during PEMFC operation. At a system level, the continuous injection of a small amount of gas- or liquid-phase ROS scavengers in the cathode air stream might be applicable. The role of methanol as a sacrificial ROS scavenger was investigated by oxidizing Fe-N-C in either an acidic solution of methanol and H_2O_2, or in the same solution but without methanol. [156] The results showed a slightly reduced deactivation in the presence of methanol, with 40% of the ORR activity remaining after 60 h in 0.2 M methanol compared to *ca* 30 % in the absence of methanol (**Figure 28e-f**).

Overall, the field of composite materials or ALs with PGM-free catalyst and ROS scavengers is burgeoning. It is a promising approach, but will require advanced syntheses approaches to locate the ROS scavengers at atomic or nanometric distance of the ORR active sites, for maintaining the durability over long operation time.

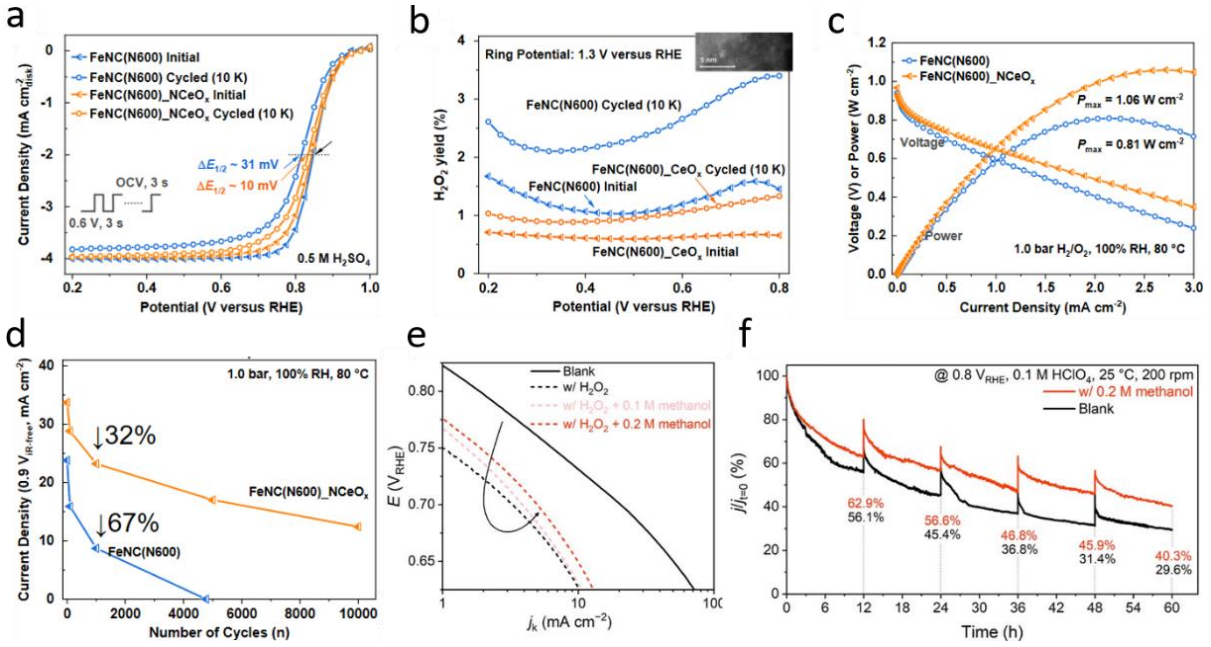

Figure 28. a) Durability of a Fe-N-C catalyst modified by N-doped CeO_x nanoparticles after ORR staircase potential steps of 0.025 V at intervals of 25 s from 1.0 to 0.0 V *vs*. RHE in O_2-saturated 0.5 M H_2SO_4 at 25°C and b) associated H_2O_2 yields measured with RRDE (catalysts loading = 0.6 mg_{powder} cm^{-2}); c) Initial performances and activities in H_2/O_2 PEMFC cathode; d) Activities losses during the DoE Electrocat Durability protocol. Anode: 0.1 mg cm^{-2} Pt/C; Cathode: 2.6 mg cm^{-2} PGM-free (Fe-N-C/$NCeO_x$), 40 wt. % Nafion ionomer; Membrane: NR211; Active area: 5 cm^2; 100% RH, 80°C, O_2+N_2=1 bar. e) ORR Tafel plots measured before (blank) and after the H_2O_2 treatment in pH 1 solutions with H_2O_2 (without methanol, or with methanol in 0.1 or 0.2 M concentration); f) Normalized current density of the Fe-N-C catalytic layer *vs*. time. The potential was set at 0.8 V *vs.* RHE for 60 h in the presence (red curve) or absence of 0.2 M methanol in an O_2-saturated 0.1 M $HClO_4$ electrolyte. Figures a, b, c, d are reprinted from Ref. [284]. Public Domain. Figures e and f, reproduced with permission from Ref. [156] Copyright [2020] American Chemical Society.

4.3.4 Selective formation of durable Fe-N_x sites

Following the identification of durable S2 sites and non-durable S1 sites in PEMFC with EoT ^{57}Fe Mössbauer spectroscopy, [103] the next logical idea was to modify the synthesis of Fe-N-C materials to selectively form the more durable S2 sites (see **Section 2.6.2**), featuring a more graphene-like long range environment for FeN_4 compared to the porphyrinic S1 site. This attractive idea seems to have been achieved in a recent study from Liu *et al*., [286] reporting a breakthrough in the durability of Fe-N-C. A recent work independently confirmed the stabilisation by N-C overlayer deposition, with a compromise between ORR activity and stability found for this approach. The Fe-N-C was prepared from a Fe_2O_3@ZIF-8 catalyst precursor, subjecting it to a first pyrolysis in argon and to a second one with ammonium chloride salt. The resulting catalyst (Fe-AC) was then modified, by placing some nanometric ZIF-8 upstream of Fe-AC, under a flow of inert gas at 1100° C. The decomposition of ZIF-8 at high temperature formed volatile products, partially redepositing onto the Fe-AC surface through a process akin to chemical vapour deposition (CVD). The final catalyst was labelled Fe-AC-CVD, and showed slightly lower initial activity but much improved durability upon load cycle AST [0.6 – 1.0 V *vs*. RHE – unspecified duration/scan rate – 30k – O_2 – RT] in 0.5 M H_2SO_4 (**Figure 29a-b**). The initial selectivity toward four-electron ORR was high and comparable for both materials, excluding the peroxide production as a key explanation for improved durability of Fe-AC-CVD. The high durability observed in RDE setup was also verified in PEMFC, with similar load cycle AST, and also during a potential hold at 0.67 V in PEMFC (**Figure 29c**). While

the XANES and EXAFS spectra were similar for Fe-AC and Fe-AC-CVD, demonstrating atomic dispersion of Fe in both cases, distinct changes in Fe speciation were revealed with ^{57}Fe Mössbauer spectroscopy performed *ex situ* on fresh catalyst powders (**Figure 29d-e**). Fitting of the spectra with three spectral components revealed a higher relative fraction of D2 (site S2) in Fe-AC-CVD, suggesting that the ZIF-8 CVD modified the coordination environment of surface Fe-N_4 sites that were present in Fe-AC. While the change in the relative fractions of D2 and D1 may not seem as dramatic as one might expect in view of the dramatic change in catalyst durability between both materials, one must recall that Mössbauer spectroscopy is a bulk technique that probes all Fe atoms in the catalysts. The change in the relative contents of D1 and D2 quadrupole doublets on the catalyst surface of Fe-AC and Fe-AC-CVD may therefore be much greater than observed experimentally. Other advanced characterisations showed that Fe-AC-CVD has a higher relative content of sp^2 carbon, and additional thin graphitic layers were observed on Fe-AC-CVD. The authors concluded that the CVD modified the surface, transforming some of the S1 sites into more durable S2 sites, also resulting in a carbon surface that is more ordered and more resistant to electrochemical oxidation. Deconvoluting these two effects is difficult as the CVD process modifies both the coordination of surface FeN_4 sites and the carbon surface morphology. The high durability observed may be the result of both these effects, or maybe one effect dominates the other in drastically improving the durability.

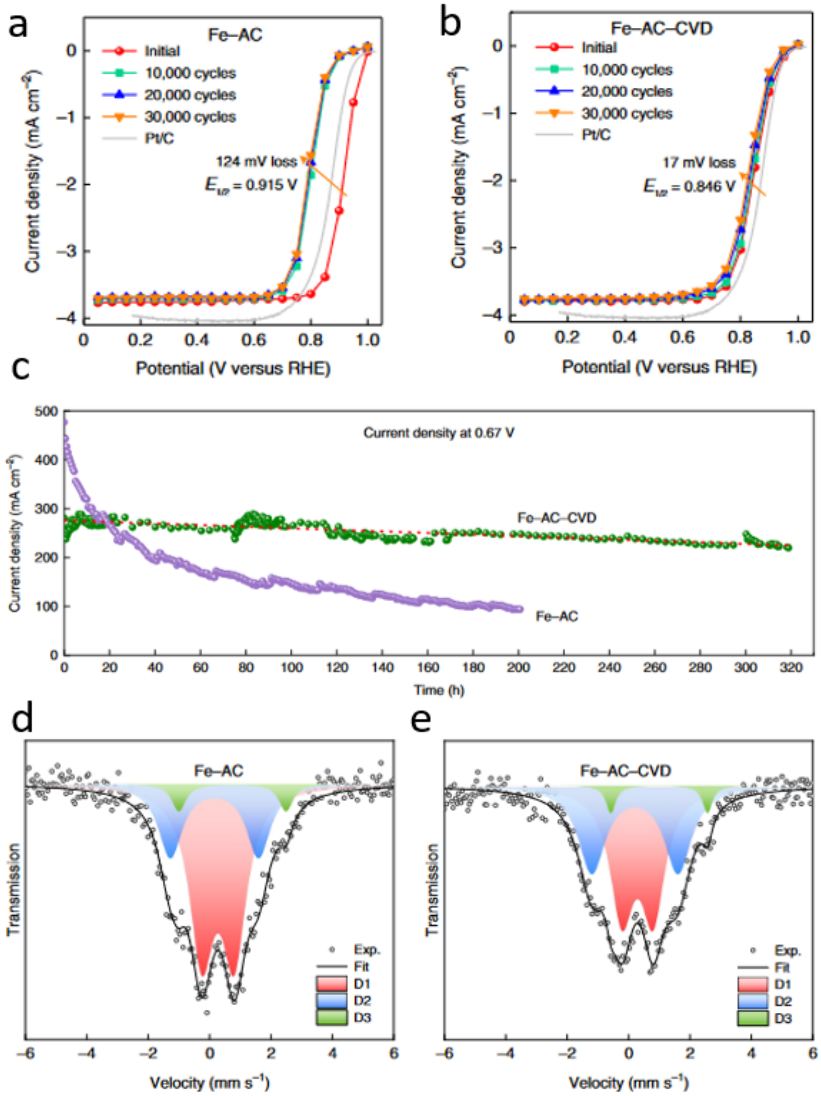

Figure 29. a) Durability of the Fe-AC and b) Fe-AC-CVD catalysts upon load cycle AST in O_2-saturated 0.5 M H_2SO_4, c) Compared durability in H_2/air PEMFC at 0.67 V cell voltage for Fe-AC-CVD and Fe-AC cathodes (80° C, 100 % RH), and d-e) *ex situ* ^{57}Fe Mössbauer spectra of the fresh catalyst powders measured at RT. Figures a, b, c, d and e, reproduced with permission from Ref. [240]. Copyright [2022] Nature Springer.

In a most recent work, the pyrolysis at the unusually high temperature of 1200 °C was found to drastically improve the durability of Fe-N-C materials during PEMFC operation. [287] A set of Fe-N-C catalysts was prepared via the pyrolysis of Fe-doped ZIF-8, changing only the pyrolysis temperature to create a set of samples, labelled as FeNC-T. All materials up to T = 1200 °C showed atomic dispersion of Fe, although with a trend of single Fe atom getting closer from each other in FeNC-1200, while Fe-oxide and α-Fe particles were detected in FeNC-1300. The initial ORR activity in RDE was comparably high for FeNC-1100 and FeNC-1200, and higher than those of FeNC-1000, FeNC-900 and FeNC-1300. The activity decrease after O_2-LC [0.6 – 1.0 V *vs.* RHE – 3s/3s – 10k – O_2 – 25°C] in 0.1 M $HClO_4$ was only 8 mV in $E_{1/2}$ values for FeNC-1100 and FeNC-1200, but larger than 20 mV for FeNC-1000 and FeNC-900. The trend of Fe amount leached in electrolyte was in line with the ORR activity decrease, indicating that a higher pyrolysis temperature mitigated the Fe demetallation. After a PEMFC durability test (50 h at 0.5 V with H_2/O_2 flows), the FeNC-1200 cathode layer showed only a very small drop in PEMFC voltage between BoT and EoT polarisation curves. EXAFS analysis revealed that the Fe-N bond

is significantly longer in FeNC-1200 than in the other materials pyrolyzed at lower temperatures (2.09 *vs*. 1.99 Å), and the Fe-N coordination number was lower (3.4 *vs*. 3.8-4.0). The XANES signature of FeNC-1200 was also significantly different, while the ^{57}Fe Mössbauer spectra revealed a marked increase in the D2/D1 ratio (jumping from 36/60 to 54/39) from the pyrolysis temperature of 1100 to 1200 °C. EXAFS also indicated a minor backscattering signal for Fe-Fe, with a bond distance of 2.7 Å. The authors rationalized all the data, suggesting the gradual transformation from a rather constant D2/D1 ratio up to 1100 °C pyrolysis temperature, then the transformation of some S1 sites (D1 signal) into S2 sites at 1200°C, but also the coexistence of a few Fe atoms as 'clusters' at 1200 °C, an intermediate structure before the strong Fe aggregation observed after pyrolysis at 1300 °C. These transformations were also paralleled by a continuous decrease of the N content with increasing pyrolysis temperature (as expected), while the signature for N-Fe species in N_{1s} XPS spectra was visible for all temperatures. Since N-groups non-coordinating Fe are known to catalyse the 2-electron ORR in acid medium, the removal of such groups may also contribute to the improved durability of the material. The carbon matrix was also shown to be slightly more ordered with increasing pyrolysis temperature.

In summary, these two recent reports certainly represent the most successful approaches hitherto to significantly improve the durability of Fe-N-C materials, by increasing the relative amount of sites S2 versus sites S1. This opens the door to Fe-N-C materials (and possibly transposable to other Metal-N-C materials) with much improved durability in acidic medium.

4.4 Mitigation of degradation phenomena with engineering approaches of the cathode active layer

All fabrication parameters of the cathode AL can potentially be used to mitigate one or several degradation phenomena, even for a given Metal-N-C catalyst. The catalyst loading, ionomer/catalyst ratio, ink formulation, and the fabrication process are perhaps the most important items to be mentioned. While we do not think that those parameters will fundamentally affect the degradation mechanisms taking place, however they can modify their rate and the predominance of a particular degradation mechanism in comparison to others. While the effect of catalyst and/or ionomer loading on the initial activity and power performance of Metal-N-C layers has been much investigated, [59, 288-290] its effect on the durability and main degradation modes is under investigated. Banham *et al.* reported improved apparent durability of Fe-N-C layers with increasing loading from 1 to 4 mg cm^{-2}. [291] The effect was evidenced by reporting the cell voltage (normalized by cell voltage at beginning of test) before and after a galvanostatic hold at 0.5 A cm^{-2}. The main degradation mechanism associated with the catalyst loading effect was assigned by the authors to carbon oxidation, on the basis of increased double layer capacitance after the PEMFC durability test (and especially broad redox peaks at 0.6 V associated to oxygen-functional groups on carbon). Indeed, for a fixed geometric current density of 0.5 A cm^{-2}, a lower catalyst loading implies a lower geometric SD (number of Fe-N_4 sites per cm^2 of geometric electrode area), which in turn implies that each active site has to work more. The higher turnover on each active site in turn implies a higher local production of H_2O_2 and ROS, which could explain the faster decay observed at low loading by Banham *et al*. [291] Slightly contrasting this report, Damjanovic *et al.* reported no clear effect of catalyst loading (0.4 and 4.0 mg cm^{-2} studied) on the performance loss observed over repeated PEMFC polarization curves. [290] The decay was significantly higher with the low loading, when looking at the cell voltage drop at 100 mA cm^{-2}, but comparable for both the loading of 0.4 and 4.0 mg cm^{-2}, when looking at the cell voltage drop at 500 mA

cm^{-2}. The authors highlighted that the different observation with Banham *et al.* [291] may be due to the different durability tests employed, galvanostatic hold on one hand and repeated polarisation curves on the other hand. The latter approach implies a broad range of electrochemical potentials experienced by the catalytic layer, which can trigger different degradation mechanisms. Of course, the Fe-N-C catalyst also differed, which can also be a reason for the different outcomes of AL thickness effect.

Nevertheless, thick catalyst layers open the possibility to use different parts of the AL at different times of the durability test, mitigating the practical cell performance decay. Banham *et al.* [291] suggested that, for thick ALs, the majority of the ORR takes place initially close to the PEM | AL interface. In the case of thick catalyst layers, the reaction front can move in deeper inside the AL after most of the Fe-N_4 sites located close to the PEM | AL interface are deactivated or destroyed, mitigating the performance loss. This is obviously impossible with thin ALs. This strategy might be useful to practically design Metal-N-C layers with improved apparent durability, but it must be kept in mind that the approach is fundamentally based on the preparation of ALs that initially present an uneven utilization of active sites, *i.e*. a by-design non-ideal AL.

Ionomer/catalyst ratio is also a key parameter for AL design and performance. Decreased Nafion ionomer content from 60 to 35 wt. % resulted in slightly decreased ORR activity at 0.8 V in H_2/air BoT PEMFC but improved cell performance above 0.5 A cm^{-2}. [292] The effects were assigned to insufficient amount of Nafion to wet the catalyst area at low ionomer content, and excess ionomer filling the macropores and increasing the layer hydrophilicity at high ionomer content. In the context of cell durability, low ionomer / catalyst ratio can exacerbate the exchange of protons by metal cations (iron and other metals used for Metal-N-C catalysts) and also the chemical degradation of Nafion ionomer in the AL. Both phenomena can decrease the proton conductivity throughout the layer, contributing to the performance decay of the cell. The re-protonation of Nafion ionomer after durability test of Fe-N-C layers was tried by Zhou *et al.* but did not lead to any partial reactivation of the PEMFC performance, whereby it was concluded that the reason for the decreased proton conductivity through the cathode layer was due to the chemical degradation of the cathode Nafion ionomer by ROS species, as supported by ^{19}F nuclear magnetic resonance. [293] Interestingly, the use of a chemically more robust inorganic solid-state proton conductor, namely cesium phosphotungstic acid, mitigated the performance loss. [293]

The study and quantification of changes of ion exchange capacity, proton conductivity and electronic conductivity throughout PGM-free cathode layers before and after durability tests certainly deserves more attention in the future.

5. Discussion

5.1 Relevant accelerated stress test protocols

ASTs are valuable tools to assess the structural degradation and ORR deactivation of different Metal-N-C catalysts in acidic environment, either in (R)RDE or in PEMFC. [73, 286, 294, 295] Combined with ORR activity measurements at different stages, ASTs allow unveiling structure-chemistry-catalytic activity-stability relationships, which can be used to design more durable Metal-N-C catalysts. ASTs can probe the effect of specific parameters: electrochemical potential, temperature, and gas atmosphere. In what follows, we discuss the key ageing parameters of

ASTs and propose the definition of ASTs that can investigate different degradation mechanisms of Metal-N-C materials, applicable in (R)RDE setup or in PEMFC.

5.1.1 Limits and alternation modes of the electrochemical potential

Load-cycling AST (LC-AST)

The electrochemical potential limits used, the frequency of alternation between the UPL and LPL limits and the mode of potential alternation are pivotal parameters, which can influence the extent of deactivation and structural changes. Various potential alternation modes are currently used in the literature, the most common ones being triangular wave (TW), square wave (SW) or hybrids of TW and SW, scanning the potential between UPL and LPL followed by a potential hold (TW-H). [296] Uchimara *et al*. [297] and Gilbert *et al*. [298] have shown that degradation of Pt-based/C catalysts is exacerbated for SW *vs*. TW both in solid and liquid electrolyte. A recent comparative study by Harzer *et al*. [296] has shown that the extent of degradation of Pt/C catalysts is similar for AST using SW and TW-H (ASTs were performed at 100 kPa abs , 80 °C, 100% RH and H_2 /N_2 flows on anode/cathode, respectively). It was hypothesized that i) carbon corrosion does not significantly occur in the 0.6 to 1.0 V *vs*. RHE potential range with Pt/C catalysts, ii) more severe electrochemically active surface area (ECSA) losses of Pt/C catalysts reported with SW *vs*. TW and TW-H are related to a larger extent of Pt oxidation at UPL and thus more Pt being dissolved during the subsequent step at LPL. The latter was supported by a less severe ECSA decrease with a TW-H AST featuring a lower UPL of 0.85 V *vs*. RHE. [296] When trying to adapt these findings to Metal-N-C catalysts, similarities but also differences appear. Similar to what has been shown for Pt/C catalysts, the corrosion of the carbon matrix does not significantly take place with Metal-N-C materials if the AST is performed in a deaerated electrolyte, these conditions avoiding ROS-induced carbon corrosion [70]. For aerated electrolyte, ROS-induced carbon corrosion with Metal-N-C catalysts leads to possible complex effects of the UPL and LPL values, and of the potential alternation mode. In this case, the extent of carbon corrosion may be proportional with the cumulative Faradaic charge during the AST, assuming the relative amount of ROS produced during ORR is relatively independent of the electrochemical potential. This possibility was recently demonstrated to take place in alkaline medium for a commercial Fe-N-C catalyst. [223] A low LPL and a SW mode would then likely result in increased carbon corrosion, while the rotation rate of the electrode during AST could also increase the carbon corrosion, by increasing the O_2 flux towards the electrode, and thus the ORR current density.

Regarding the fate of metal cations, the possible outcomes differ significantly between noble and non-noble metals. While Pt is subject to oxidation and dissolution, it can also be redeposited electrochemically as metallic Pt at the LPL. Since the rate of oxidation, dissolution and redeposition are affected by the UPL and LPL values, the time spent at the UPL/LPL, the temperature of the electrolyte and the thickness of the catalytic layer, the deactivation and ECSA losses can also be affected by all those parameters. In contrast, non-noble metals are less prone to be electrochemically oxidized at UPL since they are already typically at +II or +III oxidation states in Metal-N_x moieties, but they can also not reintegrate the □-N_x cavities after their leaching, leading to an irreversible decrease of active site density. Leached non-noble metal cations cannot be electrochemically reduced to metallic particles at typical LPL values (0.4-0.6 V *vs*. RHE) but can reprecipitate as metal(hydr)oxide, in particular, iron. This is a non-electrochemical reaction and therefore independent of potential, but dependent on the local pH and the local concentration of metal cations. Such particles have however no ORR activity in acid medium.

Recent AST proposed by Wu's group [286] suggested that the UPL should approach the OCV for Metal-N-C-materials. However, it has the disadvantage that different OCV will be used for different Metal-N-C catalysts, modifying the overall definition of the TW if a fixed scan rate is used, in turn possibly influencing the extent of corrosion of the carbon matrix in the case of aerated electrolyte. A fixed UPL value is thus recommended for load-cycles on PGM-free catalysts, for example of 0.92 V (see LC-AST presented in **Table 2**). Alternatively, to screen a broad range of catalysts with widely different initial mass activities, a fixed potential interval between LPL and UPL *e.g*. [(OCV - 0.32 V)-OCV] will be more appropriate, in order to have a constant duration (TW) or to keep a nearly constant Faradaic charge (SW), independently of the catalyst activity. These suggestions are in line, with some variations, with the recommendations of the ElectroCat consortium of the US DoE. [73] The number of cycles is another important parameter: recent studies in RDE used 30k potential cycles to evaluate the stability/durability of a given Metal-N-C catalyst. [21, 95] While this high number of cycles is valuable on down-selected materials, 10k cycles also seems acceptable and has the advantage to require less than 24 h, for most AST cycle definitions (typically 6 s duration per load cycle).

Start-up/Shutdown AST (SU/SD-AST)

The carbon matrix is prone to corrode during SU/SD ASTs. Goellner *et al.* [141] and Kumar *et al.* [21, 70] have shown that such conditions cause massive degradation of the Fe-N_x sites and of the supporting N-doped carbon matrix. The relevance of such AST for PEMFC catalyst development is however questionable. First, the potential of PEMFC cathodes does not alternate constantly between 1.0 and 1.5 V *vs*. RHE in applied PEMFC systems. Moreover, mitigation strategies at system level exist to avoid the transient polarisation of the cathode to such high potentials. Thus, while the improved resistance of Metal-N-C catalysts to the SU/SD-AST protocol is desirable, it is by no means compulsory for a practical application. However, the SU/SD-AST might provide rapid information on the corrosion resistance of the carbon matrix for both Pt-based/C [294, 299] and Metal-N-C [21] catalysts. We thus recommend performing the SU/SD-AST at T = 60 or 80°C for a small number of cycles (0.5 k) to screen the resistance to carbon corrosion and associated ORR losses of different Metal-N-C catalysts (see SU/SD-AST protocol in **Table 2**).

5.1.2 Temperature

Another important, yet often underestimated, contributor to the rate of cathode catalyst's degradation is temperature. A very representative example has been given by Dubau and Maillard [175] for Pt/C catalyst. The authors showed that the gap between 'beaker' cells (cells made of glass and filled with liquid electrolyte) and MEAs can be bridged by using similar temperature. Indeed, while ASTs performed on Pt/C electrocatalysts in liquid electrolyte at 25°C showed modest changes in morphology, AST performed at 80°C accurately reflected the situation reported after ageing in MEA configuration. The same holds true for Fe-N-C catalysts: Goellner *et al.* [117, 141] reported that the ORR mass activity decay was 18 times larger at 80°C than at 20°C for a [0.2 – 1.4 V *vs*. RHE – 10 mV s^{-1} – 0.15 k – N_2] AST in 0.1 M H_2SO_4. This increased activity decay with temperature correlated well with the corresponding 14-fold increase in the COR rate observed from 20 to 80°C. A temperature of 80°C is obviously best adapted to simulate the situation occurring in operating PEMFC cathode, however 60°C is an alternative temperature if, for practical reasons (*e.g*. corrosion of the (R)RDE set-up, excessive evaporation of electrolyte), a temperature of 80°C cannot be used. For LC-AST, the effect of temperature on the extent of deactivation is more moderate, but different temperatures can

affect the fate of leached metal cations, either remaining as free cations in electrolyte, or precipitating as iron (hydr)oxides in the AL. [103]

5.1.3 Atmosphere used to saturate the electrolyte (RDE) or to feed cathode (PEMFC)

A major finding that has been covered in Section 2.6 is that significantly different degradation mechanisms and extents of deactivation take place for Metal-N-C catalysts under O_2-free and O_2-rich atmosphere, with similar outcome seen in RDE and PEMFC. [70, 76] For most Metal-N-C materials with complete or near-complete dispersion of the metal atom as Metal-N_x sites, little degradation is observed after LC-AST with N_2-saturated electrolyte. Nevertheless, the application of such LC-AST is still useful, to assess whether the material is fully stable in acidic conditions in absence of ORR, and to establish a baseline to which the LC-AST with O_2-saturated electrolyte can be compared to.

Table 2. Accelerated stress tests proposed for Metal-N-C electrocatalysts. The AST should be combined with acquisition of full polarization curves in O_2-saturated environment, before and after the AST, for quantification of the ORR activity change due to the AST.

AST	Conditions	Main Expected Degradation Mechanisms
Load-cycling (LC-AST)	10,000 cycles between 0.6 and fixed potential (*e.g*. 0.92 V *vs*. RHE) or [(OCV-320 mV)-OCV] at *T* = 80°C, or 60°C 3 s at each potential (SW) or 100 mV s^{-1} (TW)	O_2-free atmosphere: Demetalation due only to acidic medium; protonation of N-groups
		O_2-containing atmosphere: ROS-induced carbon corrosion and associated demetalation and modification of the TOF of remaining Metal-N_x sites
Start-up/shutdown (SU/SD-AST)	500 cycles between 1.0 and 1.5 V *vs*. RHE at *T* = 80°C, or 60°C 3 s at each potential (SW) or 100 mV s^{-1} (TW)	O_2-free or O_2-containing atmosphere: Classical carbon corrosion

5.2 Advantages, limitations and pitfalls of physicochemical characterization techniques to unveil the degradation mechanisms of Metal-N-C catalysts

Researchers use various physicochemical techniques to unravel the degradation mechanisms of Metal-N-C catalysts (**Table 3**). In this section, we present some of the most important ones for characterizing Metal-N-C materials, discuss their advantages, limitations and possible pitfalls in the context of investigating degradation mechanisms.

High-resolution high-angle annular dark field scanning transmission electron microscopy (HR-HAADF-STEM) is ideally suited to visualize the distribution of transition metal atoms in the nitrogen-doped carbon matrix, whether in the form of single metal atoms or as (nano)particles or a combination thereof, before and after electrochemical ageing. [30] When combined to electron energy-loss spectroscopy (EELS), HR-STEM can provide atomic-scale insights of the transition metal atoms. For example, the technique has revealed [30] that single Fe atoms embedded into N-doped graphene feature average composition of FeN_4, consistent with the structure of the active sites deduced from XAS analysis of model Fe-N-C catalysts. The major advantage of HR-STEM is probably also its main drawback. Indeed, insights are obtained on a

limited area of the material, and are thus not necessarily representative of the average Fe speciation before or after aging, while also possibly missing inhomogeneous transformation of Fe-N-C through the thickness of a PEMFC cathode. A typical example of this assertion might be the observation of Fe oxide NPs after AST under O_2 on a thin-film RDE by Kumar, Li *et al.* [70, 103] not by Osmieri *et al*. [71] after similar AST applied in PEMFC. This difference might be related to uneven distribution of Fe oxide NPs in the MEA used by Osmieri *et al.* Indeed, the degradation of PEMFC MEAs is known to be inhomogeneous, due to gradients of O_2 concentration and electrolyte potential arising at high current density through the cathode AL, leading in turn to a distribution of volumetric current density throughout the AL. Such phenomena occur even for thin Pt/C based cathodes and certainly even more prominently in thick Metal-N-C cathodes. Thus, inhomogeneous utilization (due to gradients of O_2 concentration and electric potential in the ionomer phase) of active sites in Metal-N-C cathode catalytic layers is prone to lead to inhomogeneous degradation and metal speciation after PEMFC tests. It is therefore recommended to perform HR-STEM analyses on different areas of a cathode AL (in particular at the cathode|PEM and at the cathode|GDL interfaces) and/or to combine such analyses with other characterisation techniques that provide information on a larger scale. Another possible limitation or even pitfall of HR-STEM concerns the possible interactions between the electron beam and the transition metal atoms occurring during inelastic shocks or during its scattering at large angles. The transfer of kinetic energy may facilitate the scattering of the transition metal atoms on the surface and eventually the formation of NPs or nanoclusters. The electron beam may also modify the structure of the carbon matrix. [300, 301] Indeed, transfer of kinetic energy from the electrons to the carbon atoms displaces them from their equilibrium positions. By ripples, these atoms collide with their neighbours, which facilitates local restructuration of the carbon matrix. This effect, referred to as 'knock-on', [300] mostly takes place for accelerating voltages of 100-300 kV, classically used in TEM (60 kV accelerating voltage or cryo-holder are currently employed for HR-STEM to minimize beam damage). This phenomenon might become of major importance for *in situ* TEM studies. Two configurations are classically used in *in situ* TEM studies: environmental TEM and thin-windowed liquid cell TEM. In the former, the catalyst is exposed to a partial pressure (from 10^{-5} mbar up to some mbar) of a gas that is also found in the conditions of the application. In that frame, we note that O_2 has been reported to lead to metal oxide formation, evidenced for stainless steel or copper TEM grids during *in situ* TEM experiments. [302] Hence, caution should be taken if such configuration is used for investigating Metal-N-C catalysts, as this might lead to oxidation of the carbon matrix or formation of metal oxides. In liquid cell TEM, the sample is immersed in a liquid electrolyte between the two windows. The decomposition of water (radiolysis) leading to the formation of solvated electrons, $^{\bullet}H$, $^{\bullet}OH$ and $^{\bullet}OOH$ species is a widely documented phenomenon. Free radicals production may degrade the catalyst in a different way than that encountered in the conditions of the application. [303] Limited beam dose and/or exposure time, control 'beam on' and 'beam off' experiments and images in different zones of the catalytic layer are thus recommended to avoid artefacts. Another possibility to avoid or minimize the 'beam effect' is to perform experiments using an identical-location transmission electron microscopy (IL-TEM) set-up. In this technique, first introduced by Mayrhofer and co-workers, [304] a TEM grid made of a corrosion-resistant and electro-inactive metal (usually Au) is loaded with the electrocatalyst, used as a working electrode in a conventional electrochemical cell, and the same area or same particle of a catalyst can be observed before and after electrochemical measurements. IL-

STEM and IL-HR-STEM-HAADF experiments for Metal-N-C catalysts were first performed by Choi *et al.* [117] and Kumar *et al.* [60] as discussed in **section 2.3.1**.

Complementary to electron microscopies are X-ray absorption techniques. XANES and EXAFS provide information about the oxidation state of the x-ray absorbing element, the nature and the average distance between the absorbing element and its neighbours. The obtained information is averaged over all metal atoms of a same element present in the sample, including active Metal-N_x sites and inactive or less active metal clusters, surface sites and bulk sites. XANES and EXAFS are therefore well suited to understand the degradation mechanisms of Metal-N-C materials with only, or mostly, Metal-N_x sites at BoT. The presence of a significant fraction of metallic particles in pristine catalysts prevents an accurate tracking of coordination changes and quantitative changes of Metal-N_x sites before and after AST, due to the fact that XAS techniques provide a signal summed on all metal atoms of a same element, present in the sample. This effect is even more reinforced with EXAFS, due to exacerbated signal for ordered Fe metallic particles (with high coordination number for Fe-Fe) compared to atomically-dispersed Metal-N_x sites with lower coordination number for Metal-N bonds (typically 4) and a more disordered structure. Another limitation of XANES-EXAFS lies in the difficulty in distinguishing the XANES and EXAFS signal of Fe-N_x sites from that of nanosized FeO_x particles. Since the latter can form *operando* as a result of the destruction of Fe-N_x sites, this limitation is severe for unambiguously tracking the fate of such sites. The advantages of XANES-EXAFS are its applicability to *in situ* and *operando* measurements with fast acquisition time, and its applicability to numerous chemical elements. [305] X-ray emission spectroscopy is a complementary analysis to XAS, that gives information on the average spin state of Fe and could be envisioned to track structural reorganisation of Fe-N-C materials during ORR electrocatalysis. [306-309]

^{57}Fe Mössbauer spectroscopy has proven a unique tool to investigate the oxidation states and chemical environment of Fe in Fe-N-C catalysts. As XAS, the technique provides a signal summed on all Fe atoms present in the sample. However, due to very different spectroscopic responses, the technique is powerful to distinguish between the spectroscopic signature of Fe crystalline phases (magnetic sextet signals for *e.g.* Fe carbides, Fe oxides and α-Fe), single Fe atoms (quadrupole doublet signal), and non-magnetic gamma-iron (singlet component). Therefore, fitting the Mössbauer spectra of complex Fe-N-C materials with a set of singlet, doublets and sextets allows unveiling and quantifying how much of Fe is present as NPs/nanoclusters and how much as single Fe atoms. Two main doublets, namely D1 and D2 in the literature, are usually encountered in *ex situ* Mössbauer spectra of Fe-N-C catalysts. These doublets differ in their quadrupole splitting (QS, represented by the peak to peak "distance" of a given doublet). They have been empirically assigned from the Mössbauer spectra of well-defined Fe complexes and Fe-macrocycles with known Fe coordination, oxidation state and spin state. However, these empirical assignments are not ideal to understand Fe-N_x sites covalently embedded in a carbon matrix, as DFT calculations have shown. For example, three different sites (namely Fe(II)N_4C_{12} site with spin state 0 or 1 but also Fe(III)N_4C_{12} with spin state 5/2 or Fe(III)N_4C_{10} with spin state 5/2) all lead to QS-values around 1 mm s^{-1}, compatible with the experimental D1. [144] In contrast, only the QS-values calculated for the Fe(II)N_4C_{10} (in spin state either 0 or 1) moiety matched the experimentally observed value of D2 (2.4 - 3.0 mm s^{-1}). [144] This highlights the need to couple Mössbauer spectroscopy with other techniques. Mössbauer spectroscopy was recently combined with *in situ* (cathode fed with inert gas) electrochemistry using an isotope-enriched ^{57}Fe-N-C cathode. [103] The experiments showed

that the D1 signal was potential dependent, switching reversibly between Fe(III) and Fe(II) states. In contrast, the D2 signal was independent on the potential, supporting its previous assignment to a Fe(II) site. The experiments evidenced a limitation of ^{57}Fe Mössbauer spectroscopy, namely the long time required for spectral acquisition with sufficient signal/noise ratio. Tens of hours were necessary for acquiring one spectrum, even working with a Fe-N-C cathode prepared with the Mössbauer-active ^{57}Fe isotope. [103] For this reason, acquisition of spectra in *operando* conditions in PEMFC was not possible, due to the continuous change of Fe speciation during the course of the acquisition. Mössbauer spectra were thus acquired after *operando* PEMFC tests. It was firstly shown that a fraction of the D1 sites quickly converts to superparamagnetic Fe-nano-oxides. Measurements at -268 °C were necessary to reveal this, since at room temperature (or any temperature above *ca*. -173 °C), superparamagnetic Fe-nano-oxides contribute with a doublet signal that is very similar to the 'true' D1 signal (of Fe(III)N_4 sites or D1-like signal of other Fe-N_x species). [310] This is a significant limitation, and even a pitfall, for the application of ^{57}Fe Mössbauer spectroscopy to the understanding of the degradation of Fe-N-C catalysts. Low temperature Mössbauer spectroscopy (therefore conducted *ex situ*) allows however disentangling between these two species as Fe-nano-oxides contribute then with a sextet signal, as large Fe-oxides do, while Fe(III)N_4 sites still contribute with the D1 doublet signal.

Complementary to Mössbauer spectroscopy, nuclear inelastic scattering (NIS) reveals the full spectrum of vibrational dynamics of the probed Mössbauer nuclei and allows the identification of modes which are not available otherwise. Combined NIS measurements and DFT calculations were used by Kneebone *et al.* [311] to unveil the nature of the ORR active sites in a PANI-derived Fe-N-C catalyst. The technique was also used recently by Wagner *et al.* [234] to provide a proof of the presence of Fe-oxide and α-Fe species after pyrolysis at 600°C of carbon-supported chloro-iron tetramethoxyphenyl-porphyrin followed by acid-leaching (1 M HCl). The authors concluded that oxide species form after contact with air, while α-Fe species mostly correspond to Fe particles embedded in the carbon matrix. To the best of our knowledge however, this technique has until now never been used to investigate the degradation mechanisms of Metal-N-C catalysts.

While STEM, XAS and Mössbauer spectroscopy are powerful tools to investigate Metal-N-C catalysts before and after electrochemical aging, or even *operando* for XAS, these techniques are not surface-sensitive. The same holds true for Raman spectroscopy, used to probe the degree of graphitization of the N-doped carbon matrix carbon, X-ray diffraction, used to reveal the presence of metal-based crystalline phases and the graphitization degree of the carbon matrix, and for EDXS which can quantify the metal/(metal + carbon) ratio in different regions of a Metal-N-C catalyst.

Molecular probes and electrochemical techniques have been developed to overcome this issue. Malko *et al*. [26] first developed a nitrite adsorption/reduction method to evaluate the active site density at the surface (ASD, see **Equation 2**) of Metal-N-C catalysts before and after ageing tests in a RDE setup. [60, 70] However, the method has some limitations: (i) measurements are conducted at pH 5.2, which is less acidic than the typically operative conditions of a PEMFC device, and (ii) the ORR activity does not completely vanish after nitrite adsorption, suggesting that nitrite anions do not poison all Metal-N_x sites, but only the most active ones. [27] Finally, it was recently reported that nitrite anions probe also the surface of iron oxides. [70] Therefore the technique cannot be generally applied to measure the ASD of aged Fe-N-C materials, unless independent techniques can provide evidence of the absence of Fe oxides after aging

for particular samples or aging conditions. The number of electrons exchanged per nitrite molecule reduced also remains an open question, with direct implication on the derived ASD number. Indeed, whereas Malko *et al*. [26] suggested a 5-electron process of nitrite electroreduction to NH_3 on Fe-N_x sites, Kim *et al*. [312] recently showed that nitrite species were selectively reduced into hydroxylamine via 3-electron process onto a given Fe-N-C catalyst. The 67 % uncertainty in the number of electrons exchanged reflects directly on the value of ASD, which is highly significant. Moreover, the product of nitrite electrochemical reduction might change in the course of the AST, further introducing a source of uncertainty. It would be desirable to combine the results of the nitrite electroreduction measurements with an analytical method to achieve quantitative insights into the values of ASD in the pristine and aged states.

Recently, Sahraie *et al.* [38] developed an *ex situ* method based on CO chemisorption/desorption. The method proved applicable to measure the ASD of Fe-N_x and Mn-N_x sites, but requires low temperature (-100 °C) to favour the CO adsorption (explaining also why CO molecules do not poison Metal-N_x sites at room or application-relevant temperatures). The technique can therefore not be applied *in situ* or *operando*. Note also that the ASD values obtained by this method depend on the pre-treatment protocol because a thermal treatment (> 600°C, for Fe-N-C materials) must be performed to remove O_2 pre-adsorbed on Fe-N_x sites. [39] Because of this, the method cannot be applied to the *post mortem* investigation of Fe(Mn)-N-C cathodes, since Nafion ionomer of the cathode AL would be converted to S-doped carbon after such a heat treatment, and Fe-oxides or Mn-oxides may also be transformed to metallic particles or even possibly, reactivated to Metal-N_x sites. Recently, Bae *et al.* [313] used cyanide as a molecular probe to measure the ASD of a previously well characterized Fe-N-C material, and that of other single-metal-site Metal-N-C materials based on other 3d transition metals. The authors correlated the decrease in cyanide concentration triggered by irreversible adsorption onto a model Fe-N-C catalyst to the decrease in ORR activity. Moreover, they showed that cyanide poisoning can be performed in a broad pH range (1−13), and for sensing metallic NP surfaces, including PGM-based ORR electrocatalysts. Since cyanide anions do not seem to distinguish Metal-N_x sites from metallic surfaces, their use to investigate the fate of Metal-N_x sites during electrochemical aging is likely challenging, unless oxidized surfaces (in particular those of Fe, Co, Mn) do not adsorb cyanides.

Snitkoff-Sol *et al.* [314] developed a different approach, based on Fourier-transform alternating current voltammetry to measure the ASD values. The principle is based on the fact that under *ac* current, the active sites generate a current related to the Fe(II)/Fe(III) redox couple, which is intrinsically nonlinear *i.e*. easily distinguishable from other processes occurring in parallel (under *dc* current, the low intensity Faradaic processes are shrouded by other process such as double layer charging). The approach was used to monitor the decrease in ASD *in situ* during [0.6 V – 40 h – N_2 – 80°C] and proved valid for two different catalysts.

Table 3. Advantages, limitations and pitfalls of various techniques for studying the degradation mechanisms of Metal-N-C materials.

Techniques	Advantages	Limitations	Pitfalls
Nitrite adsorption/reduction method	Assess ASD value of pristine or aged electrodes. *In situ* ASD measurement. Simple electrochemical analysis.	Demonstrated hitherto only for Fe-N-C materials. *In situ* measurement but at pH 5.2. Sensitive to the most active Fe-N_x sites but does not count less active Fe-N_x sites.	Unclear product of nitrite reduction (NH_4^+ or NH_3OH^+, 5 or 3 e^- involved, respectively), leading to high uncertainty in ASD calculation. The method also senses FeO_x clusters, which can form *operando*, see Refs. [70, 103] .
^{57}Fe Mössbauer spectroscopy	Facile identification of relative amounts of Fe-N_x sites and Fe particles. Applicable to pristine and aged electrodes. Possible identification of oxidation and/or spin state of Fe-N_x sites.	Need of ^{57}Fe enriched samples for measurements on electrodes. Applicable mainly to ^{57}Fe and ^{119}Sn. Bulk technique. Long acquisition time for *in situ* measurements.	Needs acquisition at low *T* (typically, -268°C) in order to distinguish Fe-N_x sites with D1 signature from nanosized FeO_x clusters.
XANES and EXAFS	Can probe changes in oxidation state and coordinating environment of isolated metal centres. Applicable for *in situ* or *operando* studies.	Access to Synchrotron radiation facility. Bulk technique. Signal convoluted on all atoms of a given metal, impeding studying Fe-N_x sites in Metal-N-C materials comprising large relative amount of metal clusters. XANES quantitative analysis requires collaboration with specialists in theoretical chemistry.	Similar XANES spectra of Fe-N_x sites and FeO_x nanoclusters, a drawback for studying aged electrodes. EXAFS is unable to distinguish Metal-O from Metal-N bonds.

	Applicable to many metal elements. Fast acquisition time.		
TEM/ HRTEM/ EDXS	Study changes in carbon morphology and atomic structure. Visualisation of metal-rich particles.	Ultrathin samples required. Sample damage/alteration under beam. Local analysis.	Burn-in spots can create artefacts.
HAADF-STEM	Direct observation of single atoms, and of metal-rich particles after AST.	Sample damage/alteration under beam. Local analysis.	Fe and Zn atoms cannot be distinguished (drawback for Zn-MOF derived materials). Burn-in spots can create artefacts.
IL-TEM	Study changes in morphological surface at the nanoscale. Study the degradation mechanism in different reaction and potential/current conditions	Does not provide *in situ* information. Time-consuming. Sample alteration under beam ray. Local analysis.	Burn-in spots can create artefacts.
In situ liquid cell TEM	Study single metal atoms during electrocatalysis	Electron beam induced materials damages.	

6. Conclusions and perspectives

This review article aimed at providing a comprehensive overview of the current understanding of the degradation mechanisms of Metal-N-C catalysts used to reduce oxygen in proton-exchange membrane fuel cells, and of the material's approaches recently explored to mitigate these mechanisms.

A first major conclusion is that Fe-N-C catalysts typically suffer from major structural degradations and losses of their ORR activity in acidic medium in the presence of O_2 and at electrochemical potentials at which these materials catalyse the ORR, supporting an intimate correlation between the degradation rate and the electrocatalysis of the ORR on Fe-based sites, or on other Metal-N_x sites. The latter conclusion is directly supported by the fact that under the same electrochemical conditions but in the absence of O_2, little to no degradation of the structure and catalytic activity of Fe-N-C materials is observed. Similar trends were observed in liquid acid electrolyte and in proton-conducting polymer electrolytes, and the effects were also quantitatively comparable if the same temperature was applied in both environments. Several studies point toward the formation of reactive oxygen species (ROS) as the key reason for the poor durability of Metal-N-C materials in acidic medium. The ROS formation can either be a direct consequence of the ORR mechanism on Metal-N_x sites or an indirect consequence due to H_2O_2, a by-product of the ORR, reacting with Fe or other 3d transition metal cations. The gap between the degradation of Metal-N-C materials observed in O_2-free and in O_2-rich acidic environments is therefore a key difference with state-of-art platinum-based catalysts, for which little to no difference is observed for accelerated stress tests performed in O_2-free and O_2-rich environments.

As a result, the electrocatalysis of the ORR by Metal-N-C materials rapidly leads, in acidic medium, to electrochemical carbon corrosion and to the rapid destruction of a significant fraction of the Metal-N_x sites that were initially present. In addition, the Metal-N_x sites that survived the aging experiment likely experience a modified electronic and chemical environment as given by the surface-oxidized carbon matrix, leading to a decreased ORR turnover frequency of Metal-N_x sites. This effect is supported by experimental and theoretical works showing that the introduction on the carbon surface of a small number of oxygen groups leads to a modified binding energy of O_2 on Metal-N_x sites. While the different degradation mechanisms discussed in the present review apply to all Metal-N-C catalysts, the relative importance of each degradation type likely depends on the chemistry and morphology of the catalysts. In particular, the starting point on the SD-TOF ORR reactivity map of a fresh Metal-N-C catalyst certainly has implications on which degradation mechanism will predominate. For example, Metal-N-C materials with an initial high SD but low TOF would likely suffer mainly from SD losses while materials with an initial low SD but high TOF would suffer mainly from TOF decrease (due to mild surface oxidation).

Based on these recently acquired fundamental understandings of the key degradation or deactivation mechanisms of Metal-N-Cs, the four main approaches to mitigate the undesirable effects of ROS or of direct carbon surface oxidation have hitherto been:

a) Replacing Fe with other transition metals (such as Co, Mn, Sn), with lower production of H_2O_2 and/or ROS,

b) Integrating Metal-N_x sites in a more graphitic or more stable support matrix

c) Selectively forming durable Fe-N_4 sites on the surface

d) Identifying platinum-group metal-free ROS scavengers and interfacing them appropriately with Metal-N-C materials

By extensively reviewing the literature documenting mitigation strategies, we conclude that the approaches b)-c)-d) currently seem the most promising one. In approach a), while Metal-N-C materials based on Co, Mn and Sn have been reported that reached sufficiently high initial ORR activity to be of practical interest, their rates of degradation and decrease of ORR activity during operation do not seem tremendously lower than those of Fe-N-C materials. For b), the concept is of interest, but improved bulk graphitization has typically led to lower nitrogen content, lower defects in the carbon matrix, and hence a lower site density of Metal-N_x sites, leading to initial ORR activity below the expectations for replacing Pt-based catalysts. The recent success in improved durability while maintaining high initial ORR activity seems to lean on locally enhancing the graphitisation, or carbon ordering, on the surface. [286] At the same time, the ZIF-8 CVD approach or the pyrolysis at the unusually high temperature of 1200 °C also modified the average iron coordination, increasing the relative amount of the durable sites S2, which can be associated with the approach c) above. [287] The approach d) has the potential to offer a dynamic protection of Metal-N_x sites, without compromising the activity. To be successful and to last for a long time, ROS scavengers should be dispersed and/or integrated in Metal-N-C materials at a nanometric or atomic scale. ROS species must be inactivated by scavengers before they can react with the Metal-N_x sites or the carbon matrix, for an efficient and durable protection. We therefore stress the urgent need to develop time- and space-resolved experimental set-ups that are able to provide information on the nature and the amount of various ROS produced *operando*, in order to improve the fundamental understanding of the degradation of such composite materials, and to accelerate the development of mitigation approaches. Alternative concepts, or at least approaches, for improved durability may be found looking from the perspective of the ionomeric phase in direct contact with the Metal-N-C surface. For example, ROS scavengers could be dispersed and/or integrated in the ionomeric phase of the cathode layer rather than in the Metal-N-C materials themselves, akin to proven stabilisation approaches of proton-conducting membranes. The development of novel ionomers or inorganic proton conductors with anionic groups having a higher pKa than sulfonic acid groups may also help mitigating the formation of the most aggressive ROS (OH radicals) during ORR. [293] This is suggested by the strong pH dependency of ROS species formation and activity decay experienced by Fe-N-C when exposed to H_2O_2 in different pH environments. [156] The lower acidity would however likely reduce the proton conductivity of such ionomers or solid-state materials, but a very thin film of such an interfacial ionomer or other proton-conducting material could be used to control the local pH, while typical perfluorosulfonic acid ionomer still being used away from the electrochemical interface, for long-distance proton transport throughout the cathode AL. A slightly higher local pH would also expectedly decrease the rate of demetalation of Metal-N_4 sites. Ultimately, advanced Metal-N-C materials and ALs featuring a combination of several if not all above-mentioned approaches for improved durability, may be necessary to reach durability in all PEMFC operating conditions and comparable to that of Pt-based catalysts.

Finally, we briefly presented physicochemical techniques that have permitted fundamental advances in the field of degradation mechanisms of Metal-N-C catalysts, and have discussed their advantages, limitations and pitfalls. For example, ^{57}Fe Mössbauer spectroscopy has revealed that active sites featuring a D2 spectral signature are durable during ORR electrocatalysis in acid medium, while D1 sites quickly convert to nano-Fe oxides in the same

conditions. Besides, while a few techniques are now able to measure or assess the density of active sites in pristine catalysts (CO cryo-chemisorption, nitrite stripping, cyanide poisoning, etc), there is no report leaning on these methods, or on another method, that can yet reliably measure the site density in aged Metal-N-C cathodes. After operation in O_2-rich acidic environment, and the correlated destruction of Metal-N_x sites and possible formation of metal (hydr)oxide particles (with no or negligible ORR activity in acid), the technique must be selective and quantitative for Metal-N_x sites and, for example, should not count metal (hydr)oxides as "sites". Given that active site density measurement is the basis for the proper evaluation of the intrinsic electrocatalytic activity of different Metal-N-C materials before and after aging, there is an urgent need to develop a technique that can distinguish Metal-N_x sites from metallic or metal oxide particles, and that can be applied *operando*, *or post mortem*.

In conclusion, the challenge ahead for significantly improving the durability of Metal-N-C materials for PEMFC is admittedly a daunting one, but rational ideas are emerging to tackle the challenge, and recent experimental results are strongly promising. The high stability of Metal-N_x sites in acid medium (in O_2-free acid environment) has been demonstrated, and is a strong support for further concerted efforts between materials scientists, electrochemists and engineers to address the durability challenges, working across the scales, from atomic level, carbon particle, and AL scales, to ensure a transition towards a cleaner and greener future based on platinum group metal-free ORR catalysts.

AUTHOR INFORMATION

Corresponding Authors

* F.M. Tel: +33 476 826 592. E-mail: frederic.maillard@grenoble-inp.fr

* F.J. Tel: +33 448 792 030. E-mail: frederic.jaouen@umontpellier.fr

Notes

The authors declare no competing financial interest.

Biographies

Kavita Kumar obtained her Ph.D. in Electrochemistry from the University of Poitiers (France) in 2017 under the direction of Prof. K. Boniface Kokoh, Dr. Têko W. Napporn and Dr. Aurélien Habrioux. From 2018 to 2023, she worked as a postdoctoral research associate in the Interfacial Electrochemistry and Processes group of the Laboratory of Electrochemistry and Physicochemistry of Materials and Interfaces (LEPMI, Grenoble, France), headed by Dr. Frédéric Maillard. She is since 2023 a CNRS research fellow at LEPMI. Her current research interests mostly lie on the structure-activity-stability relationships of platinum group metal-free catalysts for oxygen electrocatalysis.

Laetitia Dubau received her PhD on Electrocatalysis from Poitiers University (France) under the supervision of Claude Lamy and Jean-Michel Léger. After five years of post-doctoral researches on durability of proton-exchange membrane fuel cell electrocatalysts in the Interfacial Electrochemistry group of the Laboratory of Electrochemistry and Physicochemistry of Materials and Interfaces (LEPMI, Grenoble, France), she became a permanent researcher from the French National Centre for Scientific Research (CNRS) in 2014 and a Research

Director in 2021. Her research interests focus on understanding the activity/stability relationships in electrocatalysis and on designing low precious metal content electrocatalysts.

Frédéric Jaouen obtained his Ph.D. from the Royal Institute of Technology – Sweden - in 2003, under the supervision of Prof. Lindbergh. Until 2011, he was a research associate in Professor Dodelet's group at Institut National de la Recherche Scientifique, Canada. He is since 2013 a CNRS research fellow at the CNRS - Université de Montpellier - ENSCM joint research unit, Institut Charles Gerhardt (UMR 5253), and since 2020, research director at the CNRS. His research interest focuses on novel catalysts based on Earth-abundant elements for catalysing O_2 electroreduction in proton-exchange-membrane and anion-exchange-membrane fuel cells, as well as for catalysing CO_2 electroreduction to valuable chemical products. In detail, the synthesis of precious-metal-free catalysts, *ex situ* and *in situ* characterisation, implementation in electrochemical devices and *operando* degradation mechanisms are central to his work.

Frédéric Maillard obtained his Ph.D. under the supervision of Dr. Frédéric Gloaguen, Dr. Jean-Michel Léger, and Prof. Claude Lamy from the University of Poitiers in 2002. After a two-year period as post-doctoral research associate in the group of Prof. U. Stimming (Pergamon Electrochimica Acta Gold Medal 2010) at the Technische Universität Muenchen (Germany), he moved back to France first as a research and development engineer at SAFT Batteries, Poitiers and then as a CNRS researcher at the Laboratory of Electrochemistry and Physicochemistry of Materials and Interfaces (LEPMI, Grenoble, France) in 2005. He is research director at the CNRS since 2018, and heads the Interfacial Electrochemistry and Processes group of LEPMI since 2021. Dr. Maillard combines physical, chemical and electrochemical techniques to unravel structure – activity – stability relationships in energy storage and conversion systems such as proton-exchange membrane/anion-exchange membrane fuel cells and water electrolysers.

Acknowledgements

This work has received partial funding from the French National Research Agency under the CAT2CAT (grant number ANR-16-CE05-0007), the ANIMA (grant number ANR-19-CE05-0039) and the DEEP (grant number ANR-21-CE05-0021) projects and from the FCH Joint Undertaking (CRESCENDO Project, Grant Agreement n°779366). The authors are grateful to Dr. Tristan Asset for his contribution to the manuscript's graphical abstract.

References

(1) BP. *Statistical review of world energy*. 2019. https://www.bp.com/content/dam/bp/business-sites/en/global/corporate/pdfs/energy-economics/statistical-review/bp-stats-review-2019-full-report.pdf (accessed 01/03/2023).
(2) Wagner, F. T.; Lakshmanan, B.; Mathias, M. F. Electrochemistry and the future of the automobile. *J. Phys. Chem. Lett.* **2010**, *1*, 2204-2219. DOI: 10.1021/jz100553m
(3) Frith, J. T.; Lacey, M. J.; Ulissi, U. A non-academic perspective on the future of lithium-based batteries. *Nat. Commun.* **2023**, *14*, 420. DOI: 10.1038/s41467-023-35933-2
(4) Cano, Z. P.; Banham, D.; Ye, S.; Hintennach, A.; Lu, J.; Fowler, M.; Chen, Z. Batteries and fuel cells for emerging electric vehicle markets. *Nat. Energy* **2018**, *3*, 279-289. DOI: 10.1038/s41560-018-0108-1
(5) Staffell, I.; Scamman, D.; Velazquez Abad, A.; Balcombe, P.; Dodds, P. E.; Ekins, P.; Shah, N.; Ward, K. R. The role of hydrogen and fuel cells in the global energy system. *Energy Environ. Sci.* **2019**, *12*, 463-491. DOI: 10.1039/c8ee01157e
(6) Nie, Y.; Li, L.; Wei, Z. Recent advancements in Pt and Pt-free catalysts for oxygen reduction reaction. *Chem. Soc. Rev.* **2015**, *44*, 2168-2201. DOI: 10.1039/c4cs00484a
(7) Pan, L.; Ott, S.; Dionigi, F.; Strasser, P. Current challenges related to the deployment of shape-controlled Pt alloy oxygen reduction reaction nanocatalysts into low Pt-loaded cathode layers of proton exchange membrane fuel cells. *Curr. Opin. Electrochem.* **2019**, *18*, 61-71. DOI: 10.1016/j.coelec.2019.10.011
(8) Dubau, L.; Castanheira, L.; Maillard, F.; Chatenet, M.; Lottin, O.; Maranzana, G.; Dillet, J.; Lamibrac, A.; Perrin, J. C.; Moukheiber, E.; et al. A review of PEM fuel cell durability: materials degradation, local heterogeneities of aging and possible mitigation strategies. *Wiley Interdiscip. Rev.: Energy Environ.* **2014**, *3*, 540-560. DOI: 10.1002/wene.113
(9) Meier, J. C.; Katsounaros, I.; Galeano, C.; Bongard, H. J.; Topalov, A. A.; Kostka, A.; Karschin, A.; Schüth, F.; Mayrhofer, K. J. J. Stability investigations of electrocatalysts on the nanoscale. *Energy Environ. Sci.* **2012**, *5*, 9319-9330. DOI: 10.1039/c2ee22550f
(10) Cherevko, S.; Kulyk, N.; Mayrhofer, K. J. J. Durability of platinum-based fuel cell electrocatalysts: Dissolution of bulk and nanoscale platinum. *Nano Energy* **2016**, *29*, 275-298. DOI: 10.1016/j.nanoen.2016.03.005
(11) Shao, M.; Chang, Q.; Dodelet, J. P.; Chenitz, R. Recent advances in electrocatalysts for oxygen reduction reaction. *Chem. Rev.* **2016**, *116*, 3594-3657. DOI: 10.1021/acs.chemrev.5b00462
(12) Duclos, L.; Chattot, R.; Dubau, L.; Thivel, P.-X.; Mandil, G.; Laforest, V.; Bolloli, M.; Vincent, R.; Svecova, L. Closing the loop: life cycle assessment and optimization of a PEMFC platinum-based catalyst recycling process. *Green Chem.* **2020**, *22*, 1919-1933. DOI: 10.1039/c9gc03630j
(13) Gasteiger, H. A.; Kocha, S. S.; Sompalli, B.; Wagner, F. T. Activity benchmarks and requirements for Pt, Pt-alloy, and non-Pt oxygen reduction catalysts for PEMFCs. *Appl. Catal., B* **2005**, *56*, 9-35. DOI: 10.1016/j.apcatb.2004.06.021
(14) Gittleman, C. S.; Kongkanand, A.; Masten, D.; Gu, W. Materials research and development focus areas for low cost automotive proton-exchange membrane fuel cells. *Curr. Opin. Electrochem.* **2019**, *18*, 81-89. DOI: 10.1016/j.coelec.2019.10.009
(15) Reshetenko, T.; Serov, A.; Artyushkova, K.; Matanovic, I.; Stariha, S.; Atanassov, P. Tolerance of non-platinum group metals cathodes proton exchange membrane fuel cells to air contaminants. *J. Power Sources* **2016**, *324*, 556-571. DOI: 10.1016/j.jpowsour.2016.05.090
(16) Reshetenko, T.; Laue, V.; Krewer, U.; Artyushkova, K. Study of degradation and spatial performance of low Pt-loaded proton exchange membrane fuel cells under exposure to sulfur dioxide in an oxidant stream. *J. Power Sources* **2020**, *458*, 228032. DOI: 10.1016/j.jpowsour.2020.228032

(17) Jaouen, F.; Proietti, E.; Lefèvre, M.; Chenitz, R.; Dodelet, J.-P.; Wu, G.; Chung, H. T.; Johnston, C. M.; Zelenay, P. Recent advances in non-precious metal catalysis for oxygen-reduction reaction in polymer electrolyte fuelcells. *Energy Environ. Sci.* **2011**, *4*, 114-130. DOI: 10.1039/c0ee00011f
(18) Zitolo, A.; Goellner, V.; Armel, V.; Sougrati, M. T.; Mineva, T.; Stievano, L.; Fonda, E.; Jaouen, F. Identification of catalytic sites for oxygen reduction in iron- and nitrogen-doped graphene materials. *Nat. Mater.* **2015**, *14*, 937-942. DOI: 10.1038/nmat4367
(19) Gewirth, A. A.; Varnell, J. A.; DiAscro, A. M. Nonprecious metal catalysts for oxygen reduction in heterogeneous aqueous systems. *Chem. Rev.* **2018**, *118*, 2313-2339. DOI: 10.1021/acs.chemrev.7b00335
(20) Martinez, U.; Komini Babu, S.; Holby, E. F.; Chung, H. T.; Yin, X.; Zelenay, P. Progress in the development of Fe-based PGM-free electrocatalysts for the oxygen reduction reaction. *Adv. Mater.* **2019**, *31*, e1806545. DOI: 10.1002/adma.201806545
(21) Kumar, K.; Gairola, P.; Lions, M.; Ranjbar-Sahraie, N.; Mermoux, M.; Dubau, L.; Zitolo, A.; Jaouen, F.; Maillard, F. Physical and chemical considerations for improving catalytic activity and stability of non-precious-metal oxygen reduction reaction catalysts. *ACS Catal.* **2018**, *8*, 11264-11276. DOI: 10.1021/acscatal.8b02934
(22) Li, J.; Ghoshal, S.; Liang, W.; Sougrati, M.-T.; Jaouen, F.; Halevi, B.; McKinney, S.; McCool, G.; Ma, C.; Yuan, X.; et al. Structural and mechanistic basis for the high activity of Fe–N–C catalysts toward oxygen reduction. *Energy Environ. Sci.* **2016**, *9*, 2418-2432. DOI: 10.1039/c6ee01160h
(23) Subramanian, N. P.; Li, X.; Nallathambi, V.; Kumaraguru, S. P.; Colon-Mercado, H.; Wu, G.; Lee, J.-W.; Popov, B. N. Nitrogen-modified carbon-based catalysts for oxygen reduction reaction in polymer electrolyte membrane fuel cells. *J. Power Sources* **2009**, *188*, 38-44. DOI: 10.1016/j.jpowsour.2008.11.087
(24) Lefevre, M.; Proietti, E.; Jaouen, F.; Dodelet, J. P. Iron-based catalysts with improved oxygen reduction activity in polymer electrolyte fuel cells. *Science* **2009**, *324*, 71-74. DOI: 10.1126/science.1170051
(25) Proietti, E.; Jaouen, F.; Lefevre, M.; Larouche, N.; Tian, J.; Herranz, J.; Dodelet, J. P. Iron-based cathode catalyst with enhanced power density in polymer electrolyte membrane fuel cells. *Nat. Commun.* **2011**, *2*, 416. DOI: 10.1038/ncomms1427
(26) Malko, D.; Kucernak, A.; Lopes, T. *In situ* electrochemical quantification of active sites in Fe-N/C non-precious metal catalysts. *Nat. Commun.* **2016**, *7*, 13285. DOI: 10.1038/ncomms13285
(27) Primbs, M.; Sun, Y.; Roy, A.; Malko, D.; Mehmood, A.; Sougrati, M.-T.; Blanchard, P.-Y.; Granozzi, G.; Kosmala, T.; Daniel, G.; et al. Establishing reactivity descriptors for platinum group metal (PGM)-free Fe–N–C catalysts for PEM fuel cells. *Energy Environ. Sci.* **2020**, *13*, 2480-2500. DOI: 10.1039/d0ee01013h
(28) Jiao, L.; Li, J.; Richard, L. L.; Sun, Q.; Stracensky, T.; Liu, E.; Sougrati, M. T.; Zhao, Z.; Yang, F.; Zhong, S.; et al. Chemical vapour deposition of Fe-N-C oxygen reduction catalysts with full utilization of dense Fe-N_4 sites. *Nat. Mater.* **2021**, *20*, 1385-1391. DOI: 10.1038/s41563-021-01030-2
(29) Zitolo, A.; Ranjbar-Sahraie, N.; Mineva, T.; Li, J.; Jia, Q.; Stamatin, S.; Harrington, G. F.; Lyth, S. M.; Krtil, P.; Mukerjee, S.; et al. Identification of catalytic sites in cobalt-nitrogen-carbon materials for the oxygen reduction reaction. *Nat. Commun.* **2017**, *8*, 957. DOI: 10.1038/s41467-017-01100-7
(30) Chung, H. T.; Cullen, D. A.; Higgins, D.; Sneed, B. T.; Holby, E. F.; More, K. L.; Zelenay, P. Direct atomic-level insight into the active sites of a high-performance PGM-free ORR catalyst. *Science* **2017**, *357*, 479-484. DOI: 10.1126/science.aan2255
(31) Wang, W.; Jia, Q.; Mukerjee, S.; Chen, S. Recent insights into the oxygen-reduction electrocatalysis of Fe/N/C materials. *ACS Catal.* **2019**, *9*, 10126-10141. DOI: 10.1021/acscatal.9b02583
(32) Jaouen, F.; Lefevre, M.; Dodelet, J. P.; Cai, M. Heat-treated Fe/N/C catalysts for O_2 electroreduction: are active sites hosted in micropores? *J. Phys. Chem. B* **2006**, *110*, 5553-5558. DOI: 10.1021/jp057135h
(33) Akula, S.; Mooste, M.; Zulevi, B.; McKinney, S.; Kikas, A.; Piirsoo, H.-M.; Rähn, M.; Tamm, A.; Kisand, V.; Serov, A.; et al. Mesoporous textured Fe-N-C electrocatalysts as highly efficient cathodes

for proton exchange membrane fuel cells. *J. Power Sources* **2022**, *520*, 230819. DOI: 10.1016/j.jpowsour.2021.230819
(34) Kabir, S.; Medina, S.; Wang, G.; Bender, G.; Pylypenko, S.; Neyerlin, K. C. Improving the bulk gas transport of Fe-N-C platinum group metal-free nanofiber electrodes via electrospinning for fuel cell applications. *Nano Energy* **2020**, *73*, 104791. DOI: 10.1016/j.nanoen.2020.104791
(35) Goellner, V.; Armel, V.; Zitolo, A.; Fonda, E.; Jaouen, F. Degradation by hydrogen peroxide of metal-nitrogen-carbon catalysts for oxygen reduction. *J. Electrochem. Soc.* **2015**, *162*, H403-H414. DOI: 10.1149/2.1091506jes
(36) Choi, C. H.; Lim, H.-K.; Chung, M. W.; Chon, G.; Ranjbar Sahraie, N.; Altin, A.; Sougrati, M.-T.; Stievano, L.; Oh, H. S.; Park, E. S.; et al. The Achilles' heel of iron-based catalysts during oxygen reduction in an acidic medium. *Energy Environ. Sci.* **2018**, *11*, 3176-3182. DOI: 10.1039/c8ee01855c
(37) Kramm, U. I.; Herranz, J.; Larouche, N.; Arruda, T. M.; Lefevre, M.; Jaouen, F.; Bogdanoff, P.; Fiechter, S.; Abs-Wurmbach, I.; Mukerjee, S.; et al. Structure of the catalytic sites in Fe/N/C-catalysts for O_2-reduction in PEM fuel cells. *Phys. Chem. Chem. Phys.* **2012**, *14*, 11673-11688. DOI: 10.1039/c2cp41957b
(38) Sahraie, N. R.; Kramm, U. I.; Steinberg, J.; Zhang, Y.; Thomas, A.; Reier, T.; Paraknowitsch, J. P.; Strasser, P. Quantifying the density and utilization of active sites in non-precious metal oxygen electroreduction catalysts. *Nat. Commun.* **2015**, *6*, 8618. DOI: 10.1038/ncomms9618
(39) Luo, F.; Choi, C. H.; Primbs, M. J. M.; Ju, W.; Li, S.; Leonard, N. D.; Thomas, A.; Jaouen, F.; Strasser, P. Accurate evaluation of active-site density (SD) and turnover frequency (TOF) of PGM-free metal–nitrogen-doped carbon (MNC) electrocatalysts using CO cryo adsorption. *ACS Catal.* **2019**, *9*, 4841-4852. DOI: 10.1021/acscatal.9b00588
(40) Yang, Q.; Jia, Y.; Wei, F.; Zhuang, L.; Yang, D.; Liu, J.; Wang, X.; Lin, S.; Yuan, P.; Yao, X. Understanding the activity of Co-N_{4-x} C_x in atomic metal catalysts for oxygen reduction catalysis. *Angew. Chem. Int. Ed.* **2020**, *59*, 6122-6127. DOI: 10.1002/anie.202000324
(41) Jaouen, F.; Charreteur, F.; Dodelet, J. P. Fe-based catalysts for oxygen reduction in PEMFCs. *J. Electrochem. Soc.* **2006**, *153*, A689-A698. DOI: 10.1149/1.2168418
(42) Charreteur, F.; Jaouen, F.; Ruggeri, S.; Dodelet, J.-P. Fe/N/C non-precious catalysts for PEM fuel cells: Influence of the structural parameters of pristine commercial carbon blacks on their activity for oxygen reduction. *Electrochim. Acta* **2008**, *53*, 2925-2938. DOI: 10.1016/j.electacta.2007.11.002
(43) Jaouen, F.; Serventi, A. M.; Lefèvre, M.; Dodelet, J.-P.; Bertrand, P. Non-noble electrocatalysts for O_2 reduction: How does heat treatment affect their activity and structure? Part II. Structural changes observed by electron microscopy, Raman, and mass spectroscopy. *J. Phys. Chem. C* **2007**, *111*, 5971-5976. DOI: 10.1021/jp068274h
(44) Fei, H.; Dong, J.; Feng, Y.; Allen, C. S.; Wan, C.; Volosskiy, B.; Li, M.; Zhao, Z.; Wang, Y.; Sun, H.; et al. General synthesis and definitive structural identification of MN_4C_4 single-atom catalysts with tunable electrocatalytic activities. *Nat. Catal.* **2018**, *1*, 63-72. DOI: 10.1038/s41929-017-0008-y
(45) Chen, M.; He, Y.; Spendelow, J. S.; Wu, G. Atomically dispersed metal catalysts for oxygen reduction. *ACS Energy Lett.* **2019**, *4*, 1619-1633. DOI: 10.1021/acsenergylett.9b00804
(46) Li, J.; Jia, Q.; Mukerjee, S.; Sougrati, M.-T.; Drazic, G.; Zitolo, A.; Jaouen, F. The challenge of achieving a high density of Fe-based active sites in a highly graphitic carbon matrix. *Catalysts* **2019**, *9*, 144. DOI: 10.3390/catal9020144
(47) Qiao, M.; Wang, Y.; Wang, Q.; Hu, G.; Mamat, X.; Zhang, S.; Wang, S. Hierarchically ordered porous carbon with atomically dispersed FeN_4 for ultraefficient oxygen reduction reaction in proton-exchange membrane fuel cells. *Angew. Chem. Int. Ed.* **2020**, *59*, 2688-2694. DOI: 10.1002/anie.201914123
(48) Yuan, K.; Lutzenkirchen-Hecht, D.; Li, L.; Shuai, L.; Li, Y.; Cao, R.; Qiu, M.; Zhuang, X.; Leung, M. K. H.; Chen, Y.; et al. Boosting oxygen reduction of single iron active sites via geometric and electronic engineering: Nitrogen and phosphorus dual coordination. *J. Am. Chem. Soc.* **2020**, *142*, 2404-2412. DOI: 10.1021/jacs.9b11852

(49) Thompson, S. T.; Wilson, A. R.; Zelenay, P.; Myers, D. J.; More, K. L.; Neyerlin, K. C.; Papageorgopoulos, D. ElectroCat: DOE's approach to PGM-free catalyst and electrode R&D. *Solid State Ionics* **2018**, *319*, 68-76. DOI: 10.1016/j.ssi.2018.01.030
(50) *Fuel cells and hydrogen 2 joint undertaking*. 2017. https://ec.europa.eu/research/participants/data/ref/h2020/other/wp/jtis/h2020-wp17-fch_en.pdf (accessed 2023-03-01).
(51) Osmieri, L.; Park, J.; Cullen, D. A.; Zelenay, P.; Myers, D. J.; Neyerlin, K. C. Status and challenges for the application of platinum group metal-free catalysts in proton-exchange membrane fuel cells. *Curr. Opin. Electrochem.* **2021**, *25*, 100627. DOI: 10.1016/j.coelec.2020.08.009
(52) Barkholtz, H.; Chong, L.; Kaiser, Z.; Xu, T.; Liu, D.-J. Highly active non-PGM catalysts prepared from metal organic frameworks. *Catalysts* **2015**, *5*, 955-965. DOI: 10.3390/catal5020955
(53) Chokai, M.; Daidou, T.; Nabae, Y. Development of Pt-free carbon-based catalyst for PEFC cathode prepared from polyacrylonitrile. In *ECS Transactions*, 2014; Vol. 64, pp 261-270. DOI: 10.1149/06403.0261ecst.
(54) Wan, X.; Liu, X.; Li, Y.; Yu, R.; Zheng, L.; Yan, W.; Wang, H.; Xu, M.; Shui, J. Fe–N–C electrocatalyst with dense active sites and efficient mass transport for high-performance proton exchange membrane fuel cells. *Nat. Catal.* **2019**, *2*, 259-268. DOI: 10.1038/s41929-019-0237-3
(55) Mehmood, A.; Gong, M.; Jaouen, F.; Roy, A.; Zitolo, A.; Khan, A.; Sougrati, M.-T.; Primbs, M.; Bonastre, A. M.; Fongalland, D.; et al. High loading of single atomic iron sites in Fe–NC oxygen reduction catalysts for proton exchange membrane fuel cells. *Nat. Catal.* **2022**, *5*, 311-323. DOI: 10.1038/s41929-022-00772-9
(56) Uddin, A.; Dunsmore, L.; Zhang, H.; Hu, L.; Wu, G.; Litster, S. High power density platinum group metal-free cathodes for polymer electrolyte fuel cells. *ACS Appl. Mater. Interfaces* **2020**, *12*, 2216-2224. DOI: 10.1021/acsami.9b13945
(57) Wang, L.; Wan, X.; Liu, S.; Xu, L.; Shui, J. Fe-N-C catalysts for PEMFC: Progress towards the commercial application under DOE reference. *J. Energy Chem.* **2019**, *39*, 77-87. DOI: 10.1016/j.jechem.2018.12.019
(58) He, Y.; Wu, G. PGM-free oxygen-reduction catalyst development for proton-exchange membrane fuel cells: Challenges, solutions, and promises. *Acc. Mater. Res.* **2022**, *3*, 224-236. DOI: 10.1021/accountsmr.1c00226
(59) Osmieri, L.; Meyer, Q. Recent advances in integrating platinum group metal-free catalysts in proton exchange membrane fuel cells. *Curr. Opin. Electrochem.* **2022**, *31*, 100847. DOI: 10.1016/j.coelec.2021.100847
(60) Kumar, K.; Asset, T.; Li, X.; Liu, Y.; Yan, X.; Chen, Y.; Mermoux, M.; Pan, X.; Atanassov, P.; Maillard, F.; et al. Fe–N–C electrocatalysts' durability: Effects of single atoms' mobility and clustering. *ACS Catal.* **2021**, *11*, 484-494. DOI: 10.1021/acscatal.0c04625
(61) Yang, L.; Larouche, N.; Chenitz, R.; Zhang, G.; Lefèvre, M.; Dodelet, J.-P. Activity, performance, and durability for the reduction of oxygen in PEM fuel cells, of Fe/N/C electrocatalysts obtained from the pyrolysis of metal-organic-framework and iron porphyrin precursors. *Electrochim. Acta* **2015**, *159*, 184-197. DOI: 10.1016/j.electacta.2015.01.201
(62) Meng, H.; Larouche, N.; Lefèvre, M.; Jaouen, F.; Stansfield, B.; Dodelet, J.-P. Iron porphyrin-based cathode catalysts for polymer electrolyte membrane fuel cells: Effect of NH_3 and Ar mixtures as pyrolysis gases on catalytic activity and stability. *Electrochim. Acta* **2010**, *55*, 6450-6461. DOI: 10.1016/j.electacta.2010.06.039
(63) Ostroverkh, A.; Johánek, V.; Dubau, M.; Kúš, P.; Khalakhan, I.; Šmíd, B.; Fiala, R.; Václavů, M.; Ostroverkh, Y.; Matolín, V. Optimization of ionomer-free ultra-low loading Pt catalyst for anode/cathode of PEMFC via magnetron sputtering. *Int. J. Hydrogen Energy* **2019**, *44*, 19344-19356. DOI: 10.1016/j.ijhydene.2018.12.206
(64) Wu, G.; More, K. L.; Johnston, C. M.; Zelenay, P. High-performance electrocatalysts for oxygen reduction derived from polyaniline, iron, and cobalt. *Science* **2011**, *332*, 443-447. DOI: 10.1126/science.1200832

(65) Ferrandon, M.; Wang, X.; Kropf, A. J.; Myers, D. J.; Wu, G.; Johnston, C. M.; Zelenay, P. Stability of iron species in heat-treated polyaniline–iron–carbon polymer electrolyte fuel cell cathode catalysts. *Electrochim. Acta* **2013**, *110*, 282-291. DOI: 10.1016/j.electacta.2013.03.183
(66) Chong, L.; Goenaga, G. A.; Williams, K.; Barkholtz, H. M.; Grabstanowicz, L. R.; Brooksbank, J. A.; Papandrew, A. B.; Elzein, R.; Schlaf, R.; Zawodzinski, T. A.; et al. Investigation of oxygen reduction activity of catalysts derived from Co and Co/Zn methyl-imidazolate frameworks in proton exchange membrane fuel cells. *ChemElectroChem* **2016**, *3*, 1541-1545. DOI: 10.1002/celc.201600163
(67) Zhang, G.; Chenitz, R.; Lefèvre, M.; Sun, S.; Dodelet, J.-P. Is iron involved in the lack of stability of Fe/N/C electrocatalysts used to reduce oxygen at the cathode of PEM fuel cells? *Nano Energy* **2016**, *29*, 111-125. DOI: 10.1016/j.nanoen.2016.02.038
(68) Rod Borup; More, K.; Weber, A. *Fuel cell performance and durability consortium*. 2018. https://www.hydrogen.energy.gov/pdfs/review18/fc135_borup_2018_o.pdf (accessed 2023-03-03).
(69) USDRIVE. *Fuel Cell Technical Team Roadmap*. 2017. https://www.energy.gov/eere/vehicles/articles/us-drive-fuel-cell-technical-team-roadmap (accessed 2023-03-04).
(70) Kumar, K.; Dubau, L.; Mermoux, M.; Li, J.; Zitolo, A.; Nelayah, J.; Jaouen, F.; Maillard, F. On the influence of oxygen on the degradation of Fe-N-C catalysts. *Angew. Chem. Int. Ed.* **2020**, *59*, 3235-3243. DOI: 10.1002/anie.201912451
(71) Osmieri, L.; Cullen, D. A.; Chung, H. T.; Ahluwalia, R. K.; Neyerlin, K. C. Durability evaluation of a Fe–N–C catalyst in polymer electrolyte fuel cell environment via accelerated stress tests. *Nano Energy* **2020**, *78*, 105209. DOI: 10.1016/j.nanoen.2020.105209
(72) Ahluwalia, R. K.; Wang, X.; Osmieri, L.; Peng, J. K.; Cetinbas, C. F.; Park, J.; Myers, D. J.; Chung, H. T.; Neyerlin, K. C. Stability of atomically dispersed Fe–N–C ORR catalyst in polymer electrolyte fuel cell environment. *J. Electrochem. Soc.* **2021**, *168*, 024513. DOI: 10.1149/1945-7111/abe34c
(73) Zhang, H.; Osmieri, L.; Park, J. H.; Chung, H. T.; Cullen, D. A.; Neyerlin, K. C.; Myers, D. J.; Zelenay, P. Standardized protocols for evaluating platinum group metal-free oxygen reduction reaction electrocatalysts in polymer electrolyte fuel cells. *Nat. Catal.* **2022**, *5*, 455-462. DOI: 10.1038/s41929-022-00778-3
(74) Iojoiu, C.; Guilminot, E.; Maillard, F.; Chatenet, M.; Sanchez, J. Y.; Claude, E.; Rossinot, E. Membrane and active layer degradation following PEMFC steady-state operation - II. Influence of Pt^{z+} on membrane properties. *J. Electrochem. Soc.* **2007**, *154*, B1115-B1120. DOI: 10.1149/1.27785282
(75) Gubler, L.; Dockheer, S. M.; Koppenol, W. H. Radical ($HO^{\bullet}$, $H^{\bullet}$ and $HOO^{\bullet}$) formation and ionomer degradation in polymer electrolyte fuel cells. *J. Electrochem. Soc.* **2011**, *158*, B755-B769. DOI: 10.1149/1.3581040
(76) Banham, D.; Ye, S.; Pei, K.; Ozaki, J.-i.; Kishimoto, T.; Imashiro, Y. A review of the stability and durability of non-precious metal catalysts for the oxygen reduction reaction in proton exchange membrane fuel cells. *J. Power Sources* **2015**, *285*, 334-348, 20836. DOI: 10.1016/j.jpowsour.2015.03.047
(77) Singh, H.; Zhuang, S.; Ingis, B.; Nunna, B. B.; Lee, E. S. Carbon-based catalysts for oxygen reduction reaction: A review on degradation mechanisms. *Carbon* **2019**, *151*, 160-174. DOI: 10.1016/j.carbon.2019.05.075
(78) Asset, T.; Atanassov, P. Iron-nitrogen-carbon catalysts for proton exchange membrane fuel cells. *Joule* **2020**, *4*, 33-44. DOI: 10.1016/j.joule.2019.12.002
(79) Weiss, J.; Zhang, H.; Zelenay, P. Recent progress in the durability of Fe-N-C oxygen reduction electrocatalysts for polymer electrolyte fuel cells. *J. Electroanal. Chem.* **2020**, *875*, 114696. DOI: 10.1016/j.jelechem.2020.114696
(80) Muñoz-Becerra, K.; Venegas, R.; Duque, L.; Zagal, J. H.; Recio, F. J. Recent advances of Fe–N–C pyrolyzed catalysts for the oxygen reduction reaction. *Curr. Opin. Electrochem.* **2020**, *23*, 154-161. DOI: 10.1016/j.coelec.2020.08.006
(81) Du, L.; Prabhakaran, V.; Xie, X.; Park, S.; Wang, Y.; Shao, Y. Low-PGM and PGM-free catalysts for proton exchange membrane fuel cells: Stability challenges and material solutions. *Adv. Mater.* **2021**, *33*, e1908232. DOI: 10.1002/adma.201908232

(82) Ma, Q.; Jin, H.; Zhu, J.; Li, Z.; Xu, H.; Liu, B.; Zhang, Z.; Ma, J.; Mu, S. Stabilizing Fe–N–C catalysts as model for oxygen reduction reaction. *Adv. Sci.* **2021**, *8*, 2102209. DOI: 10.1002/advs.202102209
(83) Deng, Y.; Luo, J.; Chi, B.; Tang, H.; Li, J.; Qiao, X.; Shen, Y.; Yang, Y.; Jia, C.; Rao, P.; et al. Advanced atomically dispersed metal–nitrogen–carbon catalysts toward cathodic oxygen reduction in PEM fuel cells. *Adv. Energy Mater.* **2021**, *11*, 2101222. DOI: 10.1002/aenm.202101222
(84) Miao, Z.; Li, S.; Priest, C.; Wang, T.; Wu, G.; Li, Q. Effective approaches for designing stable M-N_x/C oxygen-reduction catalysts for proton-exchange-membrane fuel cells. *Adv. Mater.* **2022**, *34*, 2200595. DOI: 10.1002/adma.202200595
(85) Shah, S. S. A.; Najam, T.; Bashir, M. S.; Javed, M. S.; Rahman, A. U.; Luque, R.; Bao, S. J. Identification of catalytic active sites for durable proton exchange membrane fuel cell: Catalytic degradation and poisoning perspectives. *Small* **2022**, *18*, e2106279. DOI: 10.1002/smll.202106279
(86) Wan, X.; Shui, J. Exploring durable single-atom catalysts for proton exchange membrane fuel cells. *ACS Energy Lett.* **2022**, *7*, 1696-1705. DOI: 10.1021/acsenergylett.2c00473
(87) Gloaguen, F.; Andolfatto, F.; Durand, R.; Ozil, P. Kinetic-study of electrochemical reactions at catalyst-recast ionomer interfaces from thin active layer modeling. *J. Appl. Electrochem.* **1994**, *24*, 863-869. DOI: 10.1007/BF00348773
(88) Gloaguen, F.; Convert, P.; Gamburzev, S.; Velev, O. A.; Srinivasan, S. An evaluation of the macro-homogeneous and agglomerate model for oxygen reduction in PEMFCs. *Electrochim. Acta* **1998**, *43*, 3767-3772. DOI: 10.1016/S0013-4686(98)00136-4
(89) Schmidt, T. J.; Gasteiger, H. A.; Stab, G. D.; Urban, P. M.; Kolb, D. M.; Behm, R. J. Characterization of high-surface area electrocatalysts using a rotating disk electrode configuration. *J. Electrochem. Soc.* **1998**, *145*, 2354-2358. DOI: 10.1149/1.1838642
(90) Holby, E. F.; Wang, G.; Zelenay, P. Acid stability and demetalation of PGM-free ORR electrocatalyst structures from density functional theory: A model for “single-atom catalyst” dissolution. *ACS Catal.* **2020**, *10*, 14527-14539. DOI: 10.1021/acscatal.0c02856
(91) Tan, X.; Tahini, H. A.; Smith, S. C. Unveiling the role of carbon oxidation in irreversible degradation of atomically-dispersed FeN_4 moieties for proton exchange membrane fuel cells. *J. Mater. Chem. A* **2021**, *9*, 8721-8729. DOI: 10.1039/d0ta12105c
(92) Yin, X.; Zelenay, P. Kinetic models for the degradation mechanisms of PGM-free ORR catalysts *ECS Trans.* **2018**, *85*, 1239-1250. DOI: 10.1149/08513.1239ecst
(93) Chenitz, R.; Kramm, U. I.; Lefèvre, M.; Glibin, V.; Zhang, G.; Sun, S.; Dodelet, J.-P. A specific demetalation of Fe–N_4 catalytic sites in the micropores of NC_Ar + NH_3 is at the origin of the initial activity loss of the highly active Fe/N/C catalyst used for the reduction of oxygen in PEM fuel cells. *Energy Environ. Sci.* **2018**, *11*, 365-382. DOI: 10.1039/c7ee02302b
(94) Dodelet, J.-P.; Glibin, V.; Zhang, G.; Kramm, U. I.; Chenitz, R.; Vidal, F.; Sun, S.; Dubois, M. Reply to the ‘Comment on “Non-PGM electrocatalysts for PEM fuel cells: effect of fluorination on the activity and stability of a highly active NC_Ar + NH_3 catalyst”’ by Xi Yin, Edward F. Holby and Piotr Zelenay, Energy Environ. Sci., 10.1039/D0EE02069A. *Energy Environ. Sci.* **2021**, *14*, 1034-1041. DOI: 10.1039/d0ee03431b
(95) Li, J.; Chen, M.; Cullen, D. A.; Hwang, S.; Wang, M.; Li, B.; Liu, K.; Karakalos, S.; Lucero, M.; Zhang, H.; et al. Atomically dispersed manganese catalysts for oxygen reduction in proton-exchange membrane fuel cells. *Nat. Catal.* **2018**, *1*, 935-945. DOI: 10.1038/s41929-018-0164-8
(96) Jaouen, F.; Dodelet, J.-P. O_2 reduction mechanism on non-noble metal catalysts for PEM fuel fells. Part I: Experimental rates of O_2 electroreduction, H_2O_2 electroreduction, and H_2O_2 disproportionation. *J. Phys. Chem. C* **2009**, *113*, 15422-15432. DOI: 10.1021/jp900837e
(97) van Veen, J. A. R.; Visser, C. Oxygen reduction on monomeric transition metal phthalocyanines in acid electrolyte. *Electrochim. Acta* **1979**, *24*, 921-928. DOI: 10.1016/0013-4686(79)87088-7
(98) Ren, S.; Ma, S.; Yang, Y.; Mao, Q.; Hao, C. Hydrothermal synthesis of Fe_2O_3/polypyrrole/graphene oxide composites as highly efficient electrocatalysts for oxygen reduction reaction in alkaline electrolyte. *Electrochim. Acta* **2015**, *178*, 179-189. DOI: 10.1016/j.electacta.2015.07.181

(99) Xue, Y.; Jin, W.; Du, H.; Wang, S.; Zheng, S.; Zhang, Y. Tuning α-Fe_2O_3 nanotube arrays for the oxygen reduction reaction in alkaline media. *RSC Adv.* **2016**, *6*, 41878-41884. DOI: 10.1039/c6ra06422a
(100) Sgarbi, R.; Kumar, K.; Jaouen, F.; Zitolo, A.; Ticianelli, E. A.; Maillard, F. Oxygen reduction reaction mechanism and kinetics on M-N_xC_y and M@N-C active sites present in model M-N-C catalysts under alkaline and acidic conditions. *J. Solid State Electrochem.* **2021**, *25*, 45-56. DOI: 10.1007/s10008-019-04436-w
(101) Sgarbi, R.; Ticianelli, E. A.; Maillard, F.; Jaouen, F.; Chatenet, M. Oxygen reduction reaction on metal and nitrogen–doped carbon electrocatalysts in the presence of sodium borohydride. *Electrocatalysis* **2020**, *11*, 365-373. DOI: 10.1007/s12678-020-00602-1
(102) Alves, I. C. B.; Santos, J. R. N.; Viégas, D. S. S.; Marques, E. P.; Lacerda, C. A.; Zhang, L.; Zhanga, J.; Marques, A. L. B. Nanoparticles of Fe_2O_3 and Co_3O_4 as efficient electrocatalysts for oxygen reduction reaction in acid medium. *J. Braz. Chem. Soc.* **2019**, *30*, 2681-2691. DOI: 10.21577/0103-5053.20190195
(103) Li, J.; Sougrati, M. T.; Zitolo, A.; Ablett, J. M.; Oğuz, I. C.; Mineva, T.; Matanovic, I.; Atanassov, P.; Huang, Y.; Zenyuk, I.; et al. Identification of durable and non-durable FeN_x sites in Fe–N–C materials for proton exchange membrane fuel cells. *Nat. Catal.* **2021**, *4*, 10-19. DOI: 10.1038/s41929-020-00545-2
(104) Luo, F.; Roy, A.; Silvioli, L.; Cullen, D. A.; Zitolo, A.; Sougrati, M. T.; Oguz, I. C.; Mineva, T.; Teschner, D.; Wagner, S.; et al. *p*-block single-metal-site tin/nitrogen-doped carbon fuel cell cathode catalyst for oxygen reduction reaction. *Nat. Mater.* **2020**, *19*, 1215-1223. DOI: 10.1038/s41563-020-0717-5
(105) Eisele, T. C.; Gabby, K. L. Review of reductive leaching of iron by anaerobic bacteria. *Miner. Process. Extr. Metall. Rev.* **2014**, *35*, 75-105. DOI: 10.1080/08827508.2012.703627
(106) Baranton, S.; Coutanceau, C.; Roux, C.; Hahn, F.; Léger, J. M. Oxygen reduction reaction in acid medium at iron phthalocyanine dispersed on high surface area carbon substrate: tolerance to methanol, stability and kinetics. *J. Electroanal. Chem.* **2005**, *577*, 223-234. DOI: 10.1016/j.jelechem.2004.11.034
(107) Morozan, A.; Campidelli, S.; Filoramo, A.; Jousselme, B.; Palacin, S. Catalytic activity of cobalt and iron phthalocyanines or porphyrins supported on different carbon nanotubes towards oxygen reduction reaction. *Carbon* **2011**, *49*, 4839-4847. DOI: 10.1016/j.carbon.2011.07.004
(108) Bonnett, R. Metal complexes for photodynamic therapy. In *Comprehensive Coordination Chemistry II*, Vol. 9; 2003; pp 945-1003. DOI: 10.1016/b0-08-043748-6/09204-5.
(109) Zhang, Z.; Dou, M.; Ji, J.; Wang, F. Phthalocyanine tethered iron phthalocyanine on graphitized carbon black as superior electrocatalyst for oxygen reduction reaction. *Nano Energy* **2017**, *34*, 338-343. DOI: 10.1016/j.nanoen.2017.02.042
(110) Takase, S.; Aoto, Y.; Ikeda, D.; Wakita, H.; Shimizu, Y. Effects of crystallographic structures of metal-phthalocyanine on electrocatalytic properties of oxygen reduction in acidic condition. *Electrocatalysis* **2019**, *10*, 653-662. DOI: 10.1007/s12678-019-00553-2
(111) Chen, Z.; Jiang, S.; Kang, G.; Nguyen, D.; Schatz, G. C.; Van Duyne, R. P. *Operando* characterization of iron phthalocyanine deactivation during oxygen reduction reaction using electrochemical tip-enhanced Raman spectroscopy. *J. Am. Chem. Soc.* **2019**, *141*, 15684-15692. DOI: 10.1021/jacs.9b07979
(112) Meier, H.; Tschirwitz, U.; Zimmerhackl, E.; Albrecht, W.; Zeitler, G. Application of radioisotope techniques for the study of phthalocyanine catalyzed electrochemical processes in fuel cells. *J. Phys. Chem.* **1977**, *81*, 712-718. DOI: 10.1021/j100523a007
(113) Wiesener, K.; Ohms, D.; Neumann, V.; Franke, R. N_4 macrocycles as electrocatalysts for the cathodic reduction of oxygen. *Mater. Chem. Phys.* **1989**, *22*, 457-475. DOI: 10.1016/0254-0584(89)90010-2
(114) Lalande, G.; Faubert, G.; Côté, R.; Guay, D.; Dodelet, J. P.; Weng, L. T.; Bertrand, P. Catalytic activity and stability of heat-treated iron phthalocyanines for the electroreduction of oxygen in

polymer electrolyte fuel cells. *J. Power Sources* **1996**, *61*, 227-237. DOI: 10.1016/s0378-7753(96)02356-7
(115) Hu, Y.; Jensen, J. O.; Zhang, W.; Cleemann, L. N.; Xing, W.; Bjerrum, N. J.; Li, Q. Hollow spheres of iron carbide nanoparticles encased in graphitic layers as oxygen reduction catalysts. *Angew. Chem. Int. Ed.* **2014**, *53*, 3675-3679. DOI: 10.1002/anie.201400358
(116) Wu, Z. Y.; Xu, X. X.; Hu, B. C.; Liang, H. W.; Lin, Y.; Chen, L. F.; Yu, S. H. Iron carbide nanoparticles encapsulated in mesoporous Fe-N-doped carbon nanofibers for efficient electrocatalysis. *Angew. Chem. Int. Ed.* **2015**, *54*, 8179-8183. DOI: 10.1002/anie.201502173
(117) Choi, C. H.; Baldizzone, C.; Grote, J. P.; Schuppert, A. K.; Jaouen, F.; Mayrhofer, K. J. Stability of Fe-N-C catalysts in acidic medium studied by *operando* spectroscopy. *Angew. Chem. Int. Ed.* **2015**, *54*, 12753-12757. DOI: 10.1002/anie.201504903
(118) Choi, C. H.; Baldizzone, C.; Polymeros, G.; Pizzutilo, E.; Kasian, O.; Schuppert, A. K.; Ranjbar Sahraie, N.; Sougrati, M.-T.; Mayrhofer, K. J. J.; Jaouen, F. Minimizing *operando* demetallation of Fe-N-C electrocatalysts in acidic medium. *ACS Catal.* **2016**, *6*, 3136-3146. DOI: 10.1021/acscatal.6b00643
(119) Deng, D.; Yu, L.; Chen, X.; Wang, G.; Jin, L.; Pan, X.; Deng, J.; Sun, G.; Bao, X. Iron encapsulated within pod-like carbon nanotubes for oxygen reduction reaction. *Angew. Chem. Int. Ed.* **2013**, *52*, 371-375. DOI: 10.1002/anie.201204958
(120) Castanheira, L.; Silva, W. O.; Lima, F. H. B.; Crisci, A.; Dubau, L.; Maillard, F. Carbon corrosion in proton-exchange membrane fuel cells: Effect of the carbon structure, the degradation protocol, and the gas atmosphere. *ACS Catal.* **2015**, *5*, 2184-2194. DOI: 10.1021/cs501973j
(121) Li, X.; Liu, G.; Popov, B. N. Activity and stability of non-precious metal catalysts for oxygen reduction in acid and alkaline electrolytes. *J. Power Sources* **2010**, *195*, 6373-6378. DOI: 10.1016/j.jpowsour.2010.04.019
(122) Serov, A.; Artyushkova, K.; Niangar, E.; Wang, C.; Dale, N.; Jaouen, F.; Sougrati, M.-T.; Jia, Q.; Mukerjee, S.; Atanassov, P. Nano-structured non-platinum catalysts for automotive fuel cell application. *Nano Energy* **2015**, *16*, 293-300. DOI: 10.1016/j.nanoen.2015.07.002
(123) Jaouen, F.; Goellner, V.; Lefèvre, M.; Herranz, J.; Proietti, E.; Dodelet, J. P. Oxygen reduction activities compared in rotating-disk electrode and proton exchange membrane fuel cells for highly active FeNC catalysts. *Electrochim. Acta* **2013**, *87*, 619-628. DOI: 10.1016/j.electacta.2012.09.057
(124) Herranz, J.; Jaouen, F.; Lefevre, M.; Kramm, U. I.; Proietti, E.; Dodelet, J. P.; Bogdanoff, P.; Fiechter, S.; Abs-Wurmbach, I.; Bertrand, P.; et al. Unveiling N-protonation and anion-binding effects on Fe/N/C-catalysts for O_2 reduction in PEM fuel cells. *J. Phys. Chem. C* **2011**, *115*, 16087-16097. DOI: 10.1021/jp2042526
(125) Okada, T.; Ayato, Y.; Satou, H.; Yuasa, M.; Sekine, I. The effect of impurity cations on the oxygen reduction kinetics at platinum electrodes covered with perfluorinated ionomer. *J. Phys. Chem. B* **2001**, *105*, 6980-6986. DOI: 10.1021/jp010822y
(126) Kienitz, B.; Pivovar, B.; Zawodzinski, T.; Garzon, F. H. Cationic contamination effects on polymer electrolyte membrane fuel cell performance. *J. Electrochem. Soc.* **2011**, *158*, B1175-B1183. DOI: 10.1149/1.3610986
(127) Wang, X. X.; Prabhakaran, V.; He, Y.; Shao, Y.; Wu, G. Iron-free cathode catalysts for proton-exchange-membrane fuel cells: Cobalt catalysts and the peroxide mitigation approach. *Adv. Mater.* **2019**, *31*, e1805126, 1805126. DOI: 10.1002/adma.201805126
(128) Binder, H.; Kohling, A.; Richter, K.; Sandstede, G. Über die anodische oxydation von aktivkohlen in wässrigen elektrolyten. *Electrochim. Acta* **1964**, *9*, 255-274. DOI: 10.1016/0013-4686(64)80015-3
(129) Castanheira, L.; Dubau, L.; Mermoux, M.; Berthomé, G.; Caqué, N.; Rossinot, E.; Chatenet, M.; Maillard, F. Carbon corrosion in proton-exchange membrane fuel cells: From model experiments to real-life operation in membrane electrode assemblies. *ACS Catal.* **2014**, *4*, 2258-2267. DOI: 10.1021/cs500449q
(130) Roen, L. M.; Paik, C. H.; Jarvi, T. D. Electrocatalytic corrosion of carbon support in PEMFC cathodes. *Electrochem. Solid-State Lett.* **2004**, *7*, A19-A22. DOI: 10.1149/1.1630412
(131) Stevens, D. A.; Dahn, J. R. Thermal degradation of the support in carbon-supported platinum electrocatalysts for PEM fuel cells. *Carbon* **2005**, *43*, 179-188. DOI: 10.1016/j.carbon.2004.09.004

(132) Appleby, A. J. Corrosion in low and high temperature fuel cells—An overview. *Corrosion* **1987**, *43*, 398-408. DOI: 10.5006/1.3583876
(133) Stevens, D. A.; Hicks, M. T.; Haugen, G. M.; Dahn, J. R. *Ex situ* and *in situ* stability studies of PEMFC catalysts. *J. Electrochem. Soc.* **2005**, *152*, A2309-A2315. DOI: 10.1149/1.2097361
(134) Nikkuni, F. R.; Vion-Dury, B.; Dubau, L.; Maillard, F.; Ticianelli, E. A.; Chatenet, M. The role of water in the degradation of Pt_3Co/C nanoparticles: An identical location transmission electron microscopy study in polymer electrolyte environment. *Appl. Catal., B* **2014**, *156-157*, 301-306. DOI: 10.1016/j.apcatb.2014.03.029
(135) Reiser, C. A.; Bregoli, L.; Patterson, T. W.; Yi, J. S.; Yang, J. D.; Perry, M. L.; Jarvi, T. D. A reverse-current decay mechanism for fuel cells. *Electrochem. Solid-State Lett.* **2005**, *8*, A273-A276. DOI: 10.1149/1.1896466
(136) Durst, J.; Lamibrac, A.; Charlot, F.; Dillet, J.; Castanheira, L. F.; Maranzana, G.; Dubau, L.; Maillard , F.; Chatenet, M.; Lottin, O. Degradation heterogeneities induced by repetitive start/stop events in proton exchange membrane fuel cell: Inlet *vs*. outlet and channel *vs*. land. *Appl. Catal., B* **2013**, *138-139*, 416-426. DOI: 10.1016/j.apcatb.2013.03.021
(137) Maillard, F.; Bonnefont, A.; Micoud, F. An EC-FTIR study on the catalytic role of Pt in carbon corrosion. *Electrochem. Commun.* **2011**, *13*, 1109-1111. DOI: 10.1016/j.elecom.2011.07.011
(138) Martinaiou, I.; Shahraei, A.; Grimm, F.; Zhang, H.; Wittich, C.; Klemenz, S.; Dolique, S. J.; Kleebe, H.-J.; Stark, R. W.; Kramm, U. I. Effect of metal species on the stability of Me-N-C catalysts during accelerated stress tests mimicking the start-up and shut-down conditions. *Electrochim. Acta* **2017**, *243*, 183-196. DOI: 10.1016/j.electacta.2017.04.134
(139) Linse, N.; Gubler, L.; Scherer, G. G.; Wokaun, A. The effect of platinum on carbon corrosion behavior in polymer electrolyte fuel cells. *Electrochim. Acta* **2011**, *56*, 7541-7549. DOI: 10.1016/j.electacta.2011.06.093
(140) Serov, A.; Workman, M. J.; Artyushkova, K.; Atanassov, P.; McCool, G.; McKinney, S.; Romero, H.; Halevi, B.; Stephenson, T. Highly stable precious metal-free cathode catalyst for fuel cell application. *J. Power Sources* **2016**, *327*, 557-564. DOI: 10.1016/j.jpowsour.2016.07.087
(141) Goellner, V.; Baldizzone, C.; Schuppert, A.; Sougrati, M. T.; Mayrhofer, K. J. J.; Jaouen, F. Degradation of Fe/N/C catalysts upon high polarization in acid medium. *Phys. Chem. Chem. Phys.* **2014**, *16*, 18454-18462. DOI: 10.1039/c4cp02882a
(142) Jaouen, F.; Wiezell, K.; Lindbergh, G. Transient techniques for investigating mass-transport limitations in gas diffusion electrodes: II. Experimental characterization of the PEFC cathode. *J. Electrochem. Soc.* **2003**, *150*, A1711

DOI: 10.1149/1.1624295
(143) Gaumont, T.; Maranzana, G.; Lottin, O.; Dillet, J.; Didierjean, S.; Pauchet, J.; Guétaz, L. Measurement of protonic resistance of catalyst layers as a tool for degradation monitoring. *Int. J. Hydrogen Energy* **2017**, *42*, 1800-1812. DOI: 10.1016/j.ijhydene.2016.10.035
(144) Mineva, T.; Matanovic, I.; Atanassov, P.; Sougrati, M.-T.; Stievano, L.; Clémancey, M.; Kochem, A.; Latour, J.-M.; Jaouen, F. Understanding active sites in pyrolyzed Fe–N–C catalysts for fuel cell cathodes by bridging density functional theory calculations and ^{57}Fe Mössbauer spectroscopy. *ACS Catal.* **2019**, *9*, 9359-9371. DOI: 10.1021/acscatal.9b02586
(145) Strlič, M.; Kolar, J.; Šelih, V.; Kocar, D.; Pihlar, B. A comparative study of several transition metals in Fenton-like reaction systems at circum-neutral pH. *Acta Chim. Slov.* **2003**, *50*, 619-632.
(146) Bonakdarpour, A.; Lefevre, M.; Yang, R.; Jaouen, F.; Dahn, T.; Dodelet, J.-P.; Dahn, J. R. Impact of loading in RRDE experiments on Fe–N–C catalysts: Two- or four-electron oxygen reduction? *Electrochem. Solid-State Lett.* **2008**, *11*, B105-B108. DOI: 10.1149/1.2904768
(147) Ünsal, S.; Schmidt, T. J.; Herranz, J. Effect of aggregate size and film quality on the electrochemical properties of non-noble metal catalysts in rotating ring disk electrode measurements. *Electrochim. Acta* **2023**, *445*, 142024. DOI: 10.1016/j.electacta.2023.142024
(148) Choi, C. H.; Choi, W. S.; Kasian, O.; Mechler, A. K.; Sougrati, M. T.; Bruller, S.; Strickland, K.; Jia, Q.; Mukerjee, S.; Mayrhofer, K. J. J.; et al. Unraveling the nature of sites active toward hydrogen

peroxide reduction in Fe-N-C catalysts. *Angew. Chem. Int. Ed.* **2017**, *56*, 8809-8812. DOI: 10.1002/anie.201704356
(149) Zhang, P.; Wang, Y.; You, Y.; Yuan, J.; Zhou, Z.; Sun, S. Generation pathway of hydroxyl radical in Fe/N/C-based oxygen reduction electrocatalysts under acidic media. *J. Phys. Chem. Lett.* **2021**, *12*, 7797-7803. DOI: 10.1021/acs.jpclett.1c01905
(150) Wiesener, K. N_4-chelates as electrocatalyst for cathodic oxygen reduction. *Electrochim. Acta* **1986**, *31*, 1073-1078. DOI: 10.1016/0013-4686(86)80022-6
(151) Lefèvre, M.; Dodelet, J.-P. Fe-based catalysts for the reduction of oxygen in polymer electrolyte membrane fuel cell conditions: determination of the amount of peroxide released during electroreduction and its influence on the stability of the catalysts. *Electrochim. Acta* **2003**, *48*, 2749-2760. DOI: 10.1016/s0013-4686(03)00393-1
(152) Schulenburg, H.; Stankov, S.; Schünemann, V.; Radnik, J.; Dorbandt, I.; Fiechter, S.; Bogdanoff, P.; Tributsch, H. Catalysts for the oxygen reduction from heat-treated iron(III) tetramethoxyphenylporphyrin chloride: Structure and stability and active sites. *J. Phys. Chem. B* **2003**, *107*, 9034-9041. DOI: 10.1021/jp030349j
(153) Wu, G.; Artyushkova, K.; Ferrandon, M.; Kropf, A. J.; Myers, D.; Zelenay, P. Performance durability of polyaniline-derived non-precious cathode catalysts. *ECS Trans.* **2009**, *25*, 1299-1311. DOI: 10.1149/1.3210685
(154) Jaouen, F.; Marcotte, S.; Dodelet, J.-P.; Lindbergh, G. Oxygen reduction catalysts for polymer electrolyte fuel cells from the pyrolysis of iron acetate adsorbed on various carbon supports. *J. Phys. Chem. B* **2003**, *107*, 1376-1386. DOI: 10.1021/jp021634q
(155) Jung, E.; Shin, H.; Lee, B. H.; Efremov, V.; Lee, S.; Lee, H. S.; Kim, J.; Hooch Antink, W.; Park, S.; Lee, K. S.; et al. Atomic-level tuning of Co-N-C catalyst for high-performance electrochemical H_2O_2 production. *Nat. Mater.* **2020**, *19*, 436-442. DOI: 10.1038/s41563-019-0571-5
(156) Bae, G.; Chung, M. W.; Ji, S. G.; Jaouen, F.; Choi, C. H. pH effect on the H_2O_2-induced deactivation of Fe-N-C catalysts. *ACS Catal.* **2020**, *10*, 8485-8495. DOI: 10.1021/acscatal.0c00948
(157) Lin, L.; Zhu, Q.; Xu, A. W. Noble-metal-free Fe-N/C catalyst for highly efficient oxygen reduction reaction under both alkaline and acidic conditions. *J. Am. Chem. Soc.* **2014**, *136*, 11027-11033. DOI: 10.1021/ja504696r
(158) Niu, W.; Li, L.; Liu, X.; Wang, N.; Liu, J.; Zhou, W.; Tang, Z.; Chen, S. Mesoporous N-doped carbons prepared with thermally removable nanoparticle templates: an efficient electrocatalyst for oxygen reduction reaction. *J. Am. Chem. Soc.* **2015**, *137*, 5555-5562. DOI: 10.1021/jacs.5b02027
(159) Li, Q.; Wang, T.; Havas, D.; Zhang, H.; Xu, P.; Han, J.; Cho, J.; Wu, G. High-performance direct methanol fuel cells with precious-metal-free cathode. *Adv. Sci.* **2016**, *3*, 1600140. DOI: 10.1002/advs.201600140
(160) Yang, S.; Verdaguer-Casadevall, A.; Arnarson, L.; Silvioli, L.; Čolić, V.; Frydendal, R.; Rossmeisl, J.; Chorkendorff, I.; Stephens, I. E. L. Toward the decentralized electrochemical production of H_2O_2: A focus on the catalysis. *ACS Catal.* **2018**, *8*, 4064-4081. DOI: 10.1021/acscatal.8b00217
(161) Zhou, Y.; Chen, G.; Zhang, J. A review of advanced metal-free carbon catalysts for oxygen reduction reactions towards the selective generation of hydrogen peroxide. *J. Mater. Chem. A* **2020**, *8*, 20849-20869. DOI: 10.1039/d0ta07900f
(162) Hu, Y.; Zhang, J.; Shen, T.; Li, Z.; Chen, K.; Lu, Y.; Zhang, J.; Wang, D. Efficient electrochemical production of H_2O_2 on hollow N-doped carbon nanospheres with abundant micropores. *ACS Appl. Mater. Interfaces* **2021**, *13*, 29551-29557. DOI: 10.1021/acsami.1c05353
(163) Mehta, S.; Gupta, D.; Nagaiah, T. C. Selective electrochemical production of hydrogen peroxide from reduction of oxygen on mesoporous nitrogen containing carbon. *ChemElectroChem* **2022**, *9*, e202101336. DOI: 10.1002/celc.202101336
(164) Lim, J. S.; Kim, J. H.; Woo, J.; Baek, D. S.; Ihm, K.; Shin, T. J.; Sa, Y. J.; Joo, S. H. Designing highly active nanoporous carbon H_2O_2 production electrocatalysts through active site identification. *Chem* **2021**, *7*, 3114-3130. DOI: 10.1016/j.chempr.2021.08.007

(165) Li, W.; Bonakdarpour, A.; Gyenge, E.; Wilkinson, D. P. Drinking water purification by electrosynthesis of hydrogen peroxide in a power-producing PEM fuel cell. *ChemSusChem* **2013**, *6*, 2137-2143. DOI: 10.1002/cssc.201300225
(166) Suk, M.; Chung, M. W.; Han, M. H.; Oh, H. S.; Choi, C. H. Selective H_2O_2 production on surface-oxidized metal-nitrogen-carbon electrocatalysts. *Catal. Today* **2021**, *359*, 99-105. DOI: 10.1016/j.cattod.2019.05.034
(167) Lim, J. S.; Sa, Y. J.; Joo, S. H. Catalyst design, measurement guidelines, and device integration for H_2O_2 electrosynthesis from oxygen reduction. *Cell Rep. Phys. Sci.* **2022**, *3*, 100987. DOI: 10.1016/j.xcrp.2022.100987
(168) Kattel, S.; Wang, G. A density functional theory study of oxygen reduction reaction on Me-N_4 (Me = Fe, Co, or Ni) clusters between graphitic pores. *J. Mater. Chem. A* **2013**, *1*, 10790-10797. DOI: 10.1039/c3ta12142a
(169) Sun, Y.; Silvioli, L.; Sahraie, N. R.; Ju, W.; Li, J.; Zitolo, A.; Li, S.; Bagger, A.; Arnarson, L.; Wang, X.; et al. Activity-selectivity trends in the electrochemical production of hydrogen peroxide over single-site metal-nitrogen-carbon catalysts. *J. Am. Chem. Soc.* **2019**, *141*, 12372-12381. DOI: 10.1021/jacs.9b05576
(170) Zhang, J.; Yang, H.; Gao, J.; Xi, S.; Cai, W.; Zhang, J.; Cui, P.; Liu, B. Design of hierarchical, three-dimensional free-standing single-atom electrode for H_2O_2 production in acidic media. *Carbon Energy* **2020**, *2*, 276-282. DOI: 10.1002/cey2.33
(171) Stefan, I. C.; Mo, Y.; Ha, S. Y.; Kim, S.; Scherson, D. A. *In situ* Fe K-edge X-ray absorption fine structure of a nitrosyl adduct of iron phthalocyanine irreversibly adsorbed on a high area carbon electrode in an acidic electrolyte. *Inorg. Chem.* **2003**, *42*, 4316-4321. DOI: 10.1021/ic026053u
(172) Li, W.; Yu, A.; Higgins, D. C.; Llanos, B. G.; Chen, Z. Biologically inspired highly durable iron phthalocyanine catalysts for oxygen reduction reaction in polymer electrolyte membrane fuel cells. *J. Am. Chem. Soc.* **2010**, *132*, 17056-17058. DOI: 10.1021/ja106217u
(173) Seo, M. H.; Higgins, D.; Jiang, G.; Choi, S. M.; Han, B.; Chen, Z. Theoretical insight into highly durable iron phthalocyanine derived non-precious catalysts for oxygen reduction reactions. *J. Mater. Chem. A* **2014**, *2*, 19707-19716. DOI: 10.1039/c4ta04690k
(174) Meier, J. C.; Galeano, C.; Katsounaros, I.; Witte, J.; Bongard, H. J.; Topalov, A. A.; Baldizzone, C.; Mezzavilla, S.; Schuth, F.; Mayrhofer, K. J. J. Design criteria for stable Pt/C fuel cell catalysts. *Beilstein J. Nanotechnol.* **2014**, *5*, 44-67. DOI: 10.3762/bjnano.5.5
(175) Dubau, L.; Maillard , F. Unveiling the crucial role of temperature on the stability of oxygen reduction reaction electrocatalysts. *Electrochem. Commun.* **2016**, *63*, 65-69. DOI: 10.1016/j.elecom.2015.12.011
(176) Beverskog, B.; Puigdomenech, I. Revised Pourbaix diagrams for iron at 25–300 °C. *Corros. Sci.* **1996**, *38*, 2121-2135. DOI: 10.1016/s0010-938x(96)00067-4
(177) Chen, L.-N.; Yu, W.-S.; Wang, T.; Yang, X.-D.; Yang, H.-J.; Chen, Z.-X.; Wang, T.; Tian, N.; Zhou, Z.-Y.; Sun, S.-G. Fluorescence detection of hydroxyl radical generated from oxygen reduction on Fe/N/C catalyst. *Sci. China Chem.* **2020**, *63*, 198-202. DOI: 10.1007/s11426-019-9635-2
(178) Ferrandon, M.; Kropf, A. J.; Myers, D. J.; Artyushkova, K.; Kramm, U.; Bogdanoff, P.; Wu, G.; Johnston, C. M.; Zelenay, P. Multitechnique characterization of a polyaniline–iron–carbon oxygen reduction catalyst. *J. Phys. Chem. C* **2012**, *116*, 16001-16013. DOI: 10.1021/jp302396g
(179) Santori, P. G.; Speck, F. D.; Li, J.; Zitolo, A.; Jia, Q.; Mukerjee, S.; Cherevko, S.; Jaouen, F. Effect of pyrolysis atmosphere and electrolyte pH on the oxygen reduction activity, stability and spectroscopic signature of FeN_x moieties in Fe-N-C catalysts. *J. Electrochem. Soc.* **2019**, *166*, F3311-F3320. DOI: 10.1149/2.0371907jes
(180) Ünsal, S.; Girod, R.; Appel, C.; Karpov, D.; Mermoux, M.; Maillard, F.; Saveleva, V. A.; Tileli, V.; Schmidt, T. J.; Herranz, J. Decoupling the contributions of different instability mechanisms to the PEMFC performance decay of non-noble metal O_2-reduction catalysts. *J. Am. Chem. Soc.* **2023**, *145*, 7845-7858. DOI: 10.1021/jacs.2c12751

(181) Ono, Y.; Mashio, T.; Takaichi, S.; Ohma, A.; Kanesaka, H.; Shinohara, K. The analysis of performance loss with low platinum loaded cathode catalyst layers. In *ECS Transactions*, 2010; Vol. 28, pp 69-78. DOI: 10.1149/1.3496614.
(182) Owejan, J. P.; Owejan, J. E.; Gu, W. Impact of platinum loading and catalyst layer structure on PEMFC performance. *J. Electrochem. Soc.* **2013**, *160*, F824. DOI: 10.1149/2.072308jes
(183) Kusoglu, A.; Weber, A. Z. New insights into perfluorinated sulfonic-acid ionomers. *Chem. Rev.* **2017**, *117*, 987-1104. DOI: 10.1021/acs.chemrev.6b00159
(184) Martinaiou, I.; Monteverde Videla, A. H. A.; Weidler, N.; Kübler, M.; Wallace, W. D. Z.; Paul, S.; Wagner, S.; Shahraei, A.; Stark, R. W.; Specchia, S.; et al. Activity and degradation study of an Fe-N-C catalyst for ORR in Direct Methanol Fuel Cell (DMFC). *Appl. Catal., B* **2020**, *262*, 118217. DOI: 10.1016/j.apcatb.2019.118217
(185) Chen, J.; Yan, X.; Fu, C.; Feng, Y.; Lin, C.; Li, X.; Shen, S.; Ke, C.; Zhang, J. Insight into the rapid degradation behavior of nonprecious metal Fe-N-C electrocatalyst-based proton exchange membrane fuel cells. *ACS Appl. Mater. Interfaces* **2019**, *11*, 37779-37786. DOI: 10.1021/acsami.9b13474
(186) García, Á.; Pascual, L.; Ferrer, P.; Gianolio, D.; Held, G.; Grinter, D. C.; Peña, M. A.; Retuerto, M.; Rojas, S. Study of the evolution of FeN_xC_y and Fe_3C species in Fe/N/C catalysts during the oxygen reduction reaction in acid and alkaline electrolyte. *J. Power Sources* **2021**, *490*, 229487. DOI: 10.1016/j.jpowsour.2021.229487
(187) Giordano, N.; Antonucci, P. L.; Passalacqua, E.; Pino, L.; Aricò, A. S.; Kinoshita, K. Relationship between physicochemical properties and electrooxidation behaviour of carbon materials. *Electrochim. Acta* **1991**, *36*, 1931-1935. DOI: 10.1016/0013-4686(91)85075-i
(188) Choi, J.-Y.; Yang, L.; Kishimoto, T.; Fu, X.; Ye, S.; Chen, Z.; Banham, D. Is the rapid initial performance loss of Fe/N/C non precious metal catalysts due to micropore flooding? *Energy Environ. Sci.* **2017**, *10*, 296-305. DOI: 10.1039/c6ee03005j
(189) Normile, S. J.; Sabarirajan, D. C.; Calzada, O.; De Andrade, V.; Xiao, X.; Mandal, P.; Parkinson, D. Y.; Serov, A.; Atanassov, P.; Zenyuk, I. V. Direct observations of liquid water formation at nano- and micro-scale in platinum group metal-free electrodes by *operando* X-ray computed tomography. *Mater. Today Energy* **2018**, *9*, 187-197. DOI: 10.1016/j.mtener.2018.05.011
(190) Li, J.; Brüller, S.; Sabarirajan, D. C.; Ranjbar-Sahraie, N.; Sougrati, M. T.; Cavaliere, S.; Jones, D.; Zenyuk, I. V.; Zitolo, A.; Jaouen, F. Designing the 3D architecture of PGM-free cathodes for H_2/air proton exchange membrane fuel cells. *ACS Appl. Energy Mater.* **2019**, *2*, 7211-7222. DOI: 10.1021/acsaem.9b01181
(191) Satjaritanun, P.; Zenyuk, I. V. Water management strategies for PGM-free catalyst layers for polymer electrolyte fuel cells. *Curr. Opin. Electrochem.* **2021**, *25*. DOI: 10.1016/j.coelec.2020.08.004
(192) Babu, S. K.; Spernjak, D.; Mukundan, R.; Hussey, D. S.; Jacobson, D. L.; Chung, H. T.; Wu, G.; Steinbach, A. J.; Litster, S.; Borup, R. L.; et al. Understanding water management in platinum group metal-free electrodes using neutron imaging. *J. Power Sources* **2020**, *472*, 228442. DOI: 10.1016/j.jpowsour.2020.228442
(193) Obermaier, M.; Bandarenka, A. S.; Lohri-Tymozhynsky, C. A comprehensive physical impedance model of polymer electrolyte fuel cell cathodes in oxygen-free atmosphere. *Sci. Rep.* **2018**, *8*, 4933. DOI: 10.1038/s41598-018-23071-5
(194) Okada, T.; Ayato, Y.; Yuasa, M.; Sekine, I. The effect of impurity cations on the transport characteristics of perfluorosulfonated ionomer membranes. *J. Phys. Chem. B* **1999**, *103*, 3315-3322. DOI: 10.1021/jp983762d
(195) Kelly, M. J.; Fafilek, G.; Besenhard, J. O.; Kronberger, H.; Nauer, G. E. Contaminant absorption and conductivity in polymer electrolyte membranes. *J. Power Sources* **2005**, *145*, 249-252. DOI: 10.1016/j.jpowsour.2005.01.064
(196) Wang, H.; Turner, J. A. The influence of metal ions on the conductivity of Nafion 112 in polymer electrolyte membrane fuel cell. *J. Power Sources* **2008**, *183*, 576-580. DOI: 10.1016/j.jpowsour.2008.05.077

(197) Yoshida, H.; Miura, Y. Behavior of water in perfluorinated ionomer membranes containing various monovalent cations. *J. Membr. Sci.* **1992**, *68*, 1-10. DOI: 10.1016/0376-7388(92)80145-a
(198) Xie, G.; Okada, T.; Arimura, T. Fourier transform infrared spectroscopy study of fully hydrated Nafion membranes of various cation forms. *Z. Phys. Chem.* **1998**, *205*, 113-125. DOI: 10.1524/zpch.1998.205.Part_1.113
(199) Suresh, G.; Scindia, Y.; Pandey, A.; Goswami, A. Self-diffusion coefficient of water in Nafion-117 membrane with different monovalent counterions: a radiotracer study. *J. Membr. Sci.* **2005**, *250*, 39-45. DOI: 10.1016/j.memsci.2004.10.013
(200) Jia, R.; Han, B.; Levi, K.; Hasegawa, T.; Ye, J.; Dauskardt, R. H. Effect of cation contamination and hydrated pressure loading on the mechanical properties of proton exchange membranes. *J. Power Sources* **2011**, *196*, 3803-3809. DOI: 10.1016/j.jpowsour.2010.12.066
(201) Kienitz, B.; Baskaran, H.; Zawodzinski, T.; Pivovar, B. A half cell model to study performance degradation of a PEMFC due to cationic contamination. *ECS Trans.* **2007**, *11*, 777-788. DOI: 10.1149/1.2780991
(202) Kienitz, B. L.; Baskaran, H.; Zawodzinski, T. A. Modeling the steady-state effects of cationic contamination on polymer electrolyte membranes. *Electrochim. Acta* **2009**, *54*, 1671-1679. DOI: 10.1016/j.electacta.2008.09.058
(203) Durst, J.; Chatenet, M.; Maillard, F. Impact of metal cations on the electrocatalytic properties of Pt/C nanoparticles at multiple phase interfaces. *Phys. Chem. Chem. Phys.* **2012**, *14*, 13000-13009. DOI: 10.1039/c2cp42191g
(204) Greszler, A.; Moylan, T.; Gasteiger, H. A. Modeling the impact of cation contamination in a polymer electrolyte membrane fuel cell. In *Handbook of Fuel Cells: Fundamentals, Technology, and Applications*, Vielstich, W., Gasteiger, H. A., Yokokawa, H. Eds.; Vol. 4; John Wiley & Sons, 2010. DOI: 10.1002/9780470974001.f500049.
(205) Braaten, J. P.; Xu, X.; Cai, Y.; Kongkanand, A.; Litster, S. Contaminant cation effect on oxygen transport through the ionomers of polymer electrolyte membrane fuel cells. *J. Electrochem. Soc.* **2019**, *166*, F1337-F1343. DOI: 10.1149/2.0671916jes
(206) Delacourt, C.; Newman, J. Mathematical modeling of a cation-exchange membrane containing two cations. *J. Electrochem. Soc.* **2008**, *155*, B1210-B1217. DOI: 10.1149/1.2977960
(207) Shi, S.; Weber, A. Z.; Kusoglu, A. Structure-transport relationship of perfluorosulfonic-acid membranes in different cationic forms. *Electrochim. Acta* **2016**, *220*, 517-528. DOI: 10.1016/j.electacta.2016.10.096
(208) Chung, H. T.; Won, J. H.; Zelenay, P. Active and stable carbon nanotube/nanoparticle composite electrocatalyst for oxygen reduction. *Nat. Commun.* **2013**, *4*, 1922. DOI: 10.1038/ncomms2944
(209) Unni, S. M.; Ramadas, S.; Illathvalappil, R.; Bhange, S. N.; Kurungot, S. Surface-modified single wall carbon nanohorn as an effective electrocatalyst for platinum-free fuel cell cathodes. *J. Mater. Chem. A* **2015**, *3*, 4361-4367. DOI: 10.1039/C4TA05092D
(210) Ferrero, G. A.; Preuss, K.; Marinovic, A.; Jorge, A. B.; Mansor, N.; Brett, D. J. L.; Fuertes, A. B.; Sevilla, M.; Titirici, M. M. Fe-N-Doped carbon capsules with outstanding electrochemical performance and stability for the oxygen reduction reaction in both acid and alkaline conditions. *ACS Nano* **2016**, *10*, 5922-5932. DOI: 10.1021/acsnano.6b01247
(211) Thomas, M.; Illathvalappil, R.; Kurungot, S.; Nair, B. N.; Mohamed, A. P.; Anilkumar, G. M.; Yamaguchi, T.; Hareesh, U. S. Morphological ensembles of N-doped porous carbon derived from ZIF-8/Fe-graphene nanocomposites: Processing and electrocatalytic studies. *ChemistrySelect* **2018**, *3*, 8688-8697. DOI: 10.1002/slct.201801419
(212) Peera, S. G.; Balamurugan, J.; Kim, N. H.; Lee, J. H. Sustainable synthesis of Co@NC core shell nanostructures from metal organic frameworks via mechanochemical coordination self-assembly: An efficient electrocatalyst for oxygen reduction reaction. *Small* **2018**, *14*, 1800441-1800441. DOI: 10.1002/smll.201800441
(213) Mufundirwa, A.; Harrington, G. F.; Smid, B.; Cunning, B. V.; Sasaki, K.; Lyth, S. M. Durability of template-free Fe-N-C foams for electrochemical oxygen reduction in alkaline solution. *J. Power Sources* **2018**, *375*, 244-254. DOI: 10.1016/j.jpowsour.2017.07.025

(214) Chen, Y.; Li, Z.; Zhu, Y.; Sun, D.; Liu, X.; Xu, L.; Tang, Y. Atomic Fe dispersed on N-doped carbon hollow nanospheres for high-efficiency electrocatalytic oxygen reduction. *Adv. Mater.* **2019**, *31*, 1806312. DOI: 10.1002/adma.201806312
(215) Chen, D.; Ji, J.; Jiang, Z.; Ling, M.; Jiang, Z.; Peng, X. Molecular-confinement synthesis of sub-nano Fe/N/C catalysts with high oxygen reduction reaction activity and excellent durability for rechargeable Zn-Air batteries. *J. Power Sources* **2020**, *450*, 227660-227660. DOI: 10.1016/j.jpowsour.2019.227660
(216) Sgarbi, R.; Kumar, K.; Saveleva, V. A.; Dubau, L.; Chattot, R.; Martin, V.; Mermoux, M.; Bordet, P.; Glatzel, P.; Ticianelli, E. A.; et al. Electrochemical transformation of Fe-N-C catalysts into iron oxides in alkaline medium and its impact on the oxygen reduction reaction activity. *Appl. Catal., B* **2022**, *311*, 121366. DOI: 10.1016/j.apcatb.2022.121366
(217) Ramaswamy, N.; Mukerjee, S. Fundamental mechanistic understanding of electrocatalysis of oxygen reduction on Pt and non-Pt surfaces: Acid *versus* alkaline media. *Adv. Phys. Chem.* **2012**, *2012*, 491604. DOI: 10.1155/2012/491604
(218) Zhong, W.; Wang, Z.; Han, S.; Deng, L.; Yu, J.; Lin, Y.; Long, X.; Gu, M.; Yang, S. Identifying the active sites of a single atom catalyst with pH-universal oxygen reduction reaction activity. *Cell Rep. Phys. Sci.* **2020**, *1*, 100115-100115. DOI: 10.1016/j.xcrp.2020.100115
(219) Setzler, B. P.; Zhuang, Z.; Wittkopf, J. A.; Yan, Y. Activity targets for nanostructured platinum-group-metal-free catalysts in hydroxide exchange membrane fuel cells. *Nat. Nanotechnol.* **2016**, *11*, 1020-1025. DOI: 10.1038/nnano.2016.265
(220) Dekel, D. R. Review of cell performance in anion exchange membrane fuel cells. *J. Power Sources* **2018**, *375*, 158-169. DOI: 10.1016/j.jpowsour.2017.07.117
(221) Santori, P. G.; Speck, F. D.; Cherevko, S.; Firouzjaie, H. A.; Peng, X.; Mustain, W. E.; Jaouen, F. High performance FeNC and Mn-oxide/FeNC layers for AEMFC cathodes. *J. Electrochem. Soc.* **2020**, *167*, 134505. DOI: 10.1149/1945-7111/abb7e0
(222) Adabi, H.; Shakouri, A.; Ul Hassan, N.; Varcoe, J. R.; Zulevi, B.; Serov, A.; Regalbuto, J. R.; Mustain, W. E. High-performing commercial Fe–N–C cathode electrocatalyst for anion-exchange membrane fuel cells. *Nat. Energy* **2021**, *6*, 834-843. DOI: 10.1038/s41560-021-00878-7
(223) Ku, Y. P.; Ehelebe, K.; Hutzler, A.; Bierling, M.; Bohm, T.; Zitolo, A.; Vorokhta, M.; Bibent, N.; Speck, F. D.; Seeberger, D.; et al. Oxygen reduction reaction in alkaline media causes iron leaching from Fe-N-C electrocatalysts. *J. Am. Chem. Soc.* **2022**, *144*, 9753-9763. DOI: 10.1021/jacs.2c02088
(224) Möller, S.; Barwe, S.; Masa, J.; Wintrich, D.; Seisel, S.; Baltruschat, H.; Schuhmann, W. Online monitoring of electrochemical carbon corrosion in alkaline electrolytes by differential electrochemical mass spectrometry. *Angew. Chem. Int. Ed.* **2020**, *59*, 1585-1589. DOI: 10.1002/anie.201909475
(225) Yi, Y.; Weinberg, G.; Prenzel, M.; Greiner, M.; Heumann, S.; Becker, S.; Schlögl, R. Electrochemical corrosion of a glassy carbon electrode. *Catal. Today* **2017**, *295*, 32-40. DOI: 10.1016/j.cattod.2017.07.013
(226) Domínguez, C.; Pérez-Alonso, F. J.; Salam, M. A.; Al-Thabaiti, S. A.; Peña, M. A.; García-García, F. J.; Barrio, L.; Rojas, S. Repercussion of the carbon matrix for the activity and stability of Fe/N/C electrocatalysts for the oxygen reduction reaction. *Appl. Catal., B* **2016**, *183*, 185-196. DOI: 10.1016/j.apcatb.2015.10.043
(227) Sharma, M.; Jang, J. H.; Shin, D. Y.; Kwon, J. A.; Lim, D. H.; Choi, D.; Sung, H.; Jang, J.; Lee, S. Y.; Lee, K. Y.; et al. Work function-tailored graphene via transition metal encapsulation as a highly active and durable catalyst for the oxygen reduction reaction. *Energy Environ. Sci.* **2019**, *12*, 2200-2211. DOI: 10.1039/c9ee00381a
(228) Ramaswamy, N.; Tylus, U.; Jia, Q.; Mukerjee, S. Activity descriptor identification for oxygen reduction on nonprecious electrocatalysts: Linking surface science to coordination chemistry. *J. Am. Chem. Soc.* **2013**, *135*, 15443-15449. DOI: 10.1021/ja405149m
(229) Wierzbicki, S.; Douglin, J. C.; Singh, R. K.; Dekel, D. R.; Kruczała, K. *Operando* EPR study of radical formation in anion-exchange membrane fuel cells. *ACS Catal.* **2023**, *13*, 2744-2750. DOI: 10.1021/acscatal.2c05843

(230) Cheng, Y.; Liang, J.; Veder, J. P.; Li, M.; Chen, S.; Pan, J.; Song, L.; Cheng, H. M.; Liu, C.; Jiang, S. P. Iron oxide nanoclusters incorporated into iron phthalocyanine as highly active electrocatalysts for the oxygen reduction reaction. *ChemCatChem* **2018**, *10*, 475-483. DOI: 10.1002/cctc.201701183
(231) Feng, W.; Liu, M.; Liu, J.; Song, Y.; Wang, F. Well-defined Fe, Fe_3C, and Fe_2O_3 heterostructures on carbon black: a synergistic catalyst for oxygen reduction reaction. *Catal. Sci. Tech.* **2018**, *8*, 4900-4906. DOI: 10.1039/C8CY01223G
(232) Adabi, H.; Santori, P. G.; Shakouri, A.; Peng, X.; Yassin, K.; Rasin, I. G.; Brandon, S.; Dekel, D. R.; Hassan, N. U.; Sougrati, M.-T.; et al. Understanding how single-atom site density drives the performance and durability of PGM-free Fe–N–C cathodes in anion exchange membrane fuel cells. *Mater. Today Adv.* **2021**, *12*, 100179-100179. DOI: 10.1016/j.mtadv.2021.100179
(233) Kramm, U. I.; Zana, A.; Vosch, T.; Fiechter, S.; Arenz, M.; Schmeißer, D. On the structural composition and stability of Fe–N–C catalysts prepared by an intermediate acid leaching. *J. Solid State Electrochem.* **2016**, *20*, 969-981. DOI: 10.1007/s10008-015-3060-z
(234) Wagner, S.; Auerbach, H.; Tait, C. E.; Martinaiou, I.; Kumar, S. C. N.; Kubel, C.; Sergeev, I.; Wille, H. C.; Behrends, J.; Wolny, J. A.; et al. Elucidating the structural composition of an Fe-N-C catalyst by nuclear- and electron-resonance techniques. *Angew. Chem. Int. Ed.* **2019**, *58*, 10486-10492. DOI: 10.1002/anie.201903753 (acccessed 2019/09/23).
(235) Mun, Y.; Lee, S.; Kim, K.; Kim, S.; Lee, S.; Han, J. W.; Lee, J. Versatile strategy for tuning ORR activity of a single Fe-N_4 site by controlling electron-withdrawing/donating properties of a carbon plane. *J. Am. Chem. Soc.* **2019**, *141*, 6254-6262. DOI: 10.1021/jacs.8b13543
(236) Liu, Z. Y.; Brady, B. K.; Carter, R. N.; Litteer, B.; Budinski, M.; Hyun, J. K.; Muller, D. A. Characterization of carbon corrosion-induced structural damage of PEM fuel cell cathode electrodes caused by local fuel starvation. *J. Electrochem. Soc.* **2008**, *155*, B979. DOI: 10.1149/1.2956198
(237) Kangasniemi, K. H.; Condit, D. A.; Jarvi, T. D. Characterization of Vulcan electrochemically oxidized under simulated PEM fuel cell conditions. *J. Electrochem. Soc.* **2004**, *151*, E125-E132. DOI: 10.1149/1.1649756
(238) Gallagher, K. G.; Fuller, T. F. Kinetic model of the electrochemical oxidation of graphitic carbon in acidic environments. *Phys. Chem. Chem. Phys.* **2009**, *11*, 11557-11567. DOI: 10.1039/b915478g
(239) Gallagher, K. G.; Darling, R. M.; Fuller, T. F. Carbon-support corrosion mechanisms and models. In *Handbook of fuel cells - Fundamentals, technology and applications*, Vielstich, W., Gasteiger, H. A., Yokokawa, H. Eds.; Vol. 6: Advances in Electrocatalysis, Materials, Diagnostic and Durability; John Wiley & Sons, Inc., 2009; pp 820-827. DOI: 10.1002/9780470974001.f500054.
(240) Miao, Z.; Wang, X.; Tsai, M. C.; Jin, Q.; Liang, J.; Ma, F.; Wang, T.; Zheng, S.; Hwang, B. J.; Huang, Y.; et al. Atomically dispersed Fe-N_x/C electrocatalyst boosts oxygen catalysis via a new metal-organic polymer supramolecule strategy. *Adv. Energy Mater.* **2018**, *8*, 1801226. DOI: 10.1002/aenm.201801226
(241) Kinoshita, K. *Carbon, electrochemical and physicochemical properties*; John Wiley & Sons, 1988.
(242) Charreteur, F.; Jaouen, F.; Dodelet, J. P. Iron porphyrin-based cathode catalysts for PEM fuel cells: Influence of pyrolysis gas on activity and stability. *Electrochim. Acta* **2009**, *54*, 6622-6630. DOI: 10.1016/j.electacta.2009.06.058
(243) Xia, D.; Yang, X.; Xie, L.; Wei, Y.; Jiang, W.; Dou, M.; Li, X.; Li, J.; Gan, L.; Kang, F. Direct growth of carbon nanotubes Doped with single atomic Fe–N_4 active sites and neighboring graphitic nitrogen for efficient and stable oxygen reduction electrocatalysis. *Adv. Funct. Mater.* **2019**, *29*, 1906174. DOI: 10.1002/adfm.201906174
(244) Lemire, J. A.; Harrison, J. J.; Turner, R. J. Antimicrobial activity of metals: mechanisms, molecular targets and applications. *Nat. Rev. Microbiol.* **2013**, *11*, 371-384. DOI: 10.1038/nrmicro3028
(245) Aust, S. D.; Morehouse, L. A.; Thomas, C. E. Role of metals in oxygen radical reactions. *J. Free Radicals Biol. Med.* **1985**, *1*, 3-25. DOI: 10.1016/0748-5514(85)90025-x
(246) Liu, S.; Deng, C.; Yao, L.; Zhong, H.; Zhang, H. The key role of metal dopants in nitrogen-doped carbon xerogel for oxygen reduction reaction. *J. Power Sources* **2014**, *269*, 225-235. DOI: 10.1016/j.jpowsour.2014.06.148

(247) Martinez, U.; Komini Babu, S.; Holby, E. F.; Zelenay, P. Durability challenges and perspective in the development of PGM-free electrocatalysts for the oxygen reduction reaction. *Curr. Opin. Electrochem.* **2018**, *9*, 224-232. DOI: 10.1016/j.coelec.2018.04.010
(248) Jaouen, F.; Dodelet, J.-P. Average turn-over frequency of O_2 electro-reduction for Fe/N/C and Co/N/C catalysts in PEFCs. *Electrochim. Acta* **2007**, *52*, 5975-5984. DOI: 10.1016/j.electacta.2007.03.045
(249) Xie, X.; He, C.; Li, B.; He, Y.; Cullen, D. A.; Wegener, E. C.; Kropf, A. J.; Martinez, U.; Cheng, Y.; Engelhard, M. H.; et al. Performance enhancement and degradation mechanism identification of a single-atom Co–N–C catalyst for proton exchange membrane fuel cells. *Nat. Catal.* **2020**, *3*, 1044-1054. DOI: 10.1038/s41929-020-00546-1
(250) Cheng, Q.; Yang, L.; Zou, L.; Zou, Z.; Chen, C.; Hu, Z.; Yang, H. Single cobalt atom and N codoped carbon nanofibers as highly durable electrocatalyst for oxygen reduction reaction. *ACS Catal.* **2017**, *7*, 6864-6871. DOI: 10.1021/acscatal.7b02326
(251) He, Y.; Hwang, S.; Cullen, D. A.; Uddin, M. A.; Langhorst, L.; Li, B.; Karakalos, S.; Kropf, A. J.; Wegener, E. C.; Sokolowski, J.; et al. Highly active atomically dispersed CoN_4 fuel cell cathode catalysts derived from surfactant-assisted MOFs: carbon-shell confinement strategy. *Energy Environ. Sci.* **2019**, *12*, 250-260. DOI: 10.1039/c8ee02694g
(252) Gupta, S.; Zhao, S.; Wang, X. X.; Hwang, S.; Karakalos, S.; Devaguptapu, S. V.; Mukherjee, S.; Su, D.; Xu, H.; Wu, G. Quaternary FeCoNiMn-based nanocarbon electrocatalysts for bifunctional oxygen reduction and evolution: Promotional role of Mn doping in stabilizing carbon. *ACS Catal.* **2017**, *7*, 8386-8393. DOI: 10.1021/acscatal.7b02949
(253) Zhong, Y.; Liang, X.; He, Z.; Tan, W.; Zhu, J.; Yuan, P.; Zhu, R.; He, H. The constraints of transition metal substitutions (Ti, Cr, Mn, Co and Ni) in magnetite on its catalytic activity in heterogeneous Fenton and UV/Fenton reaction: From the perspective of hydroxyl radical generation. *Appl. Catal., B* **2014**, *150-151*, 612-618. DOI: 10.1016/j.apcatb.2014.01.007
(254) Chen, M.; Li, X.; Yang, F.; Li, B.; Stracensky, T.; Karakalos, S.; Mukerjee, S.; Jia, Q.; Su, D.; Wang, G.; et al. Atomically dispersed MnN_4 catalysts via environmentally benign aqueous synthesis for oxygen reduction: Mechanistic understanding of activity and stability improvements. *ACS Catal.* **2020**, *10*, 10523-10534. DOI: 10.1021/acscatal.0c02490
(255) Ferguson-Miller, S.; Babcock, G. T. Heme/Copper Terminal Oxidases. *Chem. Rev.* **1996**, *96*, 2889-2908. DOI: 10.1021/cr950051s
(256) Zou, W.; Lu, R.; Liu, X.; Xiao, G.; Liao, X.; Wang, Z.; Zhao, Y. Theoretical insights into dual-atom catalysts for the oxygen reduction reaction: the crucial role of orbital polarization. *J. Mater. Chem. A* **2022**, *10*, 9150-9160. DOI: 10.1039/d2ta00313a
(257) Lu, Z.; Wang, B.; Hu, Y.; Liu, W.; Zhao, Y.; Yang, R.; Li, Z.; Luo, J.; Chi, B.; Jiang, Z.; et al. An isolated zinc–cobalt atomic pair for highly active and durable oxygen reduction. *Angew. Chem. Int. Ed.* **2019**, *58*, 2622-2626. DOI: 10.1002/anie.201810175
(258) Zhu, X.; Yan, J.; Gu, M.; Liu, T.; Dai, Y.; Gu, Y.; Li, Y. Activity origin and design principles for oxygen reduction on dual-metal-site catalysts: A combined density functional theory and machine learning study. *J. Phys. Chem. Lett.* **2019**, *10*, 7760-7766. DOI: 10.1021/acs.jpclett.9b03392
(259) Bauer, M.; Lei, C.; Read, K.; Tobey, R.; Gland, J.; Murnane, M. M.; Kapteyn, H. C. Direct observation of surface chemistry using ultrafast soft-X-ray pulses. *Phys. Rev. Lett.* **2001**, *87*, 025501. DOI: 10.1103/PhysRevLett.87.025501
(260) Puglia, C.; Nilsson, A.; Hernnäs, B.; Karis, O.; Bennich, P.; Mårtensson, N. Physisorbed, chemisorbed and dissociated O_2 on Pt(111) studied by different core level spectroscopy methods. *Surf. Sci.* **1995**, *342*, 119-133. DOI: 10.1016/0039-6028(95)00798-9
(261) Pedersen, A.; Barrio, J.; Li, A.; Jervis, R.; Brett, D. J. L.; Titirici, M. M.; Stephens, I. E. L. Dual-metal atom electrocatalysts: Theory, synthesis, characterization, and applications. *Adv. Energy Mater.* **2022**, *12*, 2102715. DOI: 10.1002/aenm.202102715
(262) Yang, X.; Priest, C.; Hou, Y.; Wu, G. Atomically dispersed dual-metal-site PGM-free electrocatalysts for oxygen reduction reaction: Opportunities and challenges. *SusMat* **2022**, *2*, 569-590. DOI: 10.1002/sus2.69

(263) Ye, W.; Chen, S.; Lin, Y.; Yang, L.; Chen, S.; Zheng, X.; Qi, Z.; Wang, C.; Long, R.; Chen, M.; et al. Precisely tuning the number of Fe atoms in clusters on N-doped carbon toward acidic oxygen reduction reaction. *Chem* **2019**, *5*, 2865-2878. DOI: 10.1016/j.chempr.2019.07.020
(264) Wang, Y.; Luo, E.; Wang, X.; Meng, Q.; Ge, J.; Liu, C.; Xing, W. Fe, Cu-codoped metal-nitrogen-carbon catalysts with high selectivity and stability for the oxygen reduction reaction. *Chin. Chem. Lett.* **2021**, *32*, 506-510. DOI: 10.1016/j.cclet.2020.03.061
(265) Du, C.; Gao, Y.; Chen, H.; Li, P.; Zhu, S.; Wang, J.; He, Q.; Chen, W. A Cu and Fe dual-atom nanozyme mimicking cytochrome c oxidase to boost the oxygen reduction reaction. *J. Mater. Chem. A* **2020**, *8*, 16994-17001. DOI: 10.1039/d0ta06485h
(266) Wang, J.; Huang, Z.; Liu, W.; Chang, C.; Tang, H.; Li, Z.; Chen, W.; Jia, C.; Yao, T.; Wei, S.; et al. Design of N-coordinated dual-metal sites: A stable and active Pt-free catalyst for acidic oxygen reduction reaction. *J. Am. Chem. Soc.* **2017**, *139*, 17281-17284. DOI: 10.1021/jacs.7b10385
(267) Xiao, M.; Chen, Y.; Zhu, J.; Zhang, H.; Zhao, X.; Gao, L.; Wang, X.; Zhao, J.; Ge, J.; Jiang, Z.; et al. Climbing the apex of the ORR volcano plot via binuclear site construction: electronic and geometric engineering. *J. Am. Chem. Soc.* **2019**, *141*, 17763-17770. DOI: 10.1021/jacs.9b08362
(268) Zhou, Y.; Yang, W.; Utetiwabo, W.; Lian, Y.-m.; Yin, X.; Zhou, L.; Yu, P.; Chen, R.; Sun, S. Revealing of active sites and catalytic mechanism in N-coordinated Fe, Ni dual-doped carbon with superior acidic oxygen reduction than single-atom catalyst. *J. Phys. Chem. Lett.* **2020**, *11*, 1404-1410. DOI: 10.1021/acs.jpclett.9b03771
(269) Zang, J.; Wang, F.; Cheng, Q.; Wang, G.; Ma, L.; Chen, C.; Yang, L.; Zou, Z.; Xie, D.; Yang, H. Cobalt/zinc dual-sites coordinated with nitrogen in nanofibers enabling efficient and durable oxygen reduction reaction in acidic fuel cells. *J. Mater. Chem. A* **2020**, *8*, 3686-3691. DOI: 10.1039/c9ta12207a
(270) Mechler, A. K.; Sahraie, N. R.; Armel, V.; Zitolo, A.; Sougrati, M. T.; Schwämmlein, J. N.; Jones, D. J.; Jaouen, F. Stabilization of iron-based fuel cell catalysts by non-catalytic platinum. *J. Electrochem. Soc.* **2018**, *165*, F1084-F1091. DOI: 10.1149/2.0721813jes
(271) Kosmala, T.; Bibent, N.; Sougrati, M. T.; Dražić, G.; Agnoli, S.; Jaouen, F.; Granozzi, G. Stable, active, and methanol-tolerant PGM-free surfaces in an acidic medium: Electron tunneling at play in Pt/FeNC hybrid catalysts for direct methanol fuel cell cathodes. *ACS Catal.* **2020**, *10*, 7475-7485. DOI: 10.1021/acscatal.0c01288
(272) Zatoń, M.; Rozière, J.; Jones, D. J. Mitigation of PFSA membrane chemical degradation using composite cerium oxide–PFSA nanofibres. *J. Mater. Chem. A* **2017**, *5*, 5390-5401. DOI: 10.1039/c6ta10977b
(273) Lei, M.; Yang, T. Z.; Wang, W. J.; Huang, K.; Zhang, Y. C.; Zhang, R.; Jiao, R. Z.; Fu, X. L.; Yang, H. J.; Wang, Y. G.; et al. One-dimensional manganese oxide nanostructures as radical scavenger to improve membrane electrolyte assembly durability of proton exchange membrane fuel cells. *J. Power Sources* **2013**, *230*, 96-100. DOI: 10.1016/j.jpowsour.2012.12.011
(274) Trogadas, P.; Parrondo, J.; Ramani, V. Degradation mitigation in polymer electrolyte membranes using cerium oxide as a regenerative free-radical scavenger. *Electrochem. Solid-State Lett.* **2008**, *11*, B113-B116. DOI: 10.1149/1.2916443
(275) Zatoń, M.; Rozière, J.; Jones, D. J. Current understanding of chemical degradation mechanisms of perfluorosulfonic acid membranes and their mitigation strategies: a review. *Sustainable Energy Fuels* **2017**, *1*, 409-438. DOI: 10.1039/c7se00038c
(276) Trogadas, P.; Parrondo, J.; Ramani, V. Platinum supported on CeO_2 effectively scavenges free radicals within the electrolyte of an operating fuel cell. *Chem. Commun.* **2011**, *47*, 11549-11551. DOI: 10.1039/c1cc15155j
(277) Shao, Y. *Highly active and durable PGM-free ORR electrocatalysts through the synergy of active sites*. 2019. https://www.hydrogen.energy.gov/pdfs/review19/fc172_shao_2019_o.pdf (accessed 2023-03-01).
(278) Shao, Y. *Highly active and durable PGM-free ORR electrocatalysts through the synergy of active sites*. 2018. https://www.hydrogen.energy.gov/pdfs/review18/fc172_shao_2018_o.pdf (accessed 2023-03-01).

(279) Zelenay, P.; Myers, M. *ElectroCat (Electrocatalysis Consortium)*. 2019. https://www.hydrogen.energy.gov/pdfs/review19/fc160_myers_zelenay_2019_o.pdf (accessed 2023-03-01).
(280) Wei, H.; Su, X.; Liu, J.; Tian, J.; Wang, Z.; Sun, K.; Rui, Z.; Yang, W.; Zou, Z. A CeO_2 modified phenylenediamine-based Fe/N/C with enhanced durability/stability as non-precious metal catalyst for oxygen reduction reaction. *Electrochem. Com.* **2018**, *88*, 19-23. DOI: 10.1016/j.elecom.2018.01.011
(281) Shao, Y.; Dodelet, J. P.; Wu, G.; Zelenay, P. PGM-free cathode catalysts for PEM fuel cells: A mini-review on stability challenges. *Adv. Mater.* **2019**, *31*, e1807615, 1807615. DOI: 10.1002/adma.201807615
(282) Zatoń, M.; Prélot, B.; Donzel, N.; Rozière, J.; Jones, D. J. Migration of Ce and Mn ions in PEMFC and its Impact on PFSA membrane degradation. *J. Electrochem. Soc.* **2018**, *165*, F3281-F3289. DOI: 10.1149/2.0311806jes
(283) Li, J. C.; Maurya, S.; Kim, Y. S.; Li, T.; Wang, L.; Shi, Q.; Liu, D.; Feng, S.; Lin, Y.; Shao, M. Stabilizing single-atom iron electrocatalysts for oxygen reduction via ceria confining and trapping. *ACS Catal.* **2020**, *10*, 2452-2458. DOI: 10.1021/acscatal.9b04621
(284) Shao, Y. *Highly active and durable PGM-free ORR electrocatalysts through the synergy of active sites*. 2020. https://www.hydrogen.energy.gov/pdfs/review20/fc172_shao_2020_o.pdf (accessed 2023-03-01).
(285) Xie, H.; Xie, X.; Hu, G.; Prabhakaran, V.; Saha, S.; Gonzalez-Lopez, L.; Phakatkar, A. H.; Hong, M.; Wu, M.; Shahbazian-Yassar, R.; et al. Ta–TiO_x nanoparticles as radical scavengers to improve the durability of Fe–N–C oxygen reduction catalysts. *Nat. Energy* **2022**, *7*, 281-289. DOI: 10.1038/s41560-022-00988-w
(286) Liu, S.; Li, C.; Zachman, M. J.; Zeng, Y.; Yu, H.; Li, B.; Wang, M.; Braaten, J.; Liu, J.; Meyer, H. M.; et al. Atomically dispersed iron sites with a nitrogen–carbon coating as highly active and durable oxygen reduction catalysts for fuel cells. *Nat. Energy* **2022**, *7*, 652-663. DOI: 10.1038/s41560-022-01062-1
(287) Xia, D.; Tang, X.; Dai, S.; Ge, R.; Rykov, A.; Wang, J.; Huang, T. H.; Wang, K. W.; Wei, Y.; Zhang, K.; et al. Ultrastable Fe-N-C fuel cell electrocatalysts by eliminating non-coordinating nitrogen and regulating coordination structures at high temperatures. *Adv. Mater.* **2023**, *35*, e2204474. DOI: 10.1002/adma.202204474
(288) Banham, D.; Choi, J. Y.; Kishimoto, T.; Ye, S. Integrating PGM-free catalysts into catalyst layers and proton exchange membrane fuel cell devices. *Adv. Mater.* **2019**, *31*, 1804846. DOI: 10.1002/adma.201804846
(289) Osmieri, L.; Wang, G.; Cetinbas, F. C.; Khandavalli, S.; Park, J.; Medina, S.; Mauger, S. A.; Ulsh, M.; Pylypenko, S.; Myers, D. J.; et al. Utilizing ink composition to tune bulk-electrode gas transport, performance, and operational robustness for a Fe–N–C catalyst in polymer electrolyte fuel cell. *Nano Energy* **2020**, *75*, 104943. DOI: 10.1016/j.nanoen.2020.104943
(290) Damjanovic, A. M.; Koyutürk, B.; Li, Y. S.; Menga, D.; Eickes, C.; El-Sayed, H. A.; Gasteiger, H. A.; Fellinger, T. P.; Piana, M. Loading impact of a PGM-free catalyst on the mass activity in proton exchange membrane fuel cells. *J. Electrochem. Soc.* **2021**, *168*, 114518. DOI: 10.1149/1945-7111/ac3779
(291) Banham, D.; Kishimoto, T.; Zhou, Y. J.; Sato, T.; Bai, K.; Ozaki, J.; Imashiro, Y.; Ye, S. Y. Critical advancements in achieving high power and stable nonprecious metal catalyst-based MEAs for real-world proton exchange membrane fuel cell applications. *Sci. Adv.* **2018**, *4*, eaar7180. DOI: 10.1126/sciadv.aar7180
(292) Komini Babu, S.; Chung, H. T.; Zelenay, P.; Litster, S. Resolving electrode morphology's impact on platinum group metal-free cathode performance using nano-CT of 3D hierarchical pore and ionomer distribution. *ACS Appl. Mater. Interfaces* **2016**, *8*, 32764-32777. DOI: 10.1021/acsami.6b08844

(293) Zhou, L.; Li, Y.; Chen, X.; Yang, Z.; Yang, S.; Wang, Q.; Liu, X.-Y.; Lu, S. New insights into degradation of Fe–N–C catalyst layers: ionomer decomposition. *J. Mater. Chem. A* **2022**, *10*, 20323-20330. DOI: 10.1039/d2ta03669j
(294) Garland, N.; Benjamin, T.; Kopasz, J. DOE fuel cell program: Durability technical targets and testing protocols. *ECS Trans.* **2007**, *11*, 923-931. DOI: 10.1149/1.2781004
(295) Hydrogen and Fuel Cell Technologies Office. *Fuel Cell Tech Team Accelerated Stress Test and Polarization Curve Protocols for PEM Fuel Cells*. 2013. https://www.energy.gov/sites/prod/files/2015/08/f25/fcto_dwg_usdrive_fctt_accelerated_stress_tests_jan2013.pdf (accessed 2023-03-01).
(296) Harzer, G. S.; Schwämmlein, J. N.; Damjanović, A. M.; Ghosh, S.; Gasteiger, H. A. Cathode loading impact on voltage cycling induced PEMFC degradation: A voltage loss analysis. *J. Electrochem. Soc.* **2018**, *165*, F3118-F3131. DOI: 10.1149/2.0161806jes
(297) Uchimura, M.; Kocha, S. S. The impact of cycle profile on PEMFC durability. *ECS Trans.* **2007**, *11*, 1215-1226. DOI: 10.1149/1.2781035
(298) Gilbert, J. A.; Kariuki, N. N.; Wang, X.; Kropf, A. J.; Yu, K.; Groom, D. J.; Ferreira, P. J.; Morgan, D.; Myers, D. J. Pt catalyst degradation in aqueous and fuel cell environments studied via in-*operando* anomalous small-angle X-ray scattering,. *Electrochim. Acta* **2015**, *173*, 223-234. DOI: 10.1016/j.electacta.2015.05.032
(299) Macauley, N.; Papadias, D. D.; Fairweather, J.; Spernjak, D.; Langlois, D.; Ahluwalia, R.; More, K. L.; Mukundan, R.; Borup, R. L. Carbon corrosion in PEM fuel cells and the development of accelerated stress tests. *J. Electrochem. Soc.* **2018**, *165*, F3148-F3160. DOI: 10.1149/2.0061806jes
(300) Banhart, F. Irradiation effects in carbon nanostructures. *Rep. Prog. Phys.* **1999**, *62*, 1181-1221. DOI: 10.1088/0034-4885/62/8/201
(301) Krasheninnikov, A. V.; Banhart, F. Engineering of nanostructured carbon materials with electron or ion beams. *Nat. Mater.* **2007**, *6*, 723-733. DOI: 10.1038/nmat1996
(302) Wagner, J. K. *Environmental TEM: principle, limitation and application*. http://www.fhi-berlin.mpg.de/acnew/department/pages/teaching/pages/teaching__wintersemester__2016_2017/jakob_wagner__environmental_transmission_electron_microscopy__161202.pdf (accessed 2022-04-15).
(303) Hodnik, N.; Dehm, G.; Mayrhofer, K. J. Importance and challenges of electrochemical *in situ* liquid cell electron microscopy for energy conversion research. *Acc. Chem. Res.* **2016**, *49*, 2015-2022. DOI: 10.1021/acs.accounts.6b00330
(304) Mayrhofer, K. J. J.; Meier, J. C.; Ashton, S. J.; Wiberg, G. K. H.; Kraus, F.; Hanzlik, M.; Arenz, M. Fuel cell catalyst degradation on the nanoscale. *Electrochem. Com.* **2008**, *10*, 1144-1147. DOI: 10.1016/j.elecom.2008.05.032
(305) Jia, Q.; Ramaswamy, N.; Hafiz, H.; Tylus, U.; Strickland, K.; Wu, G.; Barbiellini, B.; Bansil, A.; Holby, E. F.; Zelenay, P.; et al. Experimental observation of redox-induced Fe-N switching behavior as a determinant role for oxygen reduction activity. *ACS Nano* **2015**, *9*, 12496-12505. DOI: 10.1021/acsnano.5b05984
(306) Saveleva, V. A.; Ebner, K.; Ni, L.; Smolentsev, G.; Klose, D.; Zitolo, A.; Marelli, E.; Li, J.; Medarde, M.; Safonova, O. V.; et al. Potential-induced spin changes in Fe/N/C electrocatalysts assessed by *in situ* X-ray emission spectroscopy. *Angew. Chem. Int. Ed.* **2021**, *60*, 11707-11712. DOI: 10.1002/anie.202016951
(307) Ebner, K.; Clark, A. H.; Saveleva, V. A.; Smolentsev, G.; Chen, J.; Ni, L.; Li, J.; Zitolo, A.; Jaouen, F.; Kramm, U. I.; et al. Time-resolved potential-induced changes in Fe/N/C-catalysts studied by *in situ* modulation excitation X-ray absorption spectroscopy. *Adv. Energy Mater.* **2022**, *12*, 2103699. DOI: 10.1002/aenm.202103699
(308) Saveleva, V. A.; Kumar, K.; Theis, P.; Salas, N. S.; Kramm, U. I.; Jaouen, F.; Maillard, F.; Glatzel, P. Fe-N-C electrocatalyst and its electrode: Are we talking about the same material? *ACS Appl. Energy Mater.* **2023**, *6*, 611-616. DOI: 10.1021/acsaem.2c03736
(309) Teixeira Santos, K.; Kumar, K.; Dubau, L.; Ge, H.; Berthon-Fabry, S.; Vasconcellos, C. S. A.; Lima, F. H. B.; Asset, T.; Atanassov, P.; Saveleva, V. A.; et al. Spontaneous aerobic ageing of Fe–N–C

materials and consequences on oxygen reduction reaction kinetics. *J. Power Sources* **2023**, *564*, 232829. DOI: 10.1016/j.jpowsour.2023.232829
(310) Ni, L.; Gallenkamp, C.; Wagner, S.; Bill, E.; Krewald, V.; Kramm, U. I. Identification of the catalytically dominant iron environment in iron- and nitrogen-doped carbon catalysts for the oxygen reduction reaction. *J. Am. Chem. Soc.* **2022**, *144*, 16827-16840. DOI: 10.1021/jacs.2c04865
(311) Kneebone, J. L.; Daifuku, S. L.; Kehl, J. A.; Wu, G.; Chung, H. T.; Hu, M. Y.; Alp, E. E.; More, K. L.; Zelenay, P.; Holby, E. F.; et al. A combined probe-molecule, Mössbauer, nuclear resonance vibrational spectroscopy, and density functional theory approach for evaluation of potential iron active sites in an oxygen reduction reaction catalyst. *J. Phys. Chem. C* **2017**, *121*, 16283-16290. DOI: 10.1021/acs.jpcc.7b03779
(312) Kim, D. H.; Ringe, S.; Kim, H.; Kim, S.; Kim, B.; Bae, G.; Oh, H. S.; Jaouen, F.; Kim, W.; Kim, H.; et al. Selective electrochemical reduction of nitric oxide to hydroxylamine by atomically dispersed iron catalyst. *Nat. Commun.* **2021**, *12*, 1856. DOI: 10.1038/s41467-021-22147-7
(313) Bae, G.; Kim, H.; Choi, H.; Jeong, P.; Kim, D. H.; Kwon, H. C.; Lee, K. S.; Choi, M.; Oh, H. S.; Jaouen, F.; et al. Quantification of active site density and turnover frequency: From single-atom metal to nanoparticle electrocatalysts. *JACS Au* **2021**, *1*, 586-597. DOI: 10.1021/jacsau.1c00074
(314) Snitkoff-Sol, R. Z.; Friedman, A.; Honig, H. C.; Yurko, Y.; Kozhushner, A.; Zachman, M. J.; Zelenay, P.; Bond, A. M.; Elbaz, L. Quantifying the electrochemical active site density of precious metal-free catalysts *in situ* in fuel cells. *Nat. Catal.* **2022**, *5*, 163-170. DOI: 10.1038/s41929-022-00748-9